UNIVERSITY OF LONDON THESIS

Degree PhD Year 2004 Name of Author EVANS, R. Jane (Rosemary)

Identification and Characterisation of RP2 Interacting Proteins

R Jane Evans Bsc (Hons)

A thesis submitted for the Degree of
Doctor of Philosophy

Division of Molecular and Cellular Neuroscience
Institute of Ophthalmology
University College London
Bath Street, London
EC1V 9EL

2007

ProQuest LLC
789 East Eisenhower Parkway
P.O. Box 1346
Ann Arbor, MI 48106-1346

Declaration

I declare that this thesis submitted for the Degree of Doctor of Philosophy is composed by myself, and the work herein is my own, or that the author involved is clearly stated.

R Jane Evans

ABSTRACT

Retinitis pigmentosa (RP) is a genetically and clinically heterogenous retinal degenerative disease, which is characterised by night blindness and constriction of visual fields in the early stages which progress to blindness. X-linked RP (XLRP) is the most severe form of the disease and 2 causative genes have been identified, *RP2* and *RPGR*. *RP2* encodes a ubiquitously expressed 350 amino acid protein with a tubulin folding cofactor C (TBCC) homology domain and a C-terminal NDK homology domain. Despite the ubiquitous expression of the RP2 protein, the disease pathogenesis in patients carrying *RP2* gene mutations appears to be restricted to retina. The function of RP2 in retina, or other tissues, has yet to be determined. This study aims to increase the understanding of the pathobiology of RP2 by unravelling novel molecular pathways of RP2 function.

The approach taken to elucidate the cellular roles of RP2 in retina was to identify potential interacting partner proteins from a retina library using a yeast-two-hybrid approach. The Sos Recruitment System (SRS) was exploited, as RP2 had previously been shown to be predominantly localised on the plasma membrane. Several candidate protein partners for RP2 were identified. ADP-ribosylation like factor 3 (Arl3) was the most common cDNA identified in the yeast-two-hybrid screen. The interaction between RP2 and Arl3 was further defined using site directed mutagenesis to model pathogenic mutations in RP2 and a series of deletion mutants. RP2 preferentially interacted with the active GTP-bound form of Arl3 via the RP2 TBCC-homology domain. An altered cellular localisation and behaviour of RP2 was observed when co-transfected with GTP-bound Arl3. Both Arl3 and RP2 exhibit partial relocalisation to the Golgi and increased intracellular transport of RP2-GFP. Arl2 is structurally very similar to Arl3, and was also identified as a potential interactor of RP2, however the physiological significance of the RP2-Arl2 interaction is unclear. Interestingly, TBCC did not bind Arl2 or Arl3 confirming that RP2 and TBCC have different cellular functions.

Four other novel potential interactors were also identified from the yeast two-hybrid screen including another small GTPase, and their interaction mapped to the C-terminus of RP2. The cellular localisation and function of these novel interactors suggest RP2 may have multiple cellular functions.

PUBLICATIONS AND ABSTRACTS

Publications

Evans, R. J., Chapple, J. P., Grayson, C., Hardcastle, A. J., and Cheetham, M. E. (2005). Assay and functional analysis of the ARL3 effector RP2 involved in X-linked retinitis pigmentosa. *Methods Enzymol.* **404**, 468-480.

Evans, R. J., Hardcastle, A. J., and Cheetham, M. E. (2006). Focus on molecules: X-linked Retinitis Pigmentosa 2 protein, RP2. *Exp.Eye Res.* **82**, 543-544.

Hidalgo-de-Quintana, J, Evans, R. J, Cheetham, M. E, and van der Spuy, J. (2007). The LCA protein AIPL1 functions as part of a chaperone heterocomplex. Submitted.

Abstracts

Characterisation of the Interaction Between the X-linked Retinitis Pigmentosa Protein RP2 and Arl Proteins.
R. Jane Evans, Alison J. Hardcastle, and Michael E. Cheetham.
ARVO (2005) 5170-*B373.*

Investigation of the Interaction of RP2 and Arl3.
R. Jane Evans, Alison J. Hardcastle, and Michael E. Cheetham.
ISOCB (2006) P13.

ACKNOWLEDGEMENTS

Firstly I would like to thank my supervisors Alison Hardcastle and Mike Cheetham for giving me the opportunity to work on such a fantastic project and who have been incredibly supportive during the last four years. It's been a fabulous experience, so thank you so much. Thank you also to everyone in MCN, past and present, it's been great to work with so many lovely people. In particular I'd like to say huge thanks to Juan for all the yeast chats and to Jacqui for all the advice and perfectly written protocols!

I'd especially like to thank Simon not only for his guru-like advice but also his calm manner and friendship which has got me through many stressful times! Naheed, I can't thank you enough for your amazing patience and lovely chats which I have appreciated no end, especially in the last few months. Marghe, it's been fabulous having you in the lab this year, your cheerfulness has made us all smile! Thanks also to Suba and Neil who may have left but have always still been there. Thank you also to Shazeen, Sakina and Louise.

Thank you also to Peter Munro for all his help with the confocal microscope and to Beverley Scott who always seemed to ensure my sequencing worked!

I'd like to say a big thank you to Corin, who really has put up with a lot, I promise my constant lateness will soon be a thing of the past (I hope)! Thank you for being such a fantastic friend.

Lastly I would like to thank my family. Thank you to my parents, without all your support I'm quite sure I wouldn't be writing this now, it's hard to say quite how much I owe you and how much I appreciate everything you've done. Thanks also to Kay, Brian, Angus and Magdalen who have been so supportive. To Patrick, thank you for being so lovely! And to Bréanainn, I hope I can do the same for you one day.

Dedication

This thesis is dedicated to Bréanainn and Patrick who I think are brilliant.

TABLE OF CONTENTS

LIST OF FIGURES

LIST OF TABLES

LIST OF ABBREVIATIONS

ADP	Adenosine diphosphate
Arf	ADP-ribosylation factor
Arl	ADP-ribosylation factor-like
ATP	Adenosine triphosphate
BART1	Binder of Arl2
BSA	Bovine serum albumin
CAP	Cyclase associated protein
CC	Connecting cilia/cilium
CCT	Cytosolic chaperonin
CDKN1B	Cyclin dependent kinase inhibitor 1B
cDNA	complementary DNA
cGMP	cyclic guanosine monophosphate
CHO	Chinese hamster ovary
CIAP	Calf intestinal alkaline phosphatase
CRD	Cone-rod dystropy
DAPI	4'6-diamidimo-2-phenylindole
ddH_2O	Double distilled water
DMEM	Dulbecco's modified eagles medium
DNA	Deoxyribonucleic acid
ECL	Enhanced chemiluminescence
FBS	Fetal bovine serum
GAP	GTPase activating protein
GCL	Ganglion cell layer
GDP	Guanosine diphosphate
GEF	Guanine nucleotide exchange factor
GFP	Green fluorescent protein
GTP	Guanosine triphosphate
HBSS	Hanks balanced salt solution
HRP	Horse radish peroxidase
IPTG	Isopropyl-beta-D-thiogalactopyranoside
IMS	Industrial methylated spirit
INL	Inner nuclear layer
IPL	Inner plexiform layer

IS	Inner segment
kb	kilobase
kDa	kilo Dalton
LCA	Leber congenital amaurosis
MAP	Microtubule associated protein
mRNA	messenger RNA
MTOC	Microtubule organising centre
NP40	Nonidet P40
OLM	Outer limiting membrane
ONL	Outer nuclear layer
OPL	Outer plexiform layer
OS	Outer segment
PCR	Polymerase chain reaction
PDE	Phosphodiesterase
Pi	Phosphate
RAN	Ras-related nuclear protein
RP	Retinitis pigmentosa
RPE	Retinal pigment epithelium
RPGR	Retinitis pigmentosa GTPase regulator
SDS	Sodium dodecyl sulphate
SDS-PAGE	SDS polyacrylamide gel electrophoresis
SPAG7	Sperm associated antigen 7
SRS	Sos recruitment system
TAE	Tris acetate buffer
TEMED	N,N,N',N'-tetramethylethylenediamine
TNPO3	Transportin 3
Tris	2-amino-2-(hydroxymethyl)-1,3-propanediol
Tween 20	Polyoxyethylene sorbitan monolaurate
XLRP	X-linked retinitis pigmentosa

CHAPTER 1

INTRODUCTION

1.1 The Eye

The human eye comprises three basic layers; a fibrous (corneoscleral) coat, the uvea (formed by the choroids, ciliary body and iris) and the neural layer (retinal layer) (Figure 1.1). Light enters the eye through the lens which is able to relax and contract thus altering its shape and allowing a sharp image to be formed on the retina. The amount of light passing through the lens is controlled by the iris, a pigmented circular muscle surrounding the pupil. The transparent cornea acts as a barrier to infection and trauma as well as being partially responsible for the refractive properties of the eye. Continuous to the cornea is the sclera which is a dense fibrous opaque coat which forms the site of attachment for the intrinsic muscles of the eye.

Figure 1.1 Structure of the human eye

A cross-sectional view of the human eye, adapted from Fight for Sight (www.fightforsight.org.uk)

1.2 The Retina

The retina is the light-detecting part of the eye consisting of three major neuronal layers. The neuro sensory retina and the outer pigmented epithelium are linked by the interphotoreceptor matrix (IPM) (Bridges, 1995). Images are focused onto the retina by the cornea and lens.

1.2.1 The retinal pigment epithelium

The non-neuronal monolayer of columnar epithelial cells which separate the retina from its blood supply (the choroid) is known as the retinal pigment epithelium (RPE). The RPE cells play a role in the turnover of outer segments (OS) discs as well as functioning in the visual cycle by recycling vitamin A; all-*trans*-retinol is converted back to 11-*cis*-retinal and released across the apical membrane for reabsorbtion by the photoreceptors (Bok, 1993). The phagocytosis of the OS occurs through the apical processes of the RPE cells which surround the photoreceptor OS. Shed discs are then packaged into phagosomes which are subsequently degraded. Each RPE cell contacts approximately 45 outer segments, and the estimated turnover of outer segment discs is 10% daily (Young and Bok, 1969). The RPE also absorbs scattered light as it is rich in melanosomes. (Bron, Tripathi and Tripathi, 8th Ed, 1997).

1.2.2 The neural retina

The sensory neural retina is comprised of five layers; the outer nuclear layer (ONL), the outer plexiform layer (OPL), the inner nuclear layer (INL), the inner plexiform layer (IPL) and the ganglion cell layer (GCL) (Figure 1.1A). The ONL contains the photoreceptor cell bodies, the OPL is formed from the photoreceptor inner fibres and contains the synaptic junctions between the axon fibres of the photoreceptors and those of the second-order neurons in the retina (e.g. bipolar cells). The INL contains the cell bodies of the neural cells of the retina (e.g bipolar, amacrine, Müller and horizontal cells), and the IPL denotes the point at which the bipolar cells synapse with the third order neural cells; the ganglion cells (Figure 1.2). The GCL contains the cell bodies of the ganglion cells predominantly, but Müller cell processes are also found in this layer (Bron, Tripathi and Tripathi, 8th Ed, 1997).

The most direct way to signal to the brain is through a chain of three neurons; the photoreceptor to bipolar to ganglion cell, however the lateral synaptic connections made by the horizontal and amacrine cells exert additional control over the

transmission of the signal from the photoreceptor to the visual cortex of the brain (Rowe, 1991).

Figure 1.2 Structure of the retina

A A schematic representation of the human retina showing the organisation of the various cell types in the retina. **B** A vertical light micrograph section through the central human retina showing the distinctive layers of the retina. Adapted from http://webvision.med.utah.edu/. Outer limiting membrane (OLM), outer nuclear layer (ONL), outer plexiform layer (OPL), inner nuclear layer (INL), inner plexiform layer (IPL), ganglion cell layer (GCL) and inner limiting membrane (ILM).

The optic disc is located near the centre of the retina to the nasal side, this is the point at which the optic nerve departs and the major blood vessel enters the retina, this area of the retina contains no photoreceptors and as such is known as the 'blind spot'. Near the optic disc the fovea is located, which marks the centre of the macula region (Figure 1.3) (Hendrickson and Yuodelis, 1984). The macula region of the retina is densely populated with photoreceptors, while the central region of the fovea, the foveal pit, is populated exclusively with cone photoreceptors and is the area of most acute vision (Provis *et al.*, 1998).

1.2.3 Rod and cone photoreceptors

There are two major types of photoreceptor cell in the human retina, located in the outer layer of the retina, which are responsible for light perception; rods and cones.

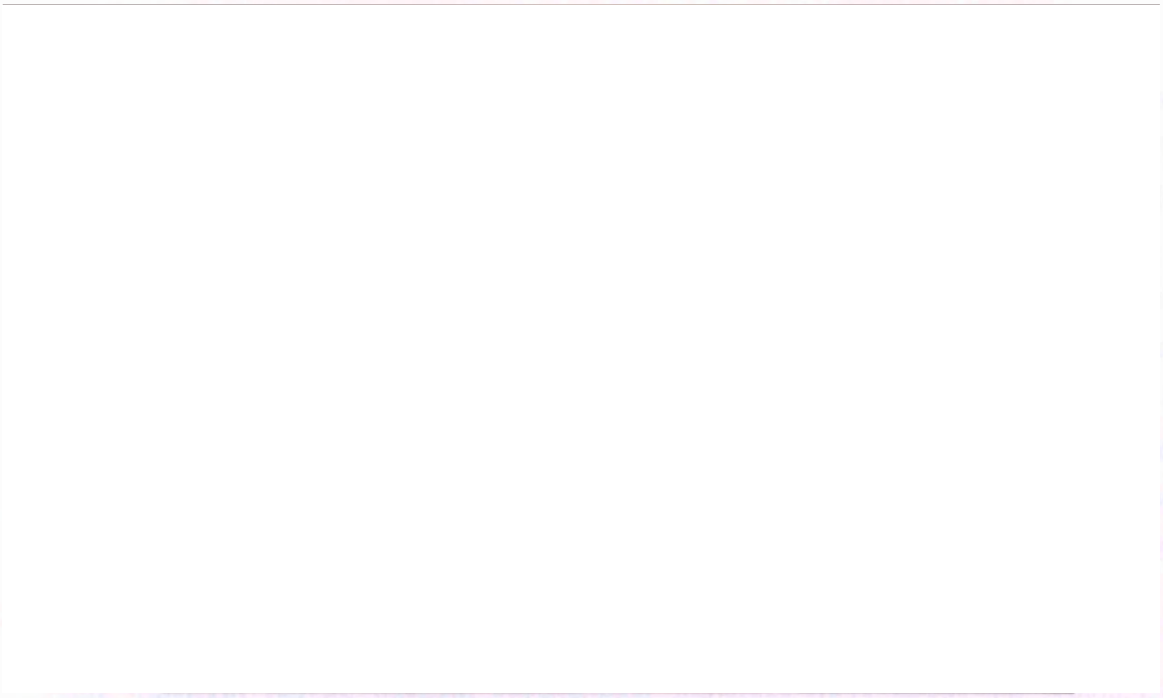

Figure 1.3 A fundus image of a human retina

An ophthalmoscopic photograph of a healthy human retina showing the optic disc, macula region and the fovea. Adapted from Webvision.

Rods are responsible for detection of dim light (scotopic vision) and for contrast sensitivity, while the cone cells are responsible for daylight (photopic) and colour perception. There are approximately 90 million rod cells in the human retina and approximately 4.5 million cones (Curcio *et al.*, 1990).

Rods and cones have a similar basic structure consisting of an outer segment (OS) and inner segment (IS) connected by the connecting cilium (CC). The cell body contains the nucleus, and a synaptic terminal (Figure 1.4). In the outer segment of photoreceptors, membranous structures known as discs are found. These are rich in visual pigment proteins and are surrounded by plasma membrane. In rods these discs are pinched off from the plasma membrane. Whereas in cones, the discs are continuous with one another and the surrounding plasma membrane except for the basal discs which are a separate structure. These discs undergo a high rate of turnover, the old discs are shed from the tip of the photoreceptor and are

phagaocytosed by the RPE cells while the OS continuously forms new discs (Bron, Tripathi and Tripathi, 8thEd, 1997, Pierce 2001).

1.2.3.1 The connecting cilium

The connecting cilium (CC) is a specialised non-motile cilium which actively transports proteins synthesised in the IS to the OS and acts as a support structure for the outer segments (Figure 1.4, Liu *et al.* 2007, Schmitt and Wolfrum, 2001). The cilium develops from the basal body, a modified centriole, which also acts as a microtubule organising centre for the photoreceptor (Figure 1.4) (Muresan *et al.*, 1993). The cilium is non-motile and as such the microtubule arrangement of a 9+0 configuration lacks the central microtubule doublet (9+2) and dynein arms seen in motile cilia (Rölich, 1975). The high turnover rate of proteins in the OS, (it has been estimated that as many as 2,000 photopigment molecules are required by the OS per minute), means that an efficient transport system is required (Besharse and Horst, 1990).

This transport occurs through intraflagellar transport (IFT) along the connecting cilium's axoneme doublet microtubules. The cargo is transported along with IFT particles that are associated with the axonemal structure (Eley *et al.*, 2005). Heterotrimeric kinesin II is the molecular motor responsible for anterograde transport and cytoplasmic dynein 1B is the motor that controls retrograde transport (Eley *et al.*, 2005). Maintenance of this process is vital to the function of the photoreceptor cell and the retina. A study by Pazour *et al* (2002) showed that mice with a mutation in the gene encoding the IFT protein IFT88 exhibited abnormal development of the outer segments and retinal degeneration, suggesting IFT based transport along the connecting cilium is vital to normal retinal function (Pazour *et al.*, 2002). Defects in IFT have also been implicated in Bardet Biedl Syndrome (BBS), a syndrome in which one of the phenotypes is RP (Blacque *et al.*, 2004). Furthermore, other retinal disease proteins have been shown to localise to the connecting cilium (e.g. RPGR) (Hong *et al.*, 2003).

A recent proteomic screen by Liu *et al* (2007) of the photoreceptor sensory cilium of mouse revealed that there is a much higher degree of complexity in mammalian cilia compared to those of unicellular organisms; of the 1968 proteins detected in the screen ~1500 were not detected in lower organisms (Liu *et al.*, 2007), although many of these were outer segment proteins rather than cilia proteins.

Figure 1.4 The rod photoreceptor

Schematic representation of a rod photoreceptor. **A** The rod cell is formed by the outer segment (OS) and the inner segment (IS) connected by the connecting cilium (CC), and the cell body which contains the nucleus (N) and the synaptic terminal (ST) which connects the rod to the bipolar cell. The OS extends toward the retinal pigment epithelium (RPE) cells which are involved in phagocytosing the shed OS disks. **B** The rod connecting cilium, which extends from the rootlet (R) through the basal body (BB) at the top of the IS all the way along the axoneme which extends to the top of the OS. From Liu *et al* (2007).

1.2.4 Phototransduction

Phototransduction is the process which converts the light detected by the photoreceptors into an electrical signal. Rod photoreceptors detect light through photoactivation of the visual pigment, rhodopsin, specifically, isomerisation of 11-*cis*-retinal to all-*trans*-retinal which leads to a conformational change in rhodopsin and consequently activates transducin, this is the first step in the phototransduction pathway (Yau, 1994).

The photoreceptor cell is kept in a depolarised state in the absence of light through the cGMP-gated cation channels on the OS plasma membrane remaining open and allowing sodium ions to enter the cell. When light is detected the consequential decrease in cGMP levels in the cell leads to the closure of the cGMP-gated cation channels. The decrease in intracellular cations leads to the plasma membrane becoming hyper-polarised and a graded decrease in neurotransmitter release at the photoreceptor synapse. This is then detected by the bipolar cells which ultimately results in the signal being interpreted in the visual cortex of the brain (Rattner *et al.*, 1999).

1.3 Inherited retinal dystrophies

Inherited retinal dystrophies are relatively common, estimated to affect 1 in 2000 people worldwide (Rivolta *et al.*, 2002). These retinal dystrophies are both clinically and genetically heterogeneous. There are currently 181 loci for diseases exhibiting an abnormal retinal phenotype with 129 of the causative genes having been identified (Daiger *et al.*, 2007). Autosomal dominant, autosomal recessive, X-linked, digenic, mitochondrial, complex and syndromic inheritance patterns have all been reported. Retinal dystrophies are often categorised according to the age of onset, severity of diease, pattern of visual loss and inheritance pattern.

1.3.1 Leber Congenital Amaurosis

Leber Congenital Amaurosis (LCA) is a rare severe retinal dystrophy with an incidence of approximately 1 in 50-100,000, the onset of disease is early and results in blindness in childhood characterised by no detectable electroretinogram (ERG) response in rods and cones. LCA is genetically heterogenous with 9 known loci, of which 7 of the causative genes are known (Allikmets, 2004, RetNet, OMIM). LCA is inherited in an autosomal recessive pattern.

1.3.2 Central retinal disorders

Central retinal disorders encompass a number of dystrophies such as cone-rod dystrophy, Stargardt disease, and macular degeneration, as well as stationary disorders such as colour blindness and achromatopsia.

Mutations in the genes encoding the red and green cone opsins can result in a stationary visual disorder called colour blindness, with no effect on rod photoreceptor function (McIntyre D, 2002). There is currently little evidence to suggest that mutations in these genes result in cone cell death, in contrast, mutations in the gene encoding rod opsin can result in severe retinal degeneration (Section 1.2.4 and 1.3.4.3).

Cone-rod dystrophies (CRD) are a group of phenotypically and genetically heterogeneous retinal disorders in which there is visual field loss or abnormalities in colour vision. Cone-rod dystrophies can be inherited in an autosomal recessive, autosomal dominant or X-linked pattern. There are currently 13 known causative genes for cone-rod dystrophy (Michaelides *et al.*, 2006, RetNet) and 6 mapped loci (RetNet). ERGs show initial impairment of the normal cone response. The disease can either remain stationary or can be progressive (Michaelides *et al.*, 2006). If stationary the disorder is often diagnosed soon after birth while if progressive the diagnosis is usually made in childhood or adolescence. The disease primarily affects the cone photoreceptors, and diagnosis is often made based on impairment of central vision. There is frequently later involvement of the rod photoreceptors (Michaelides *et al.*, 2006).

Stargardt disease is the most common form of macula degeneration in childhood with an estimated incidence of 1:10,000 (Blacharski, 1988). Disease onset is between 7 and 12 years of age and progression is rapid, visual acuity is severely reduced although peripheral vision remains normal. Mutations in three genes (*ABCA4, CNGB3* and *ELOVL4*, which causes a different form of Stargardt) have been shown to cause Stargardt disease and there is currently one mapped locus (RetNet). *ABCA4* transcripts were initially found to be expressed exclusively in the disc membrane of rod outer segments (Sun and Nathans, 1997) and ABCA4 is thought to be involved in transport between the rod outer segments and the RPE (Sun and Nathans, 1997) (Section 1.3.4.3). However, Molday *et al* showed that ABCA4 is also found in cone cells of the fovea and the peripheral retina as well as in rod cells thus explaining the loss of central vision experienced by Stargardt patients (Molday *et al.*, 2000). Interestingly, there is evidence of genotype-phenotype correlations in *ABCA4* mutations with truncation mutations causing Stargardt disease, and missense mutations affecting uncharged amino acids leading to late-onset fundus flavimaculatus (FFM), an adult onset macula degeneration (Rozet *et al.*, 1998). Mutations in *ABCA4* have also been shown to be responsible for a number of other

retinal dystrophies (Table 1.1), indicating that ABCA4 is vital to the normal function of the retina.

1.3.3 Retinitis pigmentosa

Retinitis pigmentosa (RP) is a clinically and genetically heterogenous condition which results in blindness due to photoreceptor cell death, the condition commonly presents with night blindness as the rod photoreceptors begin to dysfunction and degenerate followed by peripheral vision loss as the rods continue to die. Eventually central vision becomes compromised as the cone photoreceptors also degenerate (Bird, 1975). The incidence of RP has been estimated to be approximately 1 in 3,500 (Vervoort and Wright, 2002) The name 'RP' is derived from the distinctive clusters of pigment that can be seen to overlie a depigmented fundus in RP patients; the pigmented clusters, known as bone-spicules, result from accumulation of pigment granules from degenerating RPE cells. RP is distinguished from cone rod dystrophy as it is principally a peripheral retinal disease, whereas cone-rod dystrophy is a central retinal disease. LCA and early-onset RP are harder to distinguish but LCA has a much earlier age of onset, is a more rapid degeneration and has an increased cone involvement characterised by the rapid loss of central vision compared to the peripheral vision loss that characterises RP. There are currently 46 known loci for RP with 36 causative genes cloned (Daiger *et al.*, 2007, RetNet). RP can be inherited in an autosomal dominant, autosomal recessive or X-linked fashion.

1.3.3.1 Syndromic RP

RP can also occur as a phenotype in syndromes such as Bardet Biedl syndrome (BBS) and Usher syndrome. BBS is a genetically heterogeneous syndrome characterised by obesity, polydactyly, renal abnormalities and RP. The disorder is characterised as a cilia disease or 'ciliopathy' as primary defects in cilia, ciliary transport and signalling underlie the phenotype (Beales 2005). The implication is that the retinal phenotype may be due to defects in the connecting cilium of the photoreceptors. There are 12 known causative genes for BBS (OMIM, RetNet). Usher syndrome is a genetically heterogeneous deafness/blindness syndrome (Kremer *et al.*, 2006). Interestingly, mutations in the *USH2A* gene have been shown to be responsible for arRP without hearing loss, as well as for Usher syndrome (Eudy *et al.*, 1998, Rivolta *et al.*, 2000,). Delineation of the phenotypes of Usher is ongoing, however some explanations are emerging. Defects in morphogenesis of the stereocilia bundle in hair cells, the calycal processes of photoreceptor cells, and

defects in the synaptic processes of these cells have been shown to result in Usher syndrome. Also, connections to the dynamics of the actin cytoskeleton are emerging, more specifically the involvement of actin in cellular morphology, cell polarity and cell–cell interactions (Kremer *et al.*, 2006). There are 9 known causative genes for Usher syndrome and 2 mapped loci (RetNet).

Senior-Loken syndrome (SLSN) is another example of a syndrome in which a retinal dystrophy is a phenotype, in this case LCA or RP is reported with nephronophthisis (anemia, polyuria, polydipsia, isosthenuria, and death in uremia) (Otto *et al.*, 2002). SLSN is inherited in an autosomal recessive mode and is genetically heterogenous, there are currently 3 known causative genes and 1 mapped locus (OMIM). Joubert syndrome (JBTS), inherited in an autosomal recessive manner, has the same phenotype as SLSN but with additional cerebellar and cognitive impairments (Keeler *et al.*, 2003, Maria *et al.*, 1999), suggestive of a ciliary disease. There are currently 4 known causative genes for JBTS and 2 further mapped loci (Helou *et al.*, 2007).

1.3.4 Genes and pathways implicated in retinal diseases

Genes in which mutations have been shown to result in retinal dysfunction or degeneration can be broadly categorised according to their expression profile; those that exhibit a retina- or ocular-specific expression profile or have a known function in a retinal pathway, and those that are ubiquitously expressed (Table 1.1). Phototransduction, the visual cycle, and photoreceptor structure are all retinal-specific pathways or functions which when perturbed have been shown to result in retinal dysfunction (Sections 1.3.4.3-4).

Interestingly, mutations in ubiquitously expressed genes have also been shown to cause retinal dysfunction, either as an aspect of a syndromic disorder (e.g Usher syndrome and Bardet-Beidl syndrome) or as an isolated retinal dystrophy. For example, mutations in the ubiquitously expressed genes *PRPF31* and *RP2* cause retinitis pigmentosa (RP) (Section 1.3.4.2). Examples of the genes and the pathways implicated in retinal disease are shown in Table 1.1.

Pathway/Function	Gene	Reference	Disease caused	Expression Profile
Visual cycle	*LRAT*	Thompson *et al.*, 2001	arRP/arLCA	Retina-specific

	ABCA4	Cremers *et al.*, 1998, Valverde *et al.*, 2007 Allikmets *et al.*, 1997	arRP arCRD ar Stargardt	Retina-specific
	RPE65	Morimura *et al.*, 1998 Gu *et al.*, 1997	arRP arLCA	Retinal pigment epithelium (RPE)
Phototransduction	*PDE6A*	Dryja *et al.*, 1999	arRP	Retina-specific
	PDE6B	Bayes *et al.*, 1995 Gal *et al.*, 1994	arRP adCSNB	Retina-specific
	RHO	Dryja *et al.*, 1990 Rosenfeld *et al, 1992* Dryja *et al.*, 1993	adRP arRP adCSNB	Retina-specific
Photoreceptor structure	*RDS (PRPH2)*	Kajiwara *et al.*, 1991	adRP	Retina and nervous system
Retinal polarity	*CRB1*	den Hollander *et al.*, 1999 den Hollander *et al.*, 2001	arRP arLCA	Retina and brain
Extracellular matrix	*USH2A*	Rivolta *et al.*, 2000	ar Usher syndrome arRP	Broad but not ubiquitous
Transcription	*NRL*	Bessant *et al.*, 1999	adRP/arRP	Retina-specific
	TULP1	Banerjee *et al.*, 1998 Hanein *et al.*, 2004	arRP arLCA	Retina and nervous system
	CRX	Freund *et al.*, 1997 Freund *et al.*, 1998, Hanein *et al.*, 2004	adCRD *de novo* LCA arLCA	Retina and pineal gland
Cilia function	*RPGRIP1*	Dryja *et al.*, 2001 Hameed *et al.*, 2003	arLCA arCRD	Retina and testis
	RP1	Bowne *et al.*, 1999 Khaliq *et al.*, 2005	adRP arRP	Retina
	BBS2	Nishimura *et al.*, 2001	arBBS	Ubiquitous
mRNA splicing	*PRPF31*	Vithana *et al.*, 2001	adRP	Ubiquitous
	PRPF8	McKie *et al.*, 2001	adRP	Ubiquitous
	PRPF3	Chakarova *et al.*, 2002	adRP	Ubiquitous
	PAP1	Maita *et al.*, 2004	adRP	Ubiquitous
Unknown function	*RP2*	Schwahn *et al.*, 1998	XLRP	Ubiquitous
Mitochondrial function	*MTATP6*	Lamminen *et al.*, 1995	LHON	Mitochondrially-encoded
	MTTS2	Mansergh *et al.*, 1999	Dominant RP with hearing loss	Mitochondrially-encoded
	OPA1	Alexander *et al.*, 2000 Delletre *et al.*, 2000	ad Optic atrophy (ADOA)	Ubiquitous

Table 1.1 Examples of genes and pathways implicated in retinal diseases

1.3.4.1 Transcription

Transcription factors that control the expression of genes important for photoreceptor function have been shown to be causative for RP. NRL has been shown to promote the transcription of *Rod Opsin* and other retinal genes (Mears *et al.*, 2001, Rehemtulla *et al.* 1996). CRX has also been shown to control the expression of *Rod Opsin* and act synergistically with NRL in this function (Mitton *et al.*, 2000). Pathogenic mutations in *CRX* were shown to not only impair the DNA binding ability of CRX but also to reduce its interaction affinity for NRL, indicating that compromised control over expression of certain photoreceptor genes (e.g. *Rod opsin*) is likely to result in disease (Mitton *et al.*, 2000).

1.3.4.2 mRNA splicing

Four pre-mRNA splicing factors have been implicated in retinal disease despite being ubiquitously expressed and evolutionary conserved (Sullivan *et al.*, 2006, McKie *et al.*, 2001, Chakarova *et al.*, 2002, Maita *et al.*, 2004). The mechanism by which these splicing factors result in disease remains unclear, but other neurodegenerative disorders (e.g. amyotrophic lateral sclerosis) have also shown to be caused by defects in pre-mRNA splicing (Grabowski and Black, 2001) A study by Mordes *et al* has investigated retinal transcripts which are affected by mutations in one of this group of genes; *PRPF31*. In this study, using immunoprecipitations and microarrays, it was found that mutated *PRPF31* led to a reduced expression of *RDS/PRPH2* which is an important retinal protein involved in photoreceptor structure (Mordes *et al.*, 2007). Mutations in *RDS* also lead to RP, thus indicating that mutations in ubiquitously expressed splicing factors can result in alterations of retinal-specific gene expression (Mordes *et al.*, 2007).

1.3.4.3 Visual cycle and phototransduction

The visual cycle involves the recycling of all-*trans*-retinal back to 11-*cis*-retinal after photoactivation, which occurs in the RPE. Dysfunction of this process can result in RP. *RPE65*, for example, is involved in the isomerisation of all-*trans*-retinol to 11-*cis*-retinol and mutations in this gene can result in arRP and LCA (Morimura *et al.*, 1999, Gu *et al.*, 1997). Furthermore, another protein involved in the visual cycle has been shown to the causative gene for Stargardt retinal dystrophy, RP and CRD: ATP binding cassette transporter rods (*ABCA4*) (Allikmets *et al.*, 1997) (Section 1.3.2), has been shown to transport retinoids across the outer segments of the rods (Azarian

et al., 1997, Cremers *et al.*, 1998) and mutations in ABCA4 result in accumulation of lipofuscin in the RPE, indicating defects in the transport between the RPE and rod outer segments leading to retinal dysfunction (Sun and Nathans, 1997).

Phototransduction is a vital process for normal vision (section 1.2.4) and as such proteins involved in this process have been shown to be causative for RP. For example, mutation of the rod opsin which, combined with the chromophore 11-*cis* retinal, forms the visual pigment rhodopsin, can result in RP or CSNB (Dryja *et al.*, 1990). Rhodopsin is involved in the initiation of the phototransduction cascade when a photon of light strikes rhodopsin and causes the isomerisation of the chromophore (section 1.2.4). Mutations in rod opsin have been characterised according to the affect the mutation imparts, for example mutations have been shown to prevent the correct localisation of rhodopsin, to cause the proteins to misfold and be retained in the ER, to be constitutively active or to have an increased activation rate for transducin (Mendes *et al.*, 2005) (section 1.2.4). All of these defects in the normal function of rhodopsin lead to abnormal phototransduction and eventually RP.

Rod phosphodiesterase is a heterotrimeric enzyme responsible for the hydrolysis of cGMP in early phototransduction which leads to a decrease in cGMP and closure of the cGMP-gated channels in the photoreceptor plasma membrane (section 1.2.4). Mutations in both the alpha and beta subunits of rod phosphodiesterase have been shown to be responsible for RP (Bayes *et al.*, 1995, Bowes *et al.*, 1992, Huang *et al.*, 1995). Furthermore mutations in the gene encoding the cGMP channel also result in autosomal recessive RP (Bareil *et al.*, 2001). The exact mechanisms by which defective phototransduction leads to rod cell death and RP remains to be fully elucidated.

1.3.4.4 Photoreceptor structure and cilia

Photoreceptor structure is crucial for the detection and correct processing of light. Mutations in *RDS* which has been shown to be important for OS disc morphogenesis result in ADRP (Arikawa *et al.*, 1992). Proteins localised to the connecting cilia have been shown to cause retinal disease (e.g. RPGR and RP1) (Hong *et al.*, 2003, Liu *et al.*, 2002), as have proteins that disrupt the IFT system of the cilia (e.g. IFT88) (Pazour *et al.*, 2002). Therefore transport through the connecting cilium is absolutely required for normal retinal function and perturbation of this function can lead to disease (Sections 1.2.3.1, 1.3.3.1, 1.3.5.1).

1.3.4.5 Other retinal disease pathways

Mutations in mitochondrial genes have also been shown to result in retinal disease. Kearns-Sayre syndrome which is caused by deletions in mtDNA, can include RP and progressive hearing loss among its symptoms (Kogelnik *et al.*, 1996). Although unraveling how mitochondrial mutations result in retinal disease is inherently complex, it has been suggested that the high energy requirements of the ganglion cells may be important to pathogenesis. In Leber's hereditary optic neuropathy (LHON), caused by mutations in *MTATP6*, there is notable ganglion cell death, implying these neurons are significantly affected (Careli *et al.*, 2004). Optic atrophy, which is characterized by ganglion cell degeneration and eventual optic nerve atrophy, has also been reported to be caused by mutations in *OPA1*, a gene important for mitochondrial function (Alexander *et al.*, 2000, Delletre *et al.*, 2000). Interestingly, despite the specificity of the degeneration in optic atrophy, OPA1 was found to be expressed in the inner and outer plexiform layers and the inner nuclear layer as well as the ganglion cell layer (Aijaz *et al.*, 2004). A mouse model of autosomal dominant optic atrophy (ADOA) with a mutation in OPA1 was observed to have mitochondrial dysfunction and visual defects, indicating that the neural atrophy in ADOP may be due to abnormal mitochondrial function (Davies *et al.*, 2007).

Retinal development is also a key pathway that may be disrupted and lead to retinal dystrophy, for example mutations in the *CRB1* gene cause retinal disease (den Hollander *et al.*, 1999, den Hollander *et al.*, 2001). A study of a mouse model with a mutation in the *Crb1* gene exhibits shortened inner and outer segments of the photoreceptors as early as two weeks after birth leading the authors to suggest that there is a defect in photoreceptor development and differentiation, rather than degeneration (Mehalow *et al.*, 2003).

1.3.5 X-linked retinits pigmentosa

X-linked retinitis pigmentosa (XLRP) is regarded as the most severe form of RP with early onset and rapid disease progression resulting in clinical blindness by the fourth decade of life (Bird, 1975). Female carriers tend to exhibit a milder phenotype than hemizygous males which is due to random X-inactivation. XLRP is estimated to account for 6-17% of familial RP cases (Vervoort and Wright, 2002). There are currently six mapped loci on the X chromosome for RP (see Table 1.2). For four of these loci the causative gene is not known. The causative gene for the *RP3* locus has been shown to be *Retinitis pigmentosa GTPase regulator* (*RPGR*) (Meindl *et al.*,

1996, Roepman *et al.*, 1996) and for the *RP2* locus the disease gene has been named *RP2* (Schwahn *et al.*, 1998).

Genetic Locus	Symbol	Causative Gene	Reference
Xq26-q27	RP24	?	Gieser *et al.*, 1998
Xp11.4	RP3	*RPGR*	Musarella *et al.*, 1988
Xp21.3-p21.2	RP6	?	Ott *et al.*, 1990
Xp22	RP23	?	Hardcastle *et al.*, 2000
Xp11.23	RP2	*RP2*	Bhattacharya *et al.*, 1984
Xq28-qter	RP34	?	Melamud *et al.*, 2006

Table 1.2 The six known XLRP loci

1.3.5.1 Retinitis pigmentosa GTPase regulator (RPGR)

RPGR is a large gene which spans approximately 60 kb of genomic DNA. Originally *RPGR* was described as having 19 exons (Meindl *et al.*, 1996, Roepman *et al.*, 1996). However studies of potential alternative splicing of *RPGR* revealed the presence of an alternative 3' terminal exon, named ORF15, in which many RP-causing mutations were located (Vervoort *et al.*, 2000). ORF15 has been described as a mutational hotspot: in one study of 47 families 60% of XLRP cases were due to mutations found in ORF15 of *RPGR* (Vervoort *et* al., 2000; Breuer *et al.*, 2002). Expression studies showed that *RPGR* is ubiquitously expressed (Meindl *et al.*, 1997) but a study by Vervoort *et al* showed that the *RPGR* transcript containing the alternatively spliced ORF15 exon was only detected in testis and retina. Therefore it is possible that ORF15-containing transcripts have a retina-specific role (Vervoort *et al.*, 2000).

The RPGR protein contains a domain conserved with another protein; an RCC1-like domain. RCC1 is a guanine exchange factor (GEF) for the small GTP-binding protein RAN which has led to the speculation that RPGR may also act as a GEF for a GTPase. Many of the mutations in *RPGR*, excluding those found in ORF15, are found in this domain. Meindl *et al* showed that many of the residues affected by RP-causing missense mutations were conserved residues in the RCC1-like domain (Meindl *et al.*, 1996).

RPGR has been localised to the connecting cilia in rods and cones in retina (Hong *et al.*, 2003). The RCC1-like domain of RPGR was shown to interact with a novel

protein, RPGRIP1, using yeast two-hybrid (Boylan *et al.*, 2000, Roepman *et al.*, 2000). Interestingly *RPGRIP1* is photoreceptor-specific and has been shown to be a causative gene for LCA and CRD (Gerber *et al.*, 2001, Hameed *et al.*, 2003), (section 1.3.1), implying that this interaction is important for normal retinal function as both proteins are implicated in retinal disease. RPGR has been shown to localise to the ciliary axoneme in photoreceptors where it co-localised with RPGRIP1, furthermore this localisation pattern was lost in the *Rpgrip1* knock-out mouse, implying the interaction is important for the localisation of RPGR (Pawlyck *et al.*, 2005). Recently a homolog of RPGRIP1 has been identified; RPGRIP1L (Arts *et al.*, 2007). RPGRIP1L was found to be ubiquitously expressed and has been localised to basal bodies (Arts *et al.*, 2007). The gene has also been reported to be causative for Joubert syndrome, a syndrome consistent with defects in cilia (Arts *et al.*, 2007, Delous *et al.*, 2007, section 1.3.3.1). In retina the protein was found to localise to the connecting cilium, further strengthening the proposed role for the protein in cilia (Arts *et al.*, 2007).

Another of RPGR's interacting proteins, PDE δ, which also interacts through the RCC1-like domain of RPGR, is ubiquitously expressed (Linari *et al.*, 1999). Mutations in *RPGR* have also been shown to result in CORD, (described in 1.3.2), atrophic macular atrophy and syndromal retinal dystrophies with ciliary dyskinesia, sensorineural hearing loss, and respiratory problems thus implying a wider role for RPGR outside the retina, and a role in cilia function (Zito *et* al., 2003, Iannaccone *et al.*, 2004, Shu *et al.*, 2007). The putative retina-specific ORF15 isoform of RPGR has also been shown to interact with Nucleophosmin 1 (NPM), a nuclear chaperone thought to have a role in centrosome duplication (Shu *et al.*, 2005). Shu *et al* (2005) also report that RPGR and RPGRIP1 co-localise at basal bodies in ciliated cells and that RPGR and NPM co-localise at metaphase centrosomes (Shu *et al.*, 2005). The mechanism by which mutations in *RPGR* result in retinal disease remains unclear but the implication is that RPGR is involved in an important cilia-related pathway.

1.4 RP2

The only other identified gene in which mutations result in XLRP is *RP2*. *RP2* maps to Xp11.3 and was cloned by Schwahn and colleagues (Schwahn *et al.*, 1998). Phenotypically, mutations in *RPGR* and *RP2* are indistinguishable.

1.4.1 RP2 gene

RP2 is a ubiquitously expressed 5 exon gene which codes for a 350 amino acid protein, RP2 (Schwahn *et al.*, 1998, Chapple *et al.*, 2000). Mutations in *RP2* account for between 7-20% of XLRP cases (Hardcastle *et al.*, 1999, Sharon *et al.*, 2003; Vorster *et al.*, 2004). Mutations in RP2 have also been shown to be a cause of macular and peripapillary atrophy, thus expanding the clinical phenotype to central retina, as opposed to peripheral retina, disease (Dandekar *et al.*, 2004).

There are currently 53 reported mutations in *RP2* leading to RP (Table 1.3). The majority of RP2 mutations are predicted to result in premature truncation of the protein (67%), missense mutations account for 22% of the reported mutations in *RP2* while the other 11% are splice-site mutations. The majority of the missense mutations cluster in the N-terminus of the protein but there are 2 missense mutations in the C-terminal half of the protein (R211H and L253R). The mutated residues are likely, therefore, to be key to either the structure or function of the RP2 protein.

The most common mutation is the Arg120Stop mutation, resulting in no detectable protein (Grayson *et al.*, 2002b) (Table 1.3). It has been proposed by Vorster *et al* that this residue acts as a mutational hotspot since the mutation is found in several families with different ethnicities. Vorster and colleagues also present evidence of the mutation occurring as a *de novo* mutation, in this instance as a germ line mutation in the obligate carrier mother (Vorster *et al.*, 2004). Patient mutations also imply that the R118 residue is significant to the function of RP2. This residue has been mutated to histidine, cysteine, or leucine in different XLRP families, and while the R118H mutation is the most common variant, the high incidence of missense mutations at position 118 supports its significance to the normal function of RP2 (see Table 1.3). Furthermore the pathogenic E138G mutation has been analysed by Kuhnel *et al* and was found to disrupt the formation of a salt bridge in the protein which is required for the correct placement of the R118 residue, implying that the R118 residue must be specifically located to be catalytically active (Kuhnel *et al.*, 2006). There is currently no evidence of genotype-phenotype correlation for *RP2* mutations, suggesting that missense mutations either result in no functional protein due to misfolding, or alter the function or localisation of the protein to the equivalence of a null mutation. The mutation spectrum of *RP2* suggests that the development of RP results from a total loss of RP2 protein.

A

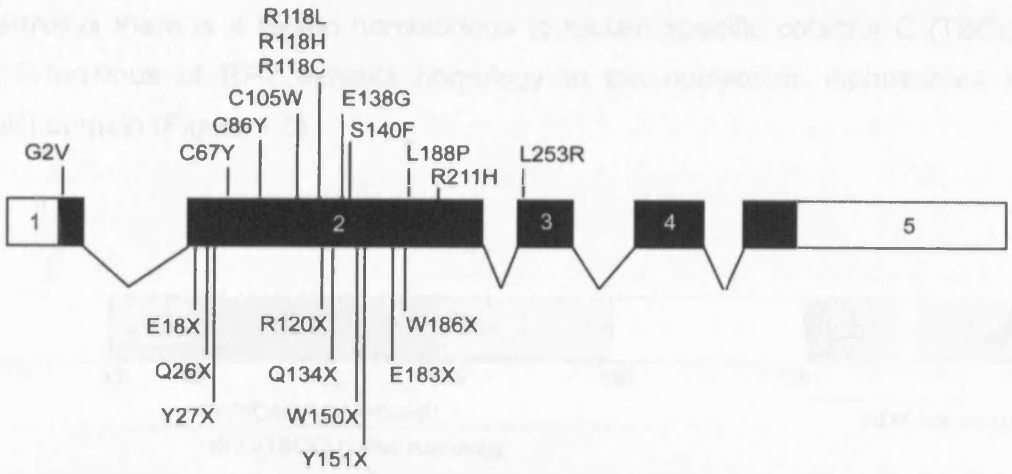

B

INTRON/ EXON	POSITION	CHANGE	CONSEQUENCE	REFERENCE
ALL		Gene deletion		Pelletier *et al.* 2007
Exon 1		delete all	Truncated protein	Bader *et al.* 2003
Exon 1	16-18	Delete 3 bp	ΔS6	Schwahn *et al.* 1998; Rosenberg *et al.* 1999;
Exon 1	77/78	Insertion CA	Q26fsX19	Mears *et al.* 1999
Intron 1		IVS1+3A>T	Splice site mutation	Sharon *et al.* 2000
Intron 1		IVS1+3A>G	Splice site mutation	Breuer *et al* .2002
Intron 1		LINE 1 retrotransposition	Not known	Schwahn *et al.* 1998
Intron 1		IVS1-2A>G	Splice site mutation	Vigo *et al.* ARVO 2000; Miano *et al.* 2001
Exon 2	292	Insert A	Gly98fsX123	Pelletier *et al.* 2007
Exon 2	297	Insert 5 bp	Ser99fsX114	Pelletier *et al.* 2007
Exon 2	301	Delete T	F101fsX11	Pelletier *et al.* 2007
Exon 2	302 or 299	Insertion T	F101fsX22	Vigo *et al.* ARVO 2000; Miano *et al* 2001; García-Hoyos *et al.* 2006
Exon 2	330-342	del 330-342	C110fsX40	Mears *et al.* 1999
Exon 2	350-351	350-351del	F117fsX38	Breuer *et al.* 2002
Exon 2	409	Del 3 bp (ATT)	ΔI137	Sharon *et al.* 2000; Breuer *et al* 2002
Exon 2	419-426	Del 8 bp	S140fsX151	Pelletier *et al.* 2007
Exon 2	453	Delete 1 bp (C)	Y151fsX1	Schwahn *et al.* 1988
Exon 2	483/484	Insertion GGGCTAA	D161fsX13	Mears *et al.* 1999
Exon 2	515	Insert G at 515	S172fsX1	Breuer *et al.* 2002
Exon 2	538-539	Del 2 bp (GT)	V180fsX38	Pelletier *et al.* 2007
Exon 2	670	Insert C at 670	R225fsX9	Breuer *et al* 2002
Exon 2	688-692	Delete 5 bp	Q229fsX2	Hardcastle *et al.* 1999; Sharon *et al.*
Exon 2	723	Delete 1 bp (T) 723delT	F241fsX12	Thiselton *et al.* 2000
Intron 2		IVS2-1G>A	Splice site mutation	Pelletier *et al.* 2007
Exon 3	796-799	Delete 4 bp (CAGA)	V265fsX3	Thiselton *et al.* 2000; Sharon *et al* 2003
Exon 3	801-804	Del 4 bp (AAAG)	T267fsX4	Pelletier *et al.* 2007
Exon 3	834	2bp insertion	Q278fsX15	Mashima *et al.* 2000
Exon 3	853	853/854insG	F284fsX4	DeLuca *et al.* 2001
Exon 4		Delete entire exon		Schwahn *et al.* 1998
Exon 4	925/926	Insertion AG	V308fsX7	Mears *et al.* 1999
Exon 4	929	Insertion 1 bp (T)	E309fsX18	Hardcastle *et al.* 1999
Intron 4		IVS4+3A→C	Splice site mutation	Sharon *et al.* 2003
Intron 4		IVS4+3A→G	Splice site mutation	Sharon *et al.* 2003

Table 1.3 All reported mutations in the *RP2* gene

A Schematic of *RP2* showing exon structure and the positions of all known missense (above) and nonsense (below) pathogenic mutations. Shaded areas indicate coding sequence **B** Table showing all reported insertion, deletion and frameshift mutations in *RP2*.

1.4.2 RP2 sequence homology

RP2 protein has sequence similarity to two defined domains of other proteins. At the N-terminus there is a region homologous to tubulin specific cofactor C (TBCC) and the C-terminus of RP2 exhibits homology to the nucleoside diphosphate kinase (NDK) domain (Figure 1.5).

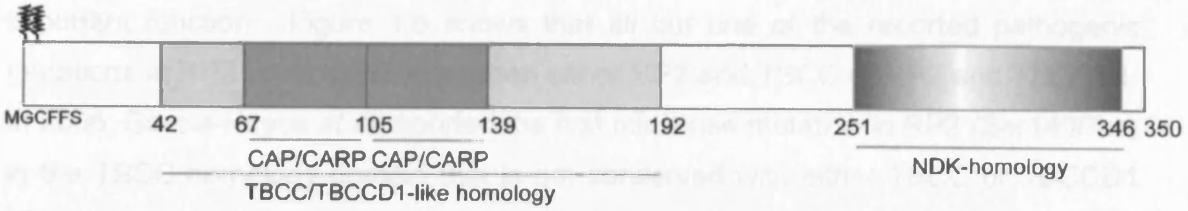

Figure 1.5 Schematic representation of the RP2 protein

Schematic diagram of RP2 showing the TBCC homology domain (42-192) and the C-terminal NDK homology domain (251-346). The N-terminal acylation motif (MGCFFS) is shown by the two tags representing the myristoylation and palmitoylation that RP2 undergoes which results in its plasma membrane localisation.

1.4.2.1 The TBCC/TBCCD1 homology domain

TBCC is involved in the folding of native tubulin and will be discussed further in section 1.5. The TBCC homology domain in RP2 stretches over 151 amino acids, from position 42-192 (Figure 1.5). This region shows 30.4% identity with TBCC and 43.7% similarity (Schwahn *et al.*, 1998). The TBCC-RP2 homology covers a region which includes homology to the C-terminal domain of cyclase associated protein (C-CAP). Cyclase associated proteins (CAPs) are involved in binding to actin monomers and regulating the remodelling of actin in response to extracellular and/or intracellular signalling and are conserved among eukayotes (Stevenson and Theurkauf, 2000). Within the C-CAP region lie 2 CARP domains, the CARP domains are the actin binding domains of C-CAP. The CARP domain is found as a tandem repeat in the C-terminal of many CAPs (Ponting *et al.*, 2001). The presence of two CARP domains in tandem suggests there may be an ability for TBCC, and RP2, to bind to actin. There is currently no experimental evidence to suggest whether the CAP/CARP domains are functional in TBCC or RP2.

A novel protein with homology to both RP2 and TBCC has been identified (personal communication, Alison Hardcastle, Celene Grayson thesis), named TBCC domain containing 1 (TBCCD1) (Accession No. AK001422.). The region of homology between the 3 proteins extends over the same residues as the RP2 TBCC-homology domain (RP2:42-192; TBCC:186-339 and TBCCD1:312-464) (shown in Figure 1.6). Many of the reported pathogenic missense mutations in *RP2* are found in the TBCC/TBCCD1 homology domain (Table 1.3), implicating the domain has an important function. Figure 1.6 shows that all but one of the reported pathogenic mutations in RP2 is conserved between either RP2 and TBCC or RP2 and TBCCD1. In 2006, García-Hoyos *et al* reported the first missense mutation in RP2 (Ser140Phe) in the TBCC homology domain that is not conserved with either TBCC or TBCCD1 (García-Hoyos *et al.*, 2006). The serine 140 residue makes up part of the "Ser/Cys" stack in the predicted RP2 structure which stabilizes the β-helix (Dodatko *et al.*, 2004, section 1.3.4), and as such a non-conservative change at this residue is likely to destabilize the protein and this is likely to be the reason for disease (see section 1.4.4).

1.4.2.2 The NDK homology domain

RP2 also has a region of homology to nucleoside diphosphate kinase (NDK) at the C-terminus of the protein. The domain spans 95 amino acids (from aa251 to aa346) and exhibits 21% identity and 43% similarity to *E.coli* NDK (Figure 1.5). Nucleoside diphosphate kinases are enzymes involved in synthesis of nucleoside triphosphates (NTP), but not ATP. They provide NTPs (including GTP) for numerous processes within the cell, for example, signal transduction and microtubule polymerisation (Nickerson and Wells, 1984, Patel-King *et al.*, 2004). There is evidence that NDK proteins may also be involved directly in DNA processing (Postel *et al.*, 2003), although this has been disputed (Bennett *et al.*, 2004). Alignment of RP2 with *E.coli* NDK indicates that the conserved catalytic histidine residue (at position 117 in *E.coli*) required for NDK function is not present in the RP2 NDK-homology domain, and is instead replaced with a phenylalanine residue. RP2 is also lacking the complete substrate-binding domains for NDK activity found in *E.coli* NDK, suggesting that it may not exhibit NDK function (Yoon *et al.*, 2006). Whether this domain exhibits any residual NDK activity or any other function associated with NDK proteins has been investigated recently and will be discussed in Chapter 5.

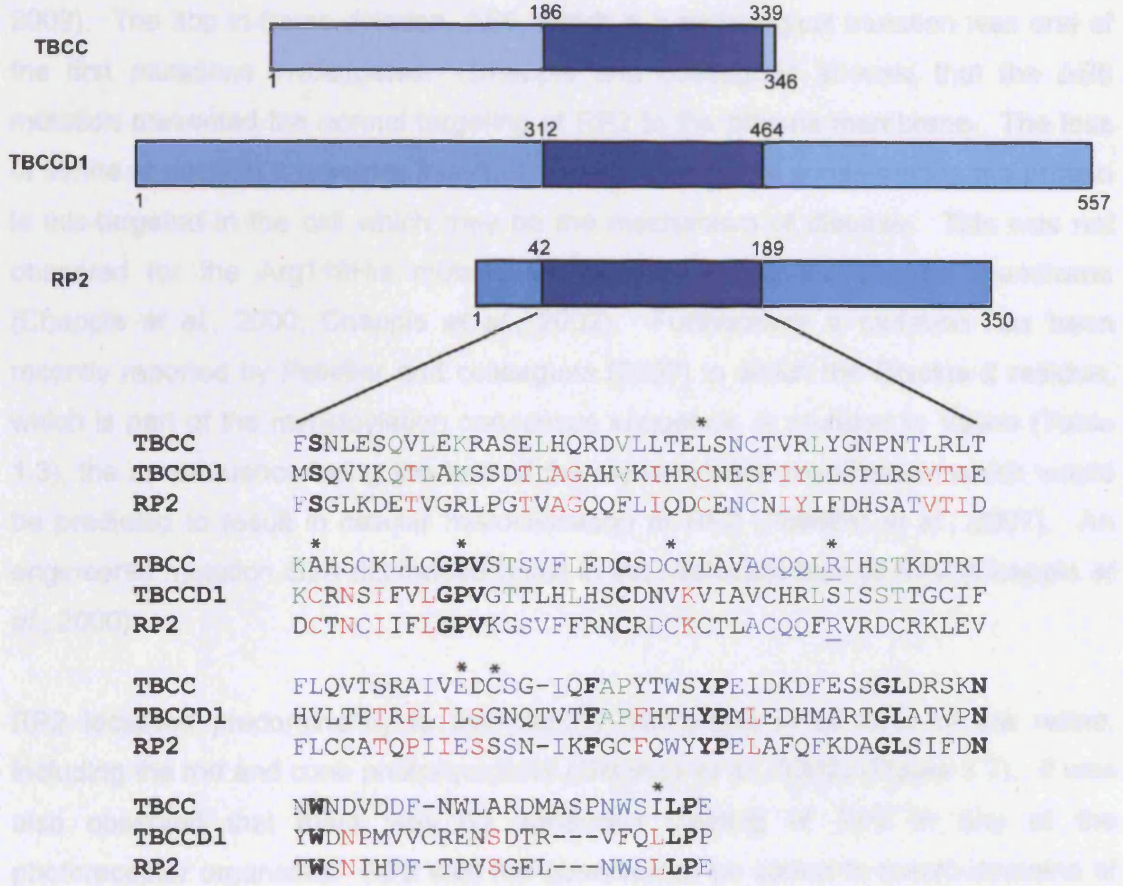

Figure 1.6 Alignment of RP2, TBCC and TBCCD1

Schematic diagram showing the region of homology shared by RP2, TBCC and TBCCD1 and the amino acid sequence of the homology domain. Residues marked in blue are those conserved between RP2 and TBCC, red are conserved between RP2 and TBCCD1 and green are conserved between TBCC and TBCCD1. Residues marked in bold are conserved between all three proteins. The R118 residue in RP2 is underlined. Asterisks denote residues that are mutated in RP2 in families with RP.

1.4.3 Cellular localisation of RP2

RP2 has a signature motif for dual acylation at its N-terminus. This motif of Met-Gly-Cys-X-X-Ser facilitates myristoylation at G2 and subsequently facilitates palmitoylation at C3. As a consequence the RP2 protein is targeted predominantly to the plasma membrane in all cell lines tested (Chapple *et al.*, 2000, Chapple *et al.*, 2002). The 3bp in-frame deletion, ΔS6, which is a pathological mutation was one of the first mutations investigated. Chapple and colleagues showed that the ΔS6 mutation prevented the normal targeting of RP2 to the plasma membrane. The loss of serine at position 6 prevents this dual acylation, and as a consequence the protein is mis-targeted in the cell which may be the mechanism of disease. This was not observed for the Arg118His mutant, which localised to the plasma membrane (Chapple *et al.*, 2000; Chapple *et al.*, 2002). Furthermore a mutation has been recently reported by Pelletier and colleagues (2007) in which the Glycine 2 residue, which is part of the myristoylation consensus sequence, is mutated to Valine (Table 1.3), the consequence being the loss of the myristoylation modification which would be predicted to result in cellular mislocalisation of RP2 (Pelletier *et al.*, 2007). An engineered mutation G2A did indeed result in the mislocalisation of RP2 (Chapple *et al.*, 2000).

RP2 localised predominantly to the plasma membrane in all cells of the retina, including the rod and cone photoreceptors (Grayson *et al.*, 2002) (Figure 1.7). It was also observed that there was no enhanced staining of RP2 in any of the photoreceptor organelles. RP2 was not observed to be sorted to macro-domains of the membrane (Grayson *et al.*, 2002) but extended from the tips of the outer segments through to the outer plexiform layer (OPL) (Grayson *et al.*, 2002) (Figure 1.7). RP2 appeared to localise to the cytoplasmic face of the plasma membrane as expected from previous staining of all cultured cells tested (Grayson *et al.*, 2002, Chapple *et al.*, 2000, Schwahn *et al.*, 2001).

1.4.4 RP2 protein structure

Dodatko *et al* (2004) reported a predicted structure for the N-terminal domain of RP2 based on the structural similarity of this region of RP2 with the C-terminal domain of cyclase associated protein (C-CAP) (see section 1.4.3.1) (Dodatko *et al.*, 2004, Evans *et al.*, 2006). The structure was predicted to be a β-helix, from this structure it can be speculated as to what effects some of the pathogenic *RP2* mutations may have on the protein. For example the Cys67Tyr and Cys86Tyr mutations would both

Figure 1.7 Localisation of RP2 in human retina

Immunohistochemical analysis of the localisation of RP2 in peripheral human retina. NFL, nerve fibre layer; GCL, ganglion cell layer; IPL, inner plexiform layer; INL, inner nuclear layer; OPL, outer plexiform layer; ONL, outer nuclear layer; IS, inner segments; OS, outer segments. Arrowheads are used to highlight plasma membrane staining for RP2. RP2 is seen in cells throughout the retina. Scale bar is 10 μm. From Grayson *et al.*, 2002.

appear to destabilise the protein as the Cys residues form part of the 'backbone' of the helix and the non-conservative change from Cys to Tyr would almost certainly cause destabilisation of the protein (Dodatko *et al.*, 2004). The crystal structure of RP2 has been solved recently and will be discussed further in section 4.7 (Kuhnel *et al.*, 2006).

1.5 Tubulin and the cytoskeleton

1.5.1 The cytoskeleton

Microtubules comprise an important part of the cytoskeleton of the cell which acts as a scaffold for the cell, maintaining shape and assisting in cellular movement and providing a network for internal vesicular trafficking. The main components of the cytoskeleton include microfilaments comprising actin, intermediate filaments comprising, for example, lamin and vimentin, and microtubules comprising tubulin.

Microtubules are polar and consist of tubulin heterodimers, made up of two subunits, α and β. Microtubules are believed to exist in either a slowly growing or a rapidly shrinking state. This is controlled by the hydrolysis and binding of GTP by the β-subunit (Kirschner and Mitchison, 1986) such that when the β-subunit is bound to GTP the tubulin dimers assemble into microtubules and when the β-subunit hydrolyses the bound GTP the microtubules disassemble. The microtubule organising centre (MTOC) is where the microtubules are nucleated and a third form of tubulin is found here, γ-tubulin, which is involved in the initial assembly of the tubulin heterodimers into microtubules (Moritz *et al.*, 1995).

1.5.2 Tubulin folding model

As described in section 1.4.3.1 RP2 contains a homology domain to TBCC. TBCC is one of five cofactors implicated in the tubulin folding pathway. TBCC has been proposed to facilitate the release of the native α/β heterodimer by inducing the formation of a complex containing α tubulin, β tubulin, Cofactor E and Cofactor D (Tian *et al*, 1996). The specific role for each of the cofactors in this pathway are not fully understood but a model for the process has been proposed by Bhamidipati *et al* (2000) (Figure 1.8).

Figure 1.8 shows the proposed pathway which leads to the generation of correctly folded tubulin forming the microtubules. Unfolded α- and β-tubulin are brought to the cytosolic chaperonin (CCT) by prefoldin (PFDN), which interacts directly with CCT to allow the transfer of the polypetides (Vainberg *et al.* 1998). The model proposed by Bhamidipati *et al* suggests that CCT then assists in the folding of tubulin monomers (Martin, 2000), and releases them to allow completion of their folding, aided by the tubulin cofactors. Tubulin specific cofactor A (TBCA) then binds to the β-tubulin monomer and tubulin specific cofactor B binds to the α-tubulin monomer. These intermediate complexes of A-β and B-α then transfer the tubulin subunits to cofactors D (TBCD) and E (TBCE) respectively, at which point cofactor C (TBCC) binds to form a complex of TBCC, TBCD and TBCE with α- and β-tubulin. This tubulin-cofactor complex exhibits tubulin-GAP activity, the hydrolysis of GTP to GDP acts as a switch mechanism for the release of the native tubulin heterodimer which can now polymerise into microtubules when the β-subunit binds GTP (see Figure 1.8) (Bhamidipati *et al.*, 2000).

RP2 was shown to be able to stimulate the GAP activity of β-tubulin in combination with TBCD, substituting for TBCC in this function (Bartolini *et al.*, 2002). However, RP2 was not able to substitute for TBCC in the heterodimer assembly pathway (Bartolini *et al.*, 2002). It is thought that GTPase activators have a relatively conserved active site which includes an arginine finger (Scheffzek *et al.*, 1998). It has been proposed that the Arg118 residue of RP2 and the Arg262 in TBCC may form a crucial part of this arginine finger, since they are the only conserved arginine residues between RP2 and TBCC (Figure 1.6). When these arginine residues in RP2 and TBCC were mutated by Bartolini and colleagues, the tubulin-GAP activity of both TBCC and RP2 was abolished (Bartolini *et al.*, 2002). This suggests the loss or mutation of the arginine residue at position 118 causes the RP2 protein to lose a crucial function which results in the development of retinitis pigmentosa (see Table 1.3). There is an Arginine residue in TBCCD1 (at position 386) (Figure 1.6) close to the conserved residue between RP2 and TBCC which may also be the catalytic residue for an arginine finger in TBCCD1.

1.5.2.1 Regulation of tubulin folding

There are some additional mechanisms of regulation throughout various aspects of the tubulin folding pathway. Gigaxonin is mutated in human giant axonal neuropathy (GAN), a neurodegenerative disorder with an autosomal recessive mode of

Figure 1.8 A model for tubulin folding

Schematic showing the proposed mechanism by which nascent tubulin is folded and incorporated to form microtubules. The cytosolic chaperonin (CCT) receives the unfolded tubulin polypetide chains from prefoldin (PFDN). The involvement of the tubulin cofactors (TBCA-E) and the regulation of TBCD by Arl2 is shown. Adapted from Bhamidipati *et al*, 2000 with additional information from Wang *et al*, 2005 and Vainberg *et al*, 1998.

inheritance (Bomont *et al.*, 2000). One of the characteristics of the disease is cytoskeletal abnormalities including reduced microtubule levels, suggesting gigaxonin has a role in normal cytoskeletal function (Yang *et al.*, 2007). Gigaxonin has also been shown to interact with TBCB (see Figure 1.8) and to target it for degradation via the ubiquitin-proteasome pathway (Wang *et al.*, 2005). The levels of TBCB were examined in gigaxonin knock out mice and found to be elevated compared to wild type animals, implying that the loss of gigaxonin directly results in accumulation of TBCB. Consequently, when TBCB was over-expressed in COS7 cells the authors noted a reduction in microtubules, thus confirming that the loss of microtubules in gigaxonin null mice can be explained by the lack of degradation of TBCB (Wang *et al.*, 2005). Overexpression of TBCD has also been shown to have a destabilising effect on microtubules implying the regulation of the levels of the tubulin cofactors is crucial to the maintentance of the cytoskeleton (Bhamidipati *et al.*, 2000, Martin *et al.*, 2000).

A novel protein related to TBCE has been identified by Bartolini and colleagues (2005). This protein, E-like, was shown to be important for microtubule dynamics (Bartolini *et al.*, 2005). Over-expression of E-like resulted in tubulin depolymerisation and degradation of microtubules, while suppression of E-like led to an increase in the amount of stable microtubules (Bartolini *et al.*, 2005). E-like appears to exert a direct effect on the folding of tubulin as when it is over-expressed, the depolymerised tubulin was noted to be misfolded and targeted to the proteosome for degradation. The authors suggest that E-like has a role in the turnover of microtubules (Bartolini *et al.*, 2005). The identification of E-like and the as yet undefined role of TBCCD1 (described in section 1.4.2.1) implies there is an additional level of control involved in the tubulin folding pathway that is still to be elucidated.

ADP-ribosylation factor (Arf)-like 2 (Arl2) has also been shown to be involved in the regulation of the tubulin cofactor TBCD (Bhamidipati *et al.*, 2000). Loss of Arl2 function has been shown to result in a loss of microtubule stability (Hoyt *et al.*, 1990, Radcliffe *et al.*, 2000). Arl2 has been shown by Bhamidipati and colleagues to regulate the binding of TBCD to tubulin and the microtubule destabilisation induced by over-expression of TBCD in HeLa cells can be rescued by co-expression of Arl2 (Bhamidipati *et al.* 2000).

1.6 ADP-ribosylation factor (Arf)-like proteins

The ADP-ribosylation factor (Arf)-like (Arl) family of proteins is part of the Ras superfamily of small GTPase proteins (Fan *et al.*, 2004) (Figure 1.9). As part of the Arf protein family, the mammalian Arls have approximately 40-60% protein sequence identity with Arfs. They have been classed as Arf-like because although they are similar in sequence to Arfs, there are considerable functional differences between the proteins. While Arfs are characterised by their ability to activate cholera toxin-catalysed ADP ribosylation, activate phospholipase D and complement the lethal arf1-/arf2- mutation in *S.cerevisiae*, Arls do not possess these functional characteristics (Tamkun *et al.*, 1991; Amor *et al.*, 2001). Arl1 is the exception with a very weak ability to act as a functional Arf (Hong *et al.*, 1998). The GTP-binding ability of Arl proteins means that they are able to adopt two conformations: an 'active' conformation when GTP-bound, and an 'inactive' conformation when GDP-bound (Burd *et al*, 2004).

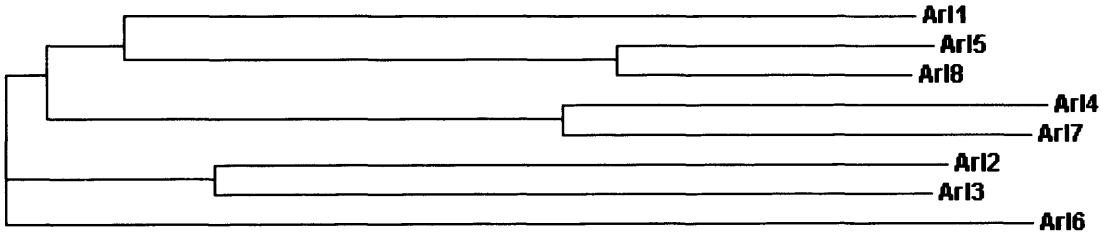

Figure 1.9 Phylogenetic analysis of Arl family members

Phylogentic tree of human Arl family members 1-8 using a ClustalW alignment programme based on human protein sequences. Arl2 and Arl3 are close phylogenetic relatives.

1.6.1 Arl3

Since Arl2 was shown to be an important regulator of tubulin biogenesis (Figure 1.7) and RP2 has a region of homology to TBCC (Figure 1.5), a targeted approach was adopted to search for an Arl that interacted with RP2. Arl2, Arl3, and Arl4 were tested for an interaction with RP2. Arl3 was shown to interact with RP2 (Bartolini *et al.*, 2002). The interaction is dependent on Arl3 being in the active GTP-bound state rather than GDP-bound, and appeared to be enhanced if RP2 was not myristoylated (Bartolini *et al.*, 2002).

Arl3 was found to be a microtubule associated protein (MAP) in a study by Grayson *et al* (2002) in which Arl3 was observed to localise to microtubule structures (Grayson *et al.*, 2002). Arl3 was shown to exhibit enhanced microtubule localisation following stabilisation of the microtubule network with taxol and shown to be redistributed to the nuclear membrane when microtubules were depolymerised (Grayson *et al.*, 2002). Arl3 was also co-purified with microtubules from bovine brain, indicating that Arl3 behaves as a MAP (Grayson *et al.* 2002).

The localisation of Arl3 in the retina has also been studied by Grayson *et al* (2002) in which it was found that Arl3 was enriched in the photoreceptor connecting cilium of both rods and cones, which was in contrast to the plasma membrane staining exhibited by RP2 throughout the photoreceptors in the retina (Grayson *et al.*, 2002). Using an RP2 patient-derived lymphoblastoid cell line (the patient had an Arg120Stop mutation) there was no effect on the expression level of Arl3 with the loss of functional RP2 (Grayson *et al.*, 2002). As such the cellular and retinal site of the RP2-Arl3 interaction has yet to be elucidated, as does the functional significance of the interaction.

Further to the reported connecting cilium localisation of Arl3 (Grayson *et al.*, 2002) there is evidence that Arl3 is important to general cilia function. A study in *Leishmania* showed that overexpression of a the GTP-bound form of *Ld*Arl3A in *Leishmania* led to shortened flagella implying *Ld*Arl3A is required for the normal development of this ciliated structure (Cuvillier *et al.*, 2000). Although *Ld*Arl3A appears to be a homolog of Arl3 the study showed that *Ld*Arl3A was myristoylated, and that when a mutant in which myristoylation is prevented (G2A) is overexpressed the resultant viability defect in the cells, and cytoplasmic staining pattern, was the same as seen with the inactive GDP-bound mutant (Cuvillier *et al.*, 2000). There is currently no evidence that human Arl3 is myristoylated or is able to localize to the membrane of any cellular organelle, and as such it is possible that *Ld*Arl3A is not functionally comparable to human Arl3. A recent report of an Arl3 knockout mouse further implicates Arl3 in normal cilia function, and this will be discussed in Chapter 4 (Schrick *et al.*, 2006). Furthermore, Arl3 was detected in the photoreceptor sensory cilium complex proteomic screen performed by Liu and colleagues (Liu *et al.*, 2007).

1.6.2 Arl2

Arl2 is the closest phylogenetic relative of Arl3 (Figure 1.9). The *S.cerevisiae* homolog of Arl2, CIN4, is essential for microtubule stability. The fission yeast homolog of CIN4, Alp41, when knocked out results in microtubule instability and polarity-based growth defects. Radcliffe and colleagues used genetic studies to show that in fission yeast Alp41 acts upstream of the TBCD homolog in the "cofactor-dependent pathway" (Radcliffe *et al.*, 2000) (Figure 1.7). Another report supports the importance of Arl2 in the cytoskeleton using the *C.elegans* Arl2 homolog, *evl-20*. Antoshechkin and Han (2002) show that the disruption of *evl-20* causes vulval malformation due to alteration of the normal developmental cell lineage as well as male gonadal defects and other effects. All of these visible defects can be attributed to cytoskeletal defects, specifically the microtubules. Antoshechkin and colleagues suggest *evl-20* has a role in the control of the cytoskeleton throughout development (Antoshechkin and Han, 2002).

1.6.3 Arl3 and Arl2 interacting partners

Arl3 has been shown to bind to the GRIP domain of Golgin-245, Arl1 has also been shown to bind to the same protein, through the same domain (van Valkenburgh *et al.*, 2001). The GRIP domain is a targeting sequence which is recruited to specific structures of the *trans*-Golgi network (TGN). Arl1 is known to be involved in mediating this targeting in a mainly hydrophobic manner. It has been shown that if this hydrophobic interaction is disrupted the correct targeting of Golgin-245 is abolished (van Valkenburgh *et al.*, 2001; Wu *et al.*, 2003). The functional importance and physiological relevance of the interaction between Arl3 and the GRIP domain is not clear. It should also be noted that in the interaction studies by van Valkenburgh and colleagues, dominant active mutants of the Arls were used for their screening (Q71L), these exhibit a GTP-bound conformation and remain constitutively active.

Arl3 has been shown to interact with the ubiquitously expressed proteins PDE δ (the δ subunit of rod-specific cGMP phosphodiesterase), and BART1 (ARL2BP) (Linari *et al.*, 1999, Sharer *et al.*, 1999, van Valkenburgh *et al.*, 2001, Hanzal-Bayer *et al.*, 2002). Arl2 has also been shown to bind to PDE δ and BART1 (Sharer *et al.*, 1999, Hanzal-Bayer *et al.*, 2002). Both Arl2 and Arl3 only bind PDE δ in their GTP-bound states (Linari *et al.*, 1999, van Valkenburgh *et al.*, 2001, Hanzal-Bayer *et al.*, 2002). PDE δ actively

increases the affinity that Arl3 has for GTP (van Valkenburgh *et al.*, 2001). Although the function of PDE δ itself is not fully understood, it is believed to act as an effector of Arl2 and it has been suggested it may be a transport mediator (Hanzal-Bayer *et al.*, 2002). It has also been proposed that PDE δ has a more general function as a prenyl-binding protein, since PDE δ interaction with farnesylated rhodopsin kinase (GRK1) was prenylation dependent (Zhang *et al.*, 2004). PDE δ interacts with several other small GTPases which are also prenylated but Arl3 and Arl2 are not prenylated, and neither is the PDE δ binding domain of RPGR (see section 1.3.5.1), so it can be assumed that it is not an absolutely essential requirement for PDE δ interactions (Zhang *et al.*, 2004, Linari *et al.*, 1999).

Arl3 and Arl2 are also known to interact with HRG4 (Unc119). HRG4 is a retina-specific protein and the first known receptor-associated activator of Src family tyrosine kinases (Cen *et al.*, 2003). HRG4 shares significant homology with PDE δ, they are 30% identical and 40% similar in their C-terminal regions, and 23% identical overall (van Valkenburgh *et al.*, 2001). HRG4 has been shown to be important to retinal function. A mutation in HRG4 in a transgenic model resulted in cone-rod dystrophy and a heterozygous premature stop codon was reported in a 57 year old woman with late onset cone-rod dystrophy (Kobayashi *et al.*, 2000). It appears to be particularly important for synaptic function in the retina (Kubota *et al.*, 2002), in transgenic mice there was evidence of vacuolation in the outer plexiform layer (where the ribbon synapses are located) and apoptosis of the neural cells in the inner nuclear layer (Kobayashi *et al.*, 2000). Therefore Arl3 appears to be involved in important retinal-specific pathways, their precise roles and the delineation of the pathways is yet to be elucidated however.

Arl2 and Arl3 are close phylogenetic relatives (see Figure 1.9), and although they have a similar structure and share interacting partners and functional similarities they appear to have some divergent capabilities. A recent study by Zhou *et al* (2006) addressed the different microtubule-associated roles of Arl3 and Arl2 and concluded that although Arl2 and Arl3 both play important roles at the centrosome, they have different functions at this cellular compartment. Arl2 has an established role in tubulin assembly and appears to be involved in the regulation of this process at the centrosome, while Arl3 seems to be involved in the regulation of cytokinesis. The proposed role of Arl3 in cytokinesis was suggested to be most likely due to its microtubule association as it was localised to the

mitotic spindle, midzone and midbodies, all of which are microtubule dense stuctures involved in cell division (Zhou *et al.*, 2006). Interestingly, although Arl3 was detected in a photoreceptor sensory cilium complex proteomic screen, Arl2 was not detected (Liu *et al.*, 2007), suggesting the proteins may have divergent functions in this specialised cytoskeletal component.

1.6.4 Arl6

Arl6 was recently reported to be the causative gene for the BBS3 locus (Fan *et al.*, 2006, Chiang *et al.*, 2006). Arl6, like all the known Arl family members exists in either a GTP-bound or GDP-bound conformation. The GTP-binding function of Arl6 was determined to be important for its wild type function as two independent mutations have been reported at the Thr31 position (T31M and T31R) which result in the protein being unable to bind GTP and thus constitutively inactive (Fan *et al.*, 2002).

1.7 Aims of this study

The main focus of this study was to further advance the understanding of the disease pathogenesis of RP caused by mutations in *RP2* through the investigation of the cellular pathways in which RP2 may be involved. The approach taken was to use a yeast two-hybrid screening strategy to discover novel RP2 interacting partners. As RP2 is ubiquitously expressed and it remains unclear how *RP2* mutations result in a retina-specific disease, a retina cDNA library was screened. Novel interactions detected and characterised could unravel important retina cellular pathways, such as photoreceptor specific or cilia function, and improve our understanding of how RP2 mutations result in retinal degeneration.

It can be hypothesised that due RP2's subcellular localisation, the ability of RP2 to partially substitute the function of TBCC, and the microtubule-associated localisation of its interacting partner Arl3, that RP2 may play a role in integrating vital cellular functions between the plasma membrane and the cytoskeleton. Furthermore, there is evidence that Arl3 and another XLRP protein, RPGR, are involved in cilia biology and therefore RP2 may have a role at the connecting cilia of photoreceptor cells, possibly in IFT or in connecting the cytoskeletal axoneme with the surrounding environment. The

identification of novel interacting partners would clarify the potential roles of RP2 at the cilia and in the broader retinal environment.

CHAPTER 2

MATERIALS AND METHODS

2.1 BASIC MOLECULAR TECHNIQUES

All solutions and media described in this thesis are listed in Appendix 1.

2.1.1 Vectors Used in this Study

•pGem T-Easy (Promega, UK). This vector was used for cloning PCR products and as a shuttle vector for subcloning into the CytoTrap vectors and other expression vectors.

•pSos (Stratagene, UK). This was the bait vector for CytoTrap, used for all RP2 constructs.

•pMyr (Stratagene, UK). The CytoTrap target vector, the cDNA library is cloned into this vector and any directed interactions are achieved by cloning the desired gene into this vector. This gene exhibits inducible expression under the control of a Galactose promoter.

•pCMV-Tag3b (Stratagene, UK). Mammalian expression vector resulting in an expressed protein with an N-terminal myc tag, used for Arl2, Arl3 and Arl3 mutants.

•pcDNA4/TO/VSV (Gift from Prof Karl Matter). A mammalian expression vector which expresses a protein with a VSV tag at the C-terminus of the protein. Used for Arl2, Arl3 and Arl3 mutants.

•pEGFP-N1 (Clontech, UK). RP2 was cloned into this vector to allow expression of a RP2-GFP fusion protein with the GFP at the C-terminus of the protein (Chapple *et al.*, 2000).

•pGEX-2T (Pharmacia, UK). RP2 (from Prof Michael Cheetham), Arl3-T31N and Arl3-Q71L (from Dr Tatyana Novoselova) were cloned into this vector to allow expression of N-terminal GST fusion proteins in bacterial cells.

Plasmid	Insert description	Genotype	Use
pSos	No insert	*LEU2*, Amp^r	Control bait vector
pMyr	No insert	*URA3*, Cam^r	Control prey vector
pMyr-cDNA	Bovine retinal cDNA library	*URA3*, Cam^r	Prey vector
pSos-RP2	Wt human RP2	*LEU2*, Amp^r	RP2 bait vector
pMyrSB	Rit protein, interacts with hSos	*URA3*, Cam^r	Positive control vector
pMyrLaminC	Human Lamin C (aa 67-230)	*URA3*, Cam^r	Negative control vector

Table 2.1 Details of the vectors used for CytoTrap yeast two-hybrid (Stratagene)

2.1.1.1 Construction of the pMyr cDNA Library

The bovine retina cDNA library was purchased from Stratagene, details can be found in section 2.2.3.

2.1.2 Subcloning

All genes and constructs were subcloned into a variety of vectors (section 2.1.1) facilitated by PCR to introduce restriction enzyme sites as required and restriction enzyme digestion. For restriction digestion between 5 and 20 µg of DNA was digested in a total reaction volume of between 20 and 100 µl with 10% (v/v) restriction enzyme(s), using x10 buffer supplied by the manufacturer. The reactions were incubated at 37°C for 2 hours. High volume restriction digests (100 µl) were used when subcloning into the pSos vector.

2.1.3 Precipitation and Purification of DNA

Following high volume restriction digests it was necessary to precipitate and purify the DNA for resuspension in a lower volume. To each aliquot of digested DNA 0.1 x volume of 3M NaOAc (pH 5.5) was added followed by 2.5-3 x volume of absolute ethanol. DNA was precipitated by incubation at -20°C for at least 30 minutes. The reactions were centrifuged at 14,000 xg for 10 minutes to pellet the DNA, and the supernatant was discarded. 0.5 ml 70% ethanol was added, samples were centrifuged for an additional 5 minutes at 14,000 xg, the supernatant was discarded and the pellet was dessicated and then resuspended in 10-15 µl of ddH_2O.

2.1.4 Alkaline Phosphatase Treatment

Digested and purified vector DNA was treated with calf intestinal alkaline phosphatase (CIAP) to dephosphorylate the 5' ends and prevent religation of the vector. 10x CIAP reaction buffer was used with 1 µl CIAP (1u/µl) (Promega) and ddH_2O to a final reaction volume of 50 µl. The reaction was incubated for 30 minutes at 37°C and a

further 1 u CIAP was added for another 30 minutes at 37°C. The reactions were then purified using the Qiagen QIAquick PCR purification kit (Qiagen, UK) to remove the enzyme and were resuspended in 30 µl of ddH_2O.

2.1.5 Agarose Gel Electrophoresis

Agarose gel electrophoresis was used to separate DNA fragments by size. DNA was visualised after staining with ethidium bromide (5µl of 5mg/ml) by viewing the gel with UV light on a transilluminator. Generally 1.0-0.8% agarose (w/v) in tris-acetate (TAE) buffer were used to separate the DNA. Samples were loaded into the wells using 6x loading dye (Promega) to a final concentration of 1x. Sizes were determined by comparison to a known marker (generally 1kb ladder Promega, UK). When necessary DNA was excised from the gel using a clean sharp scalpel and was extracted using QIAquck gel extraction kit (Qiagen) according to the manufacturer's instructions, DNA was resuspended in 30 µl ddH_2O.

2.1.6 Ligation of DNA

Digested and purified insert and vector were ligated at a molar concentration of approximately 3:1 respectively. Usually 100-500 ng of plasmid DNA was used with the corresponding amount of insert DNA. The reaction consisted of 3 units (3u/µl) of T4 DNA ligase (Promega, UK), 5 µl of 2x rapid ligation buffer (Promega, UK), DNA and ddH_2O up to a total volume of 10µl. The reaction was incubated at room temperature (approximately 22°C) for 2 hours, or to obtain the maximum number of transformants, at 4°C overnight.

2.1.7 Bacterial Transformation

Ligation reactions (5 µl aliquots) were used to transform competent *E. coli* cells. For constructs in the pSos vector 100 µl SURE® 2 supercompetent cells (Stratagene, UK) were used per transformation reaction, 2 µl 1.22 M β-mercaptoethanol was also added to each reaction to enhance the transformation efficiency. The DNA, cells and β-mercaptoethanol were incubated on ice for 30 minutes in 15 ml polypropylene tubes (Falcon, Nunc). The cell suspension was then heat shocked at 42°C in a water bath for 50 seconds and incubated on ice for 2 minutes. SOC media (preheated to 42°C) was then added to 1 ml total volume and the samples were incubated at 37°C with shaking for at least 1 hour. The cells were then centrifuged at 1000 xg for 5 minutes and resuspended in 200 µl of SOC media and the total volume was plated onto the appropriate L-agar antibiotic plates, the plates were then incubated at 37°C overnight.

All other transformations were performed using JM109 competent cells (Promega). Aliquots of ligation reactions (5 µl) were added to 50 µl of cells. The samples were incubated on ice for 30 minutes. The cells were then heat shocked in a water bath at 42°C for 45-60 seconds and incubated on ice for a further 2 minutes. SOC media (750 µl) was then added and the cells were incubated at 37°C for 1 hour, with shaking. The cells were centrifuged at 1000 xg for 10 minutes and were resuspended in 150 µl of SOC and plated onto the appropriate L-agar antibiotic plates. Plates were incubated at 37°C overnight until single colonies appeared.

2.1.8 Plasmid Purification (Miniprep)

5 ml of LB+antibiotic (See Table 2.2) was inoculated with a single transformant colony. Cultures were grown for 12-16 hours at 37°C with shaking. Cells from 1.5 ml of culture were centrifuged at 6,000 xg for 5 minutes and DNA was extracted using the GenElute Miniprep kit (Sigma) according to the manufacturer's instructions. DNA was eluted in 60 µl of ddH_2O. Glycerol stocks were made of selected cultures by adding 750 µl of culture to 750 µl of 50% sterile glycerol and freezing at -80°C.

DNA was analysed by restriction enzyme digestion: 2 µl eluted DNA was digested with 5-10% (v/v) appropriate restriction enzmye(s), in 10x buffer and ddH_2O to a total volume of 10 µl for 1-2 hours at 37°C. The samples were then analysed by gel electrophoresis (See Sections 2.1.2 and 2.1.5).

Antibiotic Used	Concentration of Stock	Concentration Used At
Ampicilin	50mg/ml	50µg/ml
Kanamycin	50mg/ml	50 µg/ml
Chloramphenicol	34mg/ml	34µg/ml

Table 2.2 Antibiotics used and their concentrations

2.1.8.1 DNA Quantification

DNA was quantified using a spectrophotometer by measuring absorbance at 260 nm. 5 µl of DNA was diluted in 1 ml dH_2O and absorbance at 260 nm was recorded, absorbance of 1 OD (A) is equivalent to 50 µg/ml dsDNA. The purity of the DNA was checked by reading the sample's absorbance at 280 nm. $A_{[260]}/A_{[280]}$ provides an estimate of purity for DNA, with approximately 1.8 indicating sufficiently pure DNA.

2.1.9 DNA Sequencing

DNA was sequenced using an automated system which employs a cycling strategy of primer annealing and DNA synthesis using a thermostable DNA polymerase. Priming occurs in only one direction for each reaction and fluorescently labelled dideoxynucleoside triphosphates (ddNTPs) are included with the deoxynucleoside triphosphates (dNTPs). The ddNTPs lead to chain termination, as when they are incorporated they prevent further elongation due to the lack of an OH at the 3' position, thus they are unable to form the phosphodiester bond.

AmpliTaq DNA polymerase is a form of DNA polymerase that contains a point mutation in its active site which results in less discrimination against the ddNTPs and a more even peak intensity. The enzyme is used in a pre-made mix (BigDye 3.1 Applied Biosystems) which also contains dye terminators, dNTPs, $MgCl_2$, and buffer (Tris-HCl pH9). Clones were sequenced using ABI BigDye terminator cycle sequencing chemistry version 3.1 on an ABI 3100 automated sequencer (Applied Biosystems).

Cycle sequencing reactions (10 µl) consisted of 1 µl primer (1.6 µM), 1.5 µl ABI buffer, 1 µl BigDye, approximately 0.5 µg DNA and made up to 10 µl total volume with ddH_2O. Samples were subjected to 30 cycles of 96°C for 30 s, 50°C for 30 s, and 60 °C for 4 minutes. The sequencing reactions were then purified to remove unincorporated primers and dNTPs: 26 µl ddH_2O and 64 µl 96% ethanol was added to the 10 µl sequencing reaction, the mixture was vortexed and incubated at room temperature for 10 minutes. Reactions were then centrifuged at 14,000 xg for 20 minutes and the supernatant was carefully removed. 200 µl of 70% ethanol was then added and the samples were centrifuged for an additional 20 minutes to pellet the DNA. The supernatant was removed without disturbing the pellet and the pellet was dried at 65°C for 5 minutes. The sample was then resuspended in 12 µl of formamide, denatured, and loaded onto the ABI 3100 automated sequencer. Sequence analysis was performed using DNAStar software.

2.1.10 Polymerase Chain Reaction

The polymerase chain reaction (PCR) was used to amplify selected regions of DNA using specifically designed oligonucleotide primers. PCR uses *in vitro* enzyme-catalysed DNA synthesis to create multiple copies of a specific region of DNA. The oligonucleotide primers are extended towards one another under appropriate

conditions by a thermostable DNA polymerase in a 3-step reaction: denaturation, primer annealing and extension.

Denaturation is achieved by heating the PCR mix to 95°C for 5 minutes to separate the dsDNA. The DNA is then put through a 3-step reaction between 15-40 times. The first step separates the dsDNA by heating to 95ºC for 30 seconds. The primer annealing step's temperature is dependent upon the melting temperature (Tm) of the primers being used; 2-5°C below the Tm, this usually varies between 50-72ºC and is usually maintained for 30 seconds. The extension step is performed at 72°C as this the optimum temperature for the Taq ploymerase. Generally the extension step runs for 1 minute/kb of DNA to be replicated. PCR was used to amplify SPAG7, Arl3 and Arl6 from IMAGE clones and to construct RP2 fragments. In some cases the reaction was spiked with 0.5 µl proofreading Taq (*Pfu Turbo*, Promega, UK) to reduce the number of PCR-induced errors.

A typical PCR was 5-50 µg miniprep DNA, 2x PCR Master Mix (Abgene, Epsom, UK), 1 µl (2µM) of each primer, sterile water up to 25 µl. The Abgene master mix consisted of 1.25 units Thermoprime Plus DNA polymerase, 75 mM Tris-HCl, 20 mM NH_4, 1.5 mM $MgCl_2$, 0.01% (v/v) Tween®20, 0.2 mM each of dATP. dCTP, dGTP, dTTP.

2.1.10.1 Primer Design

Oligonucleotide primers are designed to specific regions of DNA to allow specific amplification. Several rules were followed: Random base distribution and similar CG content for both primers, an anchoring G or C at the end of each primer, minimal secondary structure and no greater than 4ºC difference in Tm between each primer. A primer length of between 20-25 nucleotides was optimal. Restriction enzyme sites can be designed on the 5' end of the primers if the product is to be cloned to allow digestion required for a specific primer or to assist with directional cloning. All primer sequences can be found in Appendix 1.

2.1.11 TA Cloning into pGem T-Easy

The Taq used in PCR (Abgene, UK) leaves overhanging A bases on the ends of the PCR products. This is used to allow TA cloning into the pGem T-Easy vector which is engineered with T overhangs. The ligation and transformation into this vector was done according to the manufacturer's instructions (Promega, UK) and as described in section 2.1.6 but for 2 hours at room temperature rather than overnight. Ligation

reactions (5 µl aliquots) were used to transform competent *E.coli* as described in section 2.1.7. This method was used as a shuttle vector when a PCR product was to be cloned into another vector (e.g Arl6 being cloned into pMyr).

2.1.12 Site Directed Mutagenesis (SDM)

SDM was used to create missense mutations in RP2, Arl3 and RAN. Four mutations were chosen for RP2, they are all pathogenic mutations found in XLRP families. The Arl3 mutants were chosen according to findings by Bartolini and colleagues (See section 1.5) (Bartolini *et al.*, 2002). RAN mutations were chosen according to Lounsbery *et al* (1996) and Palacios *et al* (1996) (Lounsbery *et al.*, 1996, Palacios *et al.*, 1996).

Stratagene's QuikChange kit was used, the protocol was followed as stated in the manufacturer's instructions (Stratagene, UK). The method employs 12 cycles of PCR (annealing temperature of 55°C and extension temperature of 68ºC for 1 minute/kb of plasmid DNA) to introduce a base change using primers with a designed mutation (see Table 7.2 in Appendix 1). Overlapping primers were designed with the change centrally located. A proofreading Taq (*Pfu Turbo*) was used; the enzyme allows high fidelity replication without displacing the mutant primers. Incorporation of the mutant primers creates a mutant plasmid with staggered nicks. *Dpn*I digestion is then used to select for mutant plasmids by digestion of the parental plasmids. The nicked mutant vector DNA is then transformed into XL1-Blue supercompetent cells as described in section 2.1.7 but with the addition of 2 µl 1.22 M β-Mercaptoethanol. The resulting transformants were prepared and analysed as described in section 2.1.8 and were sequenced in both forward and reverse directions to check for the desired change as described in section 2.1.9.

2.2 YEAST TWO-HYBRID TECHNIQUES (CytoTrap, Stratagene)

2.2.1 Verification of Yeast Strain Phenotype

The yeast strain cdc25-2 phenotype was checked to ensure there was no aberrant growth on inappropriate selective media. The marker phenotype (ura3-*52, his3-200, ade2-101, lys2-801, trp1-901, leu2-3, 112, cdc25-2* Gal+) means that the strain should not grow on plates lacking tryptophan, leucine, histidine and uracil. This strain should also not grow at 37ºC due to a temperature sensitive mutation that affects the Ras signalling cascade (see Chapter 3.2). Yeast cells were streaked out onto SD-glucose plates each lacking one of the 4 amino acids and incubated at 24°C to check for no growth. Yeast cells were also streaked out onto YPAD plates and incubated at 37°C to ensure the phenotype had not reverted to allow growth at this temperature.

2.2.2 Yeast Glycerol Stocks

Glycerol stocks of the verified yeast strains were made. YPAD media (10ml) was inoculated with a single colony from a YPAD plate, grown for a minimal number of generations. The cells were grown until late log phase (OD_{600} = 0.8-1.0) at 24ºC. A sterile solution of 50% glycerol and 50% YPAD broth (4.5ml) was added to the 10ml culture. The glycerol-containing culture was aliquotted into 2ml cryotubes (1ml/tube) and frozen at -80ºC. These preparations can be kept for up to two years. Each week a stock was streaked out onto a fresh YPAD plate and incubated at 24°C.

2.2.3 pMyr Target Library Construction

The target library was constructed in the pMyr vector by Stratagene. The library chosen was a bovine retinal cDNA library. The library was constructed using a hybrid oligo(dT) linker-primer system. The library was amplified using the protocol from Clontech's MATCHMAKER Library User Manual (PT1020-1).

To check there was no bias or skewing of the library, 20 individual colonies were picked before and after amplification (colonies were picked from the titre plates for the 'before' analysis). These were prepared and digested with *Xho*I and *Eco*RI, as described in section 2.1.8 to check for the size of the inserts and then 10 of these were selected for sequencing to ensure the library was representative and did not contain an over-representation of ribosomal RNAs, and that the process of amplification had not biased the library towards the smaller plasmids. The average

insert size prior to amplification was 1.23 kb and after was 1.34 kb indicating there was no skewing of the library.

2.2.4 Yeast Transformation

Once the bait plasmid had been constructed (subcloning of RP2 from pGem T-Easy into pSos) the yeast strain cdc25-2 was transformed with pSos-RP2 to check for expression and transactivation of the bait fusion protein, hSos-RP2. Yeast transformation was performed using a lithium acetate based method.

The protocol was adapted from http://proteome.wayne.edu/transform.html which was itself developed from a protocol described by Gietz et al. (1992). A single colony from an YPAD plate was used to inoculate a 10 ml culture of YPAD. This was grown overnight at 24°C with shaking until the culture was saturated (approximately 12 hours). The culture was then used to inoculate 50 ml of fresh YPAD to an OD_{600} of 0.2. This culture was grown until it reached an OD_{600} of approximately 1.0 (4-5 hours).

Yeast cells were pelleted at 2000 xg for 2 minutes and supernatant was removed quickly and carefully. The yeast were resuspended in 10 ml sterile water and pelleted again under the same conditions, after removing the supernatant the yeast were resuspended in 5 ml LiOAc/TE and pelleted as before. The supernatant was removed and the yeast were resuspended in 250 µl of LiOAc/TE and incubated at room temperature for upto 15 minutes.

For each transformation 55 µl of cdc25-2 yeast were aliquotted into a sterile 1.5 ml eppendorf tube and 1 µg of plasmid DNA was added, with 5 µl of sonicated ssDNA salmon sperm (10 µg/µl Stratagene) and DMSO (Sigma, UK) to a final concentration of 10% (v/v). Finally 300 µl of 40%PEG_{4000} in LiOAc/TE was added to each reaction and mixed by gently pipetting. The cells were incubated for 1.5 hours at 24 °C. The cells were heat shocked in a water bath at 42°C for 10 minutes, the cells were then pelleted at 3000 xg for 2 minutes and the supernatant was removed. Cells were washed and resuspended in 1 ml sterile water and pelleted as before. Supernatant (750 µl) was removed and the cells were resuspended in the remaining 250 µl and plated onto appropriate selective SD/glucose plates by spreading with approximately 10-15 4 mm sterile glass beads. The plates were incubated at 24 °C until colonies appeared, usually after about 3-4 days.

2.2.5 Bait Transactivation

To ensure the bait (pSosRP2) did not cause transactivation of the system single yeast colonies transformed with the bait plasmid were resuspended in 25 µl of sterile water, and 2.5 µl of the cell suspension was then spotted onto an SD/glucose (-L) plate. The same was done for various control transformations using SD/galactose (-UL) plates. These plates were then incubated at 37ºC for 5 days and growth was compared to the positive (pSos and pMyrSB) and negative (pSos and pMyrLaminC) controls.

2.2.6 Verification of Bait Protein Expression

5 ml of SD/glucose (-L) was inoculated with a single pSosRP2 containing yeast colony. The culture was grown at 24 ºC with shaking until saturated, usually 2 days. The yeast cells were pelleted by centrifugation at 1000xg for 5 minutes. The yeast cells were resuspended in 1 ml cold dH_2O. 150 µl freshly made NaOH/β-ME buffer was added to the cell suspension. The cell suspension was vortexed for 30s and placed on ice for 15 minutes. The cells were vortexed again briefly and 150 µl of 55% TCA (v/v) in water was added to the cell suspension. After briefly vortexing the tubes were incubated on ice for a further 10 minutes. The protein extract was then pelleted by centrifugation at 12,000xg for 10 minutes at 4°C. The supernatant was removed and the protein extract resuspended in 300 µl SU buffer (2 µl 1 M Tris-base (pH 10) was added if the suspension turned yellow). Protein concentration was not quantified; 16 µl of SU buffer suspension was added to 4 µl of SDS-PAGE Sample Buffer and heated for 3 minutes at 65°C before loading onto an SDS-PAGE gel (see section 2.2.7). The same protocol was followed for other transformed yeast colonies to act as controls.

2.2.7 SDS-PAGE Analysis and Coomassie Staining

SDS-PAGE is a technique used to separate proteins according only to their molecular weights. This is achieved by coating all the proteins with an overall negative charge using the ionic detergent sodium dodecyl sulphate (SDS) ensuring the proteins have the same ratio of mass:charge and so separating them according only to size. This is done on a polyacrylamide gel.

Gels were prepared using BioRad mini-protean II SDS-PAGE equipment. Resolving gels varying between 8-15% were used in combination with a 3% stacking gel for all applications. The electophoresis was conducted at 200 V in 1 x SDS-PAGE running

buffer. A comparison with a protein ladder of known molecular weights was used to determine protein sizes once resolved (BioRad, Amersahm, Pharmacia). Samples were prepared in 2 x SDS-PAGE sample buffer and heated to 96 °C for 3 minutes prior to loading on the gel.

The resolved proteins were fixed and stained using Coomassie stain, proteins were fixed with methanol and acetic acid and stained with Coomassie brilliant blue R250. Gels were immersed in stain for approximately 4 hours and then immersed in de-stain solution for approximately 2 hours with several changes of solution in that time. Gels were then soaked in a water and glycerol (5% v/v) solution overnight and dried between two moistened sheets of cellulose film (Promega gel drying kit).

2.2.8 Western Blotting

Proteins were transferred from the polyacrylamide gel to a nitrocellulose membrane (BioRad) using semi-dry electrophoretic transfer (BioRad) at constant voltage (15 V) for 20 minutes. The nitrocellulose membrane was pre-soaked in water while the blotting paper used for the transfer was pre-wetted with 1 x transfer buffer. Non-specific binding on the membrane was blocked by immersion in Western blotting blocking buffer overnight at 4°C or for 1 hour at room temperature. The blots were then incubated with the primary antibody in blocking buffer for 1 hour at room temperature and then washed with PBS-Tween20 3 x for 10 minutes each. The membrane was subsequently incubated with the HRP-conjugated secondary antibody in blocking buffer for 1 hour at room temperature, and again washed in wash buffer for 3 x 10 minutes. Immunoreactive bands were detected using an enhanced chemiluminescence reagent ECL+ (Amersham Pharmacia) according to the manufacturer's instructions and visualised by exposure to X-Ray film (Jet X-ray, UK).

Name	Specificity	Raised In	Supplied By	Titre Used in WB	Secondary Used	Titre of Secondary
S974	RP2	Sheep	Our lab Chapple *et al* 2000	1:1000	Sigma HRP	1:2000
Sos	hSos	Mouse	Transduction	1:250	Pierce HRP	1:20,000
Arl3-854	Arl3	Rabbit	Gift Nick Cowan	1:2000	Pierce HRP	1:30,000
9E10	myc	Mouse	Sigma	1:1000	Pierce HRP	1:20,000

VSV	VSV	Rabbit	Gift Karl Matter	1:10	Pierce HRP	1:30,000
av Peptide	GFP	Rabbit	BD Biosciences	1:50	Pierce HRP	1:30,000
RAN	RAN	Mouse	Transduction	1:5000	Pierce HRP	1:20,000
p27/Kip1	p27	Mouse	Transduction	1:2000	Pierce HRP	1:20,000
TNPO3	Transportin3	Rabbit	Gift from W.Y Tarn	1:500	Pierce HRP	1:30,000
3603	SPAG7	Rabbit	This study	1:500	Pierce HRP	1:30,000

Table 2.3 Primary antibodies used for Western blotting

2.2.8.1 Antibody peptide blocking

To determine the specificity of our SPAG7 antibody it was necessary to use peptide competition and observe whether the immunoreactivity was lost. The peptide block solution was prepared by diluting the specific peptide to 10µg/ml in blocking buffer and adding the SPAG7 antibody to a final titre of 1:500 and rotate end-on-end for 2 hours at room temperature. The membrane was incubated in blocking buffer during this time and then the peptide-blocked buffer was added in parallel with the primary antibody. The rest of the procedure is carried out as in 2.2.8.

2.2.9 Library Screening

2.2.9.1 Co-transformation of yeast

Yeast was co-transformed with a total of 1 µg plasmid DNA (0.5 µg amplified library DNA and 0.5 µg pSosRP2) as described in section 2.2.4. A positive control with 0.5 µg pSosRP2 and 0.5 µg pMyrSB was also co-transformed in the same way, as was a negative control with pSosRP2 and pMyrLaminC. An additional 0.5 µg of library DNA was also transformed into the yeast strain to act as an indicator of the proportion of revertants in each individual screen (this will be explained in section 2.2.9.3). An average screen consisted of 30 individual co-transformations which were plated onto SD/glucose (-UL) 90mm plates and grown for approximately 36-40 hours at 24°C.

2.2.9.2 Replica Plating of Yeast Co-transformations

After 36-40 hours of growth on glucose plates the co-transformations were replica plated onto SD/galactose (-UL) plates, the 'library only plate' was replica plated onto an SD/galactose (-U) plate. The orientation was clearly marked on the plates. The replica plater and velevteen squares used were from Sigma. The replica SD/galactose plates were incubated at 37°C until colonies appeared.

2.2.9.3 Identification of Putative Positive Interactors

The SD/galactose plates were closely observed every day for up to 10 days after replica plating. Any colonies growing at 37°C were marked. Colonies were picked from the 30 co-transformation plates as they became apparent, from day 1 until colonies were seen on the negative control plate. Due to low level background transactivation by the bait it was necessary to have a negative control to compare growth to as eventually all colonies containing the bait would grow at 37°C. It was also necessary to know how prevalent revertant colonies were in each screen: the yeast that had only been transformed with cDNA library should not have any interactions, due to the lack of the bait, and so any colonies growing at the restrictive temperature were either revertant or contained a false positive cDNA (e.g. Ras). This provided an indication of the prevalence of revertants in each screen.

2.2.9.4 Extraction of DNA from Putative Interactors

pMyr plasmid DNA was extracted from the putative interactors to allow further analysis. 5 ml of SD/glucose (-UL) liquid media was inoculated with a portion of the yeast colony. This was grown at 24 °C with shaking until the culture was saturated. The yeast were centrifuged at 2000 xg for 2 minutes and the pellet was resuspended in 100 µl freshly made 3% SDS 0.2 M NaOH. The cell suspension was incubated at room temperature with occasional mixing by rapid inversions. TE (500 µl) was added followed by 60 µl 3 M NaOAc (no pH adjustment) with mixing, and 600 µl of phenol:chloroform:isoamyl alcohol (25:24:1) was added to the cell suspension followed by vortexing for 2 minutes. The samples were then centrifuged at 14,000 xg for 2 minutes and the resulting upper aqueous layer was transferred to a fresh 1.5 ml eppendorf tube. Another 600 µl phenol:chloroform:isoamyl alcohol was added and the sample was vortexed and centrifuged as described previously. Ice cold isopropanol (650 µl) was then added, after mixing, the samples were incubated at -20°C for at least 20 minutes, ideally 1 hour. The samples were then centrifuged for 5 minutes at 14,000 xg to pellet the DNA. The supernatant was removed and 100 µl of 70% ethanol was added followed by another 5 minute spin at 14,000 xg. The supernatant was removed, the pellet dessicated and subsequently resuspended in 15 µl ddH_2O.

2.2.9.5 Transformation of Total Yeast DNA into E. coli

Samples of the extracted yeast DNA (7 µl) were used to transform 55 µl competent JM109 *E. coli* cells as in section 2.1.7. The cell suspension was plated onto Chloramphenicol LB-agar plates. Individual colonies containing pMyr clones were

picked and grown in 5 ml LB+Chloramphenicol overnight at 37°C. The pMyr plasmid DNA was prepared and analysed using *Xho*I and *Eco*RI (Promega) restriction enzymes as described in section 2.1.8. Plasmid DNA was used to re-transform cdc25-2 yeast cells to confirm the interaction was specific to RP2 and not due to phenotypic revertancy (Section 2.2.4). In addition yeast cells were re-transformed with pSos alone to check for binding to Sos and/or transactivating the system (e.g. a Ras related molecule acting as a false positive). Any putative interactor DNA was sequenced with pMyr primers to determine the indentity of the putative interactor and whether the clone was in frame as described in section 2.1.9. Plasmid DNA from putative interactors was also re-transformed into yeast with the RP2 bait plasmid and the empty pSos plasmid to check for specific binding to RP2.

2.2.9.6 Analysis for Revertants

In order to eliminate revertants from the time-consuming procedure of DNA extraction and sequencing, other methods were assessed. Due to the weak transactivation of the bait it was not possible to test for revertants as described in the published protocol (CytoTrap System, Stratagene). Instead, 10 ml of SD/glucose (-U) was inoculated with a portion of the yeast colony to be tested, and grown at 24ºC with shaking until the culture was saturated, usually 2 days. A 200 µl aliquot of culture was then plated onto SD/glucose (-U) plates and grown at 24ºC for 40 hours. The cultures were then replica plated onto SD/glucose (-L) plates to observe which colonies were cured of the bait plasmid. These colonies were then tested at the permissive (24ºC) and restrictive temperatures (37ºC). Revertants continue to grow at 37°C even with the loss of the bait, but interactors do not.

2.2.9.7 Yeast Spheroblast PCR

An alternative method to avoid the time consuming procedure of extracting DNA and sequencing for every putative interactor is to use PCR and sequence directly. A small amount of each colony was picked with a sterile loop into 10-20 µl incubation solution (1.2 M Sorbitol, 100 mM sodium phosphate pH 7.4, 2.5 mg/ml Lyticase). The resulting mixture was incubated at 37ºC for 5 minutes. 1-3 µl was used as a template for PCR, the other PCR reagents used were as described in section 2.1.10. The cycles were 95ºC for 10 minutes to break down the protein coat and denature the DNA, followed by 95ºC for 30 s, 68ºC for 30 s and 72ºC for 1 minute (the average insert size of the library is 1.2 kb). This technique was not deemed to be reliable and therefore was not used to eliminate any putative interactors from being processed.

2.2.10 Southern Blotting

Southern blotting was used as a technique to try to eliminate the processing of Arl2 and Arl3 among putative interactors using bovine-specific Arl2 and Arl3 probes.

Putative positive yeast colonies were selected as described In section 2.2.9 and DNA from the yeast colonies was extracted as described in section 2.2.9.4. 5-7 µl of the total extracted yeast DNA was then separated on a 2% agarose gel by electrophoresis as described in section 2.1.5 and was run at 80 volts.

The gel was incubated in denaturation buffer for 30 minutes to denature the DNA to allow the probe to bind to ssDNA. The denatured gel was then used to set up the Southern blot overnight. A capillary blot was assembled using Whatman filter paper as a wick which was immersed in denauration buffer. The gel was placed on the wick with the Hybond N+ membrane on top of it, 3 sheets of Whatman filter paper were placed on top of the membrane and then paper towels were used for the final layer. The blot was then left overnight to allow transfer of the DNA from the gel to the membrane.

Arl2 and Arl3 specific probes were prepared using PCR as described in section 2.1.10 and utilising primers designed for bovine Arl2 and Arl3. The primers were designed to a central part of the cDNA sequence as the 3' and 5' ends of the cDNA clones can exhibit variability. The resulting DNA amplicons were different sizes to allow differentiation between Arl2 and Arl3. After PCR the DNA was extracted from the gel and purified using the Qiagen Gel Extraction kit, according to the manufacturer's instructions. The DNA was then quantified using a Spectrophotometer as described as in section 2.1.8.1.

The blot was dismantled the following morning and the position of the wells was clearly marked. The membrane was then dried and then baked at 80°C for 2 hours. The membrane was then prepared for hybridisation by pre-wetting the membrane in 5 X SSC. The membrane was then incubated with Hybridisation solution shaking for 1 hour at 65°C. During this time the probe was prepared. The probe was denatured by incubation at 95°C for 5 minutes and then rapidly placing on ice. A total reaction volume of 50 µl was used with 5 µl of αdCTP^{32}P and 200ng probe to re-hydrate the Ready-to-go® bead (Amersham). The reaction was incubated at 37°C for 30 minutes

and denatured for 5 minutes at 95°C. The denatured probe was then added to the hybridisation solution and incubated with the membrane overnight at 65°C.

The following morning the membrane was washed twice in 2 X SSC/0.1% SDS for 30 minutes at room temperature, and then twice in 2 X SSC/0.1% SDS for 30 minutes at 65°C. As background was still high a further wash using 1 x SSC/0.1% SDS at 65°C was also performed. The membrane was then exposed to film.

2.3 CELL CULTURE AND IMMUNOCYTOCHEMISTRY

2.3.1 Cell Culture Maintenance (Adherent cells)

Chinese hamster ovary (CHO) cells, human neuroblastoma SK-N-SH cells, monkey African green kidney fibroblast (COS7) cells, and cervical adenocarcinoma cells (HeLa) were cultured in Dulbecco's modified Eagle's Medium (DMEM)/F12 (Gibco, UK). All cells were cultured in medium containing 10% fetal bovine serum and 100 units/ml penicillin and 100 µg/ml streptomycin. Cells were maintained in an environment of 5% CO_2 and 37°C.

Cells were passaged every 3-4 days or when they were approximately 90-95% confluent and were maintained in T75 flasks with 13 ml media per flask. When cells reached 95% confluency they were washed twice with 20 ml HBSS (Gibco, UK) before being incubated with 1 ml of trypsin (Gibco, UK) for up to 5 minutes until cells were no longer adherent, 9ml of DMEM/F12 media was then added to stop the action of the trypsin. Cells were then appropriately diluted in fresh DMEM/F12 media.

2.3.2 Liquid Nitrogen Storage of Cells

Approximately $2x10^5$ cells were resuspended in 0.25 ml freezing media (20% foetal bovine serum, 72% DMEM/F12, 8% DMSO) and an alcohol bath (VWR) was used to slowly freeze the cells to -80°C over 24 hours. Cells requiring long term storage were then placed in liquid nitrogen.

2.3.3 Resuscitation of Cells from Liquid Nitrogen

Aliquots of cells were removed from liquid nitrogen and rapidly warmed to 37°C and added to pre-warmed media. The cells were then pelleted at 500 *g* and resuspended in fresh media to remove the DMSO.

2.3.4 Lipofectamine Transfection

Transient transfection of adherent cells with plasmid DNA was achieved using Lipofectamine reagent in combination with 'Plus' reagent (Invitrogen, UK).

2.3.4.1 Transfection of eight-well chamber slides

In a typical transfection reaction using eight-well chamber slides, cells were seeded at a density of 20,000 cells/well and were left at 37ºC for 24-48 hours until approximately 60% (HeLa, COS7, SK-N-SH cells) or 70% (CHO and ARPE19 cells) confluent. The following solutions were then prepared for each transfection reaction: A: 100 ng plasmid DNA was mixed with 25 µl serum free DMEM/F12 media and 1 µl 'Plus' reagent and B: 100 µl serum free media mixed with 0.5 µl Lipofectamine reagent. Solutions A and B were then incubated at 22ºC for 15 minutes, then mixed together and incubated for a further 15 minutes at 22ºC to allow DNA-liposome complexes to form. At this point the cells to be transfected were washed twice with serum free media and then 100 µl of the DNA-liposome solution was added to the appropriate well and incubated for 3 hours at 37ºC. After this incubation, 100 µl of serum containing 20% serum was added to the cells. The cells were then assayed 24 hours after transfection.

2.3.4.2 Transfection of six-well plates

Transfections of cells in six-well plates was done as described above but with variations in the quantities of solutions used and the number of cells seeded. In a well of a six-well plate 200,000 cells were seeded per well. Solution A: 25 µl serum free DMEM/F12 media was mixed with 800 ng plasmid DNA and 4 µl 'Plus' reagent, Solution B: 800 µl serum free media was mixed with 2 µl Lipofectamine reagent. After the two incubations 800 µl of the A+B solution was added to each well and 800 µl of media containing 20% serum was added after the 3 hour incubation.

2.3.4.3 Preparation of cell lysates

Cell lysates were prepared fresh when required from either T25 flasks or 6 well dishes. Lysates requiring transiently transfected cells were transfected in six-well plates as described in 2.3.4. 24 hours after transfection cells were washed twice in ice-cold PBS and then lysed in 300 µl lysis buffer per well (0.5% NP40, 5mM EDTA and 1% Protease Inhibitor Cocktail (Sigma) in PBS) for 15 minutes at 4ºC. Cell lysates were then centrifuged at 13,000 *g* for 30 minutes at 4ºC to obtain the supernantant fraction and 300 µl ice cold PBS was used to resuspend the pellet fraction when required. Untransfected cells were prepared in the same way but from T25 flasks.

2.3.5 Immunocytochemistry

Cells were seeded in eight-well chamber slides at a density of approximately 20,000 cells per well and allowed to grow for 24-48 hours. The cells were then washed twice in PBS and fixed in either 3.7% paraformaldehyde in PBS for 15 minutes or 100% ice-cold methanol for 5 minutes. Cells were permeabilised using 0.1%-0.2% Triton X-100 for 15 minutes. Non-specific binding was prevented by incubation in Blocking Buffer (3% bovine serum albumin (BSA), 10% normal donkey serum in PBS) for 1 hour at 22°C. Primary antisera were added at the appropriate titre (See Table 2.4) to Blocking Buffer and the cells were incubated with the primary antisera for 1 hour at 22°C. After 5 washes in PBS the cells were incubated with the secondary antisera in 3% BSA in PBS for 1 hour at 22 °C. The secondary antisera were cyanine-conjugated and used at the titres stated in Table 2.4. If needed, DAPI was used at 1:10,000 (to a final concentration of 0.002 mg/ml) before the penultimate PBS wash and was incubated for 5 minutes at 22°C.

Name	Specificity	Raised In	Supplier	Titre Used
Arl3-854	Arl3	Rabbit	Gift Nick Cowan	1:200-250
9E10	myc tag	Mouse	Sigma	1:1000
VSV	VSV tag	Mouse	Gift Karl Matter	1:4
S974	RP2	Sheep	Our own	1:100
TUB 2.1	β-tubulin	Mouse	Sigma	1:500
Calnexin	Calnexin	Mouse	StressGen, US	1:100
β-COP	maD clone	Mouse	Sigma, UK	1:40
EEA1	Early endosome antigen 1	Mouse	Gift Clare Futter	1:100-1:200
3603	SPAG7	Rabbit	Our lab	1:500
TNPO3	Transportin 3	Rabbit	Gift W. Y. Tarn	1:500
RAN	RAN	Mouse	Transduction	1:500
p27/Kip1	p27	Mouse	Transduction	1:200

Table 2.4 Primary Antisera for Immunocytochemistry

Specificity	Raised In	Conjugate	Supplier	Titre Used
Rabbit IgG	Donkey	Cy-3	Jackson	1:100
Sheep IgG	Donkey	Cy-2	Jackson	1:100
Mouse IgG	Donkey	Cy-3	Jackson	1:100
Sheep IgG	Donkey	Cy-3	Jackson	1:100
Rabbit IgG	Donkey	Cy-2	Jackson	1:100
Mouse IgG	Donkey	Cy-2	Jackson	1:100

Table 2.5 Secondary Antisera for Immunocytochemistry

2.3.6 Co-Immunoprecipitations

Co-immunoprecipitations were performed on cells transiently co-transfected in six-well plates as described in 2.3.4. Each reaction was done in duplicate and cell lysates of the same transfection were pooled at the stage of adding the antibody. 24 hours after transfection cells were washed twice in ice-cold PBS and then lysed in 300 µl lysis buffer per well (0.5% NP40, 5 mM EDTA and 1% protease inhibitor cocktail (Sigma) in PBS) for 15 minutes at 4°C. Cell lysates were then centrifuged at 13,000 *g* for 30 minutes at 4°C, and 500 µl of each lysate was used for the Co-IP while the rest was kept as 'Input' sample. 4 µl of 9E10 antibody (α-myc) was added to each 500 µl sample and this was incubated overnight at 4°C with rotation. 25 µl packed bed volume of protein G sepharose equilibriated in lysis buffer (without CPI) was added to each sample and incubated at 4°C for 3 hours with rotation. The sepharose was then washed five times with lysis buffer, pelleting beads in between at 500 *g* for 30 seconds. The bound protein was eluted from the sepharose with 50 µl sample buffer. The sample was denatured at 96°C for 3 minutes and the beads were pelleted before loading on an SDS-PAGE gel (See section 2.2.7), 10 µl of the Co-IP sample was loaded onto the gel with 10 µl of the 'Input' in the adjacent lane and was resolved on an SDS gel. Bound protein was then detected by Western blotting with specific antibodies (See section 2.2.8 and Table 2.4).

2.3.7 GST-Pulldown Assay

RP2, Arl3-T31N and Arl3-Q71L were cloned into the pGEX-2T vector (by Dr Tatyana Novoselova) and transformed into Top10 OneShot *E.*coli bacteria. Having checked for the presence of the plasmid in the bacteria (see sections 2.1.8, 2.1.2 and 2.1.5), the bacterium were used to inoculate an overnight 5 ml culture of L-Broth with

Ampicilin (see Table 2.1). The following morning the overnight cultures were used to inoculate larger LB+Ampicilin cultures (RP2 – 1 litre cultures; Arl3 – 200 ml cultures) at a dilution of 1:100. The cultures were grown for 2 hours and then expression of the GST-fusion proteins were induced by addition of IPTG to a final concentration of 1 mM. RP2 cultures were then grown for a further 4 hours while Arl3 cultures were grown for another 2 hours. In all experiments empty pGEX-2T was used as a control.

Bacteria were then centrifuged at 6,000 xg for 15 minutes at 4 °C. The resulting pellets were then resuspended in PBS with added bacterial cell protease inhibitor cocktail (Sigma, UK) (5 ml PBS for 200 ml original culture volume) and the cells were lysed by sonication on ice (5 x 30 sec pulses) using a 9mm probe on a Soniprep150 (80% power). Lysates were centrifuged at 14,000 g for 30 minutes at 4°C and the supernatant was then passaged through a 0.45 µm filter. Small scale versions of this protocol were initially employed to check for optimum conditions for the expression of the fusion proteins, samples were resolved on SDS-PAGE and gels were stained with Coomassie stain to visualise proteins (see section 2.2.7).

1 ml of a 50% slurry of previously equilibriated glutathione sepharose 4B (Amersham Biosciences) was added and the lysates were then incubated with rotation for 1 hour at 4°C. After binding the GST-resin was washed with 10 x volume ice-cold PBS.

Cell lysates were prepared from confluent T75 flasks of cells (see section 2.3.1), after trypsin treatment cells were resuspended in 50 ml ice-cold PBS and centrifuged at 800 g for 5 minutes, the wash was then repeated before cells were lysed in 1 ml of lysis buffer (50 mM Tris-HCl (pH8), 150 mM NaCl, 1% Triton, 1% protease inhibitor cocktail) at 4°C for 15 minutes. In cases where transfected cells were used the cells were seeded and transfected in 6 well dishes as described in section 2.3.4.2 and then trypsinised in 300 µl 1 x Trypsin, resuspended in 50 ml ice-cold PBS and centrifuged at 800 g for 5 minutes, the wash was then repeated before cells were subsequently lysed in 300 µl lysis buffer as described above.

Lysates were subsequently centrifuged at 14,000 g for 15 minutes at 4°C. Protein concentration was determined using the BCA assay (Novagen). Cell lyastes were pre-cleared on GST-bound glutathione sepharose 4B resin for 1 hour at 4°C with rotation (400 µg cell lysate, 50 µl glutathione sepharose 4B, 10 µl mammalian cell protease inhibitor cocktail (Sigma, UK), made up to 900 µl with PBS). Pre-cleared lysates were then incubated with the GST-fusion proteins bound to the resin overnight

at 4°C with rotation (900 µl pre-cleared lysate, 10 µl mammalian cell protease inhibitor cocktail, 50 µl GST-fusion resin, made up to 1 ml with PBS).

The following morning the GST resin was washed 5 x with PBS, the resin was centrifuged at 500 g for 30seconds between each wash, beads were then resuspended in 80 µl of 2 x sample buffer and incubated at 100°C for 5 minutes to elute bound proteins from the resin. Samples were then resolved using SDS-PAGE and coomassie staining and proteins were detected using Western blotting and specific antibodies (see sections 2.2.7 and 2.2.8).

2.3.8 Live Cell Imaging

Cells were seeded into 35mm dishes with a central glass coverslip (MatTek, USA) at density of 200,000 cells/dish and were transfected as described in 2.3.4.2. 24 hours after transfection the cells were observed using a Zeiss Axiovert M100 microscope and Improvison software, the GFP channel (excitatation at 488 nm) was used to visualise the transfected GFP protein. A program was set up to take a photo of the cells every 15 seconds for a duration of ten minutes. Single frames were then used to construct video files of the cells showing the movement of the GFP-tagged protein in that time.

2.3.8.1 Confocal scanning microscopy

For all other immunocytochemical imaging applications a Zeiss LSM 510UV confocal scanning microscope was used with LSM510 and Adobe Photoshop software. Excitation wavelengths were 354 nm (DAPI), 488 nm (Cy2/GFP) and 543 nm (Cy3).

CHAPTER 3

IDENTIFICATION OF RP2 INTERACTING PROTEINS

3.1 Introduction

In order to investigate the putative pathways that RP2 may be involved in and how these may be important in retina a yeast two-hybrid approach was adopted to discover novel RP2 interacting partners. Yeast two-hybrid systems have been shown to successfully identify interacting partners for other retinal proteins, for example the delineation of the interaction between the nuclear receptor Nr2e3 and the transcription factor CRX (Peng *et al.*, 2005). In the case of the Nr2e3-CRX interaction both the proteins are retina-specific, however yeast two-hybrid has also been used for ubiquitously expressed retinal disease proteins, such as RPGR. The RCC1 domain of RPGR was used as a bait in yeast two-hybrid which led to the identification of retina-specific RPGRIP1 as an interacting partner (Boylan *et al.*, 2000), RPGRIP1 was subsequently found to be a causative gene for LCA and as such the interaction enhanced the knowledge of RPGR's role in retinal degeneration (Dryja *et al.*, 2001).

3.1.1 Yeast two-hybrid

The yeast two-hybrid system was developed by Fields and Song (1989). The system was designed on the principle that the two functional domains (DNA binding domain and transcriptional activation domain) of a transcription factor (TF) are able to exist and fold independently as part of fusion proteins which can be functionally active when they are physically brought back together. The DNA binding domain of the yeast Gal4 TF was used as the 'bait' domain and the transcriptional activation domain was used as the 'target' or 'prey' domain in the system. The gene of interest is cloned into a vector that results in the protein of interest being fused to the Gal4 TF DNA binding domain, and a cDNA library cloned into a vector resulting in expression of the cDNA clones as fusion proteins with the Gal4 TF transcriptional activation domain. Thus the bait/DNA binding domain fusion protein binds to the reporter gene in the nucleus of the yeast. When there is an interaction between two proteins the

transcriptional activation domain is brought together with the DNA binding domain to activate transcription of a β-galactosidase reporter gene (Figure 3.1) (Fields and Song, 1989). The methodology provides a powerful system for screening a cDNA library for putative interactions with a protein of interest by co-transforming yeast cells with the 'bait' (gene of interest) and 'target' (cDNA library) plasmids and assaying for β-galactosidase activity.

Figure 3.1 Schematic representation of the transcription-based yeast two-hybrid system

The schematic illustrates how the system operates in the yeast cell nucleus and how this translates into growth on *HIS*- media and the result of the β-Galactosidase assay. Adapted from http://www1.imperial.ac.uk/medicine/about/institutes/nhli/cardio/heart/cellbio/myogene/. Dr Nigel Brand, National Heart and Lung Institute, Imperial College.

Variations on this methodology have been developed since the original system was published, such as the use of alternative transcription factors, for example the LexA

TF, and the addition of dual reporter genes to allow increased stringency of testing for an interaction. For example the *HIS3* gene is often used as an additional reporter gene. Thus putative interactors can be initially screened using *HIS*- growth media such that the number of colonies requiring screening with the β-galactosidase (X Gal) assay is much reduced (Miller and Stagljar, 2004).

There are potential problems to consider in the use of this system to identify protein:protein interactions: for example an artificial environment can lead to false positive interactions, possibly due to proteins that would never come into contact in a physiological environment interacting in a non-specific manner. On the other hand it has also proved to be a useful system for observing transient interactions that would perhaps otherwise have been difficult to identify; often proteins involved in these interactions are of low abundance or interact briefly while 'in transit' from one organelle to another. Yeast two-hybrid may be of limited use if the protein of interest used as the bait in the screen is able to activate the system independently of an interaction, termed transactivation, this problem usually occurs when the bait is a transcription factor (Causier and Davies, 2002). An alternative yeast two-hybrid system has been developed more recently in which the interaction does not occur in the nucleus of the yeast cell, this system, which is described below, enables a two-hybrid assay to be performed using bait proteins which are not amenable to the transcription-based system.

3.1.2 Son of Sevenless Recruitment System

The SOS (Son of Sevenless) recruitment system (SRS) is a modified yeast two-hybrid system that utilises a variation on the TF-based yeast two-hybrid principle to find potential interacting partners for a protein. The system uses a strain of yeast (cdc25-H) which contains a point mutation at position 1328 of the *CDC25* gene, the human homolog of which is hSos. The mutation is temperature sensitive and so allows normal growth of the yeast at 22-25°C (permissive temperature) but prevents the cells from being able to grow at 37°C (restrictive temperature) (Aronheim *et al.*, 1994). The *CDC25* and *hSos* gene products act as guanyl nucleotide exchange factors (GEFs) that are able to induce the Ras signalling cascade by directly activating Ras, which is required for yeast growth through the activation of the adenylyl cyclase pathway (Broder *et al.*, 1998). The hSos protein which is expressed as a fusion protein with the gene of interest is able to complement this mutation at the restrictive temperature only when it is localised to the plasma membrane where yeast

Ras is localised, and it is this principle that forms the basis of the system (Aronheim *et al.*, 1994) (See Figure 3.2).

The cDNA library to be screened is cloned into a vector that tags each cDNA with a myristoylation signal at the N-terminus, thus targeting all the expressed proteins from the library to the plasma membrane. The expression of the cDNAs is under the control of the Gal1 promoter, such that expression is induced only in the presence of galactose in the media. The gene of interest is cloned into the pSos vector and is expressed as a fusion protein with hSos. Therefore, when yeast are grown at 37°C in the presence of galactose an interaction between 'bait' and 'target' proteins will result in the artificial recruitment of hSos to the membrane. This will complement the *CDC25* mutation and activate Ras allowing growth at the restrictive temperature (See Figure 3.2).

This system does not rely on transcription and so does not have the problem of traditional transactivation. Another potential advantage is that the interaction occurs in the cytoplasm at the plasma membrane as opposed to the nucleus (see section 3.1) and therefore can be used for larger proteins which may not easily translocate to the nucleus and also allows limited post-translational protein modifications that may occur in the cytoplasm which may be important for an interaction. This system can also be used for proteins which are themselves transcription factors and thus can cause transactivation of the traditional two-hybrid system. A further advantage of the SRS system is that it is capable of detecting weaker interactions due to the sensitivity and cascading nature of the Ras signalling pathway. It should be noted, however, that this system does still have the inherent problem of false positives and non-specific interactions as do other yeast two-hybrid strategies (Huang *et al.*, 2001).

A challenge with any yeast two-hybrid assay is the potential large number of false positives that are generated. For the SRS system this is due to the ability of mammalian Ras and Ras-related cDNAs from the cDNA library being able to complement the mutation without the need for hSos at the membrane. The hSos is able to stimulate the conversion of GDP-Ras to GTP-Ras and the cDNA myristoylation tag means the Ras is recruited to its site of action at the plasma membrane, for example p21-Ras has been a commonly reported false positive (Huang *et al.*, 2001).

Figure 3.2 Schematic showing how the SRS system is used to identify interacting proteins for a protein of interest

A At the permissive temperature the yeast are able to grow due to the mutation in *CDC25* having no effect. **B** At the restrictive temperature when there is no interaction between the 'bait' and 'target cDNA' the mutation in *CDC25* means the protein is unable to stimulate the conversion of Ras-GDP to Ras-GTP and thus the yeast do not grow. **C** At the permissive temperature the cells grow whether there is an interaction or not. **D** At the restrictive temperature if there is an interaction the loss of function of the CDC25 protein is compensated for by the recruitment of hSos to the plasma membrane which stimulates the conversion of Ras from GDP-bound to the active GTP-bound form. Modified from Evans *et al* (2006), Methods in Enzymology.

The SRS system relies on the temperature sensitive yeast strain cdc25-H, however, yeast are prone to mutation such that the cdc25-H mutant yeast strain may 'revert back' to the wildtype phenotype, and so grow at the restrictive temperature. As this is the phenotype used to select putative interactors it can be time consuming to distinguish a genuine interaction from a revertant colony. The SRS has been used

successfully in identifying the GABAp1 interaction with cellular retinoic acid binding protein (CRABP), an interaction potentially important in retinal neuron signalling (Song *et al.*, 2005). This suggests that the system is an effective method for the detection of novel interactions important to retinal biology.

The SRS yeast two-hybrid system was chosen as the most suitable for detecting potential physiologically relevant RP2 interactors. RP2 is dually aceylated and targeted to the cytosolic face of the plasma membrane (see section 1.4.2) in retina and all cell types tested (Chapple *et al.,* 2000, Chapple *et al.,* 2002). As such the localisation of the 'prey' to the cytosolic face of the plasma membrane of the yeast cell is closer to the normal physiological environment in which RP2-mediated interactions are likely to occur.

3.2 Optimisation of CytoTrap for screening a retina cDNA library using RP2 as bait

The system used in this study is the CytoTrap® system, Stratagene's version of the SRS system. Considerable optimisations of the standard protocols provided by Stratagene for CytoTrap were necessary in order to efficiently screen a bovine retina cDNA library (Stratagene) for RP2 interacting partners. The methods used are described in Chapter 2 but details of the strategies behind the final methodologies are described in this chapter.

3.3.1. Sub-cloning of RP2 into the pSos vector

The pSos plasmid is a relatively large plasmid at 11.3kb. RP2 was subcloned into the pSos vector as described in sections 2.1.2-8. The large size of the vector meant that bacterial transformation efficiency was low. Rearrangements and recombination events were observed with pSos and RP2 as shown in Figure 3.3.

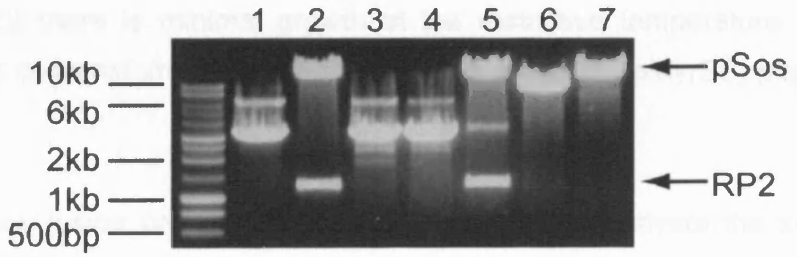

Figure 3.3 Rearrangements of pSos/RP2 plasmids

RP2/pSos plasmids from *E.coli* transformations of RP2/pSos ligations, DNA was digested with *Nco*I and *Not*I. Lane 2 contains a correctly ligated RP2 insert in the pSos plasmid. Control pSos digested with *Nco*I and *Not*I is shown in Lane 7. Lanes 1, 3, 4, and 6 show rearranged pSos plasmid. Lane 5 shows an apparently correctly ligated RP2 insert in the pSos vector which appears to be partially digested.

The pSos rearrangements were overcome by using SURE® 2 supercompetent *E.coli* cells (Stratagene). These bacteria have altered *E.coli* genes involved in DNA repair and recombination, thus reducing the likelihood that these events will occur and result in deletion and/or alteration of the plasmid construct. Homologous recombination events are reduced by the introduction of *recB* and *recJ* mutations which is similar to

a mutation in the *recA* gene. Mutations in genes involved in DNA repair, specifically in the UV and SOS repair systems, allows the cloning of usually unstable DNA, for example DNA containing long inverted repeats. The manufacturer does not recommend using these cells for constructs larger than 10kb which may explain why there are still rearrangements (Figure 3.3) even when using cells intended to prevent such occurrences. All subsequent cloning into pSos was successful when this protocol was followed.

3.3.2 Functional analysis of pSos-RP2 in CytoTrap

It was necessary to establish if RP2 was functional in the SRS system and this was done as described in section 2.2.5. The expression level of the hSos-RP2 fusion protein was assessed as described in sections 2.2.4 and 2.2.6-8. The functionality of hSos-RP2 in CytoTrap was then analysed by co-transforming cdc25H yeast with pSos-RP2 and pMyr control plasmids (Table 2.1) and checking that they are able to grow as predicted. Figure 3.4 shows that hSos-RP2 expresses in the transformed cdc25-H yeast and that when co-transformed with the pMyr negative control plasmid (pMyrLaminC) there is minimal growth at the restrictive temperature and there is growth when co-transformed with the pMyr positive control (pMyrSB) plasmid (Figure 3.4).

The RP2-hSos fusion protein was found to slightly transactivate the system; when hSos-RP2 is expressed alone or in combination with a negative control (pMyrLaminC) there was some growth at the restrictive temperature. This growth was minimal and was usually noticeable after approximately 6-7 days at the restrictive temperature (see Figure 3.4). Whenever a screen was performed, a negative control using pSos-RP2 and pMyrLaminC was included, which was used as a direct comparison to the library screen. As soon as any colonies became visible on the negative control plate no further colonies were selected from the screen.

3.3.3 Screening strategies

In order for any yeast two-hybrid method to be successful, efficient transformation with plasmid DNA is important. The recommended manufacturer's protocol for transformation of the cdc25-Hα yeast were found to be insufficient (efficiency of 5-7x10^2/μg DNA) for large-scale library screening and so adjustments to the protocol were made, the final protocol used is described in sections 2.2.4 and 2.2.9.

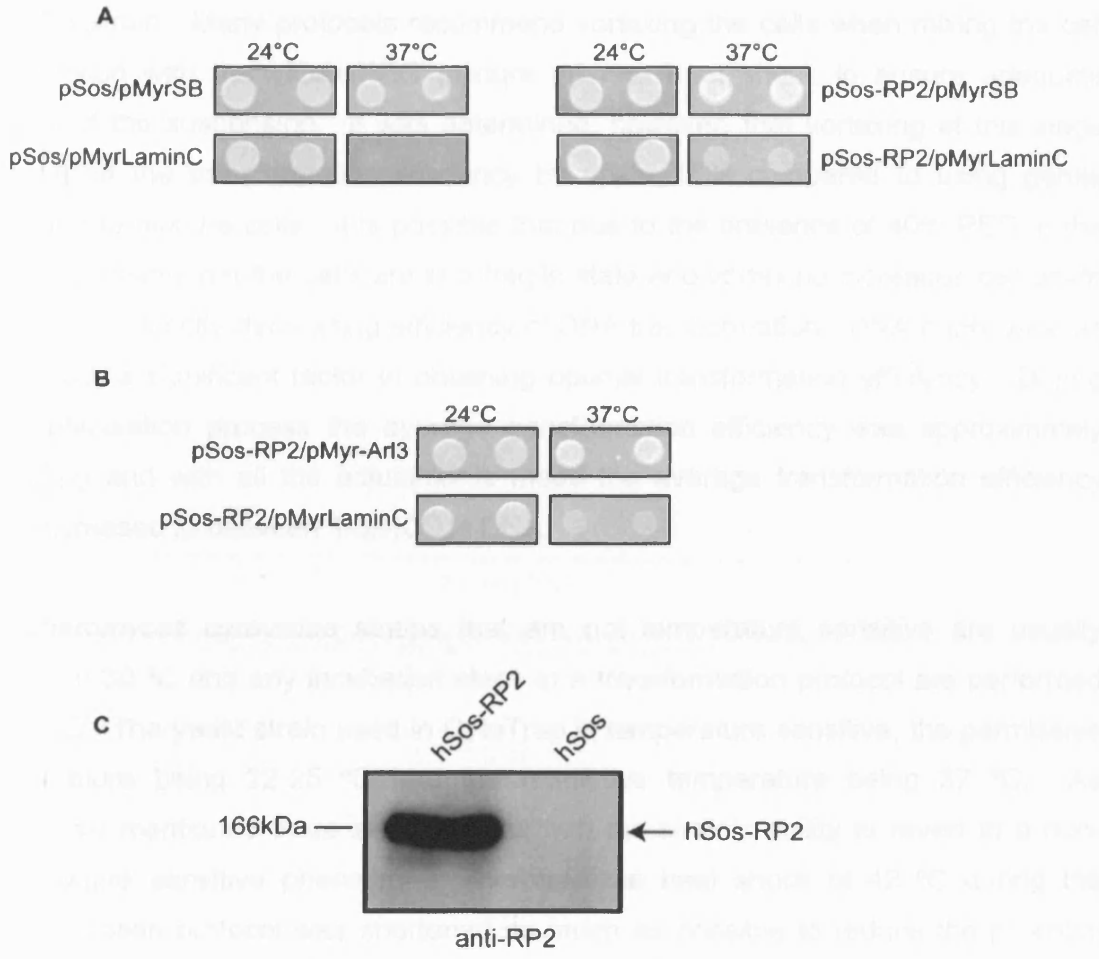

Figure 3.4 Functional analysis of the hSos-RP2 bait

A Yeast co-transformed with plasmid combinations as indicated and grown for 120 hours at the permissive and restrictive temperatures. The hSos-RP2 'bait' is able to grow to a limited degree at the restrictive temperature whereas when hSos is expressed without RP2 there is no growth at 37°C. The pMyrSB plasmid expresses Rit1 protein, which binds to hSos, pMyrLaminC expresses Lamin C which does not bind to either hSos or RP2. **B** Yeast co-transformed with pSos-RP2 and either pMyr-Arl3 or pMyr-LaminC after 96 hours, showing that the RP2-Arl3 interaction can be detected above the background transactivation. **C** Yeast protein extracts transformed with pSos-RP2 or pSos alone probed using an antibody to RP2 showing expression of the hSos-RP2 fusion protein.

The method developed was based on the standard LiOAc method (Ito *et al.*1983), as modified by Gietz *et al.* (1992). There were several adjustments made to this standard protocol in order to achieve the highest transformation efficiency of the cdc25H strain. Many protocols recommend vortexing the cells when mixing the cell suspension with the LiOAc/PEG mixture prior to heat shock to ensure adequate mixing of the suspension. It was determined, however, that vortexing at this stage decreased the transformation efficiency by up to 15% compared to using gentle pipetting to mix the cells. It is possible that due to the presence of 40% PEG in the cell suspension that the cells are in a fragile state and vortexing increases cell death rather than directly decreasing efficiency of DNA transformation. DNA purity was, as expected, a significant factor in obtaining optimal transformation efficiency. During the optimisation process the average transformation efficiency was approximately $1x10^3$/µg and with all the adjustments made the average transformation efficiency was increased to between $1\text{-}3x10^4$/µg DNA.

Saccharomyces cerevisiae strains that are not temperature sensitive are usually grown at 30 ºC and any incubation steps in a transformation protocol are performed at 30 ºC. The yeast strain used in CytoTrap is temperature sensitive; the permissive temperature being 22-25 ºC and the restrictive temperature being 37 ºC. As previously mentioned there are problems with the strain's ability to revert to a non-temperature sensitive phenotype. Therefore the heat shock of 42 ºC during the transformation protocol was shortened as much as possible to reduce the potential environmental pressure for the yeast to revert. The recommended length of heat shock for most published protocols is 15-20 minutes, it was determined empirically that a heat shock of 10 minutes resulted in an efficient transformation while reducing the environmental pressure on the yeast and hence reducing the likelihood of revertants.

There are two common approaches to transforming yeast for two-hybrid screening: co-transformation and sequential transformations. Sequential transformations involve first transforming the yeast with the bait plasmid and then to transform these yeast strains with the cDNA library plasmid. This is generally achieves high efficiency transformation to screen a library. Sequential transformations were less suitable for this yeast strain, partially due to the low level transactivation by hSos-RP2, so the approach taken in this study was co-transformation which also minimised revertancy events. In order to reduce the number of yeast able to revert to the non-temperature

sensitive phenotype the amount of time the yeast were grown was kept to a minimum.

Two different conditions of screening were employed in this study. The different conditions had different limits of detection for interacting partners. The standard procedure of using replica plating onto SD/Galactose plates, as described in section 2.2.9.2, after initially plating onto SD/Glucose plates, was used for 12 screens during optimisation and for 4 optimal screens ("normal stringency screens"). Unlike the transcription-based yeast two-hybrid system, CytoTrap requires the transformed yeast to be grown at the permissive temperature for up to 40 hours on SD/Glucose plates and then replica plated onto SD/Galactose plates and incubated at the permissive temperature. This procedure allows the yeast to grow before being subjected to selection at the restrictive temperature. The procedure of replica plating does however decrease the efficiency of the screen. It was calculated that replica plating led to a 3-5% loss in total colonies screened, probably due to the yeast colonies still being too small to be successfully picked up by the velvet, however the method was more likely to detect weaker interactors than the alternative condition described below (see table 3.1).

An alternative method was attempted to bias the detection parameters towards the identification of higher affinity interactors. The yeast was transformed with the RP2 bait and cDNA library plasmids as described in section 2.2.9.1 but were plated directly onto SD/Galactose plates rather than SD/Glucose plates. The plates were incubated at 24 °C for 24 hours before being transferred to 37°C where they were incubated until colonies were visible, thus eliminating the need for replica plating. Due to there being no need for replica plating it was possible to plate colonies at a much higher density and there was no colony loss due to the replica plating procedure. Therefore, this method allowed a higher number of colonies to be screened in a single screen (see Table 3.1). This screening strategy (referred to as a "high stringency screen") resulted in only revertants and strong interactors being detected (Table 3.1) and was not used for further screening as weaker interactors may be missed if this protocol was used exclusively for screening. Following the optimisation of the system for RP2, involving replica plating, it was possible to screen approximately 300,000 colonies in a single low stringency screen.

Normal Stringency Screen	
No. Colonies Screened	300,000
No. Putative Interactors	82
No. Revertants/False Positives	71
No. Interacting Clones	11
No. Interactors	5
RP2 Interactors confirmed	Arl3 (6), Arl2 (1), RAN (2), CDKN1B (1), TNPO3 (1),
% Putative Interactors that were false positives or revertants	87%
% Interactors that were Arl clones	64%

High Stringency Screen	
No. Colonies Screened	$>1x10^6$
No. Putative Interactors	87
No. Revertants/False Positives	55
No. Interacting Clones	32
No. Interactors	2
RP2 Interactors confirmed	Arl3 (30), Arl2 (2)
% Putative Interactors that were false positives or revertants	63%
% Interactors that were Arl clones	100%

Table 3.1 A comparison of screening strategies

A comparison of the results of screening with RP2 bait using two different strategies illustrated by comparing a representative screen for each strategy.

Finally, adjustments to the recommended protocol for extracting the yeast DNA for transforming *E.coli* were necessary. The final protocol is described in section 2.2.9.4-5. The cell lysis method suggested by the manufacturer was relatively inefficient and inconsistent but using an adapted version of a phenol/chloroform/isoamyl alcohol-based extraction method provided sufficient amounts and quality of DNA to efficiently transform the *E.coli*.

3.3 Strategies to expedite processing of revertant and Arl clones

During the development of the system it became clear that a method to eliminate the large number of false positives (approximately 90% of an average screen) and known strong interactors (i.e. Arl3, see Chapter 4) was necessary. A method to determine whether or not a putative positive yeast colony was either a revertant or a positive

was recommended by Dr Gina Scott, University of Leeds. This method was based on the yeast losing the RP2 bait plasmid through growth in non-selective media as described in section 2.2.9.6 and then testing the yeast for growth at the restrictive temperature. If the yeast has reverted to the non-temperature sensitive phenotype it would continue to grow at the restrictive temperature despite losing the bait plasmid. This method allowed the elimination of approximately 75% of the revertants without having to extract DNA from the yeast cells and the subsequent analyses required. Using this method, however, did not eliminate any false positives that may bind specifically to the hSos protein or any Ras false positives that require the hSos protein to stimulate the yeast growth.

Arl3 is an established RP2 interacting partner (Bartolini *et al.,* 2002) (see section 1.6.1). During the screening process Arl3 was detected 45 times, and as such strategies to identify Arl3 at an earlier stage of screening were developed. The Arl3-RP2 interaction was relatively 'strong' and well above the background level of RP2 transactivation (see Figure 3.4). Arl2 was also found to be a strong RP2 interactor in this system. These interactions will be discussed further in Chapter 4.

3.3.1 Identifying Arl clones

Arl3 was the most common positive cDNA identified in this screen with Arl2 being the second most common (see section 3.4 and Table 3.1). In order to process and prioritise novel putative interactors more quickly, two methods were developed to detect the presence of Arl2 and Arl3 at an earlier stage in the processing of the screening.

The first method used to identify Arl clones was yeast colony PCR. Yeast spheroblast PCR (as described in 2.2.9.7) did successfully identify some Arl clones but was inconsistent, the positive control was not always successfully amplified. An alternative Southern blotting method was then used, as described in section 2.2.10. Southern blotting did not provide results as rapidly as PCR but appeared, initially, to be more consistent and therefore, more useful. Analysis of Southern blots of plasmid DNA extracted from potentially positive yeast colonies showed high background hybridisation, perhaps to yeast genomic DNA. However only 66% of the tested putative Arl cDNAs were subsequently confirmed Arl clones by sequence analysis. Therefore, this method was thought not reliable enough.

The final approach to reducing the need to fully process Arl2 and Arl3 clones was colony PCR of bacterial colonies. *E.coli* were transformed with extracted yeast DNA as previously described in section 2.2.9.4-5 and then small portions of bacterial colonies were re-suspended in PCR MasterMix (Abgene, UK) with bovine-specific Arl2 or Arl3 primers. The primers were designed based on previously sequenced bovine Arl clones. The PCR reaction and conditions are as described in section 2.2.10. The bovine Arl3 primers amplify a 201 bp region from base pair number 175 to 376. This was the most reliable method used and was consistently able to detect Arl2 and Arl3 plasmids when they were present, as well as being able to distinguish between the two genes (see Arl3 in Figure 3.5). The disadvantage of the method was that it did not eliminate the need for DNA extraction and bacterial transformations; it did, however, prevent the need to re-transform yeast cells to check the specificity of the interaction as well as making it unnecessary to subsequently sequence the clone.

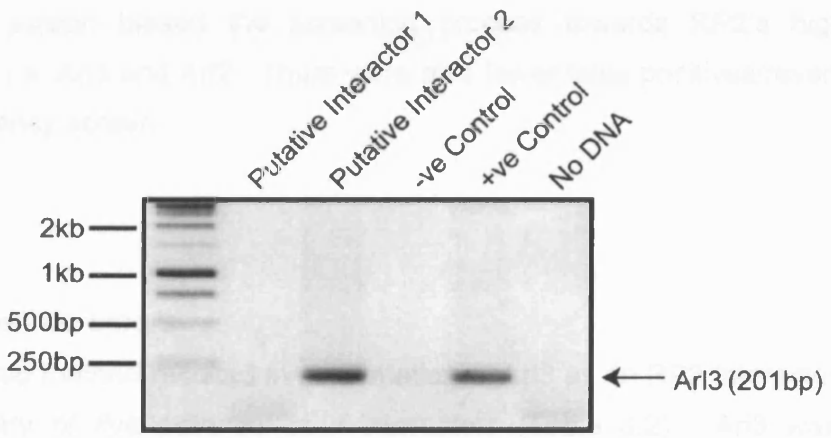

Figure 3.5 Bacterial colony PCR to detect Arl clones

Specific detection of an Arl3 plasmid from a putative interactor (Putative Interactor 2) by PCR was confirmed by sequencing. Putative interactor 1 was later confirmed to be RAN (see Chapter 5). The negative control was a bacterial colony known to contain bovine Arl2.

3.4 Overview of bovine retina cDNA library screening

The cDNA library from Stratagene was characterised both before and after in-house amplification as described in section 2.2.3. The titre of the library on delivery was calculated to be 5 x 10^8 cfu/ml. The average insert size pre-amplification was determined to be 1.23kb. Post-amplification the average insert size was found to be

1.34kb, indicating that the amplification process did not preferentially amplify the smaller cDNAs. The quality of library clones was also checked as described in section 2.2.3 and was found to contain known retinal genes such as *rhodopsin* and *CRX*, therefore the library was deemed to be representative enough for screening.

Overall approximately 2.6 million clones were screened, the majority of which were screened using the recommended replica plating strategy, only one screen was conducted using the 'high stringency' parameters which accounted for approximately 1 million of the screened colonies. Screening 2.6 million colonies resulted in 564 putative interactors of which 508 were false positives/revertants (90%) Of the 56 interacting clones, 51 were Arl3 (45) or Arl2 (6), two thirds of the detected Arl3 clones were found in the single 'high stringency screen' (see Table 3.2). In total, six potential RP2 interactors were discovered using CytoTrap. Table 3.1 shows the differences in screening when using the two previously described strategies by comparing a representative screen from each, the clear difference being that the high stringency screen biased the screening process towards RP2's higher affinity interactors, i.e. Arl3 and Arl2. There were also fewer false positives/revertants in the 'high stringency screen'.

3.5 Putative Interactors

The CytoTrap method resulted in confirmation of Arl3 as an RP2 interactor as well as the discovery of five potential new interactors (Table 3.2). Arl3 was the most common cDNA detected in the screen with 80% of the putative interacting clones being Arl3 clones. Arl2 was the second most common putative interactor discovered, six clones were identified which were all identical. Four other novel putative RP2 interactors were also identified and will be discussed in the following chapters.

Total for all screens	
No. Colonies Screened	~2,600,000
No. Putative Interactors	564
No. Revertants/False Positives	508
No. Interacting Clones	56
No. Interactors	6
RP2 Interactors confirmed	Arl3 (45), Arl2 (6), RAN (2), CDKN1B (1), TNPO3 (1), SPAG7 (1)
% Putative Interactors that were false positives or revertants	90%
% Interactors that were Arl clones	91%

Table 3.2 Summary of all screens for RP2 interactors

In total 17 screens were performed, 16 of these utilised the 'normal stringency' parameters, of these 4 were optimal screens and the other 12 were used to optimise the screening conditions. One screen was conducted using the 'high stringency' parameters.

3.6 Discussion

The choice of method when investigating interacting partners for a given protein is very important. Most approaches have both advantages and disadvantages. The use of yeast two-hybrid may lead to the discovery of transient interactors, which can be hard to detect in cellular studies but can be key to a particular pathway in the cell. CytoTrap was utilised to investigate novel RP2 interactors due to the fact that RP2 undergoes post-translational modifications and thus the SRS system reflects RP2's endogenous localisation more accurately than a nuclear-based yeast two-hybrid assay, and it does appear to have been a suitable system for this purpose. The choice of cDNA library is also crucial to any investigation of this kind. One of the fundamental aims of this study is to explore why mutations in *RP2* lead to the development of RP when the gene is expressed in every tissue tested (Schwahn *et al.*, 1998, Chapple *et al.*, 2000). The approach taken therefore was to use a retina cDNA library as potentially important retina-specific RP2 interactors will be well represented in the library as well as ensuring that any ubiquitously expressed RP2 interactors are not ignored.

The use of a temperature sensitive yeast strain that has the inherent capability of reversion to the wild type genotype, and the resultant high number (90% of all putative positives) of revertants encountered in the CytoTrap system was the most significant disadvantage of the system. The dual reporter system utilised by transcription-based yeast two-hybrid tends to reduce the number of false positives, however the nuclear location of the interaction in this system has its own set of disadvantages as discussed in section 3.1.1. During the development of CytoTrap for screening a cDNA library, obtaining good transformation efficiency for the yeast was problematic. However, through optimisation of a LiOAc based method the efficiency was increased by at least ten-fold. Although a transformation efficiency of at least $1x10^6$ colonies/µg DNA is ideal for such applications the lower efficiency was compensated for through increasing the amount of DNA and yeast cells used for each reaction, and as such was found to be sufficient for screening the cDNA library.

The use of different detection parameters through the exclusion of replica plating in the 'high stringency' screen biased the screen towards the detection of 'stronger' interactors. Although in the case of RP2 this meant that all the detected interactors were Arl2 or Arl3, the strategy was successful and has been used to screen other retinal disease genes in the lab (Hidalgo *et al.*, submitted). In order to ensure that weaker interactors were not missed, the use of replica plating for the remainder of

screening was employed. There appeared to be a higher percentage of putative positive yeast colonies subsequently determined as revertants when replica plating was used, which may be explained by the reduced number of generations of growth when replica plating is omitted from the protocol and so reducing the likelihood of revertancy.

As mentioned in section 3.1.2, CytoTrap has been successfully used to identify the interaction of GABA ρ1 with CRABP; this interaction was discovered using the same commercial bovine retina cDNA library (Stratagene) that was used in this project (Song *et al.* 2005). In this instance 1.3 million colonies were screened and of these 200 colonies grew at the restrictive temperature, consequently 23 colonies were determined to contain CRABP cDNAs that were specifically interacting with the GABA ρ1 bait. Therefore 0.015% of colonies screened were putative positives and 11.5% turned out to be CRABP clones (Song *et al.*, 2005). Using RP2 as bait to screen 2.6 million colonies 0.02% of colonies screened were putative positives and of those 10% were specific interactors (8% were Arl3). The comparable level of revertants (90% in this screen and 88.5% in the screen by Song *et al*) and highest frequency interactors (8% Arl3 compared to 11.5% CRABP) indicates that the screening process was consistent with published studies using the same system and library.

Since the development of the SRS, a new Ras-based recruitment system has been developed (RRS). The principles are the same and the same cdc25H mutant yeast strain is used, however activated mammalian Ras lacking the prenylation CAAX motif is used for the fusion protein rather than hSos. The loss of the prenylation motif means that the active Ras cannot associate with the membrane unless recruited to the membrane through interaction with a myristoylated cDNA (Broder *et al.*, 1998). This system addresses the problem of Ras false positives; the lack of hSos in the yeast prevents stimulation of the conversion of Ras cDNAs from Ras-GDP to Ras-GTP which occurs in SRS. As Ras is a smaller protein than hSos, some technical difficulties, which occur due to the large size of the *hSos* gene and hence protein, can be overcome (Broder *et al.*, 1998). The RRS would be even better for screening for RP2 interactors than the SRS, however a suitable library would need to constructed.

SRS (CytoTrap) was chosen to investigate RP2 interacting partners for the reasons described previously (Section 3.1.2). There are however other approaches to the analysis of protein:protein interactions. Yeast-two hybrid systems are usually chosen

for use as a screening method to discover new putative interactors, however, directed interactions can also be tested using a yeast-two hybrid approach. Yeast-two hybrid systems have many advantages and disadvantages as previously discussed (Section 3.1), the main problem being the detection of false positives. One of the fundamental advantages of SRS as a Yeast-two hybrid system is that the interactions occur in cytoplasm as opposed to the nucleus, allowing proteins such as transcription factors to be used. However, SRS is a lower throughput system than the traditional transcription-based system requiring more time and optimisation to achieve good results. Furthermore the design of the transcription-based system means that multiple reporter constructs are used which further reduces the processing of false positives. In the SRS system false positives can be generated due to the natural ability of yeast cells to revert to a preferable genotype. Despite the lower throughput and increased incidence of false positives, SRS was the system of choice as it reflects the physiological environment for RP2; RP2 is post-translationaly modified in the cytoplasm and localises to the plasma membrane and CytoTrap is not only cytoplasmic-based but also utilises a myristoylation signal to target prey proteins to the plasma membrane.

Another approach for identifying new interacting partners for a protein is pull down assays followed by mass spectrometrical analysis of the resulting proteins. The success of this approach relies heavily on the parameters set by the investigator and careful analysis of the raw data, for example low abundance proteins may be missed due to falling outside the set conditions. A further advantage of such an approach is the ability to generate interaction profiles by altering the tissue or cell type being used or to use different developmental time points to create a more detailed picture of how a proteins function may alter depending on the conditions. This can also be achieved through using different cDNA libraries for yeast-two hybrid, but library screening is a more time intensive process and so this approach may be more suited to a mass spectrometrical analysis method. A major disadvantage in using mass spectrometry is the lack of distinction between proteins which are direct interactors and those that form part of complex, therefore there is an additional consideration when analysing any results from this method.

Bioinformatics can also provide a starting point for a targeted search for potential interacting partners, using predicted domains and protein families established knowledge about a particular protein can guide a search for novel interacting partners.

All novel interactors discovered through a screening method should be corroborated using a different assay such as a pull-down, yeast two-hybrid or co-immunoprecipitation. Co-immunoprecipitations using endogenous protein provide the most compelling evidence that an interaction is at the very least, physiological. This is not always possible however due to the requirement for specific antibodies and optimal cellular conditions for the interaction. If one of the proteins being investigated is of low abundance this may be a difficult approach, the interaction may also be transitory or may only occur at a very specific time or in response to a particular cellular event, therefore making it hard to detect. Co-immunoprecipitations or pull down assays using over-expressed tagged proteins can overcome these problems but do not provide such robust evidence for an interaction as the conditions are not as physiological and over-expression and tagging can alter the normal properties of a protein. Once identified it is then possible to use interaction assays to map interaction domains and identify important residues for the interaction, it is also important therefore to determine where and when the interaction may occur, usually through the use of co-localisation studies.

The process of optimising the CytoTrap system for the application of identifying RP2 interactors has resulted in a system that has successfully identified RP2 interacting partners. The suitability of the system was confirmed when the previously described RP2 interactor, Arl3, was the most commonly detected cDNA in the screen. This indicates hSos-RP2 fusion protein is expressed, that RP2 is properly folded and that hSos does not occlude interaction sites. Arl3 can be regarded as a very strong interacting partner for RP2. In this system, growth of yeast can be seen as early as day 2 post-replica plating when this interaction occurs which is comparable, if not stronger, than the strong positive control of pSos and pMyrSB (hSos and Rit1). The system was also useful for mapping the RP2 interaction domain of the novel interactors which will be discussed in the next chapters.

The work described in this chapter has been published in part in Evans *et al* (2006).

CHAPTER 4

CHARACTERISATION OF THE INTERACTION OF RP2 AND ARL3

4.1 Introduction

The function of RP2 is still unknown, however, the acylation and localisation of RP2 to the plasma membrane is necessary for the normal function of the protein (Chapple *et al.*, 2000). RP2 was first shown to interact with Arl3 by Bartolini *et al* (2002) as described in section 1.6 , however little else was known about the function of Arl3 or the nature of the RP2-Arl3 interaction at the outset of this research. Arl3 remains the only currently published RP2 interacting protein. During the period of the research described here two important studies were published which have contributed to our understanding of the function of Arl3 and the importance of the RP2-Arl3 interaction. The crystal structure of RP2 has now been solved and the RP2-Arl3 interaction was further investigated by Kuhnel and colleagues (2006), and this will be discussed further in section 4.7 (Kuhnel *et al.*, 2006).

Arl3 and RP2 are both ubiquitously expressed, which leaves the question as to how RP2 mutations exclusively cause RP unresolved. Importantly, Arl3 was recently implicated directly in photoreceptor function and maintenance in a report by Schrick and colleagues describing an Arl3 knockout mouse (Schrick *et al.*, 2006). Homozygous mice lacking Arl3 were born at a sub-Mendelian ratio implying there is a degree of embryonic lethality associated with loss of Arl3 function. The surviving mice died within three weeks and exhibited multiple abnormalities. The abnormalities described in the mice were all cilia-associated defects: renal, hepatic and pancreatic epithelial tubule defects were present which mimicked the symptoms of polycystic kidney disease (PKD), the mice also suffered from retinal dystrophy. Abnormal retinal development was apparent from postnatal day 9. Knockout mice had under-developed inner and outer segments when compared to wild type mice. By postnatal day 13 mice lacking Arl3 had many TUNEL positive cells in the outer nuclear layer (ONL), as well as impaired transport of rhodopsin to the outer segments indicating

compromised photoreceptor development and cell death (Schrick *et al.*, 2006). Arl3 knockout mice have structurally normal cilia, including the photoreceptor connecting cilium, suggesting Arl3 is not important for the cilia structure per se but perhaps is important in cilia function or plays an alternative role such as a regulatory protein or as part of a signalling pathway. The mice also had abnormal cell proliferation patterns, for example with multiple renal cysts resulting from increased cell proliferation. These data implied a direct role for Arl3 in correct development and survival of the photoreceptor cells as well as a possible role in regulation of cell proliferation of other ciliated cells (Schrick *et al.*, 2006). Dysfunction of essential cilia genes is recognised as a common mechanism leading to retinal degeneration (Sections 1.2.3.1, 1.3.3.1, 1.3.4.4). Therefore there is a possibility that the RP2-Arl3 interaction plays a role in the integrity of the photoreceptor connecting cilium and that the progression of disease due to mutations in RP2 may be due to disruption of this function.

This chapter aims to investigate the nature of the RP2-Arl3 interaction and build on the previously known information regarding the interaction in order to elucidate the role of RP2 and Arl3 in the pathogenesis of RP resulting from mutations in RP2.

4.2 Arl3 and Arl2

4.2.1 RP2 interacts with Arl3

Arl3 was the most commonly detected RP2 interactor in the yeast two-hybrid screen as described in Chapter 3. Several different Arl3 cDNAs were identified. Predicted amino acid sequences of three different clones are shown in Figure 4.1A. These clones have different N-termini; cDNA 1 is missing the first 3 amino acids of the predicted sequence, cDNA 2 has an arginine codon prior to the methionine start codon, and cDNA 3 is missing the methionine start codon. This demonstrates that they originated from different cDNA clones. There was no evidence of alternatively spliced isoforms. The cDNAs express nearly full length Arl3, thus giving no indication of the RP2 binding site for Arl3 except that the first 3 amino acids of Arl3 are not necessary for RP2 binding as seen in 'Arl3 cDNA 1' (Figure 4.1). Not all of the Arl3 clones were sequenced as colony PCR was used to identify Arl3 clones during processing as described in sections 2.1.10 and 3.3.1. The predicted bovine Arl3 amino acid sequence is 98.6% identical to human Arl3 with only three amino acid substitutions at positions 79, 152 and 178, two of which are conservative (79 Lysine to Arginine and 178 Asparagine to Serine) (Figure 4.1A).

Arl3 is a member of the Ras superfamily of small GTPases and as such it was possible that it was acting as a false positive in this system. Yeast were re-transformed with the pMyr-Arl3 plasmid and either pSos or pSos-RP2 to ensure that Arl3 was binding specifically to RP2 and not hSos, as described in section 2.2.4. Arl3 was shown to bind specifically to RP2 as there was no growth at the restrictive temperature when hSos and Arl3 are co-expressed (Figure 4.1B).

In order to further test the interaction human Arl3 was cloned into pSos as described in 2.1.2-9 by PCR amplification from an IMAGE clone (No. 3926032) (see section 2.1.10-11). Cdc25-Hα yeast cells were transformed with pSos-Arl3 and grown at the restrictive and permissive temperatures for 10 days (as described in section 2.2.4). The hSos-Arl3 fusion protein appeared to transactivate the SRS system as 50% of the transformed yeast colonies were able to grow at the restrictive temperature in the absence of an interaction. In repeat experiments approximately 50% of pSos-Arl3 transformants grew at 37°C, and 50% did not. Therefore pSos-Arl3 could not be used reliably in the CytoTrap system.

A

```
Bovine Arl3    -MGLLSILRKLKSAPDQEVRILLLGLDNAGKTTLLKQLASE  40
Arl3 cDNA 1    ----LSILRKLKSAPDQEVRILLLGLDNAGKTTLLKQLASE
Arl3 cDNA 2    RMGLLSILRKLKSAPDQEVRILLLGLDNAGKTTLLKQLASE
Arl3 cDNA 3    --GLLSILRKLKSAPDQEVRILLLGLDNAGKTTLLKQLASE
Human Arl3     -MGLLSILRKLKSAPDQEVRILLLGLDNAGKTTLLKQLASE

Bovine Arl3     DISHITPTQGFNIKSVQSQGFKLNVWDIGGQRKIRPYWRN  80
Arl3 cDNA 1     DISHITPTQGFNIKSVQSQGFKLNVWDIGGQRKIRPYWRN
Arl3 cDNA 2     DISHITPTQGFNIKSVQSQGFKLNVWDIGGQRKIRPYWRN
Arl3 cDNA 3     DISHITPTQGFNIKSVQSQGFKLNVWDIGGQRKIRPYWRN
Human Arl3      DISHITPTQGFNIKSVQSQGFKLNVWDIGGQRKIRPYWKN

Bovine Arl3     YFENTDILIYVIDSADRKRFEETGQELAELLEEEKLSCVP  120
Arl3 cDNA 1     YFENTDILIYVIDSADRKRFEETGQELAELLEEEKLSCVP
Arl3 cDNA 2     YFENTDILIYVIDSADRKRFEETGQELAELLEEEKLSCVP
Arl3 cDNA 3     YFENTDILIYVIDSADRKRFEETGQELAELLEEEKLSCVP
Human Arl3      YFENTDILIYVIDSADRKRFEETGQELAELLEEEKLSCVP

Bovine Arl3     VLIFANKQDLLTAAPASEIAEGLNLHTIRDRFWQIQSCSA  160
Arl3 cDNA 1     VLIFANKQDLLTAAPASEIAEGLNLHTIRDRFWQIQSCSA
Arl3 cDNA 2     VLIFANKQDLLTAAPASEIAEGLNLHTIRDRFWQIQSCSA
Arl3 cDNA 3     VLIFANKQDLLTAAPASEIAEGLNLHTIRDRFWQIQSCSA
Human Arl3      VLIFANKQDLLTAAPASEIAEGLNLHTIRDRVWQIQSCSA

Bovine Arl3     LTGEGVQDGMNWVCKNVSAKKK  182
Arl3 cDNA 1     LTGEGVQDGMNWVCKNVSAKKK
Arl3 cDNA 2     LTGEGVQDGMNWVCKNVSAKKK
Arl3 cDNA 3     LTGEGVQDGMNWVCKNVSAKKK
Human Arl3      LTGEGVQDGMNWVCKNVNAKKK
```

B

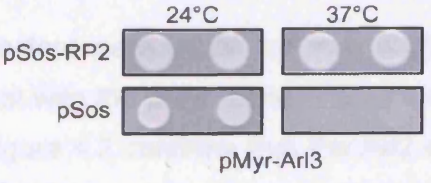

Figure 4.1 Arl3 cDNAs that interacted with RP2

A Predicted amino acid sequences of three different Arl3 cDNAs detected as RP2 interactors using CytoTrap. Residues coloured red indicate differences between the human and bovine Arl3 sequences. **B** Cdc25-Hα yeast transformed with pMyr-Arl3 and pSos-RP2 or pSos showing no growth at 37°C with hSos, and specific growth with Arl3 and hSos-RP2.

4.2.2 RP2-Arl2 interaction

Arl3's closest phylogenetic relative is Arl2, they share 53% primary amino acid sequence identity and 63% similarity (Hillig *et al.*, 2000, Hanzal-Bayer *et al.*, 2002). It has been previously reported that Arl2 and Arl3 share some interacting partners, as described in section 1.6. Arl2 has not been previously reported to bind to RP2 (e.g. Bartolini *et al.*, 2002). In this study, Arl2 was identified as an RP2 interacting partner with six clones isolated from library screening. Two of the Arl2 clones detected as RP2 interactors were sequenced as described in 2.1.9, and were identical in their nucleotide sequence. Other Arl2 clones detected in the screen were identified using bacterial colony PCR as described in 2.1.10 and 3.3.1. The predicted amino acid sequence translated from the Arl2 cDNA clones is shown in Figure 4.2, the 5' sequence prior to the methionine start codon represents in-frame 5'UTR sequence. The predicted amino acid sequence for bovine Arl2 is 99% identical to human Arl2 with amino acid substitutions at positions 108 and 182. There was a single residue in the bovine Arl2 cDNA clone at amino acid position 134 which differed from the predicted bovine Arl2 protein sequence on the UCSC database. UCSC and Genbank databases were used to search for bovine Arl2 cDNAs to compare predicted amino acid sequences. All mRNAs, cDNAs and ESTs on the database were S134, coded by TCC, whereas the two cDNAs isolated from the CytoTrap screen were F134, coded by TTC. This sequence variation may represent a rare polymorphism present in the library or may be due to a mistake in the reverse transcription reaction used to make the library. Human Arl2 (IMAGE clone no. 3140402) was cloned into pSos and used in parallel with the bovine Arl2 cDNA. There was no difference in behaviour when the 2 clones were compared, indicating that the S134F mutation made no difference to the ability of Arl2 to bind to RP2 in this system (data not shown).

All putative interactors were tested for their ability to bind specifically to RP2 by re-transforming yeast with the pMyr clone and either pSos-RP2 or pSos as described in section 2.2.4. Figure 4.2 confirms that the Arl2 cDNA identified in the library screen is only able to stimulate growth of transformed yeast when hSos-RP2 is also present (Figure 4.2).

Having established that both Arl2 and Arl3 could interact with RP2, the relative affinity of each interaction was investigated further. Cdc25-Hα yeast were co-transformed with pSos-RP2 and either pMyr-Arl2 or pMyr-Arl3 as described in section 2.2.4. Tenfold serial dilutions were prepared and 5 µl of the cell suspensions were plated onto appropriate selective media in duplicate and incubated at 24°C and 37°C. Cells

A

```
Bovine Arl2     -------MGLLTILKKMKQKERELRLLMLGLDNAGKTTILKK 35
Arl2 cDNA 1     PGGGYRDMGLLTILKKMKQKERELRLLMLGLDNAGKTTILKK
Human Arl2      -------MGLLTILKKMKQKERELRLLMLGLDNAGKTTILKK

Bovine Arl2     FNGEDIDTISPTLGFNIKTLEHRGFKLNIWDVGGQKSLRSYW 77
Arl2 cDNA 1     FNGEDIDTISPTLGFNIKTLEHRGFKLNIWDVGGQKSLRSYW
Human Arl2      FNGEDIDTISPTLGFNIKTLEHRGFKLNIWDVGGQKSLRSYW

Bovine Arl2     RNYFESTDGLIWVVDSADRQRMQDCQRELQNLLVEERLAGAT 119
Arl2 cDNA 1     RNYFESTDGLIWVVDSADRQRMQDCQRELQNLLVEERLAGAT
Human Arl2      RNYFESTDGLIWVVDSADRQRMQDCQRELQSLLVEERLAGAT

Bovine Arl2     LLIFANKQDLPGALSSNAIREALELDSIRSHHWCIQGCSAVT 161
Arl2 cDNA 1     LLIFANKQDLPGALFSNAIREALELDSIRSHHWCIQGCSAVT
Human Arl2      LLIFANKQDLPGALSSNAIREALELDSIRSHHWCIQGCSAVT

Bovine Arl2     GENLLPGIDWLLDDISSRIFMAD 184
Arl2 cDNA 1     GENLLPGIDWLLDDISSRIFMAD
Human Arl2      GENLLPGIDWLLDDISSRIFTAD
```

B

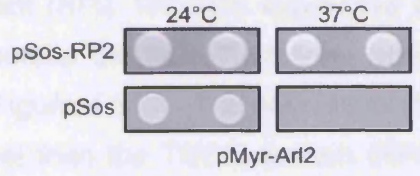

Figure 4.2 RP2-Arl2 interaction detected with CytoTrap

A Predicted amino acid sequence of Arl2 cDNA detected as an RP2 interactor using CytoTrap. Red residues show residues that differ between the bovine and human Arl2 sequences. The blue residue indicates a residue in the cDNA clone that differs from both the human and bovine Arl2 sequences on the database (UCSC). **B** Cdc25-Hα yeast cells transformed with pMyr-Arl2 and pSos-RP2 or pSos showing no growth at 37°C for hSos, and specific binding of Arl2 to RP2.

transformed with pSos-RP2 and pMyr-Arl3 grew at a faster rate compared to RP2-Arl2 co-transformed cells. Figure 4.3A shows the difference observed. Although more yeast were plated in the Arl2 dilutions (as seen at 24°C), at 37°C yeast transformed with Arl3 exhibited more growth. This would indicate that the RP2-Arl3 interaction was of a higher affinity than the RP2-Arl2 interaction.

4.2.3 Domain mapping

RP2 constructs were designed to map the interaction domain of RP2 for any interacting proteins identified. These constructs are shown in the schematic in Figure 4.3B. The constructs were designed to maximise stability of the peptides based on a predicted structure (Evans *et al.*, 2006). The RP2 constructs were designed to determine if the N-terminus (RP2 1-200) or C-terminus (RP2 190-350) contained the binding domain for the putative interacting partner. To further characterise potential binding domains two smaller constructs were designed to include the two known homology domains in RP2: the TBCC homology domain (RP2 41-200) and the NDK homology domain (RP2 238-350) as described in section 1.4.2. The domains were amplified by PCR and cloned into pSos as described in sections 2.1.10-11 and 2.1.2-9. The expression levels of all RP2-hSos constructs were investigated by Western blotting of transformed yeast protein extracts with an antibody to hSos (as described in 2.2.6-8). The expression level of the constructs was different (Figure 4.3C). The C-terminal fragment (RP2 190-350) expressed at a level comparable to full length RP2 (wtRP2), whereas the NDK homology domain (RP2 238-350) expressed at a lower level (see Figure 4.3C). The N-terminal domain (RP2 1-200) expressed at a slightly higher level than the TBCC domain (RP2 41-200), but both expressed at a higher level than the NDK domain (RP2 238-350) and less than full length RP2 (Figure 4.3C).

Having established that the RP2 domain constructs were expressed in Cdc25-Hα cells at detectable levels, the yeast were co-transformed with the RP2-hSos constructs and either pMyr-Arl2 or pMyr-Arl3 (see section 2.2.4). Arl2 required full length RP2 to grow, while the Arl3 interaction was observed with the N-terminus of RP2 (RP2 1-200) (see Figure 4.3D). Yeast growth was also detected with the RP2 41-200 construct co-expressed with Arl3, although less growth was observed compared to wild type RP2 or RP2 1-200. This may be because the RP2 41-200 construct expressed at lower levels than RP2 1-200 (Figure 4.3C).

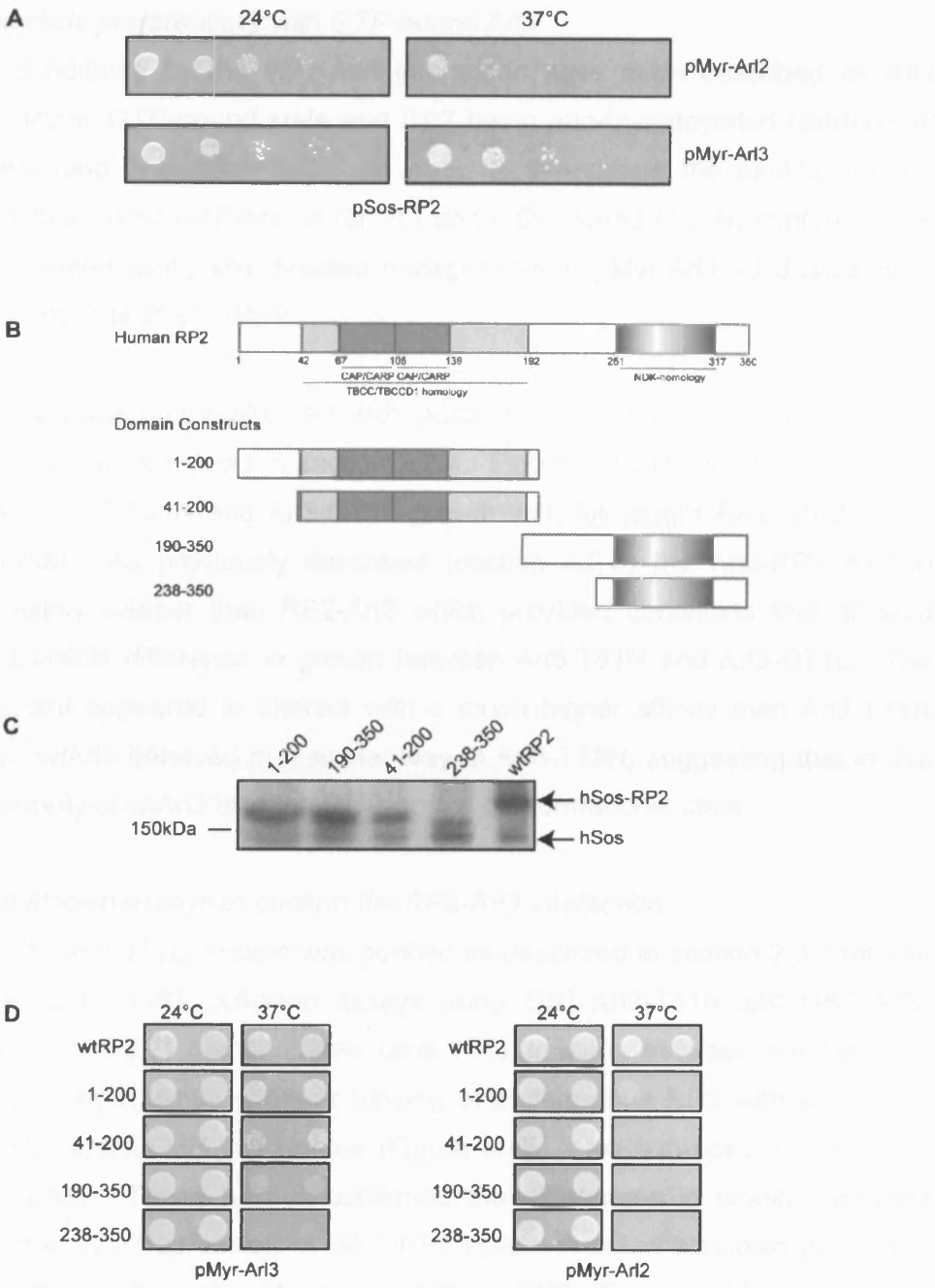

Figure 4.3 Delineation of the Arl binding domain of RP2

A Cdc25-Hα yeast cells co-transformed with pSos-RP2 and pMyr-Arl2 or pMyr-Arl3 grown for 70 hours at the restrictive and permissive temperatures as indicated. **B** Schematic showing RP2 homology domains and the constructs designed for mapping the interaction domain of RP2. **C** Western blot using an antibody to hSos showing the expression levels of RP2 constructs in Cdc25-Hα yeast. **D** Cdc25-Hα yeast co-transformed and grown for 96 hours indicating that Arl3 interacts with the N-terminus of RP2 (1-200). RP2 41-200 was sufficient for growth. Arl2 required full length RP2 for growth.

4.2.4 RP2 interacts preferentially with GTP-bound Arl3

The optimal conditions for the RP2-Arl3 interaction have been described as Arl3 being in the 'active' GTP-bound state and RP2 being non-myristoylated (Bartolini *et al.*, 2002) described in section 1.6.1. In order to investigate the binding further, 'locked' forms that mimic GTP-bound (Q71L) and GDP-bound (T31N) conformations of Arl3 were created using site directed mutagenesis in pMyr-Arl3 as described in section 2.1.12 (Bourne *et al.*, 1990).

Cdc25-Hα cells were co-transformed with pSos-RP2 constructs and each of the pMyr-Arl3 mutants as described in section 2.2.4. Figure 4.4A shows the differences between wtArl3, Arl3-T31N and Arl3-Q71L growth with full length RP2, RP2 1-200 and RP2 41-200. As previously described (section 4.2.3) the Arl3-RP2 41-200 growth was visibly weaker than RP2-Arl3 which provided conditions that allowed detection of a visible difference in growth between Arl3-T31N and Arl3-Q71L. The Arl3-Q71L mutant appeared to interact with a much higher affinity than Arl3-T31N (Figure 4.4A). wtArl3 behaved in a similar way to Arl3-T13N, suggesting that in this system the majority of wtArl3 is in the GDP-bound conformational state.

4.2.4.1 GST pulldown assays to confirm the RP2-Arl3 interaction

GST-Arl3 (T31N and Q71L) protein was purified as described in section 2.3.7 for use in pulldown assays. GST pulldown assays using GST-Arl3-T31N and GST-Arl3-Q71L (see section 2.3.7) demonstrated clear differentiation between the two Arl3 mutants showing significantly stronger binding of endogenous RP2 with Arl3-Q71L using both HeLa and COS7 cell lysates (Figure 4.4B). No non-specific binding to GST was detected. These assays confirmed the differences in binding affinities detected with the CytoTrap assay. A GST-RP2 pulldown assay was also performed to investigate the binding of endogenous Arl3 to RP2 (Figure 4.4C). No clear, specific signal for endogenous Arl3 was detected as binding to GST-RP2 or to GST alone.

4.2.4.2 Co-immunoprecipitations to confirm an RP2-Arl3 interaction

Co-immunoprecipitations were performed to confirm RP2's enhanced binding affinity for Arl3-GTP (Figure 4.5). Co-immunoprecipitations were performed as described in section 2.3.6 using myc-tagged Arl3 constructs and RP2-GFP. The optimal DNA ratios for transfection, in order to obtain good expression of both proteins, was determined to be 1:19 (RP2:Arl3). In control experiments with no RP2-GFP or no myc-Arl3-Q71L no non-specific immunoprecipitation was detected (Figure 4.5A).

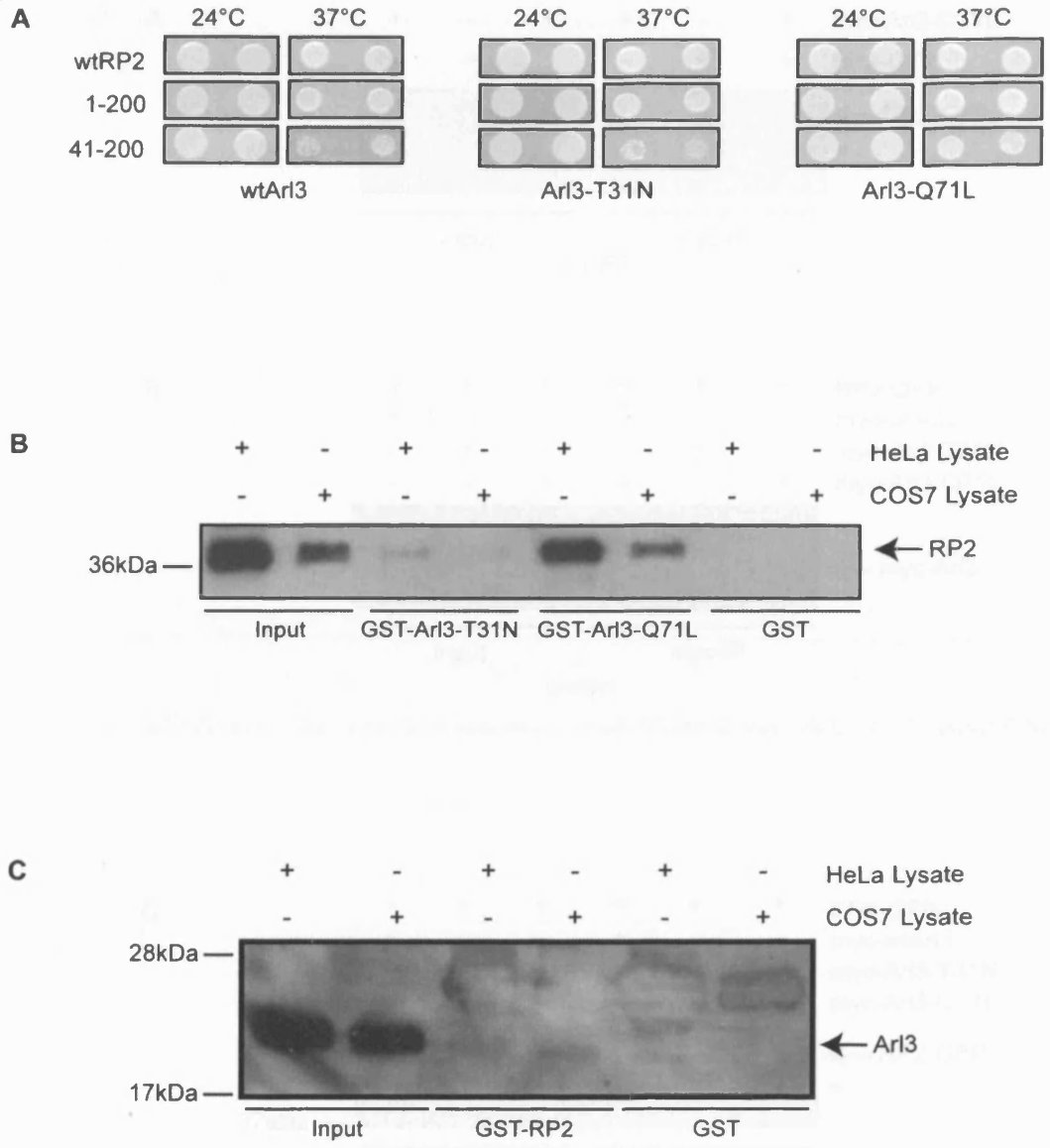

Figure 4.4 RP2 preferentially interacts with Arl3-GTP

A Wild type Arl3 (wtArl3), Arl3-T31N, and Arl3-Q71L pMyr constructs in Cdc25-Hα yeast co-transformed with hSos-RP2 constructs grown at 24°C and 37°C for 72 hours. Comparison of RP2 41-200 with the Arl3 mutants shows more growth with Arl3-GTP. **B** GST pull-down assay using GST-Arl3-T31N, GST-Arl3-Q71L and GST alone with HeLa or COS7 cell lysates. Endogenous RP2 bound to the GST-fusion proteins was detected using an RP2 antibody. **C** GST pull-down assay using GST-RP2 and GST alone with HeLa or COS7 cell lysates. Endogenous Arl3 was detected using an Arl3 antibody.

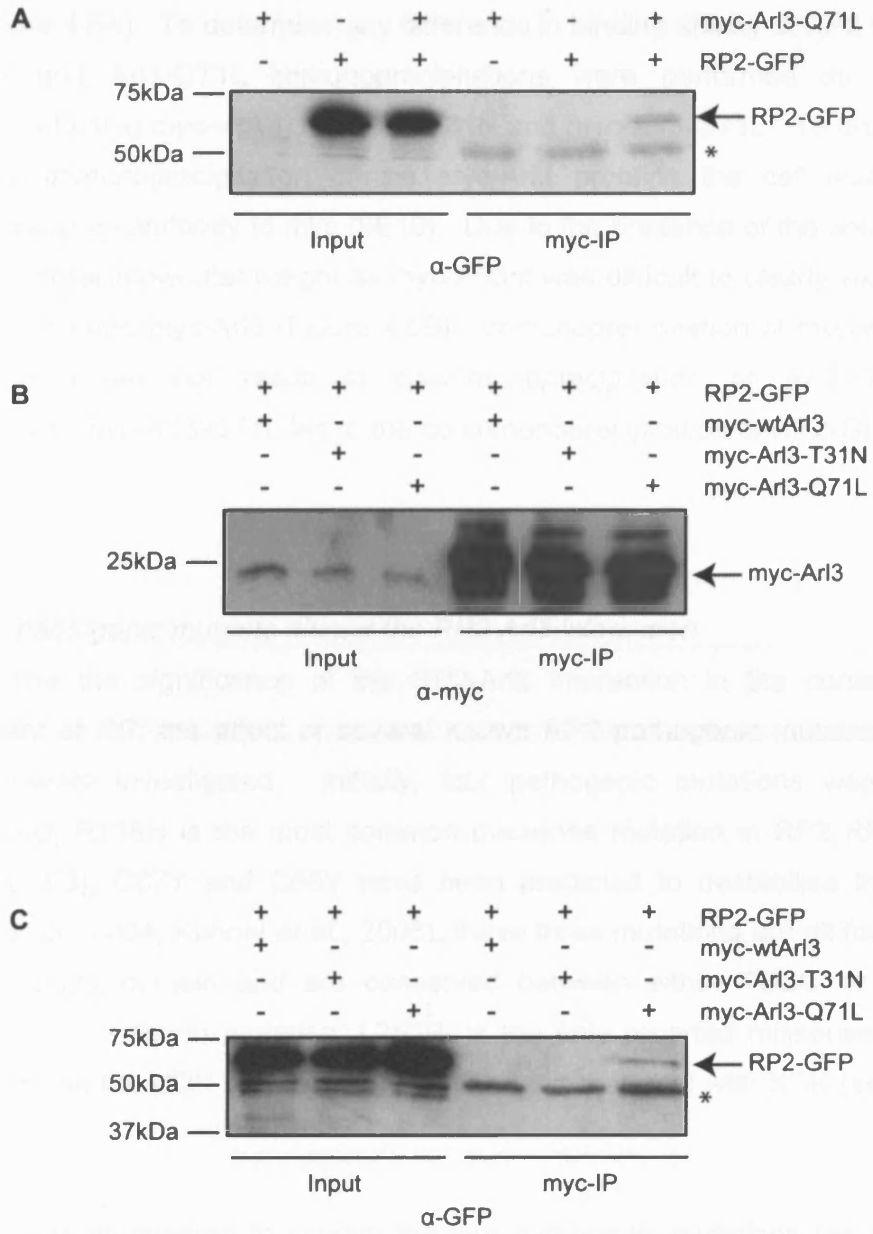

Figure 4.5 Analysis of the RP2-Arl3 interaction using co-immunoprecipitation
A Co-immunoprecipitations of CHO cell lysates transfected with myc-Arl3-Q71 and RP2-GFP, immunoprecipitated with an anti-myc (9E10) antibody and immunoblotted with an antibody to GFP. **B** Analysis of the immunoprecipitated protein was performed using an antibody to myc (9E10). The antibody light chain (at 25kDa) prevented clear visualisation of the immunoprecipitated myc-Arl3 proteins. **C** Co-immunoprecipitations of CHO cell lysates transfected with myc-Arl3 (wt, T31N, Q71L) constructs as indicated and RP2-GFP using the same antibodies as in **A**. * indicates the antibody heavy chain.

There was only detectable co-precipitation of RP2-GFP in the presence of myc-Arl3-Q71L (Figure 4.5A). To determine any difference in binding affinity of RP2 for wtArl3, Arl3-T31N and Arl3-Q71L immunoprecipitations were performed as described previously but using myc-wtArl, myc-Arl3-T31N and myc-Arl3-Q71L. To ensure there was equal immunoprecipitation of the myc-Arl3 proteins the cell lysates were analysed using an antibody to myc (9E10). Due to the presence of the antibody light chain at a similar molecular weight as myc-Arl3 it was difficult to clearly visualise the immunoprecipitated myc-Arl3 (Figure 4.5B). Immunoprecipitation of myc-wtArl3 and myc-Arl3-T31N did not result in co-immunoprecipitation of RP2-GFP, only precipitation of myc-Arl3-Q71L led to the co-immunoprecipitation of RP2-GFP (Figure 4.5C).

4.2.5 RP2 pathogenic mutants disrupt the RP2-Arl3 interaction

To determine the significance of the RP2-Arl3 interaction in the context of the development of RP, the effect of several known RP2 pathogenic mutations on the interaction were investigated. Initially, four pathogenic mutations were chosen (Figure 4.6A); R118H is the most common missense mutation in RP2 RP patients (see Table 1.3), C67Y and C86Y have been predicted to destabilise the protein (Dodatko *et al.*, 2004, Kuhnel *et al.*, 2006), these three mutations are all found in the TBCC homology domain and are conserved between either TBCC or TBCCD1 (Figure 1.4). The fourth mutation, L253R, is the only reported missense mutation which lies within the NDK homology domain and is conserved with NDK (see section 1.4.2.2).

RP2-hSos was engineered to contain the four pathogenic mutations (as previously described in 2.1.12) and these constructs were then used in the CytoTrap system to observe the effects of the mutations on the RP2-Arl3 interaction. The expression levels of the hSos-RP2 fusion proteins were checked, as described in sections 2.2.6-8, and were observed to have different expression levels (Figure 4.6B). The C86Y mutant expressed at a comparatively very low level, with L253R also expressing well below wild type. C67Y and R118H appeared to express at a comparable level to wild type RP2. Each pSos-RP2 mutant was tested for their ability to allow growth at 37°C with pMyr-Arl3, pMyr-Arl3-T31N and pMyr-Arl3-Q71L (Figure 4.6C). Again, wtArl3 and Arl3-T31N behaved similarly while Arl3-Q71L appeared to bind to all the mutant RP2 proteins with a higher affinity. All the RP2 mutants were still able to stimulate growth with Arl3 except C86Y which was only able to grow with Arl3-Q71L, albeit to a

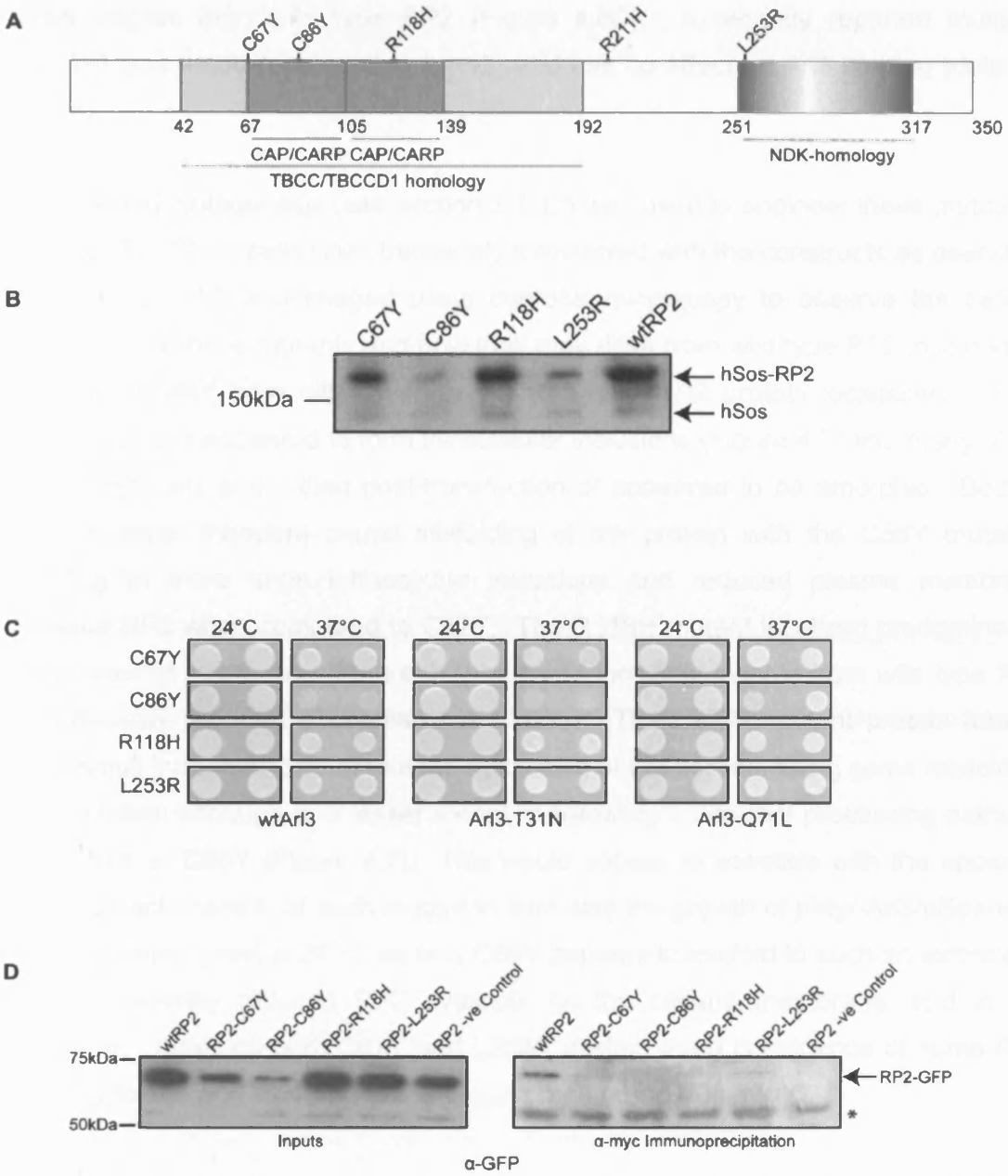

Figure 4.6 Effects of RP2 missense mutations on the affinity of the RP2-Arl3 interaction

A RP2 schematic showing the position of the missense mutations studied. **B** Western blot using an antibody to hSos showing expression levels of the hSos-RP2 mutants in Cdc25-Hα cells. **C** Cdc25-Hα yeast co-transformed with the pSos-RP2 mutants and pMyr-Arl3, pMyr-Arl3-T31N or pMyr-Arl3-Q71L at the restrictive and permissive temperatures. Reduced growth was observed with RP2-C86Y. **D** Co-immunoprecipitations of myc-Arl3-Q71L and RP2-GFP mutants. myc-Arl3-Q71L was precipitated using an antibody to myc and bound RP2-GFP was detected using an antibody to GFP. * indicates the antibody IgG heavy chain.

lesser degree than wild type RP2 (Figure 4.6C). A recently reported mutation (R211H) was made (see section 2.1.12) and has no effect on Arl3 binding (data not shown).

Site directed mutagenesis (see section 2.1.12) was used to engineer these mutations in RP2-GFP. CHO cells were transiently transfected with the constructs as described in section 2.3.4-5 and imaged using confocal microscopy to observe the cellular localisation of these mutants and how they may differ from wild type RP2 localisation. C67Y and C86Y both differed from the wild type RP2 protein localisation. Both mutant proteins appeared to form intracellular inclusions (Figure 4.7) and many of the transfected cells either died post-transfection or appeared to be amorphic. Both of these mutants therefore cause misfolding of the protein with the C86Y mutation resulting in more large intracellular inclusions and reduced plasma membrane localised RP2 when compared to C67Y. The R118H mutant localised predominantly to the plasma membrane (Figure 4.7) and was indistinguishable from wild type RP2 as previously reported (Chapple *et al.*, 2000). The L253R mutant protein formed many small inclusions throughout the cytoplasm of the cell indicating some misfolding of the protein although to a lesser extent or following a different processing pathway than C67Y or C86Y (Figure 4.7). This would appear to correlate with the apparent ability, or lack thereof, of each mutant to stimulate the growth of pMyr-Arl3/pSos-RP2 co-transformed yeast at 37°C, as only C86Y appears to misfold to such an extent that there is severely reduced RP2 available on the plasma membrane, and in the cytoplasm. Although both C67Y and L253R misfold there is evidence of some RP2 correctly folded and localised to the plasma membrane (Figure 4.7).

Co-immunoprecipitations were also used to analyse the binding of RP2 mutants to Arl3. This method had previously provided a complementary method to distinguish binding affinities (section 4.2.3.2). Co-immunoprecipitations were performed as previously described in 2.3.6 and are shown in Figure 4.6D. The 'Inputs' panel shows the amount of expressed and soluble RP2 and this appears to correlate with the immunocytochemistry (Figure 4.7) and hSos-RP2 expression levels (Figure 4.6B). C86Y was expressed at the lowest level, most likely due to misfolding and subsequent degradation or insolubility. wtRP2 was expressed at the highest level and was immunoprecipitated with Arl3-Q71L. Longer exposures revealed both C67Y and L253R were co-immunoprecipitated, but at considerably lower levels than wtRP2. There was no evidence of C86Y being precipitated with Arl3-Q71L but this is most likely due to the low level of protein input in the assay, it could be predicted that

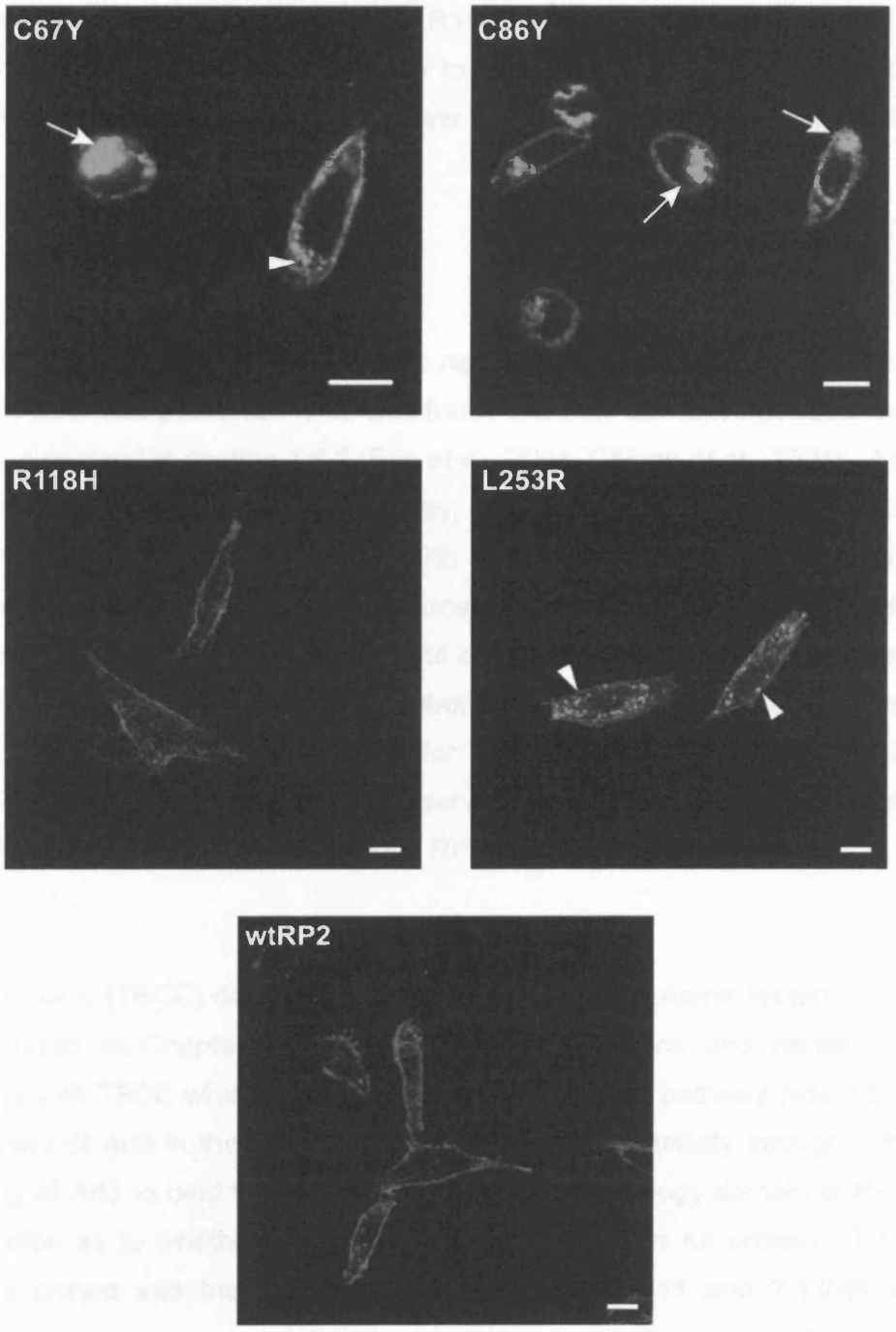

Figure 4.7 Subcellular localisation of RP2 pathogenic mutants

Immunofluorescence confocal microscopy of CHO cells transfected with RP2-GFP mutant constructs, showing mis-localisation of RP2 for C67Y (small and large inclusions), C86Y (large inclusions) and L253R (small cytoplasmic inclusions) mutants. Plasma membrane staining was observed for wtRP2 and R118H-RP2. The larger peri-nuclear inclusions are marked by arrows and smaller inclusions are highlighted with arrowheads. Scale bars are 10 μm.

if there was a comparable level of soluble protein as wild type, binding to Arl3-Q71L may have been detected. Interestingly, R118H was not immunoprecipitated despite being expressed at a level comparable to wild type RP2. Arl2 could not be co-immunoprecipitated with RP2 under any conditions (see Figure 4.6D negative control).

4.3 Arl6 does not interact with RP2

During the course of this study the first reported role in human disease for an Arl family member was published. Arl6 was found to be the causative gene for the BBS3 locus as discussed in section 1.6.3 (Fan *et al.*, 2004, Chiang *et al.*, 2004). As one of the phenotypes of BBS is retinal dystrophy, and Arl6 is also involved in cilia function, Arl6 was tested for its ability to bind to RP2. Arl6 was amplified from an IMAGE clone as described in section 2.1.10-11 and cloned into the pMyr vector. Cdc25-Hα yeast cells were transformed with pSos-RP2 and either pMyr-Arl6, pMyrSB (positive control plasmid) or pMyrLaminC (negative control plasmid) and tested for growth at the permissive and restrictive temperatures for 7 days (see section 2.2.4). As shown in Figure 4.8A, there was no growth observed for the RP2-Arl6 two-hybrid assay suggesting that Arl6 is not able to bind to RP2.

4.4 Cofactor C (TBCC) does not interact with any Arl proteins tested

As discussed in Chapter 1, RP2 shares both sequence and partial functional homology with TBCC which functions in the tubulin folding pathway (see 1.5.2). The involvement of Arl2 in the regulation of the tubulin GAP activity through TBCD and the ability of Arl3 to bind to RP2 through the TBCC homology domain of RP2 led to the question as to whether TBCC was able to bind to an Arl protein. TBCC was therefore cloned into the pSos vector (sections 2.1.10-11 and 2.1.2-9) and the expression level was analysed after transforming yeast with the plasmid as described in sections 2.2.6-8 (Figure 4.8B). The hSos-TBCC protein expressed at a level similar to wtRP2 as shown in Figure 4.8B and the hSos moiety was functional, as yeast growth was observed using the positive control pMyrSB plasmid (Figure 4.8C). Cdc25-Hα yeast were co-transformed with pSos-TBCC and pMyr-Arl2, wtArl3, Arl3-T31N, Arl3-Q71L, and Arl6 as described in section 2.2.4. After 10 days of observation at the restrictive and permissive temperatures there was no evidence of an interaction between TBCC and any of the Arl proteins tested (Figure 4.8C).

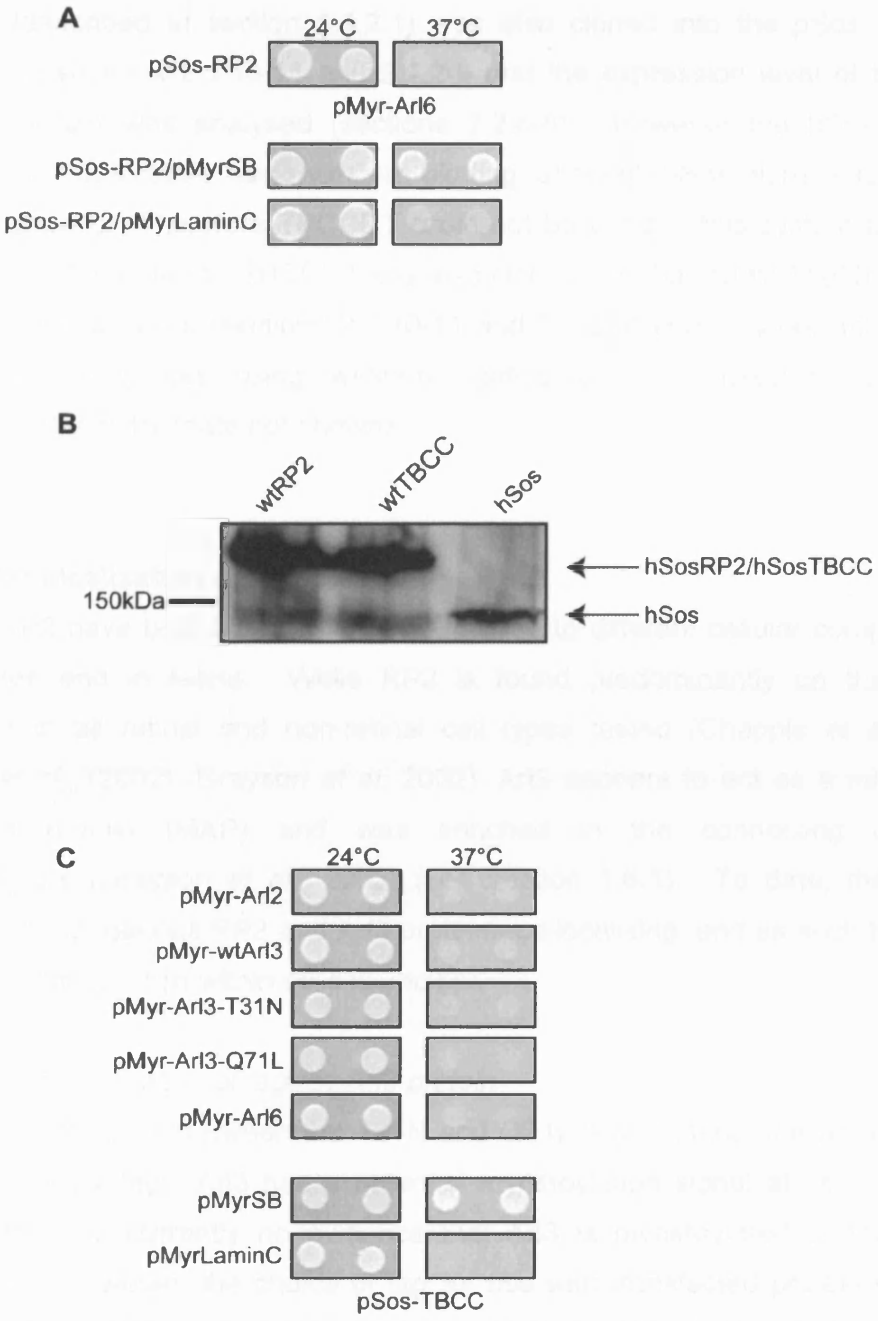

Figure 4.8 Interaction of the Arl family of proteins with RP2 and its homolog TBCC

A Cdc25-Hα yeast co-transformed with pSos-RP2 and pMyr-Arl6 and control plasmids grown for 96 hours at the restrictive and permissive temperatures. **B** Western blot of co-transformed yeast total protein using an antibody to hSos shows that hSos-TBCC protein is expressed. **C** Cdc25-Hα yeast co-transformed with pSos-TBCC and various pMyr-Arl plasmids and grown for 120 hours at the restrictive and permissive temperatures. The positive control shows the hSos moiety of the hSos-TBCC fusion protein is functional in the system.

TBCCD1 (described in section 1.4.2.1) was also cloned into the pSos vector as described in sections 2.1.10-11 and 2.1.2-9 and the expression level of the hSos-TBCCD1 protein was analysed (sections 2.2.6-8). However the hSos-TBCCD1 protein was undetectable using western blotting, although hSos alone was detected (data not shown). Therefore TBCCD1 could not be used in this system to analyse binding to the Arl proteins. TBCCD1 was also cloned into the pCMV-Tag3b vector for use in mammalian cells (sections 2.1.10-11 and 2.1.2-9) and was not detectable in transfected cell lysates using western blotting or in transfected cells using immunocytochemistry (data not shown).

4.5 Cellular localisation of RP2 and Arl3

Arl3 and RP2 have both been reported to localise to different cellular compartments in cell lines and in retina. While RP2 is found predominantly on the plasma membrane in all retinal and non-retinal cell types tested (Chapple *et al* (2000), Chapple *et al.*, (2002), Grayson *et al.* 2002), Arl3 appears to act as a microtubule associated protein (MAP) and was enriched in the connecting cilium in photoreceptors (Grayson *et al.*, 2002) (see section 1.6.1). To date, there is no evidence of endogenous RP2 and Arl3 proteins co-localising, and as such the site of the RP2-Arl3 interaction within cells is unclear.

4.5.1 Cellular localisation of tagged Arl3 protein

In order to distinguish between the T31N and Q71L Arl3 mutants the proteins were expressed with a tag. Arl3 has a potential myristoylation signal at its N-terminus, although there is currently no evidence that Arl3 is myristoylated or targeted to membranes. However, the choice of tag for use with transfected protein may alter the potential for this post translational modification. The Arl3 mutant constructs (T31N and Q71L) were, therefore, cloned into vectors with N- and C-terminal tags and all experiments were performed with Arl3 tagged at both termini. myc-wtArl3, myc-Arl3-T31N, myc-Arl3-Q71L, wtArl3-VSV, Arl3-T31N-VSV, and Arl3-Q71L-VSV were transfected into CHO cells as described in section 2.3.4-5 and all had a similar subcellular localisation. The protein was observed diffusely throughout the cell, predominantly localised to the cytoplasm with some nuclear staining evident (Figure 4.9).

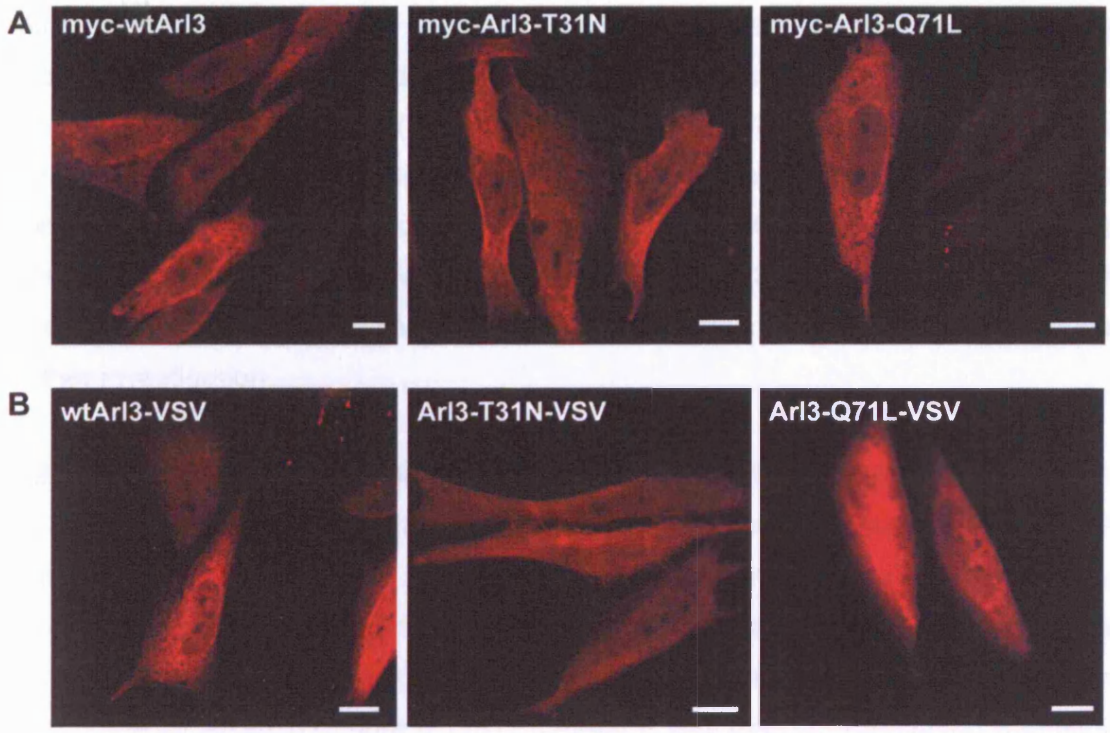

Figure 4.9 Subcellular localisation of tagged Arl3

A Immunofluorescence of CHO cells transiently transfected with myc-wtArl3, myc-Arl3-T31N, or myc-Arl3-Q71L. **B** Immunofluorescence microscopy of CHO cells transiently transfected with wtArl3-VSV, Arl3-T31N-VSV or Arl3-Q71L-VSV. All scale bars are 10μm.

4.5.2 Localisation of endogenous RP2 when Arl3 was over-expressed

Endogenous RP2 localisation was investigated in HeLa cells (see sections 2.3.4-5) and was observed to localise predominantly to the plasma membrane and exhibited some cytoplasmic staining (Figure 4.10A) as previously reported (Chapple *et al.*, 2000, Chapple *et al.*, 2002, Grayson *et al.*, 2002). The effect of excess Arl3 on RP2 localisation was investigated. HeLa cells were transiently transfected with myc-Arl3 mutants and were stained for endogenous RP2 and the transfected Arl3 protein (see sections 2.3.4 and 2.3.5. Endogenous RP2 localisation did not appear to alter in the presence of myc-Arl3-T31N (Figure 4.10B). However, an increase in intracellular RP2 surrounding the nucleus was observed in the presence of myc-Arl3-Q71L in approximately 30% of transfected cells (see Figure 4.10C). This localisation pattern was also occasionally observed in cells lacking myc-Arl3-Q71L (approximately 10% of cells observed). The significance of this re-localisation of RP2, therefore, required further investigation.

4.5.3 Investigation of the co-localisation of RP2-GFP and myc-Arl3-Q71L

To further investigate the ability of Arl3-Q71L to promote the relocalisation of RP2 and to determine if there was any co-localisation between RP2 and Arl3, the effect of co-expressing RP2-GFP and myc-Arl3 was investigated. RP2-GFP alone was transfected into CHO cells (see 2.3.4-5) and exhibited a predominantly plasma membrane localisation (Figure 4.11A). RP2-GFP was then co-transfected with either myc-Arl3-T31N or myc-Arl3-Q71L into CHO cells and the cells were stained with an antibody to the myc tag. When RP2-GFP and myc-Arl3-T31N were co-transfected there was no alteration in the localisation of either protein and no evidence of any co-localisation (Figure 4.11B). Importantly, when RP2-GFP and myc-Arl3-Q71L were co-transfected both proteins exhibited an alteration in their localisation and apparent co-localisation (Figure 4.11C). RP2-GFP was enriched intracellularly, in particular there was enhanced staining for RP2-GFP around the nucleus in a triangular pattern, suggestive of Golgi staining. myc-Arl3-Q71L co-localised with RP2-GFP and was also enriched in an apparent Golgi-like pattern. Myc-Arl3-Q71L was also occasionally observed on the plasma membrane when co-transfected with RP2-GFP.

4.5.4 Characterisation of the RP2 and Arl3-Q71L interaction

To investigate the re-localisation of RP2-GFP and myc-Arl3-Q71L a range of cellular markers were used for double labelling. CHO cells were transfected as described above but Arl3 was not stained and instead antibodies to resident proteins of the ER and Golgi were used. Calnexin was chosen as an ER marker as, it is an ER

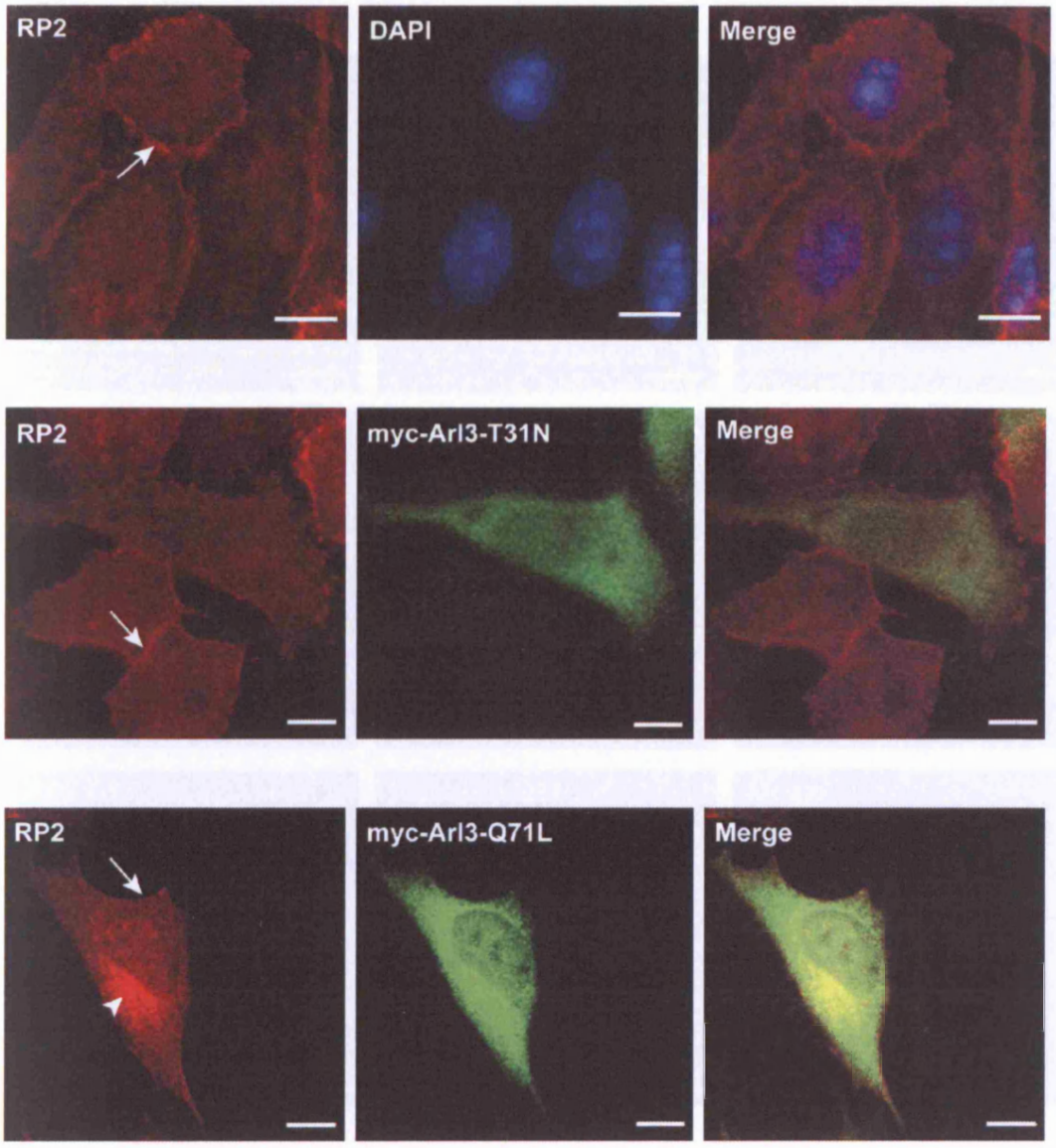

Figure 4.10 Localisation of endogenous RP2 with Arl3 over-expression

A Immunofluorescence of HeLa cells stained with an anti-sheep RP2 antibody. Endogenous RP2 was localised to the cytoplasm and the plasma membrane (arrows highlight plasma membrane staining). **B** Transient transfection with myc-Arl3-T31N and stained for endogenous RP2 and myc-tagged Arl3 in HeLa cells. **C** Transient transfection with myc-Arl3-Q71L and stained for endogenous RP2 and myc-tagged protein. Arrowhead highlights intracellular RP2. All scale bars are 10 μm.

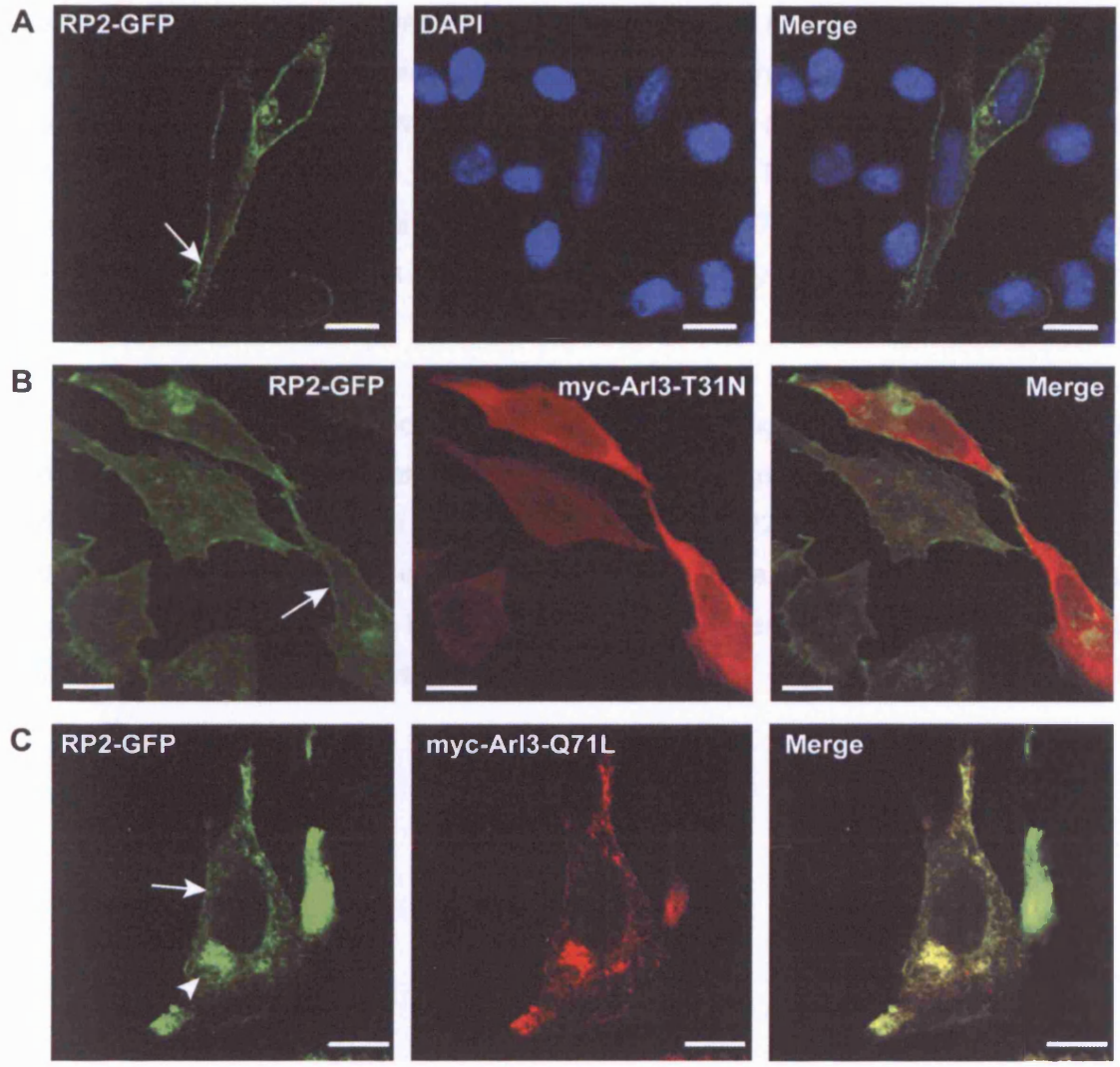

Figure 4.11 RP2-GFP co-localised with myc-Arl3-Q71L

A Immunofluorescence of CHO cells transfected with RP2-GFP showed predominant plasma membrane localisation. Arrows highlight plasma membrane staining. **B** CHO cells transfected with RP2-GFP and myc-Arl3-T31N and stained with an antibody to myc. There was no evidence of co-localisation between RP2-GFP and myc-Arl3-T31N. **C** CHO cells transfected with RP2-GFP and myc-Arl3-Q71L and stained using an antibody to myc showing extensive co-localisation between RP2-GFP and myc-Arl3-Q71L, highlighted by the arrowhead. All scale bars are 10 μm.

resident chaperone. No co-localisation was observed between the intracellular RP2-GFP and calnexin (see Figure 4.12A). β-COP was used as a Golgi marker and in this case co-localisation between intracellular RP2-GFP and β-COP was observed, suggesting the intracellular re-localisation pattern is consistent with Golgi staining (Figure 4.12B). In cells transfected with RP2-GFP alone, RP2-GFP was not observed to co-localise with β-COP (Figure 4.12C). These data show that the intracellular RP2 observed in the presence of myc-Arl3-Q71L is Golgi associated and in the absence of Arl3-Q71L is not Golgi localised but may correspond to an inclusion from over-expression.

Further investigation of the increased intracellular staining pattern of RP2-GFP was done using a vesicular marker. Early endosome antigen 1 (EEA1) is a marker for early endosomes. CHO cells were transfected with RP2-GFP and myc-Arl3-Q71L and then stained for EEA1 as described in 2.3.4-5. Figure 4.13 shows that there was no evidence of co-localisation between the two proteins and it is unlikely that RP2 is involved in early endosome vesicle trafficking.

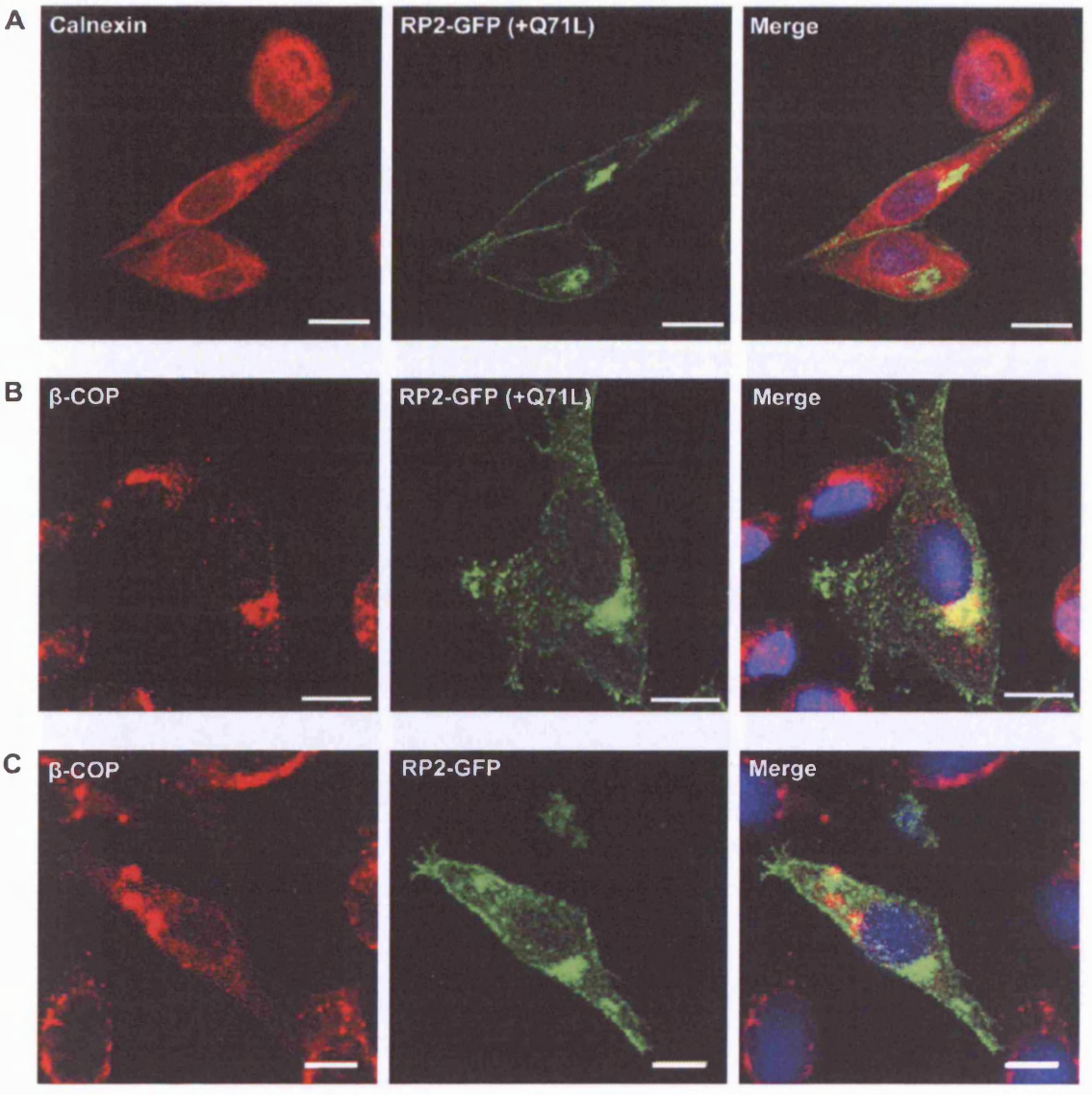

Figure 4.12 RP2-GFP co-localised with β-COP in the presence of Arl3-GTP

A Immunofluorescence of CHO cells transfected with RP2-GFP and myc-Arl3-Q71L and stained with calnexin showed no co-localisation between intracellular RP2-GFP and calnexin. **B** CHO cells transfected with RP2-GFP and myc-Arl3-Q71L and stained with β-COP showed co-localisation between intracellular RP2-GFP and β-COP. **C** CHO cells transfected with RP2-GFP alone and stained with β-COP showed no co-localisation between intracellular RP2-GFP and β-COP. All scale bars are 10 μm.

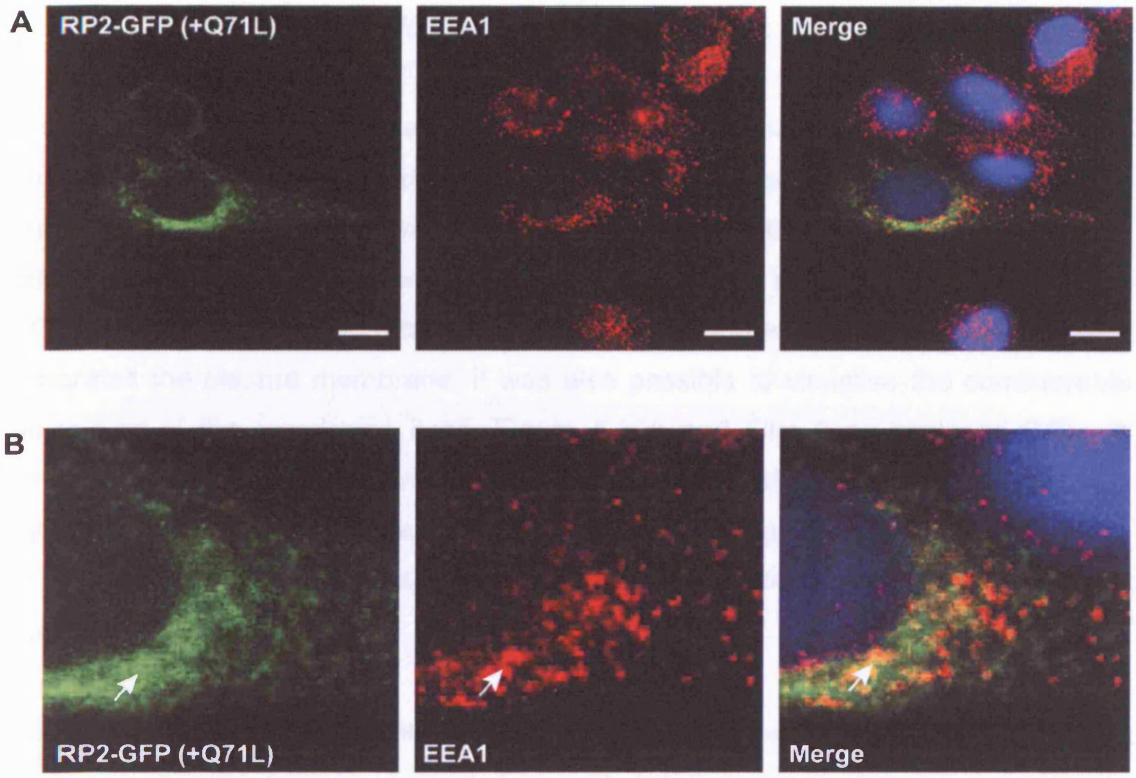

Figure 4.13 RP2-GFP did not co-localise with EEA1

A Immunofluorescence of CHO cells transfected with RP2-GFP and myc-Arl3-Q71L and stained with EEA1. **B** Zoom of panel A showed no evidence of extensive co-localisation between RP2-GFP and EEA1. Arrow highlights a region of potential co-localisation. All scale bars are 10 µm.

4.6 Live imaging of RP2-GFP

The data from the study described above showed a possible site of interaction for RP2 and Arl3 at the Golgi. Interestingly other studies show that Arl proteins are involved in protein trafficking at the Golgi (Zhou *et al.*, 2006, van Valkenburgh *et al.*, 2001). These data suggest that RP2 may have a novel role in the regulation of, or a direct involvement in, protein trafficking to or from the Golgi. To investigate this hypothesis further and to visualise the normal movement of RP2 in the cell, live imaging of RP2-GFP was performed.

CHO cells were transfected with RP2-GFP and myc-Arl3 constructs and the cells were then imaged in real time using a Zeiss Axiovert 100M microscope and Improvision software for ten minutes as described in section 2.3.8. RP2-GFP alone exhibited the expected predominant plasma membrane staining with some protein visible in small vesicles moving intracellularly (Figure 4.14B). Because RP2 decorates the plasma membrane, it was also possible to visualise the considerable movement of the membrane itself (Figure 4.14A and Film 1 on enclosed CD). A similar localisation and movement was seen when RP2-GFP was co-transfected with myc-Arl3-T31N (Figure 4.15 and Film 2). However, a significant difference in RP2-GFP cellular localisation was observed when co-transfected with myc-Arl3-Q71L (Figure 4.16 and Film 3).

The previously observed altered localisation with an increase in intracellular RP2 in a Golgi-like staining pattern (section 4.5) was noted in these imaging experiments (Figure 4.11C and 4.12B). There was also a change in behaviour of the RP2-GFP. In the presence of myc-Arl3-Q71L the RP2-GFP became more dynamic and there appeared to be more intracellular vesicles containing RP2 in the cell (Figure 4.16).

In order to ensure the change in RP2 behaviour was specific and due to the RP2-Arl3 interaction and not an indirect effect of Arl3-Q71L on membrane traffic, a severely truncated RP2-GFP construct was used. The first 15 amino acids of RP2 fused to GFP (Chapple *et al.*, 2002) is sufficient for the construct to be localised to the plasma membrane and as Arl3 was not able to interact with RP2 through the first 15 amino acids (see section 4.2.3) this acts as an RP2 control which should not be directly affected by the presence of myc-Arl3-Q71L. The truncated-RP2-GFP when co-transfected with myc-Arl3-Q71L, did not exhibit the intracellular staining observed with wtRP2 but did localise to the membrane (Figure 4.17A and Film 4).

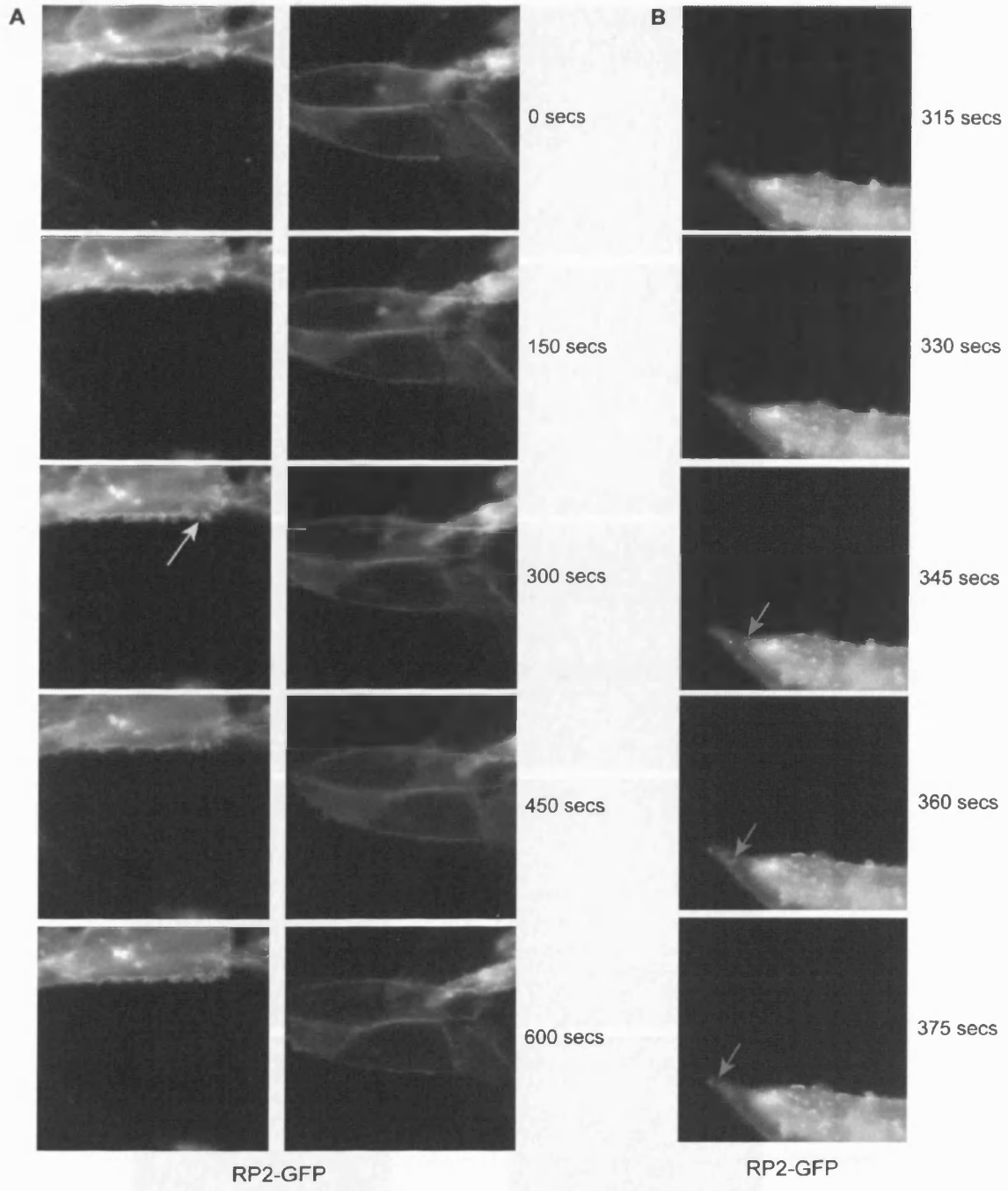

Figure 4.14 Live imaging of RP2-GFP

A CHO cells transfected with RP2-GFP and imaged in real time using a Zeiss Axiovert 100M microscope and Improvision software. The majority of movement seen is due to RP2-GFP highlighting the movement of the plasma membrane, an example is highlighted with the yellow arrow. **B** CHO cells treated as in **A**, the stills are taken over a one minute period and show an example of a vesicle moving to the plasma membrane, highlighted with the red arrow.

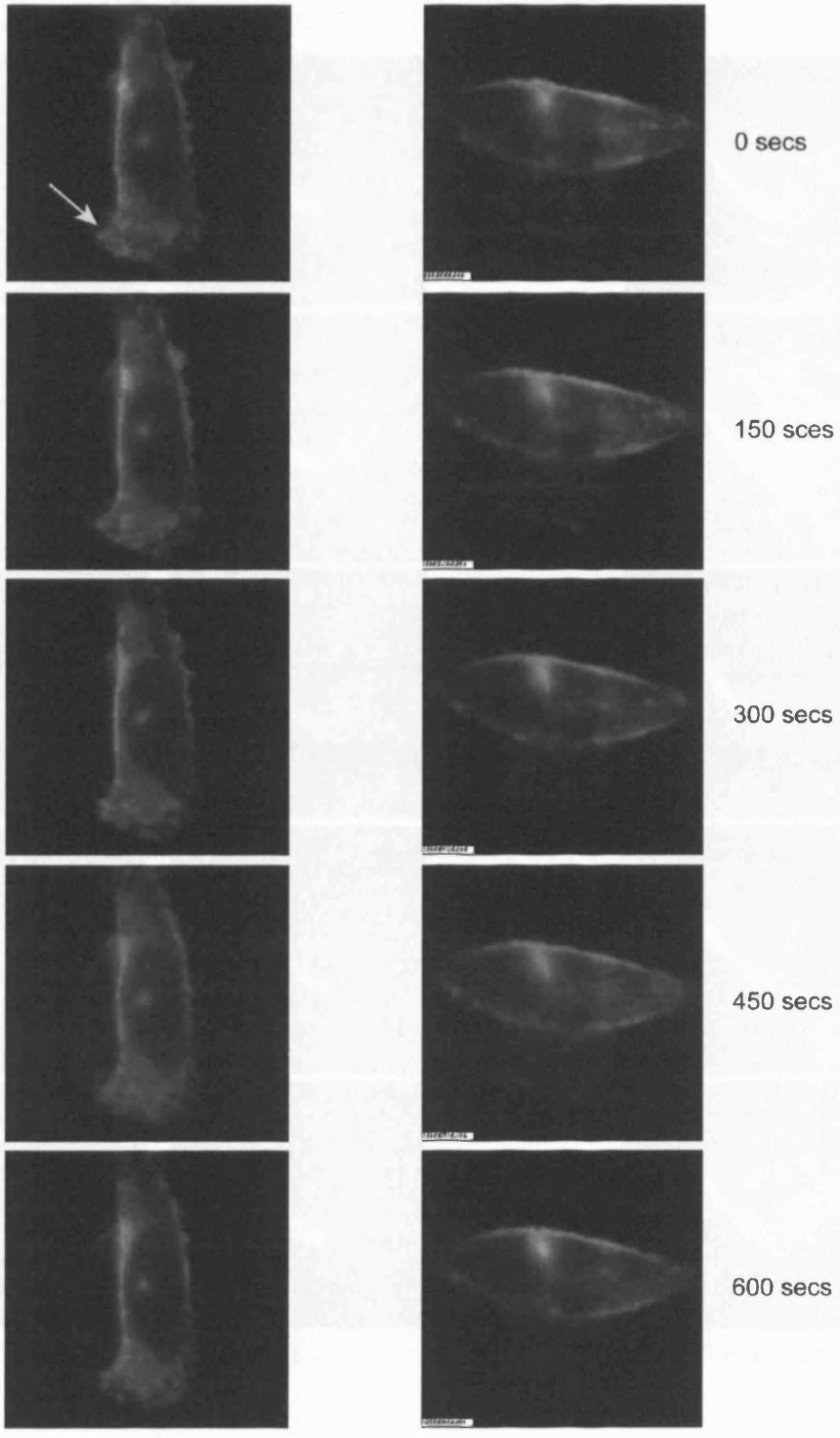

Figure 4.15 Live imaging of RP2-GFP co-expressed with myc-Arl3-T31N

CHO cells transfected with RP2-GFP and myc-Arl3-T31N and imaged in real time using a Zeiss Axiovert 100M microscope and Improvision software. The yellow arrow indicates an area of plasma membrane 'blebbing'. There is relatively little intracellular movement of RP2-GFP.

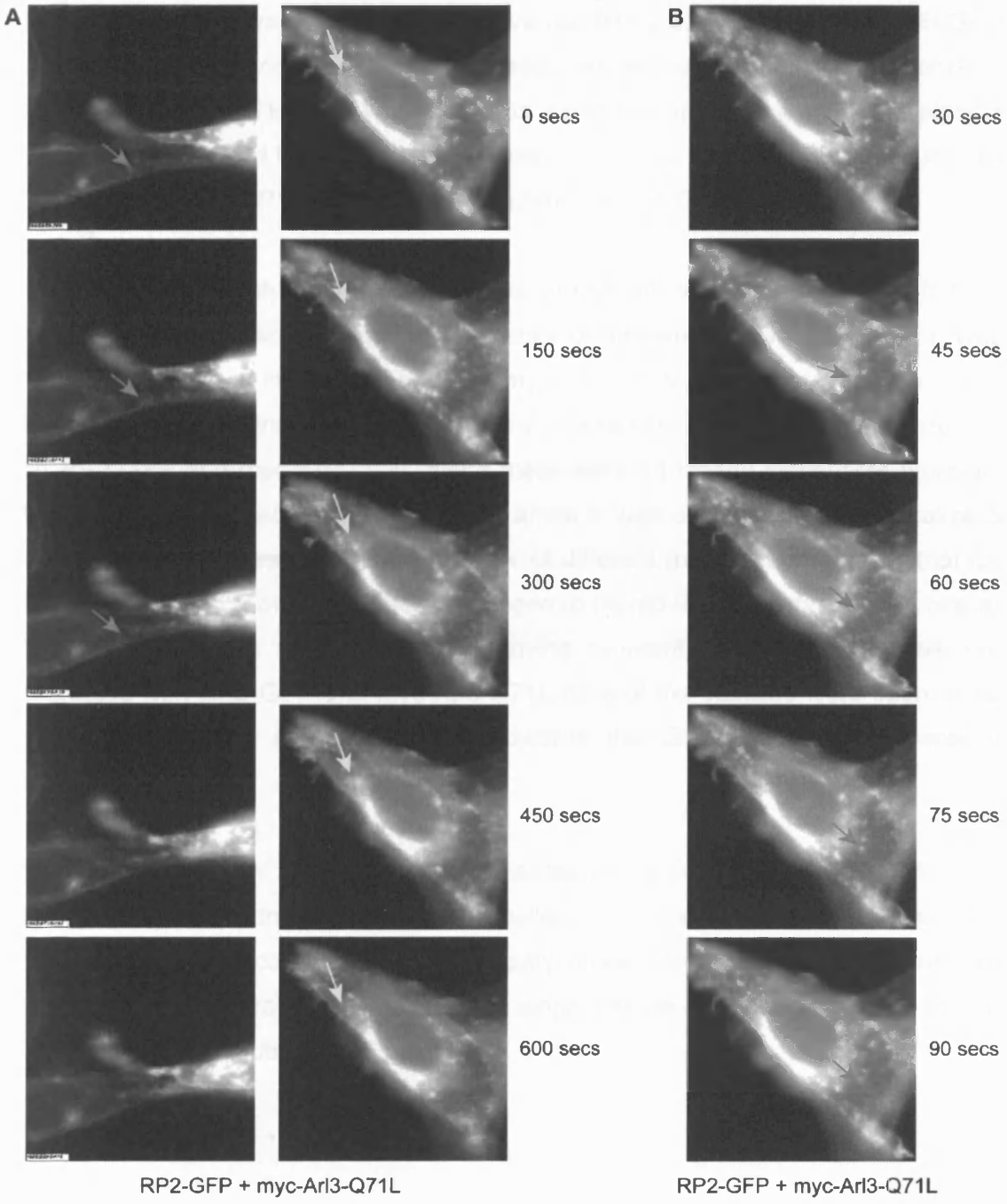

Figure 4.16 Live imaging of RP2-GFP co-expressed with myc-Arl3-Q71L

A CHO cells transfected with RP2-GFP and myc-Arl3-Q71L and imaged in real time using a Zeiss Axiovert 100M microscope and Improvision software. The pink arrow shows an example of a vesicle moving toward the Golgi. The yellow arrow shows where vesicles appear to bud out from the Golgi. **B** CHO cells treated as in **A**, the stills are taken over a one minute period and show an example of a vesicle moving to the plasma membrane, highlighted by the red arrow.

RP2-R118H-GFP was co-transfected into CHO cells with myc-Arl3-Q71L and the RP2-GFP was observed as described above (section 2.3.8). The RP2-R118H-GFP did not show altered localisation and increased vesicle movement in the presence of Arl3-GTP (Figure 4.17B and Film 5) but was visualised predominantly at the plasma membrane. The R118H mutant was used in these experiments because as previously shown the R118H is not able to interact with Arl3 (section 4.2.4).

Some preliminary analysis of the intracellular movement of RP2-GFP was performed by counting vesicles and measuring their rates of movement. When RP2-GFP was transfected alone or in the presence of myc-Arl3-T31N there were notably fewer intracellular vesicles than with Arl3-Q71L. For example, in one cell co-transfected with RP2-GFP and myc-Arl3-Q71L alone there were 23 clearly identifiable vesicles, whilst in a cell transfected with RP2-GFP alone it was only possible to visualize 5 vesicles. Counting vesicles from a number of different movies it was noted that for RP2-GFP alone 66% of the vesicles were seen to be moving towards the membrane, while the other 34% appeared to be moving randomly. When cells were co-transfected with RP2-GFP and myc-Arl3-Q71L 65% of the vesicles were seen to be moving towards the membrane, 25% towards the Golgi and 10% apparently randomly.

The rate of movement of the RP2-GFP vesicles in the presence of Arl3-Q71L was estimated by measuring the distance travelled over time. However the estimate obtained may be inaccurate due to the difficulty in precisely following a single vesicle. An estimation for the rate of movement of a single vesicle (for an example see Figure 4.16B) was 4 μm/minute or 0.06 μm/s.

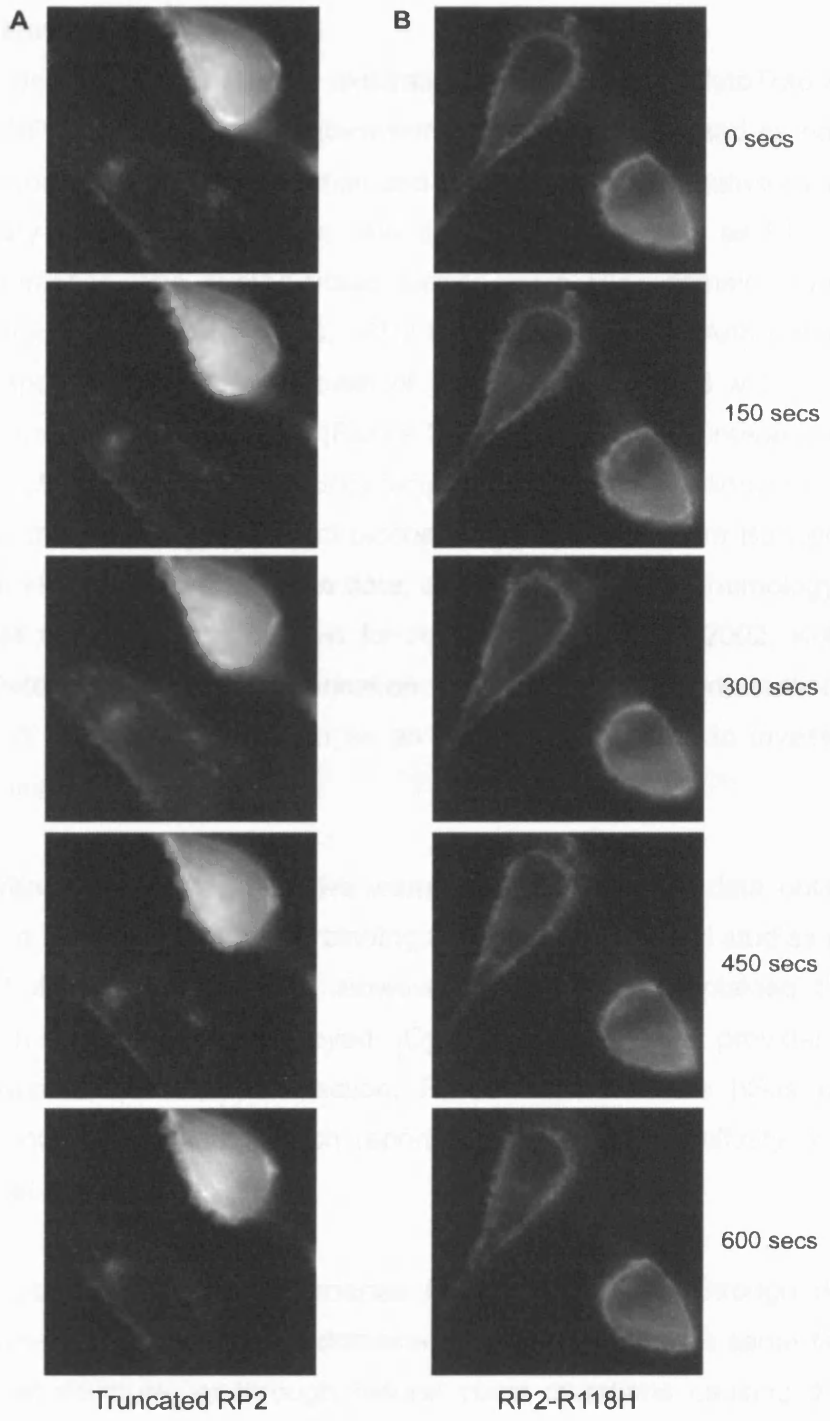

Figure 4.17 Live imaging of a truncated RP2-GFP construct and RP2-R118H-GFP co-expressed with myc-Arl3-T31N

A CHO cells transfected with truncated RP2-GFP and myc-Arl3-Q71L and imaged in real time using a Zeiss Axiovert 100M microscope and Improvision software. **B** CHO cells transfected with RP2-R118H-GFP myc-Arl3-Q71L and imaged in real time using a Zeiss Axiovert 100M microscope and Improvision software. All the RP-GFP movement appears to occur at the membrane.

4.7 Discussion

The data presented in this chapter illustrates the suitability of CytoTrap as a tool to investigate RP2's protein-protein interactions. CytoTrap was used to independently confirm the known RP2-Arl3 interaction and identified a novel putative RP2 interactor; Arl2. Library screening resulted in detection of 45 Arl3 clones as RP2 interactors, and the interaction was characterised further using RP2 domain constructs and pathogenic mutants (Section 4.2.3). RP2 has high affinity for Arl3 in the CytoTrap system as shown by the faster growth of yeast co-transformed with pSosRP2 and pMyrArl3 than the positive control (Figure 3.4). The RP2-Arl3 interaction was then further characterised using co-immunoprecipitations and GST pulldown assays which showed that the proteins do interact biochemically. Studies from Bartolini *et al* and Kuhnel *et al* also corroborated these data, confirming the TBCC-homology domain of RP2 acts as the interaction domain for Arl3 (Bartolini *et al.*, 2002, Kuhnel *et al.*, 2006). Detection and characterisation of the RP2-Arl3 interaction provided confidence in the CytoTrap system as an appropriate method to investigate novel RP2 interacting partners.

Some differences in binding affinities were observed between data obtained using CytoTrap and data from alternative binding assays and published studies (Bartolini *et al.*, 2002, Kuhnel *et al.*, 2006). However, this may be explained through the differences in methodologies employed. CytoTrap by its design provides one of the optimum conditions for this interaction; RP2 is fused to the hSos protein and therefore is not myristoylated which reportedly enhances the affinity of interaction (Bartolini *et al.*, 2002).

Yeast two-hybrid methods can generate false positive data through detection of interactions mediated by common domains, or proteins from the same family which exhibit similar structure, or through natural yeast mutations causing the yeast to behave as if an interaction was detected. It is possible that Arl2 is a false positive given the sequence and structural similarity with Arl3, which may account for the 6 Arl2 clones detected. The interaction was not confirmed using co-immunoprecipitation or GST pulldowns and it was not possible to map the RP2 interaction domain. Other reports also have not been successful in showing an Arl2-RP2 interaction (Bartolini *et al.* 2002, Kuhnel *et al.*, 2006). Hence, the physiological relevance of this interaction is not clear.

It was unclear why hSos-Arl3 resulted in growth of yeast at the restrictive temperature, but only 50% of the time. It is possible Arl3 causes transactivation possibly through direct activation of the Ras pathway, or that the hSos-Arl3 is expressed at such a high level that some protein reaches the plasma membrane even in the absence of an interacting partner.

During the progress of this study, a paper was published defining the crystal structure of RP2 and examining the interaction with Arl3 (Kuhnel *et al.*, 2006). Kuhnel *et al* (2006) confirmed the previously published work by Dodatko *et al* (2004) and Evans *et al* (2006) in which the TBCC homology domain of RP2 was predicted to be a β-helix based on the C-terminal actin binding domain of cyclase associated protein (C-CAP) (Dodatko *et al.*, 2004, Evans *et al.*, 2006). Kuhnel and colleagues determined that the N-terminus of RP2 had a right-handed β-helical structure, with seven coils. The C-terminus of RP2 contained a ferredoxin-like α/β domain which was structurally related to NDK. The first 33 amino acids of the structure were not visible and therefore it is not known how they fit into the overall structure. The ability of RP2 to bind to Arl2 and Arl3 was analysed using a quantitative fluorescence polarization assay and it was concluded that RP2 only binds to Arl3 and not to Arl2. Although these data conflict with the CytoTrap data presented here, the two systems used to analyse binding are different and it is likely they have very different detection levels in regard to relative interaction affinities.

Kuhnel and colleagues also used fluorescence polarization assays to analyse the binding of Arl3 to either the N-terminus (1-230) or the C-terminus (229-350) of RP2. Arl3 was only able to bind to the N-terminal domain of RP2, and when a deletion mutant missing the first 34 amino acids was also used in this assay it was found that this deletion mutant had an affinity for Arl3 300 times lower than full length RP2, leading to the authors suggesting that the first 34 amino acids were necessary for Arl3 binding.

The data presented in this chapter also show that Arl3 bound to the N-terminus of RP2 and, furthermore, that the TBCC-homology domain was sufficient for binding (aa 41-200). These data conflict slightly with data from Kuhnel *et al*, in which it was suggested that the first 34 amino acids of RP2 are necessary for Arl3 binding. However the CytoTrap system is very sensitive to any interaction due to the cascading nature of the Ras signalling pathway which the system exploits. The RP2-Arl3 interaction is strong in this system, comparable, if not stronger, than the positive

control (hSos and Rit1). The growth of yeast with pMyr-Arl3 and pSos-RP2 41-200 was weaker however than wtRP2 and RP2 1-200 which agrees with Kuhnel *et al* (2006), however it is not accurate to directly compare the yeast growth due to the lower expression level of the RP2 41-200 construct compared to the wt RP2 or RP2 1-200 constructs.

Comparison of yeast growth rates between Arl3-T31N and Arl3-Q71L with the RP2 41-200 domain indicated that RP2 preferentially binds to Arl3-Q71L. These observations corroborate the binding assays used by Kuhnel and colleagues which state that the binding affinity of RP2 for Arl3-GDP is 400 times lower than for Arl3-GTP. Kuhnel *et al* also found that RP2 has the ability to act as a guanine nucleotide dissociation inhibitor (GDI) for GTP-bound Arl3 (Kuhnel *et al.*, 2006). It was not possible to detect endogenous Arl3 bound to GST-RP2 in a GST pulldown assay, however, this may reflect the guanine nucleotide-bound state of endogenous Arl3. As RP2 preferentially binds to GST-Arl3, it is likely that endogenous Arl3 is predominantly GDP-bound making it difficult to detect the small proportion of GTP-bound Arl3 that may bind to RP2 (Figure 4.6B).

Using CytoTrap to study pathogenic RP2 mutations it was not clear whether the lack of interaction between RP2-C86Y and Arl3 was due to the low expression level of the hSos-RP2-C86Y (the ability to bind to Arl3-Q71L would suggest not) or whether this mutation affects RP2's ability to interact with Arl3. The lack of interaction may be non-specific as the misfolded protein may not be able to interact with any potential interacting partners. Co-immunoprecipitation assays indicated the misfolding mutations (C67Y and C86Y) no longer interacted due to there being insufficient correctly folded protein. Immunocytochemical analysis showed the misfolded protein appears to form inclusions suggesting it was not available for binding to Arl3. The L253R mutation would be predicted not to directly affect the interaction with Arl3 as the residue is outside the interaction domain. Thus, one would predict that the mutation may affect the interaction with Arl3 through a global misfolding effect. The R118H mutation, despite being expressed at a level comparable to wild type and being correctly localised did not appear to be able to bind to the Arl3-Q71L, which suggests the Arginine 118 residue is important for the functionality of the RP2-Arl3 interaction.

The data presented in this Chapter investigating pathogenic RP2 mutants and their ability to bind to Arl3 were in general agreement with the structure published in the

Kuhnel study (Kuhnel *et al.*, 2006) and predictions based on this structure. Firstly, the C67 and C86 residues lie along the 'backbone' of the N-terminal helix and their substitution to tyrosine residues could result in the destabilisation of the hydrophobic core set around these amino acids. The L253R mutation would also be predicted to destabilise the protein due to clashes between residues in the hydrophobic core of the C-terminal domain (Kuhnel *et al.*, 2006). However, RP2-L253R was able to bind to Arl3. The R118H mutation, in contrast, has been predicted to be catalytically important, as discussed in Chapter 1, and does not lead to an incorrectly folded protein. In their study, Kuhnel *et al* analysed the effect of the R118H mutation on the ability of RP2 to bind to Arl3. They found that this mutation led to an 800 fold decrease in affinity for Arl3, this was determined to be below physiological relevance leading to the conclusion that the R118H mutation would most likely *in vivo* result in an inability of RP2-R118H to bind to Arl3 which was reflected in the co-immunoprecipitation experiments (described in this chapter).

CytoTrap was uniquely sensitive to the RP2-Arl3 interaction which meant that a range of affinities were detectable, for example according to Kuhnel *et al* the interaction between Arl3 and RP2-R118H is of an affinity 800 times lower than for wtRP2 and yet it was still detectable using CytoTrap, suggesting the method is suitable for detecting interactions with a wide range of affinities from low to high. The data obtained from CytoTrap, GST pulldown assays and co-immunoprecipitations illustrated the importance of using several different types of binding assay when analysing interactions and also their individual limitations. The GST-RP2 pulldown for example did not detect endogenous Arl3 binding to GST-RP2 due to the low levels Arl3-GTP found endogenously.

Prior to the study described in this chapter, there was no strong evidence of where in the cell the RP2-Arl3 interaction may occur, the proteins appeared to be expressed in a different pattern in the retina (Grayson *et al.*, 2002). When excess RP2 and Arl3-GTP were expressed there was a distinctive shift in the localisation of both proteins (Figure 4.11C) to the Golgi (Figure 4.12B) which offers a potential cellular interaction site. The preference of RP2 to bind to GTP-bound Arl3 and then to prevent the dissociation of GTP suggests that the RP2-Arl3 interaction plays an important role in stabilising Arl3 in the GTP-bound state which goes against the natural nucleotide binding affinity of the protein (Kuhnel *et al.*, 2006). RP2's ability to act as a GDI and the re-localisation of RP2 and Arl3-GTP shown in this chapter suggests that RP2 may

play an important role in keeping Arl3 in the active GTP-bound form, suggesting RP2 is an Arl3 effector.

The data obtained using live imaging of RP2 has also provided novel data on RP2's dynamic nature as well as showing a potential role for RP2 and Arl3 in vesicular trafficking. Live imaging also clarified that RP2-GFP was not being retained in the Golgi in the presence of Arl3-GTP. The presence of Arl3-GTP appears to increase the movement of RP2-GFP towards the plasma membrane and also towards the Golgi, overall an estimated 5-10 fold increase in intracellular RP2-GFP content was observed. The vesicles often move in and out of focus and it is only possible to follow them for short periods of time, therefore making accurate rate estimations difficult. More accurate calculations of the rate of movement of the RP2-GFP vesicles would assist in elucidating the protein trafficking pathway they may be involved in.

Table 4.1 Estimated rates for components of the axonal transport system
Adapted from Brady (1991).

The rate of movement for kinesin has been calculated to be 2 μm/sec in an *in vitro* study using purified microtubules (Alberts, 1994), the direction of movement has been shown to be toward the microtubule plus end, therefore kinesin motors transport in an anterograde direction. The kinesin Ncd motor moves cargo in the opposite direction at a slower rate of 0.1 μm/sec (Alberts, 1994). The estimated rate of RP2 vesicles movement was 0.06 μm/sec, which is slower than that reported for kinesin. The

kinesin calculation was generated using purified components *in vitro* and as such is likely to be an over-estimation of the true rate *in vivo*. An accurate estimation of the rate of movement of RP2-GFP vesicles would allow a more accurate preposition as to the transport mechanism being utilised, and thus more specific experiments to determine the nature of the transport.

The possibility of elucidating potential RP2 roles in trafficking and signalling is significant when using the technique of live imaging. Fluorescent markers could be used to characterise the vesicle-like bodies that contain RP2 which would provide clues as to the pathway that RP2 plays a role in. Alternative markers for late endosomes (e.g. Lamp1) or other vesicle markers, and vesicle coat markers (e.g. clathrin) and using fluorescent transferrin receptor in live imaging may provide more information on the nature of the RP2 trafficking in the cell and whether it is itself involved in the processing and trafficking of proteins.

The use of drugs to disrupt various pathways is possible in live imaging and the cells can be directly observed to directly see the effect on the RP2 protein. A potentially interesting drug to use would be Brefeldin A which causes disruption of the Golgi through inhibiting the action of Arf1. As the likely site of interaction for RP2 and Arl3 is the Golgi, it would be interesting to see what the effects of fragmenting the Golgi would be on RP2 and whether Arl3-GTP still alters the cellular localisation of RP2. It would also be interesting to disrupt exocytosis and endocytosis and observe whether there is a change in the vesiclular-like movement of RP2. The data from the live imaging experiments presented here, combined with an investigation by Yoon *et al* showing that RP2 can translocate to the nucleus under DNA damaging conditions indicates that RP2 has the potential to move throughout the cell and is not restricted to a plasma membrane association.

Currently the guanine nucleotide exchange factor (GEF) for Arl3 is unknown, thus there is relatively little known about the regulatory pathways involved in controlling the nucleotide binding state of Arl3. Similarly, the GAP for Arl3 is not known and the regulation of the conversion of Arl3-GTP back to Arl3-GDP is unresolved. Considering the ability of RP2 to act as a GDI for GTP-bound Arl3 it would be interesting to investigate the potential effect of GEFs and GAPs for Arl3 on RP2 function.

Live imaging could also be used as a tool to alter the cellular environment to induce an increase in endogenous GTP-bound Arl3. RP2-GFP was observed to behave differently in the presence of GDP- or GTP-bound Arl3. RP2-GFP could be used as a surrogate marker for the levels of GTP/GDP-bound Arl3 in the cell. Using various drugs and treatments, RP2-GFP localisation could be observed to investigate the conditions which lead to increases in Golgi associated RP2. This could provide insight into the cellular circumstances in which the RP2-Arl3 interaction may occur or in which pathway it is important.

The elucidation of a potential interaction site at the Golgi and a mutual role in vesicular trafficking indicates that the RP2-Arl3 interaction has physiological significance. The role of Arl3 in cilia (Schrick *et al.*, 2006, Lai *et al.*, 2007) and the importance of the connecting cilium and IFT in photoreceptor function also imply that the RP2-Arl3 interaction may have an important role in cilia function. Furthermore data from this chapter shows that pathogenic mutations in RP2 appear to disrupt the RP2-Arl3 interaction. It could be hypothesised that RP2 and Arl3 act together to regulate or utilise vesicular transport to and from the Golgi, perhaps through exploiting the microtubule network and as such link the membrane and the cytoskeleton through vesicular trafficking.

The data in this chapter has highlighted further the importance and location of the RP2-Arl3 interaction, however there is still a considerable amount to discover to understand the specific role this interaction plays in the development of RP.

CHAPTER 5

CHARACTERISATION OF NOVEL PUTATIVE RP2 INTERACTORS

5.1 RAN

5.1.1 Introduction

RAN is a Ras-related small GTPase that localises predominantly to the nucleus and has multiple cellular roles. RAN has been shown to be involved in nucleo-cytoplasmic transport (Macara, 2001), as well as mitosis, nuclear assembly and cell cycle progression (Kornbluth *et al.*, 1994). Although RAN is a member of the Ras superfamily it differs from other family members in that it is not prenylated through its C-terminus. RAN exists in either a GTP- or GDP-bound form, which is a feature of the Ras-related small GTPases. The cellular localisation of RAN is altered accordingly, GDP-bound RAN is found in the cytoplasm and the cytoplasmic face of the nuclear pore complex (NPC) (Weis *et al.*, 1996, Lounsbury *et al.*, 1996), whilst GTP-bound RAN localises to the nucleus and nuclear envelope (Carazo-Salas *et al.*, 1999). The subcellular localisation of RAN is key to its function and is maintained by specific exchange and activating factors. RAN's nucleotide exchange factor (GEF) RCC1 is a chromatin-bound protein thus maintaining GTP-bound RAN in the nucleus while RAN's GTPase activating protein, RanGAP1, is found predominantly in the cytoplasm (Figure 5.1 and 5.2) (Matunis *et al.*, 1996).

Interestingly, RanGAP1 does not act though an arginine finger, as suggested for TBCC and RP2 for the stimulation of the GAP activity of tubulin, and as reported for other small GTPases (e.g. Ras and Rho) (Scheffzek *et al.*, 1997, Rittinger *et al.* 1997, Bartolini *et al.*, 2002) (see section 1.5.2). Instead the machinery for GTP hydrolysis comes from RAN's intrinsic ability to correctly position the catalytic glutamine residue (Q69) for the hydrolysis to occur (Seewald *et al.*, 2002).

RAN-GTP is involved in the formation of the bipolar mitotic spindle and has been shown by Kalab *et al* (2002) and Caudron *et al* (2005) to achieve this by establishing a spatial concentration gradient of RAN-GTP. As RCC1 is a nuclear protein which is

chromatin-bound, a high concentration of RAN-GTP is found surrounding the chromosomes which consequently facilitates microtubule nucleation and stabilisation around the chromosomes which is necessary for the organisation of the microtubules into a mitotic spindle (Kalab *et al.*, 2002, Caudron *et al.*, 2005).

RAN also plays a key role in bidirectional transport across the nuclear envelope. Figure 5.1 shows the role that RAN plays in nuclear import. A protein with a nuclear localisation signal (NLS) binds to Importin-α which in turn binds to Importin-β and the complex is relocalised to the nucleus. In the nucleus RAN-GTP binds to Importin-β which causes the Importin/NLS complex to dissociate resulting in the nuclear import of the target protein. RAN-GTP bound to Importin-β is transported into the cytoplasm where RanGAP1 converts RAN-GTP to RAN-GDP following GTP hydrolysis. Importin-β is released and able to bind to another NLS-protein-Importin-α complex. This process reduces the concentration of RAN-GTP in the nucleus. Levels of RAN-GTP in the nucleus are thought to be restored by RAN-GDP binding to nuclear transport factor 2 (NTF2), which transports RAN back into the nucleus where it can be converted to RAN-GTP by RCC1 (Ribbeck *et al.*, 1998).

RAN is also involved in nuclear export and Figure 5.2 illustrates the proposed mechanism for RAN function in nuclear export. The binding of RAN to Exportin 1 is the key interaction in the process. Exportin 1 binds to the protein to be exported through its nuclear export signal (NES) and RAN-GTP then binds to this complex and is exported through the nuclear pore. Once in the cytoplasm the NES-protein is released by the conversion of RAN-GTP to RAN-GDP by RanGAP1. Exportin 1 and RAN then translocate back to the nucleus, where RAN can then be converted back to RAN-GTP by RCC1.

RAN has also been implicated in nuclear envelope assembly. A model for the involvement of RAN in this process proposes that due to the high RAN-GTP concentration near the chromosomes, RAN-GTP is able to bind to the chromosomal histones and recruit nuclear pore complex (NPC) proteins in vesicles, as well as Importin-β. Fusion of the vesicles and formation of the nuclear envelope occurs following GTP hydrolysis of RAN (Hetzer *et al.*, 2000 and Zhang and Clarke, 2001).

RAN was identified as a putative RP2 interaction partner using CytoTrap and the following section describes the identification and characterisation of the interaction.

Figure 5.1 RAN is involved in nuclear import

Schematic diagram showing the role that RAN plays in nuclear import. The binding of RAN-GTP to the nuclear import cargo through Importin-β (Imp-β) causes the complex to dissociate thus releasing the nuclear protein in the nucleoplasm. The RAN-GTP-Importin-β complex is then exported through the nuclear pore to the cytoplasm where the conversion of RAN-GTP to RAN-GDP by RanGAP1 releases Importin-β ready to bind to Importin-α. Adapted from Joseph (2006).

Figure 5.2 RAN is involved in nuclear export as well as nuclear import

Schematic showing the role RAN plays in nuclear export. Exportin1 binds to the target protein through its nuclear export signal, RAN-GTP then binds to Exportin1 and the complex is exported through the nuclear pore complex. The conversion of RAN-GTP to RAN-GDP by RanGAP1 causes the complex to dissociate thus releasing the cargo. RAN-GDP then binds Exportin1 and the complex is imported through the nuclear pore into the nucleoplasm where RCC1 converts the RAN-GDP back to RAN-GTP. Adapted from Joseph (2006) and Ohno et al., (1998).

5.1.2 Characterisation of the RP2-RAN interaction

RAN was detected as an RP2 interactor using CytoTrap. Two clones were independently identified as interacting clones as described in section 2.2.9. cDNA clones were processed and sequenced as described in sections 2.2.9.4-5 and 2.1.9 and both clones contained the complete open reading frame of RAN (Figure 5.3A). The two clones identified contained different lengths of in-frame 5'UTR sequence indicating they were amplified from different original cDNAs. Bovine RAN protein sequence is 100% identical to human RAN (Figure 5.3A). Cdc25-Hα yeast were co-transformed with pSos-RP2 or pSos and pMyr-RAN as described in section 2.2.4 and grown at the restrictive and permissive temperatures for up to 7 days. Figure 5.3B shows that RAN interacts specifically with RP2 and there was no evidence of growth at 37°C for the pSos and pMyr-RAN co-transformants

5.1.2.1 RAN interacts with the C-terminal domain of RP2

Cdc25-Hα yeast were co-transformed with deletion and pathogenic missense pSos-RP2 constructs (Figure 4.3B) and pMyr-RAN as described in section 2.2.4. Transformed yeast were diluted and spotted onto appropriate selective media and grown at 24°C and 37°C for up to 7 days. pMyr-RAN was only able to induce growth at the restrictive temperature with either wild type RP2 or the C-terminal domain construct of RP2 (190-350) indicating that RP2 interacts with RAN through its C-terminus (Figure 5.4A). No growth was observed with the N-terminal 1-200 or 41-200 RP2 constructs. No growth was detected using the shorter C-terminal domain of RP2 (RP2 238-350). However, it is possible that the shorter C-terminal fragment of RP2 (RP2 238-350) did not express at sufficient levels to allow an interaction to be detected.

The RP2-RAN interaction was characterised further by observing the effect of pathogenic RP2 mutations on the ability of RP2 to bind to RAN. Cdc25-Hα yeast were co-transformed with various pSos-RP2 mutants (Figure 4.5A) and pMyr-RAN. hSos-RP2-R118H was the only mutant for which growth was observed in a manner comparable to wild type. hSos-RP2-C67Y was still able to stimulate growth of yeast at 37°C but growth was reduced which is most likely explained by the reduced expression level compared to wild type. No growth was observed with the hSos-RP2-C86Y mutant which is again most likely explained by the low expression level of this mutant and the previously characterised misfolding of the protein (section 4.2.4).

A

```
Human RAN       --------MAAQGEPQVQFKLVLVGDGGTGKTTFVKRHLTGE 34
RAN cDNA1       DASGSNIAMAAQGEPQVQFKLVLVGDGGTGKTTFVKRHLTGE
RAN cDNA2       -ASGSNIAMAAQGEPQVQFKLVLVGDGGTGKTTFVKRHLTGE
Bovine RAN      --------MAAQGEPQVQFKLVLVGDGGTGKTTFVKRHLTGE

Human RAN       FEKKYVATLGVEVHPLVFHTNRGPIKFNVWDTAGQEKFGGLR 76
RAN cDNA1       FEKKYVATLGVEVHPLVFHTNRGPIKFNVWDTAGQEKFGGLR
RAN cDNA2       FEKKYVATLGVEVHPLVFHTNRGPIKFNVWDTAGQEKFGGLR
Bovine RAN      FEKKYVATLGVEVHPLVFHTNRGPIKFNVWDTAGQEKFGGLR

Human RAN       DGYYIQAQCAIIMFDVTSRVTYKNVPNWHRDLVRVCENIPIV 118
RAN cDNA1       DGYYIQAQCAIIMFDVTSRVTYKNVPNWHRDLVRVCENIPIV
RAN cDNA2       DGYYIQAQCAIIMFDVTSRVTYKNVPNWHRDLVRVCENIPIV
Bovine RAN      DGYYIQAQCAIIMFDVTSRVTYKNVPNWHRDLVRVCENIPIV

Human RAN       LCGNKVDIKDRKVKAKSIVFHRKKNLQYYDISAKSNYNFEKP 160
RAN cDNA1       LCGNKVDIKDRKVKAKSIVFHRKKNLQYYDISAKSNYNFEKP
RAN cDNA2       LCGNKVDIKDRKVKAKSIVFHRKKNLQYYDISAKSNYNFEKP
Bovine RAN      LCGNKVDIKDRKVKAKSIVFHRKKNLQYYDISAKSNYNFEKP

Human RAN       FLWLARKLIGDPNLEFVAMPALAPPEVVMDPALAAQYEHDLE 202
RAN cDNA1       FLWLARKLIGDPNLEFVAMPALAPPEVVMDPALAAQYEHDLE
RAN cDNA2       FLWLARKLIGDPNLEFVAMPALAPPEVVMDPALAAQYEHDLE
Bovine RAN      FLWLARKLIGDPNLEFVAMPALAPPEVVMDPALAAQYEHDLE

Human RAN       VAQTTALPDEDDDL 216
RAN cDNA1       VAQTTALPDEDDDL
RAN cDNA2       VAQTTALPDEDDDL
Bovine RAN      VAQTTALPDEDDDL
```

B

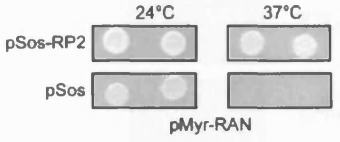

C

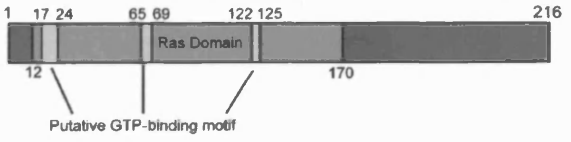

Figure 5.3 RAN interacts with RP2

A Alignment of the predicted amino acid sequence of two different RAN cDNAs detected as RP2 interactors using CytoTrap. Different N-terminal ends show they were derived from different cDNA clones. The predicted amino acid sequence is 100% conserved between human and bovine. Putative GTP-binding motifs are underlined. The catalytically important T24, L43 and Q69 residues are highlighted in red, green and blue respectively. **B** Cdc25-Hα yeast transformed with pMyr-RAN and either pSos-RP2 or pSos alone grown for 96 hours showing specific binding to RP2. **C** Schematic of RAN showing the predicted GTP-binding motifs and the Ras domain.

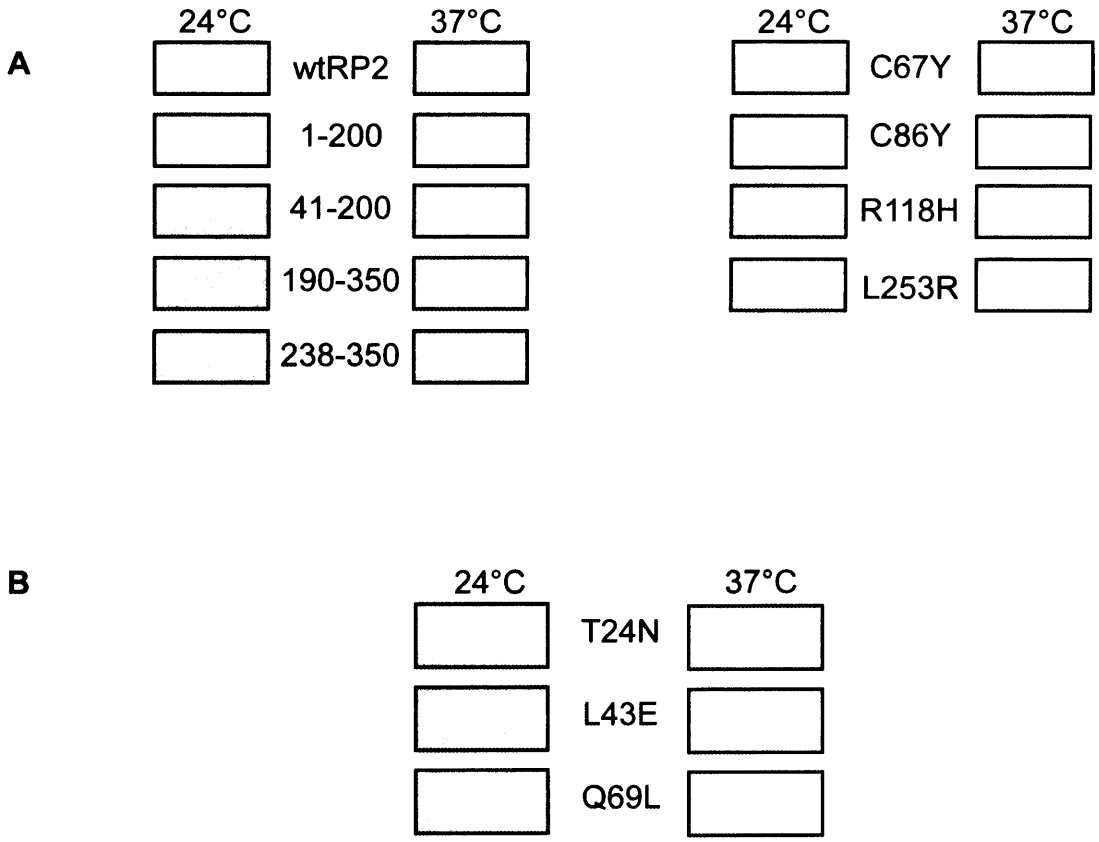

Figure 5.4 Characterisation of the RP2-RAN interaction

A Cdc25-Hα yeast co-transformed with various pSos-RP2 constructs and pMyr-RAN showing that RP2 and RAN interact, and that RP2 interacts with RAN through its C-terminus (RP2 190-350). The L253R mutation which is located in the C-terminal domain of RP2 disrupts the interaction. Yeast were grown for 96 hours. **B** Yeast co-transformed with pSos-RP2 and GDP- and GTP-locked conformations of pMyr-RAN, grown for 96 hours, indicated that the RP2-RAN interaction was enhanced when RAN was in a GDP-locked (T24N) rather than GTP-locked conformation (L43E and Q69L).

Importantly, the only pathogenic mutation in the C-terminal domain of RP2 tested (L253R) caused disruption of the RP2-RAN interaction. This highlights the importance of this residue for the function of the C-terminal domain, but it may also be possible that the mutant expresses at an insufficient level for this interaction to occur (Figure 5.4A).

5.1.2.2 GDP-bound RAN preferentially interacts with RP2

As RAN is known to exist in either a GTP- or GDP-bound form, mutants which lock the protein into both conformations were engineered in pMyr using site directed mutagenesis (see section 2.1.12). The mutants generated were based on well characterized Ras mutants: T24N locks RAN in a GDP conformation and Q69L locks RAN in a GTP conformation (Palacios *et al.*, 1996) (Figure 5.3A). An additional mutation in the effector domain of RAN which mimics a GTP-bound state was created (L43E) (Lounsbury *et al.*, 1996).

Yeast were co-transformed with pSos-RP2 and the GDP and GTP 'locked' conformations of pMyr-RAN as described in section 2.2.4 and observed for up to 7 days. Figure 5.4B shows that there was a faster rate of growth between RP2 and RAN-T24N compared to L43E or Q69L which suggests that the RP2-RAN interaction is enhanced when RAN is in the GDP conformational state.

5.1.2.3 Pulldown assays for the RP2-RAN interaction

In order to corroborate the RP2-RAN interaction a GST-pulldown assay was utilised as described in section 2.3.7. Initially, using GST-RP2 as the bait, pulldown of endogenous RAN from HeLa cell lysates was investigated. RAN migrated at approximately 25kDa as expected. Figure 5.5A shows that RAN was detected as being bound to GST-RP2. However, due to the molecular weight of RAN being similar to that of GST, it was not possible to determine whether there was any RAN bound to the GST control and as such whether the binding to GST-RP2 was specific or not. Further resolution of the samples was attempted, but unfortunately it was not possible to separate the RAN and GST sufficiently for a definitive answer.

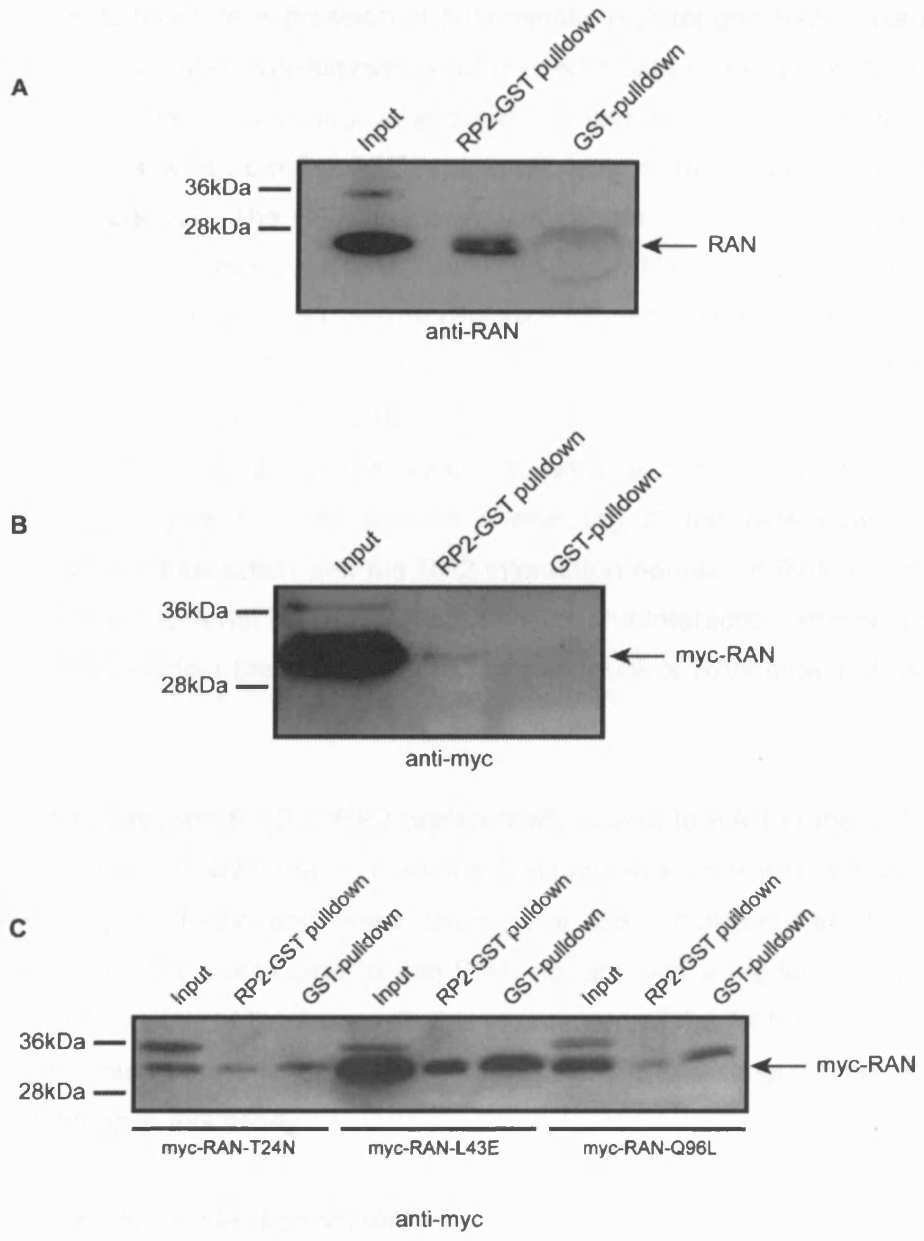

Figure 5.5 RP2-GST pulldown assays using RAN as a target

A GST pulldown assays were performed using HeLa cell lysates to test if endogenous RAN was able to specifically bind to RP2. The presence of GST protein at a similar molecular weight to RAN masked the negative control. **B** Pulldown assays using CHO cell lysates transfected with myc-RAN and subsequently blotted with anti-myc. RAN bound to RP2-GST was detected. **C** GST pulldown assays to investigate whether RP2 preferentially bound to GDP-locked myc-RAN (T24N) using CHO cell lysates transfected with myc-RAN mutants and blotted for myc. Non-specific binding of myc-RAN to the GST control was detected in this assay.

RAN was sub-cloned from the pMyr vector into the pCMV-Tag3b vector (see sections 2.1.2, 2.16-8) to facilitate expression of N-terminally myc-tagged RAN. Transfection of this construct allowed over-expression of myc-RAN and investigation of GDP/GTP forms of RAN, rather than relying on endogenous levels. Furthermore, the tagged-RAN could be resolved from the GST protein allowing more accurate analysis of the GST pulldown control. The GST pulldown was carried out as previously described but using CHO cell lysates transfected with myc-RAN. RAN bound to GST-RP2 and none was detectable in the GST control (Figure 5.5B) indicating that RP2 can bind to myc-RAN in this assay. The myc-RAN used in this assay is different from the endogenous RAN detected in the HeLa cell lysates which appears to bind to RP2 with a higher affinity, as it has the additional in-frame 5'UTR sequence of bovine cDNA clone 2 (Figure 5.3), as well as a myc tag at the N-terminus. As the mechanism of this interaction and the RP2 interaction domain of RAN is not known, the effect of this additional N-terminal sequence on the interaction affinity is also not known and may explain the apparently reduced amount of RAN detected as binding to RP2.

As described in section 5.1.2.2, RP2 preferentially bound to RAN in the GDP-locked conformation (RAN-T24N mutant), therefore RAN mutants were also sub-cloned into the pCMV-Tag3b vector and were used in a GST pulldown assay with the expectation that RP2 would bind to the T24N mutant with a higher affinity. Figure 5.5C shows the results of the assay. In this experiment all the RAN mutants bound to GST-RP2 but also bound to GST. It was not possible to distinguish between RP2 and GST binding in this assay.

5.1.2.4 Subcellular localisation of RAN

In order to investigate the subcellular location of the RP2-RAN interaction immunocytochemical studies were performed to observe the localisation of endogenous and over-expressed RAN with RP2-GFP. RAN's subcellular localisation in SK-N-SH cells was detected using a commercial antibody to RAN as described in section 2.3.5. As previously reported, RAN was observed to be predominantly nuclear but was also detected in the cytoplasm of the cell (see Figure 5.6A) (Macara *et al.*, 2001). To investigate potential co-localisation between RP2 and RAN and therefore a subcellular site of interaction, SK-N-SH cells were transfected with RP2-GFP and stained for RAN as described in section 2.3.4.1-2.3.5. Apart from some distribution of both proteins in the cytoplasm, no subcellular co-localisation was observed.

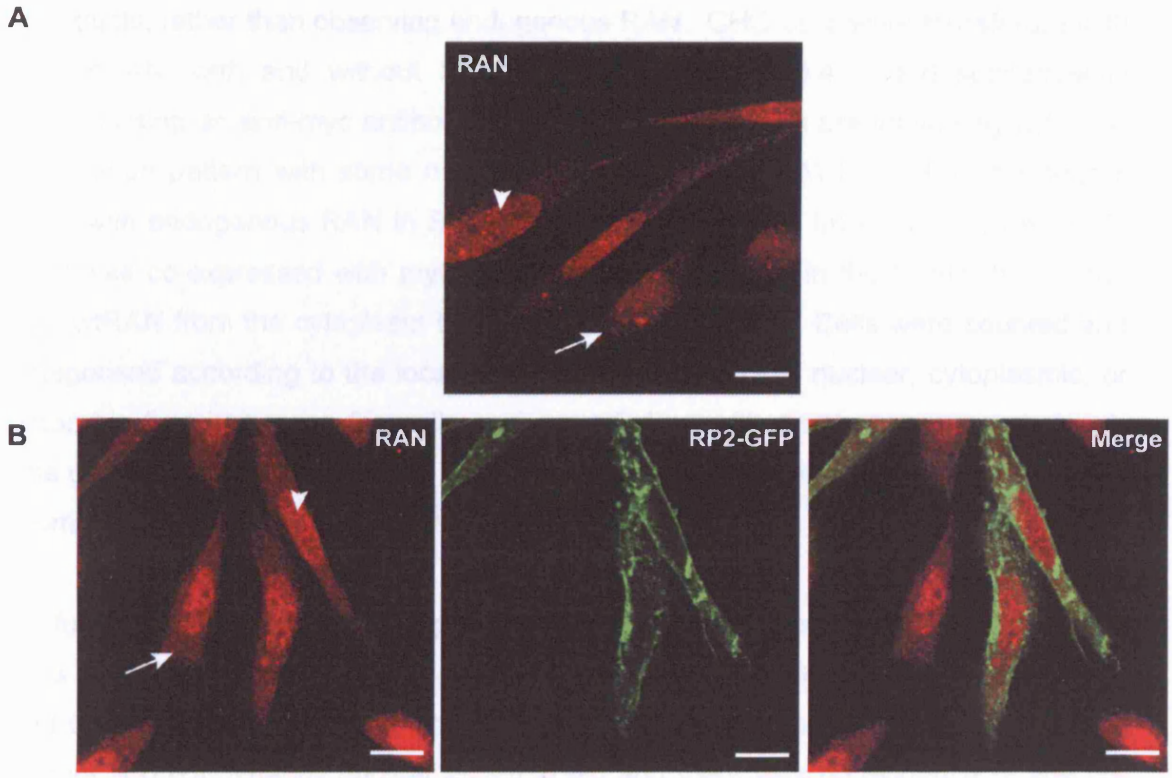

Figure 5.6 Subcellular localisation of endogenous RAN and RP2-GFP

A Immunofluorescence of SK-N-SH cells stained for endogenous RAN showing a predominantly nuclear (see arrowheads) localisation pattern with evidence of cytoplasmic RAN (see arrows). **B** Immunofluorescence of SK-N-SH cells transfected with RP2-GFP and stained for endogenous RAN. RAN and RP2-GFP did not appear to co-localise. All scale bars are 10 μm.

There was also no obvious change in the localisation of endogenous RAN in the presence of RP2 (Figure 5.6A). RAN predominantly localised to the nucleus while RP2-GFP was predominantly localised to the plasma membrane (Figure 5.6B).

Further subcellular localisation experiments were performed with RAN expression constructs, rather than observing endogenous RAN. CHO cells were transfected with myc-wtRAN, with and without RP2-GFP (see section 2.3.4-5) and subsequently stained using an anti-myc antibody. The myc-wtRAN had a predominantly cytosolic localisation pattern with some nuclear staining (Figure 5.7A) but not to the degree seen with endogenous RAN in SK-N-SH cells (Figure 5.6). Importantly, when RP2-GFP was co-expressed with myc-wtRAN there was a shift in the localisation of the myc-wtRAN from the cytoplasm to the nucleus (Figure 5.7). Cells were counted and categorised according to the localisation of the myc-wtRAN; nuclear, cytoplasmic, or amorphic (in which case the cells were rounded up with an abnormal morphology). The cell counts corroborated the immunocytochemistry imaging suggesting RP2-GFP promotes myc-wtRAN shuttling to the nucleus (Figure 5.7C).

To further investigate this interesting change in RAN's subcellular localisation, CHO cells were transfected with myc-tagged GDP and GTP locked RAN mutants T24N and Q69L and co-transfected with RP2-GFP. Figure 5.8 shows that the RAN-Q69L mutant is predominantly nuclear as expected and there was no evidence of any co-localisation between RP2 and the GTP conformation of RAN (RAN-Q69L). This subcellular localisation did not alter when RP2 was co-expressed (Figure 5.8). CHO cells transfected with the myc-RAN-T24N mutant appeared extremely sick after transfection, both with and without RP2-GFP. The morphology of the cells was abnormal; they were rounded up and dying. Careful titration of the amount of transfected DNA and shorter time points post-transfection may help to resolve the issue and allow more detailed examination of the co-expression of RP2-GFP and myc-RAN-T24N.

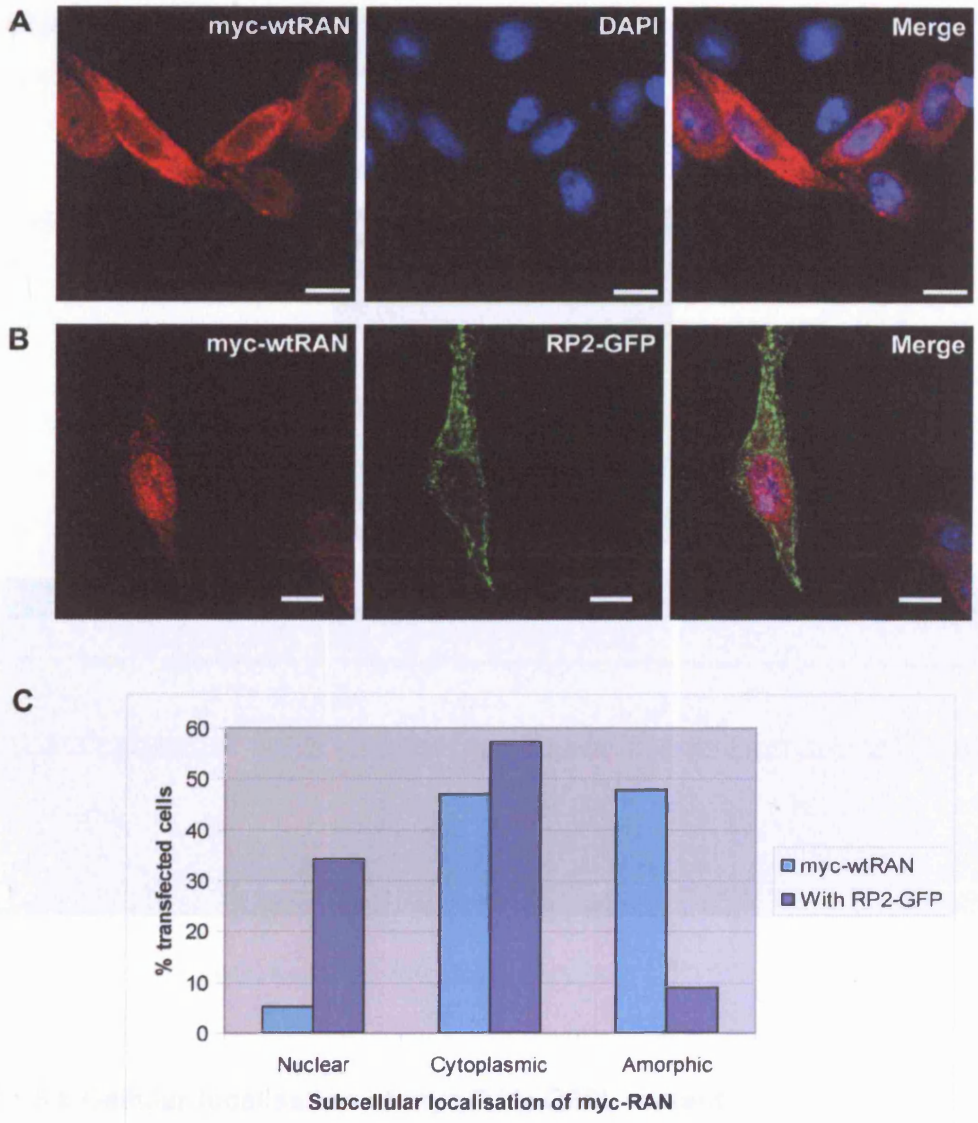

Figure 5.7 Altered localisation of myc-RAN in the presence of RP2-GFP

A Immunofluorescence of CHO cells transfected with myc-wtRAN stained with an antibody to myc showing a cytoplasmic distribution of myc-RAN. **B** Immunofluorescence of CHO cells transfected with myc-wtRAN and RP2-GFP and stained with an antibody to myc indicating that the myc-wtRAN is localised predominantly in the nucleus and on the nuclear envelope in the presence of RP2-GFP. All scale bars are 10 µm. **C** Cell counts of CHO cells transfected with myc-wtRAN with and without RP2-GFP showing that there is a shift in localisation of myc-wtRAN in the presence of RP2-GFP.

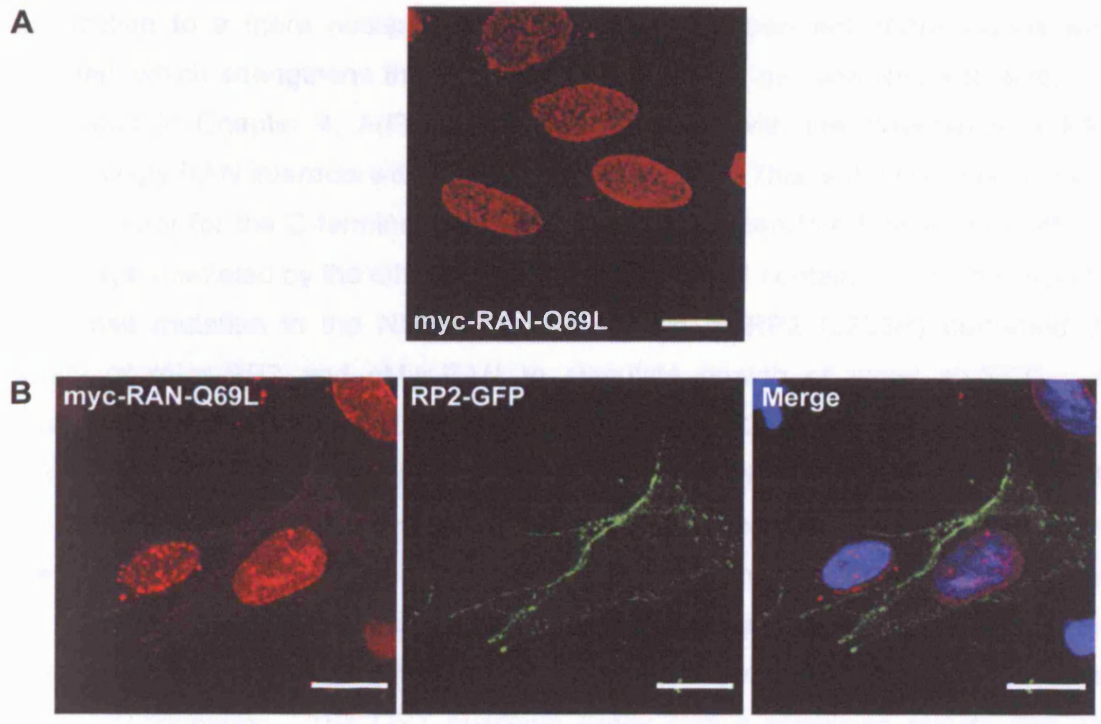

Figure 5.8 Cellular localisation of myc-RAN-Q69L mutant

A Immunofluorescence of CHO cells 24 hours after transfection with myc-RAN-Q69L stained with anti-myc indicating a nuclear and nuclear envelope staining pattern for RAN-Q69L. **B** Immunofluorescence of CHO cells 24 hours after transfection with myc-RAN-Q69L and RP2-GFP stained with anti-myc. No co-localisation was observed between RP2-GFP and myc-Ran-Q69L. The presence of RP2-GFP did not alter the localisation of RAN nor did the RP2-GFP appear any different to the plasma membrane staining pattern seen previously. All scale bars are 10μm.

5.1.3 Discussion

RAN was detected as an interactor of RP2, and it was shown that RP2 preferentially interacts with RAN when in the GDP-bound conformation. Over-expressed RP2 was able to alter the subcellular localisation of RAN from a predominantly cytoplasmic distribution to a more nuclear distribution. Two independent cDNA clones were isolated, which strengthens the likelihood that RAN is a genuine RP2 interactor. As described in Chapter 4, Arl3 was found to interact with the N-terminus of RP2, interestingly RAN interacts with the C-terminus of RP2. This is the first description of an interactor for the C-terminal domain of RP2. RP2 therefore functions in different pathways, mediated by the different functional domains it contains. The only reported missense mutation in the NDK-homology domain of RP2 (L253R) perturbed the ability of pSos-RP2 and pMyr-RAN to stimulate growth of yeast at 37°C. As described in Chapter 4 (section 4.8) the pathogenic L253R mutation is thought to destabilise the protein by causing clashes in the hydrophobic core. The same L253R mutation in RP2 did not perturb the interaction between RP2 and Arl3, which was mediated through the N-terminus of RP2, suggesting that the mutation is important for the structure and function of the C-terminus of RP2, and thus any interactions that may occur through the C-terminus. The interaction between RAN and RP2 needs further confirmation. The GST pulldown assay shows promising results and with optimisation may provide the required corroboration.

Recently the potential function of the C-terminus of RP2 has been investigated by Yoon and colleagues. Yoon *et al* investigated whether the NDK homology domain of RP2 exhibited any functional properties of human or *E.coli* NDK proteins (Yoon *et al.*, 2006). The study showed that RP2 did not exhibit any residual NDK function but revealed the ability of RP2 to act as a 3' to 5' exonuclease, as has been observed for human NDK1 (Yoon *et al.*, 2006). RP2 was also shown to be able to localise to the nucleus under certain conditions. RP2 was reported to translocate to the nucleus upon DNA damage. Solar light and UVA radiation were found to be the most potent inducers of this effect (Yoon *et al.*, 2006). These data provide evidence that RP2 may not be required exclusively at the plasma membrane and cytoplasm and highlights the potential for RP2 to act in other cellular compartments perhaps with as yet undescribed functions.

RP2 was shown to preferentially interact with GDP-form of RAN in yeast two-hybrid. RAN-GDP has been localised to the cytoplasm and the cytoplasmic side of the nuclear pore complex (NPC) (Weis *et al.*, 1996, Lounsbury *et al.*, 1996). Therefore,

the likely site of interaction for RP2 and RAN is in the cytoplasm. A change in the cellular localisation of myc-wtRAN was observed in the presence of RP2-GFP, from a cytoplasmic to nuclear staining pattern (see Figure 5.7). The mechanism for this is unclear, however it is possible that RP2 is stimulating GEF activity for wtRAN, which explains the re-localisation to the nucleus. This would not be possible using the T24N mutant as it is incapable of exchanging GDP for GTP.

It is likely there is a considerable amount of RAN-GDP in the nucleus as RAN's GEF, RCC1, is localised to the nucleus. Lounsbury *et al* show that a T24N RAN mutant localises to the nucleus in BHK21 cells (Lounsbury *et al.*, 1996) which indicates GDP-bound RAN is also found in the nucleus. It is possible, therefore, that the RP2-RAN interaction may also occur in the nucleus or at the nuclear envelope. Considering the data from Yoon *et al* showing RP2 has the ability to translocate to the nucleus, RP2 may have a role in the regulation of RAN's guanine nucleotide bound state by modulating RAN's movement between its GEF in the nucleus and GAP protein in the cytoplasm. It is interesting to note that RP2's preference for RAN-GDP is in contrast to RP2's preference for Arl3-GTP (described in Chapter 4).

The retinal localisation of RAN was investigated by Mavlyutov *et al* (2002) using bovine retinal sections. RAN was described as being localised to the nucleus and nuclear envelopes of all retinal cell bodies and was localised to the inner segments of photoreceptors but appeared to be excluded from the outer segments, as well as being localised to the synaptic endings of cells in the outer plexiform layer (OPL) and nerve fibre layer (NFL). RAN was highly expressed in ganglion cell neurons and in these cells formed a continuous nuclear rim, which the authors speculate is due to the high abundance of nuclear pore complexes at the nuclear envelope (Mavlyutov *et al.*, 2002). It is clear that RAN is extensively expressed in retina and may have a key role in normal retinal function. Although RP2's retinal localisation is distinct, i.e. predominantly plasma membrane and cytoplasmic, RP2 is also found throughout the retina (see Figure 1.7). Co-staining retina sections with both RP2 and RAN antibodies may reveal any co-localisation.

The possibility that RAN was a false positive interacting partner for RP2 must be considered, however this seems unlikely as two different RAN clones were identified in different screens. Importantly, data presented in this chapter shows a clear difference in the interaction affinities with RP2 detected between the GDP- and GTP-locked conformations of RAN. There also appears to be a functional consequence of

over-expressing RP2 and RAN; RP2 was able to alter the predominantly cytoplasmic distribution of myc-RAN to the nucleus. The mechanism of this sub-cellular re-localisation and the physiological relevance remains unclear, however it is interesting to speculate that RP2 has the potential to assist in the sub-cellular localisation of RAN, and that this may support the hypothesis proposed in Chapter 4 that RP2 has a role in protein trafficking (Section 4.6). As described previously, Arl3 has been shown to have an important role in ciliated tissues, and interestingly RAN has been shown to localise to the centrosome (Nakamura *et al.*, 1998), therefore it is possible that RP2 has a cilia function role mediated through its interacting partners.

The identification of RAN as an RP2 interacting protein is particularly interesting when considering the broader spectrum of RP related genes and pathways. As previously described, RAN's GEF is RCC1 which shares homology with RPGR (see section 1.3.3.3). Many of the RP-associated mutations in RPGR occur in the RCC1-homology domain which suggests the domain is important for RPGR's normal retinal function. It is possible to speculate, therefore, that RP2 may act as an adaptor protein for RAN in an important retinal pathway, and that RPGR is a potential GEF for RAN, such that RP2 and RPGR act in the same retinal pathway.

It will be important to confirm the RP2-RAN interaction and that this interaction is mediated through the C-terminus of RP2, as well as corroborating RP2's preference to bind to GDP-bound RAN. Having confirmed these aspects of the interaction it will be necessary to determine how and where in the cell the interaction takes place and more specifically where in the retina the interaction occurs. It would be interesting to utilise live cell imaging to analyse the effects of RP2 on key nucleo-cytoplasmic trafficking pathways (see Figure 5.1 and 5.2) in which RAN plays a role. It would also be interesting to investigate further the conditions in which RP2 translocates to the nucleus (Yoon *et al*, 2006) and determine whether this enhances the RP2-RAN interaction using treated cell lysates or immunocytochemistry. The RP2-RAN interaction warrants considerable investigation, as the implications of this interaction are very exciting, potentially linking RP2 with novel pathways and functions, including other known retina degeneration proteins.

5.2 Cyclin dependent kinase inhibitor 1B

5.2.1 Introduction

Cyclin dependent kinase (CDK) inhibitors block the kinase activity of cyclin-CDK complexes. Cyclin dependent kinase inhibitor 1B (also known as CDKN1B, p27Kip1, CDKN4, KIP1) is involved in the control of the cell cycle and the progression from G1 to S phase. The regulation of CDKN1B levels in the cell controls cell cycle progression (Figure 5.9). When CDKN1B levels are high it binds to Cyclin D-Cdk4 and prevents these proteins from phosphorylating Retinoblastoma (Rb), which results in upregulation of Cyclin E. As Cyclin E is able to phosphorylate CDK2, keeping the levels of Cyclin E low results in low levels of phosphorlyated-CDK2. Phosphorylated CDK2-Cyclin E is able to bind to and phosphorylate CDKN1B, thus targeting it for degradation and continuing the cycle to deplete the cell of CDKN1B. At this point, the cell is able to progress into S phase (Figure 5.9) (Caldon *et al.*, 2006). The recognition of phosphorylated CDKN1B is thought to occur by SKP2 which is able to recognise phosphorylated CDKN1B predominantly in S-phase and acts as the ubiquitin-protein ligase needed for CDKN1B to be correctly targeted for ubiquitination and eventual degradation by the 26S proteasome (Carrano *et al.*, 1999).

5.2.2 Characterisation of the RP2-CDKN1B interaction

CDKN1B was detected as a novel RP2 interacting partner using CytoTrap; a single cDNA clone was identified. The cDNA clone was processed and sequenced as described in sections 2.2.9.4-5 and 2.1.9 and was found to be lacking the first 54 amino acids of the predicted amino acid sequence of full length CDKN1B (Figure 5.10A). The CDKN1B clone was tested for specific binding to RP2 by co-transforming yeast with the pMyr-CDKN1B cDNA clone and either pSos-RP2 or pSos alone. This experiment confirmed that CDKN1B only stimulated growth of yeast at 37°C with hSos-RP2 not hSos alone (Figure 5.10B). The interaction of CDKN1B with RP2 did not require the first phosphorylation site and N-terminal sequence (Figure 5.10C).

5.2.2.1 The RP2-CDKN1B interaction is mediated through the C-terminus of RP2

In order to ascertain whether CDKN1B interacted with RP2 through the C- or N-terminus of RP2, yeast were co-transformed with various deletion and pathogenic missense mutation pSos-RP2 constructs and pMyr-CDKN1B (see section 2.2.4) and growth was observed under the permissive and restrictive conditions for up to 7 days.

Figure 5.9 CDKN1B is involved in cell cycle control

CDKN1B acts in concert with a number of other proteins to allow exit from the cell cycle. During G1 CDKN1B is not phosphorylated and is able to bind to Cyclin D1 and Cdk4 which prevents Cyclin D1 phosphorylating Rb which results in upregulation of E2F and subsequently Cyclin E upregulation. Cyclin E phosphorylates Cdk2 and when these two proteins form a complex with CDKN1B, CDKN1B becomes phosphorylated and is targeted for ubiquitination and degradation. Thus by binding to Cyclin D1 and Cdk4, CDKN1B prevents its own degradation and by blocking this interaction the cell is able to progress to S-phase through the depletion of CDKN1B. Adapted from Caldon *et al* (2006).

A

```
Human CDKN1B    MSNVRVSNGSPSLERMDARQAEHPKPSACRNLFGPVDHEELT 42
CDKN1B cDNA     ----------------------------------------
Bovine CDKN1B   MSNVRVSNGSPSLERMDARQAEYPKPSACRNLFGPVNHEELT

Human CDKN1B    RDLEKHCRDMEEASQRKWNFDFQNHKPLEGKYEWQEVEKGSL 84
CDKN1B cDNA     ---------MEEASQRKWNFDFKNHKPLEGKYEWQEVEKGSL
Bovine CDKN1B   RDLEKHCRDMEEASQRKWNFDFKNHKPLEGKYEWQEVEKGSL

Human CDKN1B    PEFYYRPPRPPKGACKVPAQESQDVSGSRPAAPLIGAPANSE 126
CDKN1B cDNA     PEFYHRPPRPPKGACKVPAQEGQDASGARPAVPLLGSQANPE
Bovine CDKN1B   PEFYHRPPRPPKGACKVPAQEGQDASGARPAVPLLGSQANPE

Human CDKN1B    DTHLVDPKTDPSDSQTGLAEQCAGIRKRPATDDSSTQNKRAN 168
CDKN1B cDNA     DTHLVDQKTDAPDSQTGLAEQCPGIRKRPAADDSSPQNKRAN
Bovine CDKN1B   DTHLVDQKTDAPDSQTGLAEQCPGIRKRPAADDSSPQNKRAN

Human CDKN1B    RTEENVSDGSPNAGSVEQTPKKPGLRRRQT 198
CDKN1B cDNA     RTEENVSDGSPNAGSVEQTPKKPGLRRRQT
Bovine CDKN1B   RTEENVSDGSPNAGSVEQTPKKPGLRRRQT
```

B

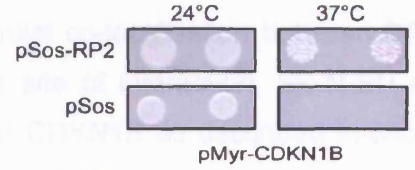

C

Figure 5.10 CDKN1B interacts with RP2

A Alignment of predicted amino acid sequences of human CDKN1B, bovine CDKN1B, and the cDNA clone of CDKN1B detected as an RP2 interactor. The first 54 amino acids of CDKN1B are missing from the cDNA clone. Red residues are those that differ between bovine and human sequences. **B** Yeast Cdc25-Hα co-transformed with pMyr-CDKN1B and either pSos-RP2 or pSos after 96 hours growth indicating that RP2 and CDKN1B interact specifically. **C** Schematic of CDKN1B showing the putative nuclear localisation signal in the C-terminus of the protein and the three known phosphorylation sites (Ser10, Thr157 and Thr187) in CDKN1B.

The interaction between RP2 and CDKN1B occurred through the C-terminus of RP2 (Figure 5.11A). When RP2 pathogenic mutants were used as bait for the interaction there was loss of the ability to stimulate yeast growth between CDKN1B and RP2 with the RP2-L253R mutation (Figure 5.11A) as well as with the RP2-C86Y mutation. Although the RP2-C67Y mutation appeared to grow at a slower rate than wild type RP2, the interaction was evidently still detectable. RP2-R118H had no effect on RP2's ability to interact with CDKN1B in this system (Figure 5.11A).

5.2.2.2 Cellular localisation studies of CDKN1B and RP2

Immunocytochemistry and confocal microscopy were used to analyse the subcellular localisation of CDKN1B and co-localisation between RP2 and CDKN1B. Endogenous CDKN1B was examined in SK-N-SH cells which were transfected with RP2-GFP and then stained using an antibody to CDKN1B (described in 2.3.4.1 and 2.3.5). CDKN1B's subcellular localisation in SK-N-SH cells was detected using a commercial antibody to CDKN1B as described in section 2.3.5. Figure 5.12A shows that CDKN1B was detected predominantly in the nucleus but also in the cytoplasm. To investigate potential co-localisation between RP2 and CDKN1B and therefore a potential subcellular site of interaction, SK-N-SH cells were transfected with RP2-GFP and stained for CDKN1B as described in section 2.3.4.1-2.3.5. Despite some distribution of both proteins in the cytoplasm, no subcellular co-localisation was observed (Figure 5.12B).

5.2.3 Discussion

The identification of CDKN1B as a putative RP2 interactor provides further evidence that the C-terminus of RP2 may have a novel role. As CDKN1B is involved directly in the regulation of the cell cycle it will be important to try and establish at which point during the cell cycle the RP2-CDKN1B interaction occurs. CDKN1B is localised to the nucleus when the cell is in a state of quiescence (e.g. due to contact inhibition) (Wang *et al.*, 1999). Although RP2 may be able to translocate to the nucleus it is possible that the interaction occurs in the cytoplasm during S phase when CDKN1B moves to the cytoplasm to be degraded by the 26S proteasome. Co-localisation between RP2 and CDKN1B was not detected in the immunocytochemical experiments performed, however it is possible that the interaction occurs at a specific point in the cell cycle and some further investigations involving examination of RP2 and CDKN1B expression at specific points of the cell cycle would be necessary to determine whether the interaction is cell cycle dependent.

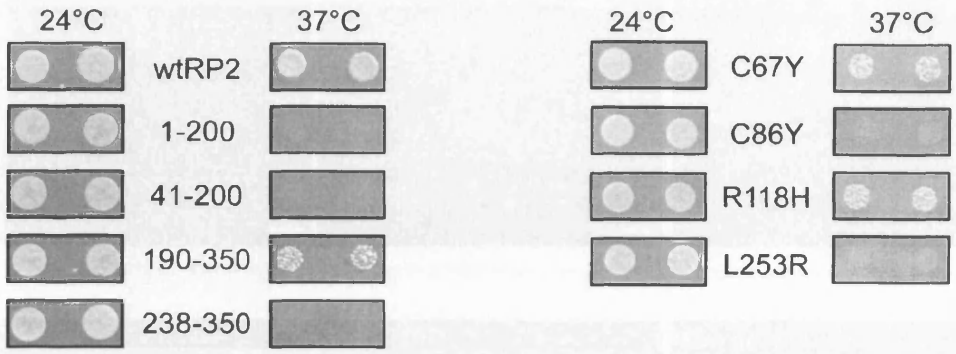

Figure 5.11 CDKN1B interacts with RP2 through the C-terminus of RP2
Yeast Cdc25-Hα co-transformed with various pSos-RP2 constructs show that CDKN1B interacts through the C-terminus of RP2 (190-350) and that the pathogenic mutation L253R in that domain perturbs the interaction. Yeast were grown for 96 hours.

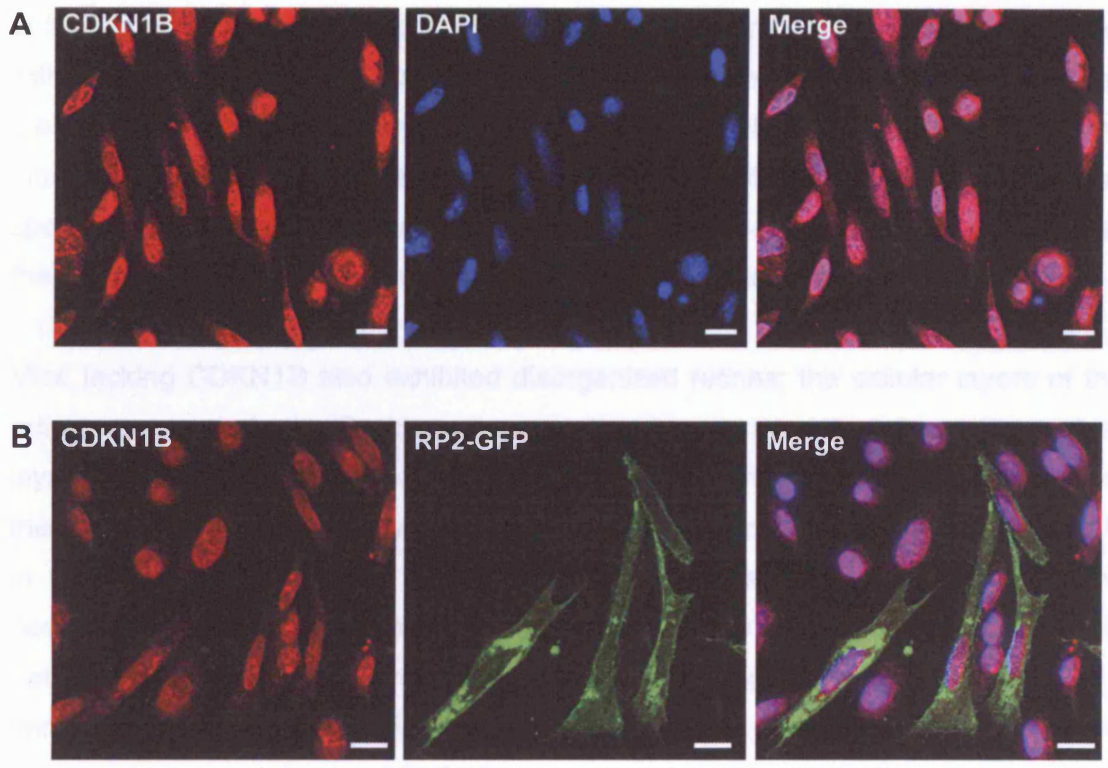

Figure 5.12 Cellular localisation of endogenous CDKN1B

A Immunofluorescence of SK-N-SH cells stained for endogenous CDKN1B showing a cytoplasmic and predominant nuclear staining pattern. **B** SK-N-SH cells transfected with RP2-GFP and stained for CDKN1B 24 hours after transfection. No specific co-localisation between CDKN1B and RP2-GFP was detected and the presence of excess RP2 appeared to have no effect on CDKN1B localisation. All scale bars are 10μm.

It is also possible that the interaction is transitory and so would be hard to detect.

There is evidence that CDKN1B is important for normal retina function as well as for correct development of other organs. Nakayama *et al* show that mice without CDKN1B have multiple abnormalities including retinal dysplasia (Nakayama *et al.*, 1996). These knockout mice are larger than their wild type litter mates but were born at the expected Mendelian ratios indicating there is no embryonic lethality associated with loss of CDKN1B. The larger size of the mice was not attributable to obesity but there was evidence of enlarged organs such as the thymus, spleen, testes and pituitary glands thus indicating abnormal cell proliferation. The mice also spontaneously developed pituitary tumours further supporting a role for CDKN1B in the control of cell replication in a variety of cell types (Nakayama *et al.*, 1996).

Mice lacking CDKN1B also exhibited disorganised retinas; the cellular layers of the retina were perturbed. On closer examination it was noted that the outer nuclear layer, where the photoreceptor nuclei are located, had entered the retinal layer below the outer limiting membrane pointing to a role in correct cell proliferation for CDKN1B in retinal development (See Figure 1.2 for the normal retinal structure). During development, CDKN1B is expressed in various retinal progenitor cells in mice and is not restricted to a photoreceptor-specific pattern (Dyer and Cepko, 2001). Immunohistochemistry investigations of retina by Nakayama and colleagues show that in wild type adult mice CDKN1B is expressed exclusively in the photoreceptors suggestive of an important role for CDKN1B in adult mouse photoreceptor function beyond its role in retinal development (Nakayama *et al.*, 1996). The retinal pigment epithelial (RPE) cells have also been shown to be affected by the loss of CDKN1B, the cells exhibit increased levels of nuclear division but without a corresponding increase in cell division suggesting a defect in mitosis (Defoe *et al.*, 2007). As CDKN1B is expressed exclusively in the photoreceptors in adult mice it can be speculated that an alteration of the normal function of CDKN1B may indeed result in RP.

Interestingly, RAN has been directly implicated in the regulation of CDKN1B levels in the cell. As described in section 5.2.1 the levels of CDKN1B in the cell are crucial to this feedback-based mechanism of cell cycle control. A study investigating how these levels were regulated found that RAN-GTP was directly involved in the transport of CDKN1B from the nucleus to the cytoplasm and that this resulted in the proteolysis of CDKN1B (Connor *et al.*, 2003). When the proteasome was inhibited it

was found that CDKN1B accumulated in the cytoplasm and, therefore, that the transport of CDKN1B out of the nucleus occurred before degradation, implicating RAN in the regulation of CDKN1B and thus the cell cycle. This most likely occurs through the model proposed in Figure 5.2 as CDKN1B has been shown to interact with Exportin 1 (Connor *et al.*, 2003).

CDKN1B was identified as a putative RP2 interacting partner using CytoTrap and was shown to interact with RP2 through the C-terminus of RP2. This putative interaction requires confirmation using different methodology in order to further understand the relevance of the interaction both in the retina and other tissues. It is possible that, if physiologically important, the RP2-CDKN1B interaction may have a role divergent, but related, to the cell cycle, especially as the photoreceptors are post-mitotic cells. For example, in its role as a cell cycle regulator, CDKN1B also plays an important role in centrosome replication (Hinchcliffe *et al.*, 1999) which potentially ties RAN, CDKN1B and RP2 into a regulatory function at the centrosome.

CDKN1B may represent a false positive, as the interaction has not yet been corroborated and only one clone was identified in the CytoTrap screen. This potential interaction merits further investigation as the CDKN1B knock out mouse shows that CDKN1B is important for normal retinal function and development, and therefore the RP2-CDKN1B interaction may indeed play an important role in normal retinal function.

5.3 Transportin 3

5.3.1 Introduction

Transportin 3 (TNPO3) is a member of the human Importin-β family of proteins. It is involved in the transport of proteins into the nucleus. TNPO3 was originally described as being the nuclear import receptor for a group of proteins known as SR proteins. SR proteins are relatively abundant and are rich in arginine/serine (RS) dipeptides (RS domain). They are involved in pre-mRNA splicing and alternative splicing regulation. SR proteins are localised to the nucleus through their RS domain acting as a nuclear localisation signal (Graveley, 2000). TNPO3 binds to the RS domain of these proteins and transports them to the nucleus in a similar mechanism as shown in Figure 5.1. The interaction between TNPO3 and the SR proteins is perturbed by RAN-GTP, indicating that RAN-GTP causes the dissociation of the TNPO3-SR protein complex once in the nucleus (Kataoka *et al.*, 1999).

A study by Lai *et al* described an alternatively spliced form of TNPO3, specifically Isoform 2 (see Figure 5.13), which appears to interact exclusively with phosphorylated SR proteins (Lai *et al.*, 2000), suggesting that Isoform 1 and Isoform 2 of TNPO3 have differing roles. Further investigations led to the observation that TNPO3 is localised in the nucleus and the nuclear membrane, facilitated by its ability to bind to a nucleoporin (p62). A TNPO3 mutant defective in RAN binding (ΔN281, deletion of the N-terminal 281 amino acids) co-localises with an anti-SC35 antibody which indicates that TNPO3 can localise to nuclear speckles due to the TNPO3-SR protein interaction not being disrupted by RAN (Lai *et al.*, 2000). Nuclear speckles are a nuclear compartment thought to be storage sites for pre-mRNA splicing factors (Lamond and Spector, 2003, Lai *et al.*, 2000). This suggests that TNPO3 not only targets SR splicing factors to the nucleus but may also be involved in correctly localising them to the subcellular compartment in which they are stored, thus acting as an import receptor for phosphorylated SR proteins (Lai *et al.* 2000).

It has also been shown that TNPO3 is able to import a non-SR protein to the nucleus using the same pathway it uses for SR proteins (Lai *et al.*, 2003). RNA-binding motif protein 4 (RBM4) is a splicing regulator with antagonistic actions to SR splicing factors and yet through its interaction with TNPO3 utilises the same pathway to translocate to the nucleus. This interaction is also RAN-dependent. These data show that TNPO3 is not restricted to binding and importing only SR proteins but may also recognise alternative proteins (Lai *et al.*, 2003). All the interactions between TNPO3 and the splicing factors described occur through the C-terminus of TNPO3.

The N-terminus of the protein appears to be important for mediating binding to RAN-GTP (Lai *et al.* 2000).

TNPO3 clearly has an important role in assisting splicing factors in reaching their correct cellular compartment, but whether it has any other functions either in the nucleus or the cytoplasm remains to be elucidated.

5.3.2 Characterisation of the RP2-TNPO3 interaction

TNPO3 was detected as an RP2 interactor using CytoTrap (as described in section 2.2.9). The cDNA was sequenced as described in section 2.1.9. Database searches and bioinformatic analysis were performed following identification of the TNPO3 clone to further understand the potential expression patterns (UCSC, ExPasy, NCBI). *TNPO3* was found to be alternatively spliced and potentially codes for at least five different protein isoforms (Figure 5.13). Two of the five isoforms have been described by Kataoka *et al* (Isoform 1) and Lai *et al* (Isoform 2), Isoforms 3 and 4 are annotated on the ExPasy database and Isoform 5 is not currently annotated on the databases (Kataoka *et al.*, 1999, Lai *et al.*, 2000). The gene contains 22 exons and has two potential methionine 'start' codons, the first in exon 1 and the second in exon 2 (see Figure 5.13). The gene also appears to contain a cryptic splice site in exon 11 resulting in a loss of 32 amino acids from Isoforms 2 and 4. Isoforms 3 and 4 also have an alternative C-terminus due to the final exon 22 being spliced out. The gene appears to be ubiquitously expressed based on EST expression data (NCBI, Unigene).

The TNPO3 clone detected was found to be a cDNA originating from an Isoform 2 mRNA (see Figure 5.13). The TNPO3 cDNA is predicted to express full length in-frame TNPO3 and was also found to have in-frame 5'UTR sequence at the N-terminus (Figure 5.14A). Yeast were co-transformed with pMyr-TNPO3 and pSos-RP2 or pSos, and TNPO3 was found to only stimulate growth of yeast with hSos-RP2, not hSos alone (Figure 5.14B).

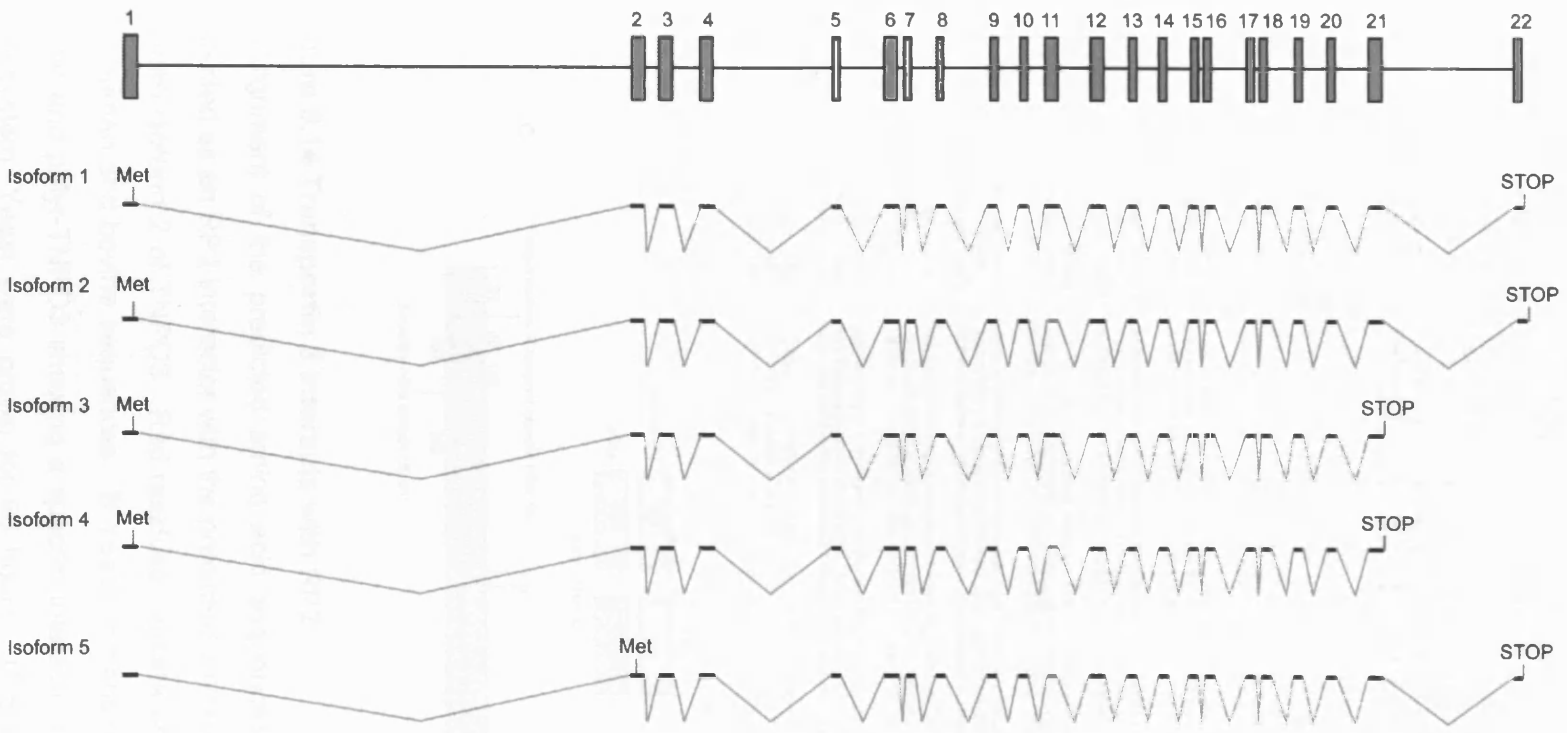

Figure 5.13 Alternative splicing of the TNPO3 gene

A schematic of the gene structure of TNPO3 showing the different isoforms that may result from alternative splicing of the gene. Isoforms 2, 4 and 5 contain a smaller spliced exon 11 (coloured in red). Isoform 5 has an alternative Methionine start codon in exon 2 and exon 22 is spliced out in isoforms 3 and 4 resulting in a different C-terminus to the protein.

A

```
Human TNPO3     ------------------------------------MEGAKPLQLVYQAVQALYHDPDPSGKEKASF  32
TNPO3 cDNA      RQSGSGRGRHSEEARGRSNRRSLGRRARTVAAATTATMEGAKPLQLVYQAVQALYHDPDPSGKERASF
Bovine TNPO3    ------------------------------------MEGAKPLQLVYQAVQALYHDPDPSGKEKASF

Human TNPO3     WLGELQRSVHAWEISDQLLQIRQDVESCYFAAQTMKMKIQTSFYELPTDSHASLRDSLLTHIQNLKDLS 101
TNPO3 cDNA      WLGELQRSVHAWEISDQLLQIRQDVESCYFAAQTMKMKIQTSFYELPTDSHASLRDSLLTHIQNLKDLS
Bovine TNPO3    WLGELQRSVHAWEISDQLLQIRQDVESCYFAAQTMKMKIQTSFYELPTDSHASLRDSLLTHIQNLKDLS

Human TNPO3     PVIVTQLALATADLALQMPSWKGCVQTLVEKYSNDVTSLPFLEILTVLPEEVHSRSLRIGANRRTEII 170
TNPO3 cDNA      PVIVTQLALATADLALQMPSWKGCVQTLVEKYSNDVTSLPFLEILTVLPEEVHSRSLRIGANRAYEII
Bovine TNPO3    PVIVTQLALATADLALQMPSWKGCVQTLVEKYSNDVTSLPFLEILTVLPEEVHSRSLRIGANRRTEII

Human TNPO3     EDLAFYSSTVVSLLMTCVEKAGTDEKKLMKVFRCLGSWFNLGVLDSNFMANNKLLALLFEVLQQDKTSS 239
TNPO3 cDNA      EDLAFYSSTVVSLLMTCVEKAGTDEKKLMKVFRCLGSWFNLGVLDSNFMANNKLLALLFEVLQQDKTSS
Bovine TNPO3    EDLAFYSSTVVSLLMTCVEKAGTDEKKLMKVFRCLGSWFNLGVLDSNFMANNKLLALLFEVLQQDKTSS

Human TNPO3     NLHEAASDCVCSALYAIENVETNLPLAMQLFQGVLTLETAYHMAVAREDLDKVLNYCRIFTELCETFLE 308
TNPO3 cDNA      NLHEAASDCVCSALYAIENVETNLALAMQLFQGVLTLETAYHMAVAREDLDKVLNYCRIFTELCETFLE
Bovine TNPO3    NLHEAASDCVCSALYAIENVETNLALAMQLFQGVLTLETAYHMAVAREDLDKVLNYCRIFTELCETFLE

Human TNPO3     KIVCTPGQGLGDLRTLELLLICAGHPQYEVVEISFNFWYRLGEHLYKTNDEVIHGIFKAYIQRLLHALA 377
TNPO3 cDNA      KIVCTPGQGLGDLRTLELLLICAGHPQYEVVEISFNFWYRLGEHLYKTNDEVIHGIFKAYIQRLLHALA
Bovine TNPO3    KIVCTPGQGLGDLRTLELLLICAGHPQYEVVEISFNFWYRLGEHLYKTNDEVIHGIFKAYIQRLLHALA

Human TNPO3     RHCQLEPDHEGVPEETDDFGEFRMRVSDLVKDLIFLIGSMECFAQLYSTLKEGNPPWEVTEAVLFIMAA 446
TNPO3 cDNA      RHCQLEPDHEGVPEETDDFGEFRMRVSDLVKDLIFLIGSMECFAQLYSTLKEGNPPWEVTEAVLFIMAA
Bovine TNPO3    RHCQLEPDHEGVPEETDDFGEFRMRVSDLVKDLIFLIGSMECFAQLYSTLKEGNPPWEVTEAVLFIMAA

Human TNPO3     IAKSVDPENNPTLVSVLEGVVRLPETVHTAVRYTSIELVGEMSEVVDRNPQFLDPVLGYLMKGLCEKPL 515
TNPO3 cDNA      IAKSVDPENNPTLVSVLEGVVRLPETVHTAVRYTSIELVGEMSEVVDRNPQFLDPVLGYLMKGLCEKPL
Bovine TNPO3    IAKSVDPENNPTLVSVLEGVVRLPETVHTAVRYTSIELVGEMSEVVDRNPQFLDPVLGYLMKGLCEKPL

Human TNPO3     ASAAAKAIHNICSVCRDHMAQHFNGLLEIARSLDSFLLSPEAAVGLLKGTALVLARLFLDKITECLSEL 584
TNPO3 cDNA      ASAAAKATHNICSVCRDHMAQHFNGLLEIARSLDSFMLSPEAAVGLLKGTALVLARLFLDKITECLSEL
Bovine TNPO3    ASAAAKAIHNICSVCRDHMAQHFNGLLEIARSLDSFMLSPEAAVGLLKGTALVLARLFLDKITECLSEL

Human TNPO3     CSVQVMALKKLLSQEPSNGISSDPIVFLDRLAVIFRHTNPIVENGQTHPCQKVIQEIWPVLSETLNKHR 653
TNPO3 cDNA      CSVQVLALKKLLSQEPSNGISSDPIVFLDRLAVIFRHTNPVVENGQTHPCQKVIQEIWPILSETLNKHR
Bovine TNPO3    CSVQVLALKKLLSQEPSNGISSDPIVFLDRLAVIFRHTNPVVENGQTHPCQKVIQEIWPILSETLNKHR

Human TNPO3     ADKRIVERCCRCLRFAVRCVGKGSAALLQPLVTQMVNVYRVHQHSCFLYLGSILVDEYGMEGCRQGLL 722
TNPO3 cDNA      ADKRIVERCCRCLRFAVRCVGKGSAALLQPLVTQMVNVYQVHQHSCFLYLGSILVDEYGMEGCRQGLL
Bovine TNPO3    ADKRIVERCCRCLRFAVRCVGKGSAALLQPLVTQMVNVYQVHQHSCFLYLGSILVDEYGMEGCRQGLL

Human TNPO3     DMLQALCIPTFQLLEQQNGLQKHPDTVDDLFRLATRFIQRSPVTLLRSQVVIPILQWAIASTTLDHRDA 791
TNPO3 cDNA      DMLQALCIPTFQLLEQQNGLQKHPDTVDDLFRLATRFIQRSPVTLLRSQVVIPILQWAIASTTLDHRDA
Bovine TNPO3    DMLQALCIPTFQLLEQQNGLQKHPDTVDDLFRLATRFIQRSPVTLLRSQVVIPILQWAIASTTLDHRDA

Human TNPO3     NCSVMRFLRDLIHTGVANDHEEDFELRKELIGQVMKQLGQQLVSQLLETCCFCLPPYTLPDVAEVLWEI 860
TNPO3 cDNA      NCSVMRFLRDLIHTGVANDHEEDFEVRKELIGQVMKQLGQQLVSQLLETCCFCLPPYTLPDVAEVLWEI
Bovine TNPO3    NCSVMRFLRDLIHTGVANDHEEDFEVRKELIGQVMKQLGQQLVSQLLETCCFCLPPYTLPDVAEVLWEI

Human TNPO3     MQVDRPTFCRWLENSLKGLPKETTVGAVTVTHKQLTDFHKQVTSAEECKQVCWALRDFTRLFR 923
TNPO3 cDNA      MQVDRPTFCRWLENSLKGLPKETTSGAVTVTHKQLTDFHKQVTSAEECKQVCWALRDFTRLFR
Bovine TNPO3    MQVDRPTFCRWLENSLKGLPKETTSGAVTVTHKQLTDFHKQVTSAEECKQVCWALRDFTRLFR
```

B

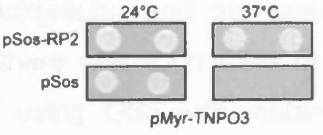

C

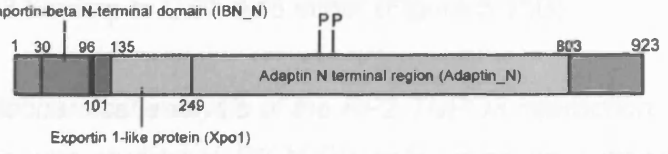

Figure 5.14 Transportin 3 interacts with RP2

A Alignment of the predicted amino acid sequences of the TNPO3 cDNA clone detected as an RP2 interactor with the predicted amino acid sequences of bovine and human isoform 2 of TNPO3. Red residues indicate amino acids that differ between the human and bovine sequences. **B** Yeast co-transformed with pSos-RP2 or pSos alone and pMyr-TNPO3 showing a specific interaction between RP2 and TNPO3 in this system. Yeast were grown for 96 hours. **C** Schematic of TNPO3 isoform 2 protein structure showing functional domains and putative phosphorylation sites at T578 and S586.

5.3.2.1 TNPO3 interacts with the C-terminal domain of RP2

TNPO3 was tested to determine which RP2 domain mediated the interaction. Cdc25-Hα yeast were co-transformed with various deletion and pathogenic missense mutation pSos-RP2 constructs and pMyr-TNPO3 (see section 2.2.4) and growth was observed at 24°C and 37°C for up to 7 days. RP2 was also found to bind to TNPO3 through its C-terminal domain due to only being able to stimulate growth of yeast at the restrictive temperature with full length RP2 or the RP2 190-350 domain (Figure 5.15A). The RP2-TNPO3 interaction, therefore, occurs in the same RP2 domain as the potential RAN and CDKN1B interactions. TNPO3 was able to induce growth with C67Y-RP2 and RP2-R118H mutations; however the interaction was perturbed by the RP2-L253R and RP2-C86Y mutations (Figure 5.15A).

A GST-RP2 pulldown assay was used to test the RP2-TNPO3 interaction detected using CytoTrap. The assay was conducted as described in section 2.3.7 using a GST-RP2 bait and HeLa cell lysates to investigate binding of endogenous TNPO3 to GST-RP2. A TNPO3 antibody was provided as a gift from W.Y.Tarn (Institute of Biomedical Sciences, Academia Sinica, Taipei, Taiwan). An immunoreactive band running at approximately 100kDa was detectable in the HeLa lysates using the TNPO3 antibody which is likely to be endogenous TNPO3, but there appeared to be no endogenous TNPO3 bound to RP2-GST or to the GST control (Figure 5.15B) and there was considerable background and non-specific immunoreactivity from the antibody. To test whether there was a complex of Arl3 with RP2 and TNPO3 the assay was also conducted using GST-Arl3 mutants as baits and there was no evidence of TNPO3 binding to GST-Arl3 either (Figure 5.15B).

5.3.2.2 Immunocytochemical analysis of the RP2-TNPO3 interaction

TNPO3 expression was studied in SK-N-SH cells using an antibody to TNPO3 as described in 2.3.4.1-2.3.5 (Figure 5.16A). TNPO3 was observed to be predominantly localised to the nucleus however plasma membrane staining was also observed in a few cells (Figure 5.16A). SK-N-SH cells were transfected with RP2-GFP (as described in section 2.3.4.1) and stained for TNPO3 (Figure 5.16B). Despite TNPO3 being observed to occasionally localise to the plasma membrane in untransfected cells there was no evidence of extensive co-localisation between RP2-GFP and TNPO3 (Figure 5.16B). The cellular localisation of TNPO3 appeared unchanged when cells with and without RP2-GFP were compared, the majority of TNPO3 was still observed to localise to the nucleus (Figure 5.16B).

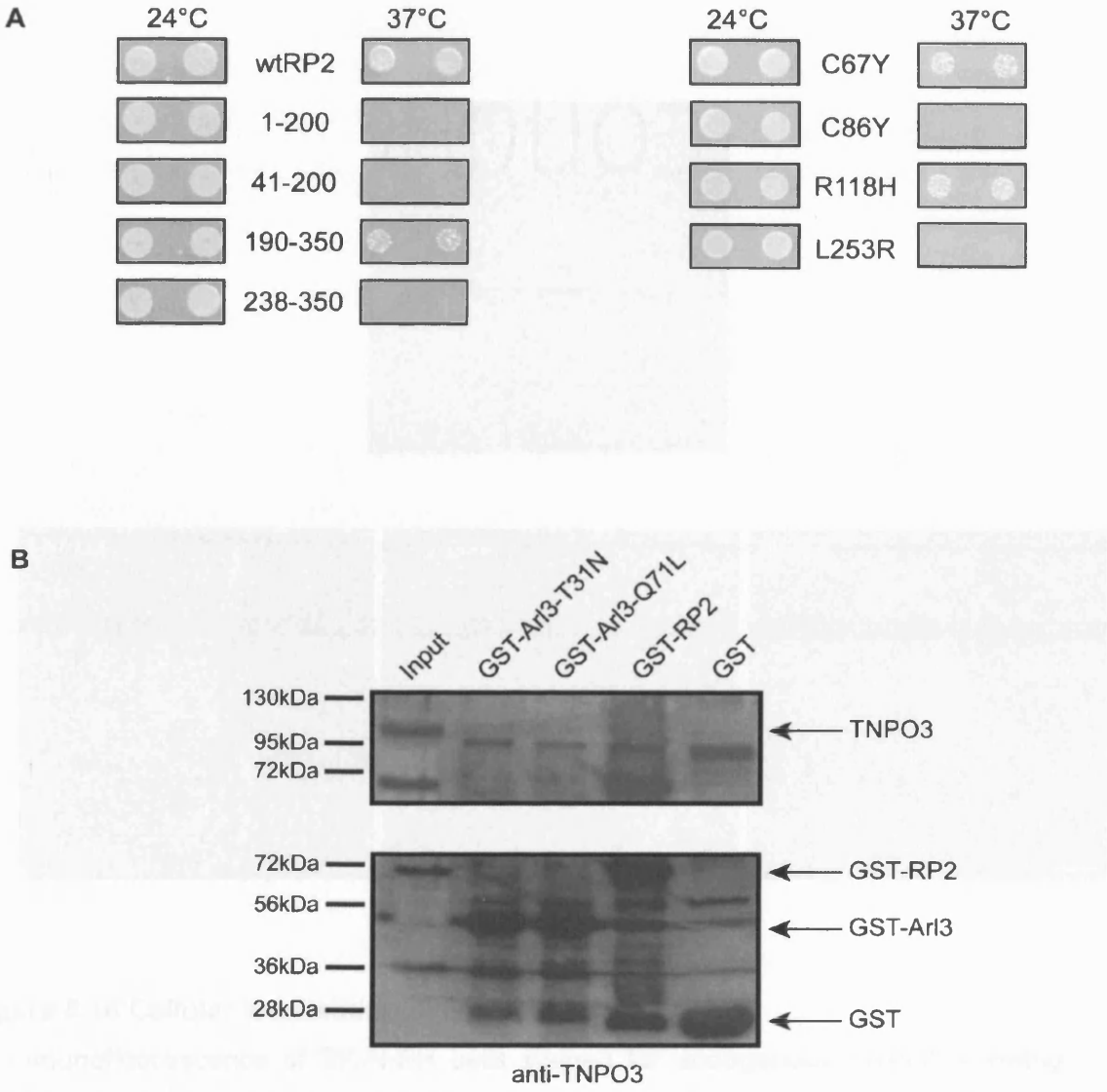

Figure 5.15 TNPO3 interacts with the C-terminus of RP2

A Cdc25-Hα yeast co-transformed with various pSos-RP2 constructs and mutants and pMyr-TNPO3 grown at the permissive and restrictive temperature showing TNPO3 interacts with RP2 through the C-terminus of RP2 (190-350) and that the L253R mutation perturbs the interaction. **B** GST pulldown assays to corroborate the interaction, however no endogenous TNPO3 was detected as binding to GST-RP2 or GST-Arl3.

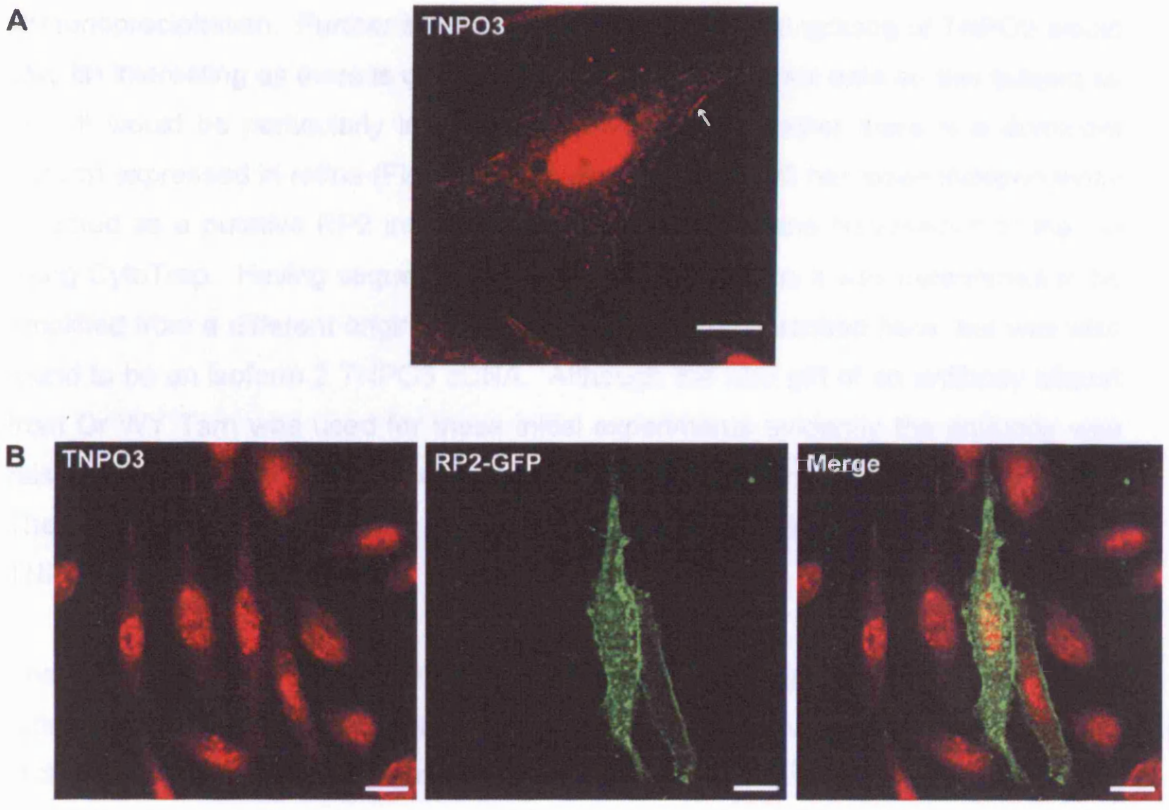

Figure 5.16 Cellular localisation of endogenous TNPO3

A Immunofluorescence of SK-N-SH cells stained for endogenous TNPO3 showing that the protein is localised predominantly in the nucleus, although some localisation of TNPO3 was detected at the plasma membrane (marked by the white arrow). **B** SK-N-SH cells transfected with RP2-GFP and stained for endogenous TNPO3. No co-localisation was observed between TNPO3 and RP2-GFP, there was no alteration in the localisation of either TNPO3 or RP2-GFP. All scale bars are 10µm.

5.3.3 Discussion

TNPO3 interacts with RP2 through the C-terminus of RP2 and was detected through the use of the CytoTrap yeast-two hybrid system. The interaction requires confirmation, possibly utilising an alternative interaction assay such as co-immunoprecipitation. Further investigation of the alternative splicing of TNPO3 would also be interesting as there is comparatively little experimental data on this subject so far. It would be particularly interesting to investigate whether there is a dominant isoform expressed in retina (Figure 5.13). Recently, TNPO3 has been independently detected as a putative RP2 interacting partner by Dr Tatiana Novoselova in the lab using CytoTrap. Having sequenced the second cDNA clone it was determined to be amplified from a different original mRNA than the clone described here, but was also found to be an isoform 2 TNPO3 cDNA. Although the kind gift of an antibody aliquot from Dr WY Tarn was used for these initial experiments evidently the antibody was raised against a GST-fusion protein as it shows strong immunoreactivity with GST. The antibody for TNPO3 is now being purified for further characterisation of the RP2-TNPO3 interaction.

The localisation of TNPO3 in retina has not been investigated and so a potential retinal role for TNPO3 has yet to be elucidated. Ubiquitously expressed splicing factors have been implicated in retinal disease, e.g. *PRPF31, PRPC8, PAP1* and *HPRP3* are all splicing factors in which mutations cause RP (McKie *et al.*, 2001, Vithana *et al.*, 2001, Chakarova *et al.*, 2002, Martinez-Gimeno *et al.*, 2003, Maita *et al.*, 2004). Therefore there is substantial evidence that the seemingly non-retinal-specific function of splicing, when perturbed, can result in retinal degeneration, implying TNPO3 may have a vital role in retinal function. The mechanism of disease pathogenesis for splicing factor mutations remains to be elucidated but represents another group of proteins known to be ubiquitously expressed that cause a retina-specific phenotype.

As with all putative interacting partners detected in yeast-two hybrid screens there is a possibility that TNPO3 represents a false positive interactor. However, the protein has been independently detected twice, with both proteins originating from different cDNA clones, thus strengthening the likelihood that TNPO3 is a real interactor. The importance of splicing in RP has already been highlighted (Section 1.3.4.2) which further supports a role for an RP2-TNPO3 interaction in retina function.

Both TNPO3 and CDKN1B interact with GTP-bound RAN. As described previously, TNPO3 is involved in the transport of SR splicing factors to the nucleus. However, it has been shown that in the presence of GTP-bound RAN the interaction between TNPO3 and its client SR protein is disrupted implying RAN is involved in the regulation of the importation of these SR proteins. As with CDKN1B, the regulation of TNPO3 by RAN may be independent from the role RAN has in regard to RP2, but it also suggests that there is a novel pathway being unravelled by the data presented in this thesis involving RP2 and these novel interacting proteins.

5.4 Sperm associated antigen 7

5.4.1 Introduction

There is comparatively little known about the function of Sperm associated antigen 7 (SPAG7). The protein was first isolated from the acrosome of *Vulpes vulpes* sperm using a monoclonal antibody and was named fox sperm antigen 1 (FSA-1) (Beaton *et al.*, 1994), and was subsequently renamed SPAG7. It was reported that FSA-1/SPAG7 was expressed in the acrosomal region of the sperm; more specifically it was found within the inner acrosomal compartment and only in developing or elongating spermatids, and the authors suggested FSA-1/SPAG7 may play a structural role in the developing acrosome. It was also shown that in fox, the FSA-1/SPAG7 RNA transcript was also expressed in heart (Beaton *et al.*, 1994). SPAG7 has been reported to interact with HLA-B-Associated transcript 5 (BAT5) (Lehner *et al.*, 2004) a protein thought to be involved in the major histocompatability complex and immunity. SPAG7 has been reported as a housekeeping gene by Eisenberg and Levanon (2003) indicating it is ubiquitously expressed (Eisenberg and Levanon, 2003).

Human SPAG7 is a 32kDa protein and has a putative R3H domain spanning amino acids 31-109. R3H domains are thought to mediate binding to single stranded nucleic acids. The major feature of the domain is an invariant arginine (at position 78 in SPAG7) and a highly conserved histidine located three residues away (position 82 in SPAG7) (see Figure 5.17C). SPAG7 also contains a bipartite nuclear localisation signal and so it may be involved in a nuclear function, for example in DNA repair. SPAG7 also has a putative phosphorylation site at residue S161 (Figure 5.17C).

5.4.2 Characterisation of the RP2-SPAG7 interaction

SPAG7 was detected as an RP2 interacting partner using CytoTrap. The cDNA was sequenced (as described in 2.1.9) and it was revealed that the clone was lacking the N-terminal 45 amino acids of the predicted amino acid sequence of the full length amino acid sequence of SPAG7 (Figure 5.17A) indicating the N-terminus and the first nuclear localisation signal of SPAG7 were not required for this interaction. Cdc25-Hα yeast were co-transformed with pMyr-SPAG7 and either pSos or pSos-RP2 as described in section 2.2.4. After 7 days growth at the permissive and restrictive temperatures there was no growth of cells lacking RP2, indicating that SPAG7 specifically requires RP2 to stimulate growth at the restrictive temperature (Figure 5.17B).

A

```
Human SPAG7     MADLLGSILSSMEKPPSLGDQETRRKAREQAARLKKLQEQEK  42
SPAG7 cDNA      -------------------------------------------
Bovine SPAG7    MADLLGSILSSMEKPPSLGDQETRRKAREQAARLKKLQEQEK

Human SPAG7     QQKVEFRKRMEKEVSDFIQDSGQIKKKFQPMNKIERSILHDV  84
SPAG7 cDNA      ---VEFRKRMEKEVSDFIQDSGQIKKKFQPMNKIERSILHDV
Bovine SPAG7    QQKVEFRKRMEKEVSDFIQDSGQIKKKFQPMNKIERSILHDV

Human SPAG7     VEVAGLTSFSFGEDDDCRYVMIFKKEFAPSDEELDSYRRGEE  126
SPAG7 cDNA      VEVAGLTSFSFGEDDECRYVMIFKKEFAPSDEELDSYRRGEE
Bovine SPAG7    VEVAGLTSFSFGEDDECRYVMIFKKEFAPSDEELDSYRRGEE

Human SPAG7     WDPQKAEEKRKLKELAQRQEEEAAQQGPVVVSPASDYKDKYS  168
SPAG7 cDNA      WDPQKAEEKRRLKELAQRQEEEAAQQGPVVVSPASDYKDKYS
Bovine SPAG7    WDPQKAEEKRRLKELAQRQEEEAAQQGPVVVSPASDYKDKYS

Human SPAG7     HLIGKGAAKDAAHMLQANKTYGCVPVANKRDTRSIEEAMNEI  210
SPAG7 cDNA      HLIGKGAAKDAAHMLQANKTYGCVPVANKRDTRSIEEAMNEI
Bovine SPAG7    HLIGKGAAKDAAHMLQANKTYGCVPVANKRDTRSIEEAMNEI

Human SPAG7     RAKKRLRQSGEELPPTS  227
SPAG7 cDNA      RAKKRLRQSGEELPSTS
Bovine SPAG7    RAKKRLRQRGEELPSTS
```

B

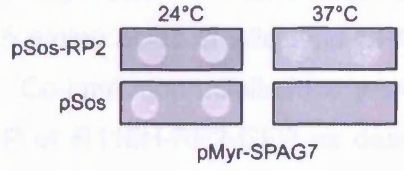

C

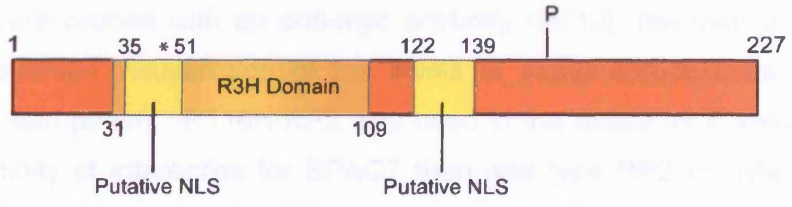

Figure 5.17 SPAG7 interacts with RP2

A Alignment of the predicted amino acid sequences of the SPAG7 cDNA clone with human and bovine SPAG7 sequences, the N-terminal 45 amino acids are missing from the cDNA. Red residues denote residues that differ between the human and bovine sequences. **B** Cdc25-Hα yeast transformed with pMyr-SPAG7 and either pSos-RP2 or pSos alone indicating that SPAG7 specifically binds to RP2. Yeast were grown for 96 hours **C** Schematic of human SPAG7 showing putative nuclear localisation signals, the R3H domain and a putative phosphorylation site at S161. * marks where the detected cDNA sequence starts.

5.4.2.1 SPAG7 interacts with the C-terminus of RP2

Cdc25-Hα were co-transformed with deletion and pathogenic missense mutation pSos-RP2 constructs and pMyr-SPAG7 (as described in section 2.2.4). SPAG7 interacts with RP2 with a relatively low affinity when compared to the previously described interactors in this system. Yeast co-transformed with pMyr-SPAG7 and pSos-RP2 constructs were observed for up to 9 days to ensure slow growth was not over-looked. Figure 5.18A shows that despite the weaker interaction affinity, it is still possible to observe that SPAG7 interacted with RP2 through the C-terminus of RP2 (Figure 5.18A) and that this interaction is abolished by the RP2-C86Y and RP2-L253R mutations (Figure 5.18A). Interestingly, the interaction between RP2 and SPAG7 was enhanced when the RP2-R118H mutant was tested; yeast co-transformed with pMyr-SPAG7 and pSos-RP2-R118H grew quicker than cells transformed with pSos-RP2.

The SPAG7 cDNA clone identified from CytoTrap screening was cloned directly into pCMV-Tag3b (see section 2.1.2 and 2.1.6-8) to provide an N-terminally myc-tagged SPAG7 protein for expression in mammalian cells. The myc-SPAG7 clone was missing the first 45 amino acids of wild type SPAG7 and will be referred to as myc-SPAG7 (45-227). Co-immunoprecipitations were attempted using myc-SPAG7(42-227) and RP2-GFP or R118H-RP2-GFP as described in section 2.3.6 using a myc antibody to immunoprecipitate protein and an antibody to GFP to detect any bound RP2. To ensure that the myc-tagged proteins were immunoprecipitated successfully lysates were probed with an anti-myc antibody (9E10), however the antibody light chain prevented visualisation of the levels of immunoprecipitated protein (Figure 5.18B bottom panel). R118H-RP2 was used in the assay as it appeared to have a higher affinity of interaction for SPAG7 than wild type RP2 in CytoTrap. No RP2-GFP, either wild type or R118H, was detected as being bound to SPAG7 in this assay (Figure 5.18B top panel).

5.4.3 Characterisation of a SPAG7 antibody

An anti-peptide antibody for SPAG7 was designed to the C-terminus of SPAG7 and was synthesised conjugated to KLH by Sigma Genosys. The peptide chosen for the antibody production was the final 13 amino acids of SPAG7 (see Figure 5.17A RLRQSEGEELP**P**TS). The proline residue (amino acid 225) marked in bold above exhibits species variation, in human and dog the residue is proline, while in mouse and rat it is a threonine and in cow it is a serine (Figure 5.17).

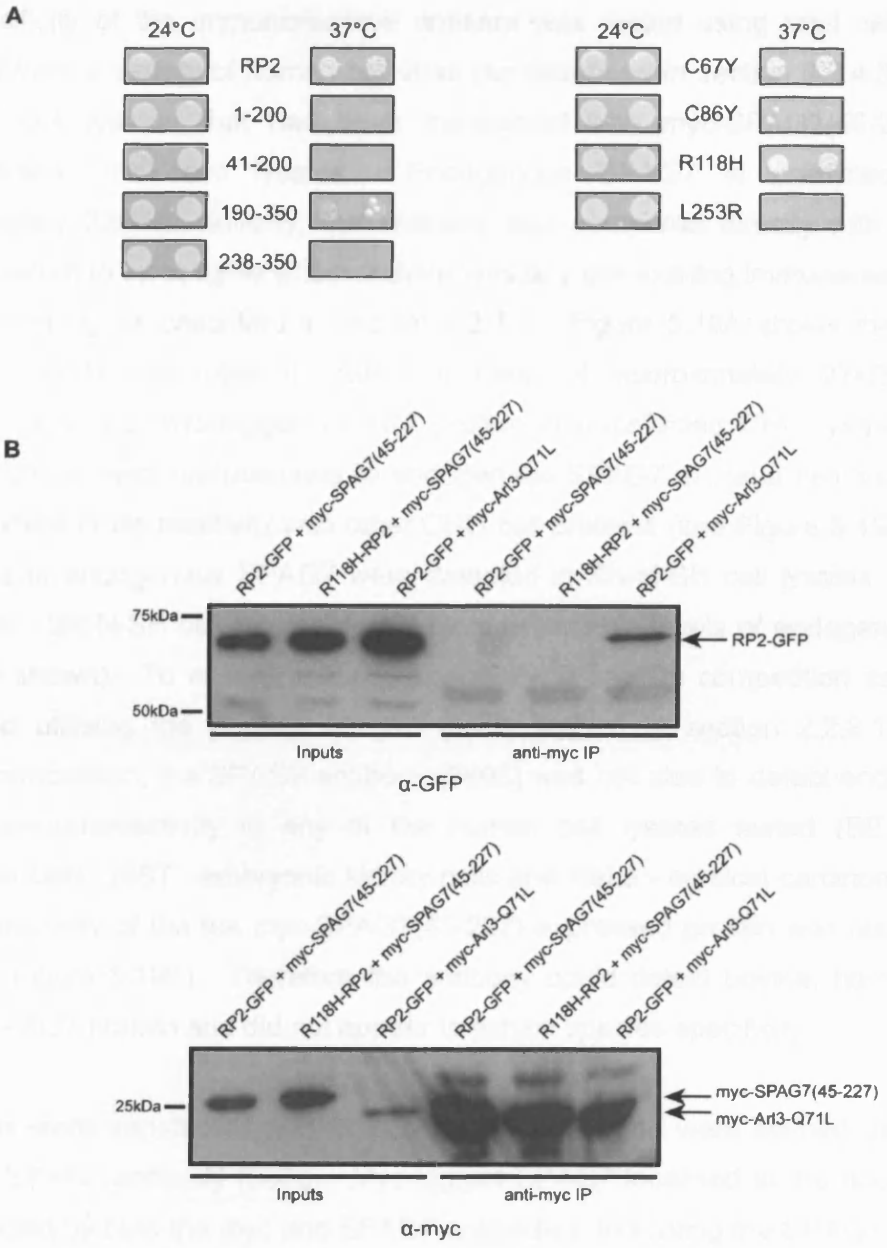

Figure 5.18 SPAG7 interacts with the C-terminus of RP2

A Cdc25-Hα yeast co-transformed with various pSos-RP2 constructs and mutants and pMyr-SPAG7 indicating that SPAG7 interacts with RP2 through RP2's C-terminal domain (190-350) and the L253R mutation abolishes this interaction. Yeast were grown for 96 hours. **B** Co-immunoprecipitations of myc-tagged SPAG7 or Arl3-Q71L and RP2-GFP constructs, an antibody to myc was used to immunoprecipitate. The top panel shows no RP2-GFP was detected as being bound to SPAG7 but was observed to bind to myc-Arl3-Q71L. To check that the myc-tagged proteins were immunoprecipitated lysates were probed with an anti-myc antibody (9E10), the antibody light chain prevented accurate determination of the levels of immunoprecipitated protein.

The specificity of the immunoreactive antisera was tested using total cell lysates prepared from a variety of human cell lines (as described in section 2.3.4.3) as well as CHO cell lysates that had been transfected with myc-SPAG7(45-227) and untransfected CHO cell lysates. Endogenous SPAG7 is predicted to be approximately 32kDa. Initially, the antibody was compared directly with the pre-immune serum to investigate whether there was any pre-existing immunoreactivity by Western blotting as described in section 2.2.7-8. Figure 5.19A shows the SPAG7 antibody (3603) was able to detect a band of approximately 27kDa which corresponds to the myc-tagged SPAG7 protein in transfected CHO lysates and a band of 32kDa which corresponds to endogenous SPAG7 in HeLa cell lysates and did not exhibit cross reactivity with other CHO cell proteins (see Figure 5.19A). Very low levels of endogenous SPAG7 were detected in SK-N-SH cell lysates at higher exposures. SK-N-SH cell lysates do not have detectable levels of endogenous RP2 (data not shown). To ensure antibody specificity, a peptide competition assay was conducted utilising the peptide antigen (as described in section 2.2.8.1). After peptide competition, the SPAG7 antibody (3603) was not able to detect endogenous SPAG7 immunoreactivity in any of the human cell lysates tested (BE - colon carcinoma cells, 293T - embryonic kidney cells and HeLa - cervical carcinoma cells), immunoreactivity of the the myc-SPAG7(45-227) expressed protein was also greatly reduced (Figure 5.19B). Therefore the antibody could detect bovine, hamster and human SPAG7 protein and did not appear to exhibit species specificity.

CHO cells were transfected with myc-SPAG7(45-227) and were stained using anti-myc and SPAG7 antibody (3603). Myc-tagged SPAG7 localised to the nucleus and was detected by both the myc and SPAG7 antibodies, indicating the SPAG7 antibody worked efficiently for immunocytochemistry (Figure 5.19C). The SPAG7 antibody was, therefore, used to stain for endogenous SPAG7 in HeLa cells, where it was observed to be predominantly nuclear with some protein localised throughout the cytoplasm (Figure 5.19D).

5.4.2.3 Immunocytochemical analysis of SPAG7 and its interaction with RP2

SK-N-SH cells were stained using SPAG7 (3603) antibody as previously described in section 2.3.5, predominant localisation of SPAG7 was detected in the nucleus despite low levels of endogenous SPAG7 being detected from SK-N-SH cell lysates (Figure 5.20A and Figure 5.19A).

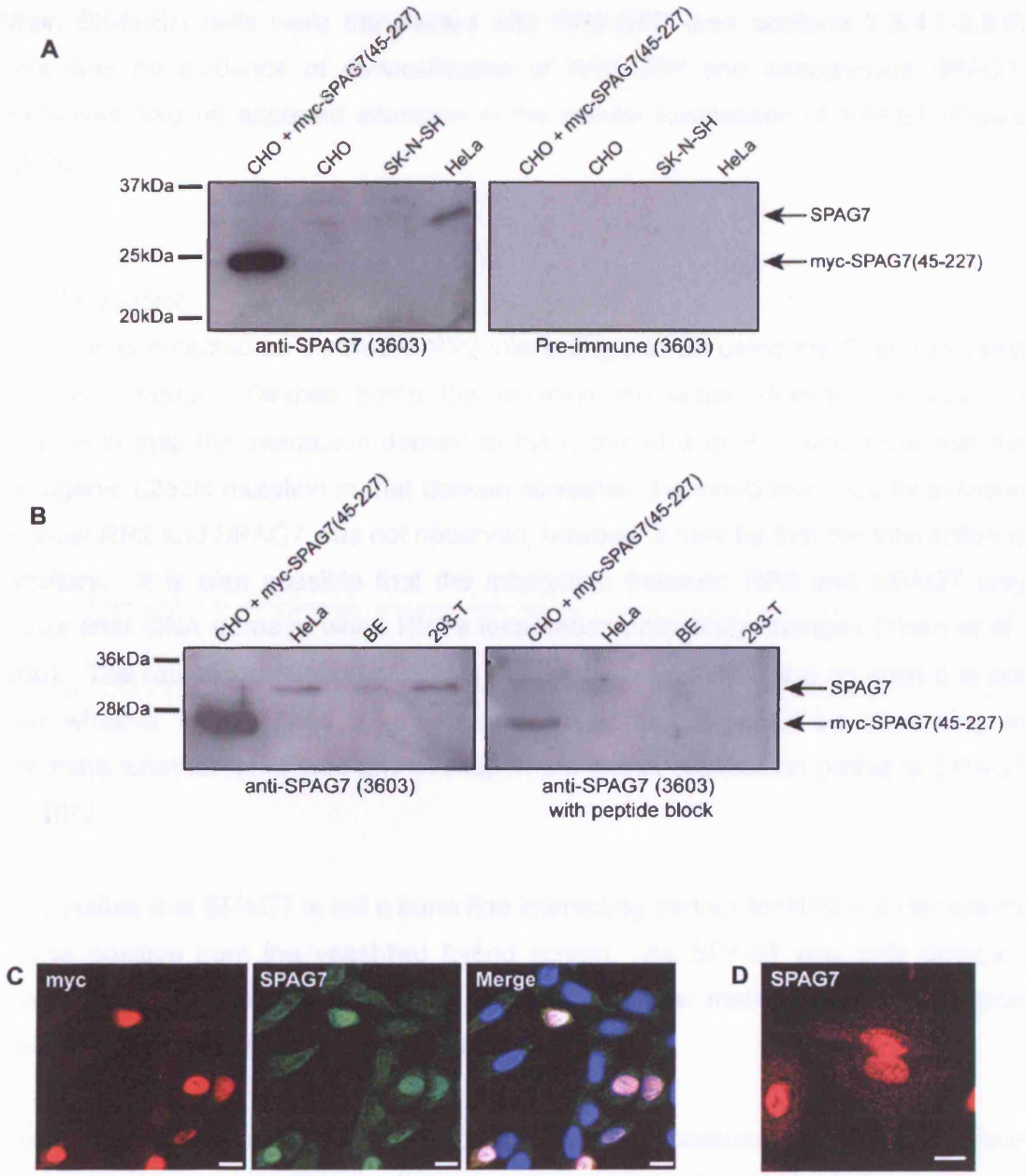

Figure 5.19 Characterisation of an antibody to SPAG7

A Western blots using an antibody to SPAG7 showing that the pre-immune sera does not exhibit any immunoreactivity. The antibody detects myc-SPAG7(45-227) and endogenous SPAG7 in HeLa cell lysates. **B** Western blots using SPAG7 (3603) antibody with and without peptide block (10µg/ml peptide in block) showing specific detection of SPAG7. **C** Immunofluorescence of CHO cells transfected with myc-SPAG7(45-227) construct and stained for myc and SPAG7 (3603) showing extensive overlapping signals. **D** Detection of endogenous SPAG7 in HeLa cells indicating SPAG7 was predominantly nuclear. All scale bars are 10µm. Antibody titres are stated in Tables 2.5 and 2.6.

When SK-N-SH cells were transfected with RP2-GFP (see sections 2.3.4.1-2.3.5) there was no evidence of co-localisation of RP2-GFP and endogenous SPAG7. There was also no apparent alteration in the cellular localisation of SPAG7 (Figure 5.20B).

5.4.3 Discussion

SPAG7 was detected as a putative RP2 interacting partner using the CytoTrap yeast two-hybrid system. Despite being the weakest interaction detected, it was still possible to map the interaction domain to the C-terminus of RP2 and show that the pathogenic L253R mutation in that domain abolished the interaction. Co-localisation between RP2 and SPAG7 was not observed, however it may be that the interaction is transitory. It is also possible that the interaction between RP2 and SPAG7 only occurs after DNA damage when RP2's localisation potentially changes (Yoon *et al.*, 2006). The retinal localisation of SPAG7 is currently unknown and as such it is not clear whether it may have a key function in retina. It would be interesting to determine whether there was any overlap in the retinal expression profile of SPAG7 and RP2.

It is possible that SPAG7 is not a bona fide interacting partner for RP2 but represents a false positive from the yeast-two hybrid screen. As SPAG7 was only detected once, and has not been corroborated through any other method, the physiological relevance of the interaction remains unclear.

Interestingly all the novel RP2 interactors are localised predominantly to the nucleus which was unexpected. The prediction prior to the start of two-hybrid screening was that most of RP2's interacting partners would be cytosolic or membrane-associated. However, the data from Yoon *et al* shows that RP2 is able to translocate to the nucleus and data shown in Chapter 4 shows that RP2 is not static. The reported conditions for RP2 to translocate to the nucleus involve DNA damaging agents. Interestingly, SPAG7 contains an R3H domain which is believed to be a single stranded nucleic acid binding domain and as such has the potential to bind to single stranded damaged DNA. This suggests that RP2 may have a novel function involving SPAG7 in the nucleus in the mediation of some aspect of DNA repair.

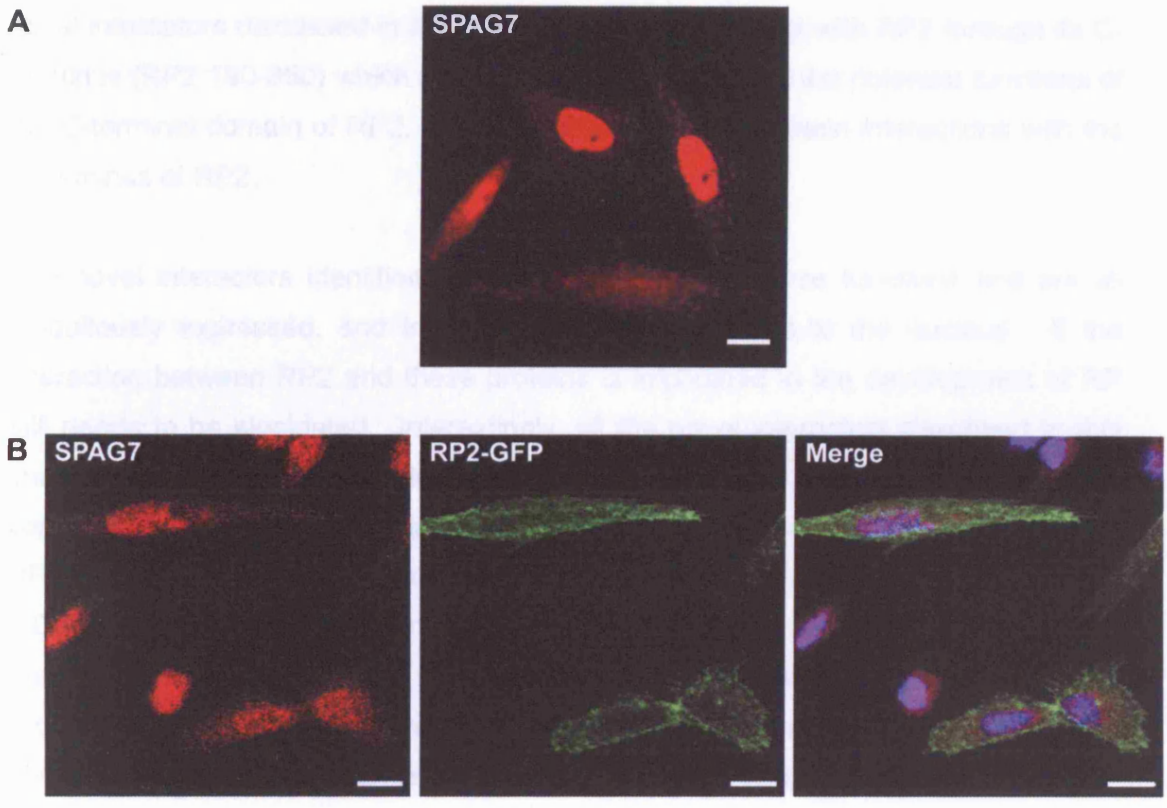

Figure 5.20 SPAG7 is localised predominantly in the nucleus

A Immunofluorescence of SK-N-SH cells stained with an antibody to SPAG7 (3603) showing that endogenous SPAG7 was localised predominantly to the nucleus in SK-N-SH cells but was also detected in the cytoplasm. **B** SK-N-SH cells transfected with RP2-GFP and stained for SPAG7. There is no evidence of co-localisation of SPAG7 and RP2-GFP. All scale bars are 10µm. SPAG7 (3603) antibody was used at a titre of 1:500.

5.5 Discussion

The data presented in this thesis show that the CytoTrap method of yeast two-hybrid for detection of RP2 interactors was successful as five novel putative interactors have been identified and a known interactor has been independently confirmed. All the novel interactors discussed in this chapter appear to interact with RP2 through its C-terminus (RP2 190-350) which provides new information on the potential functions of the C-terminal domain of RP2. This is the first report of protein interactions with the C-terminus of RP2.

The novel interactors identified using CytoTrap have diverse functions and are all ubiquitously expressed, and interestingly are all localised to the nucleus. If the interaction between RP2 and these proteins is implicated in the development of RP still needs to be elucidated. Interestingly, all the novel interactors described in this chapter were not able to interact with RP2 when the L253 residue, which is conserved with NDK, was mutated to an arginine residue. The L253R mutation in RP2 is a reported pathogenic mutation (Table 1.3) and was predicted by Kuhnel *et al* (2006) to cause destabilisation of the protein (Kuhnel *et al.*, 2006). It is notable therefore that the presence of this mutation leads to the abolishment of interaction with all the interactors that bind to RP2 through the C-terminal domain (RP2 190-350), but not with Arl3 which binds to RP2 through the N-terminal domain (RP2 41-200). In order to further define the interaction domain for each of the novel interactors it would be interesting to mutate other residues conserved with the NDK domain, as it can be predicted they will be important functionally or structurally, to delineate the binding domain in RP2 more concisely. If it was found that more than one of the interactors utilised the same binding site with RP2 it would be interesting to use a competition assay to determine the circumstances in which RP2 would bind to one or the other. Therefore, just as the ΔS6 and R118H pathogenic mutations have been shown to have functional consequences (Chapple *et al.*, 2000, Bartolini *et al.*, 2002, Kuhnel *et al.*, 2006 and Chapter 4) (see sections 1.4.3 and 1.5.2), the functional consequence of the L253R mutation may be the loss of the ability of RP2 to interact with these novel interactors.

CytoTrap reflects the reportedly ideal conditions for the RP2-Arl3 interaction (Bartolini *et al.* 2002). It may be therefore that these novel interactors would not have been detected using the transcription-based yeast-two hybrid systems that tag the bait protein at the C-terminus as RP2 would potentially be myristoylated. None of the novel putative interacting partners appear to localise to the plasma membrane and

therefore the function of the plasma membrane localisation of RP2 remains unclear, although it is known to be important in the development of RP (Chapple *et al.*, 2000, Chapple *et al.*, 2002). It is possible that the RP2 involved in these interactions comprises a small portion of the total RP2 pool, i.e the non-myristoylated RP2, or that the interaction is transient yet physiologically significant. Therefore, in order to confirm these interactors it would be necessary to optimise co-immunoprecipitation assays to reflect the likely physiological conditions of these novel interactions, possibly by using an RP2 myristoylation mutant to shift the subcellular pool of RP2 away from plasma membrane localised RP2.

GST pulldown assays proved inconclusive. These techniques were optimised for characterising the RP2-Arl3 interaction and as such the assay may require further optimisation for each of the putative interactors as, for example, expression levels of the each protein will vary. This approach could be complemented by cellular and subcellular localisation studies and observing the effects, on RP2 and cell viability and function, of depleting cells of the protein partners (and vice versa).

The ability of RP2 to bind to these novel interactors through its C-terminus illustrates the importance of the C-terminal domain and highlights the fact that RP2 is a multifunctional protein potentially involved in pathways mediated through different domains of the protein. The interactions could be important for regulating a common convergent pathway in retina. Surprisingly, none of the putative RP2 interactors described are retina-specific, however potential convergent pathways with other retinal disease genes are emerging, for example the RCC1-homology domain in RPGR and potential interaction between RAN and RP2, and the RP2-TNPO3 interaction and its potential link with the splicing factors that are known to cause RP. Further work to delineate these putative retinal pathways could unravel the disease pathogenesis of RP2 mutations in RP.

CHAPTER 6

DISCUSSION

6.1 Discussion and future work

Inherited retinal dystrophies are a major cause of blindness, of which retinitis pigmentosa (RP) is the most common form. Although many of the causative genes for RP have been identified the pathogenesis of disease remains unclear. *RP2* was identified by Schwahn (1998) as the causative gene for the RP2 locus on the X chromosome and was found to encode a ubiquitously expressed protein (Schwahn *et al.*, 1998, Chapple *et al.*, 2000). RP2 has been shown to localise to the plasma membrane in cultured cells and in all cells throughout the retina through dual acylation (Chapple *et al.*, 2000, Chapple *et al.*, 2002, Grayson *et al.*, 2002). The only known interacting partner for RP2 at the start of this thesis was ADP ribosylation factor (Arf)–like 3 (Arl3), which was shown to interact with RP2 in a myristoylation and nucleotide-dependent manner (Bartolini *et al.*, 2002). However, the mechanism by which mutations in the ubiquitously expressed RP2 result in a retinal phenotype is still to be elucidated.

The aim of this thesis was to use yeast-two hybrid to investigate the role RP2 plays in the retina and how this can lead to the development of RP when perturbed. The use of CytoTrap to find novel interacting partners for RP2 was successful, a previously known interaction (Arl3) was confirmed and characterised further and putative novel interactors were also identified. The data presented has confirmed the significance of the RP2-Arl3 interaction by showing a functional consequence of the interaction, as well as a potential cellular interaction site at the Golgi. Arl3 was determined to interact with RP2 through the TBCC homology domain at the N-terminus of RP2 and the interaction was disrupted by pathogenic mutations in RP2. Novel putative interacting partners for RP2 were also been identified: RAN, CDKN1B, TNPO3 and SPAG7. All these novel putative interacting partners were shown to interact with RP2 through the C-terminus of RP2, potentially under competition with each other. It was also found that the only currently reported missense mutation in the NDK homology

domain of RP2 perturbed RP2's interaction with all the novel interactors, strengthening the significance of these proteins as bona fide protein partners and their potential role in RP. The diverse functions of these putative interactors provide further insight into the multiple roles RP2 may have, and tentatively link RP2 with other known retinal degeneration proteins.

The identification of Arl2 as a putative RP2 interacting partner led to further investigation as to whether Arl3 was in fact the major interactor for RP2 from the Arl family. The growth of yeast co-transformed with RP2 and Arl3 was faster than for yeast transformed with Arl2 suggesting that the affinity of interaction between RP2 and Arl2 was lower than for RP2 and Arl3. Furthermore, Arl2 needed full length RP2 to interact whereas using Arl3 it was possible to define the interaction domain, again suggesting the Arl2 interaction may be non-physiological. Arl3 has been shown to be a microtubule associated protein (MAP) and to localise to the connecting cilium in photoreceptors (Grayson *et al.* 2002), it has also been detected in a cilia proteomic screen (Liu *et al.*, 2007), and the phenotype of the Arl3 knock out mouse further supports its role in cilia function and retinal degeneration (Schrick *et al.*, 2006). It is interesting to note that there is currently not an RP2 animal model available, however studies using the Arl3 knock out mouse may provide further information on the RP2-Arl3 interaction. Grayson *et al* (2002b) reported that in RP2-Arg120Stop patient lymphoblastoid cells there was no effect on the expression level of Arl3, therefore it would be interesting to investigate the effect on RP2 retinal localisation and expression in the absence of Arl3 by using the Arl3 knock out mouse (Grayson *et al.*, 2002b, Schrick *et al.*, 2006).

Data from Bartolini and colleagues (2002) suggesting the RP2-Arl3 interaction is enhanced when Arl3 is GTP-bound was corroborated in this study (Bartolini *et al.* 2002). Furthermore, the data from Kuhnel *et al* (2006) implying that RP2 is able to act as a GDI for Arl3 was supported by this study showing the relocalisation of RP2 and Arl3-GTP to the Golgi (Kuhnel *et al.*, 2006). Data presented in this thesis also suggest that RP2 may be involved in vesicular trafficking in the cell in the presence of Arl3-GTP.

Further investigation into this aspect of the interaction is required but it would also be interesting to examine whether this trafficking may be related to the intraflagellar transport (IFT) in cilia. Studies have shown that rates of movement along sensory cilia are approximately 0.65 μm/sec in the anterograde direction and approximately

1.08 µm/sec in the retrograde direction (Orozco *et al.*, 1999, Signor *et al.*, 1999). After more detailed determination of the rate of movement of RP2-GFP it may be interesting to observe RP2 and Arl3-GTP in ciliated cells and to investigate any potential role in IFT. There is also the possibility that RP2 may be utilising the actin network for the intracellular movement described in Chapter 4. Actin-based transport is believed to be slower and occurs over shorter distances than microtubule-based transport (Apodaca, 2001). In contrast to microtubule-based transport which utilises dynein and kinesin motors (Brady, 1991), actin-based transport involves myosin motors. The speed of actin-based transport has been estimated to be approximately 0.1 µm/sec (Apodaca, 2001) which is close to the 0.06 µm/sec estimation for RP2-GFP rates (section 4.6). The ability of RP2 to bind to actin has not been investigated but the presence of the two CARP domains in the TBCC homology domain suggests it is possible RP2 may have some association with actin. Interestingly, one of the myosin motors implicated in actin-based transport which is localised to the connecting cilium in photoreceptors, Myosin VIIa is the most common gene mutated in Usher syndrome one of the phenotypes of which is RP (Weil *et al.*, 1995, Liu *et al.*, 1997, Jaijo *et al.*, 2007). Therefore, further investigation of the exact mechanism of the vesicular transport system that RP2 may be involved in is an interesting avenue to explore.

The homology between RP2 and TBCC has been investigated (Bartolini *et al.*, 2002, Grayson *et al.*, 2002) revealing that RP2 and TBCC do share some functions (Bartolini *et al.*, 2002). There is no experimental evidence currently available however as to the potential function of TBCCD1. Bartolini (2005) and colleagues reported the tubulin destabilising properties of another protein homologous to another tubulin-specific cofactor, TBCE, called E-like (Bartolini *et al.*, 2005). It is possible, therefore, that studies involving TBCCD1 and other potential cofactor homologs may reveal the fine control and regulation of the microtubule cytoskeleton.

The Sos recruitment system (SRS) was used to identify five novel putative interacting partners for RP2. The use of domain constructs and pathogenic mutants was used to define the RP2 interaction domain. Interestingly, all the novel interactors identified, except Arl2, interact with RP2 through the C-terminus and were all nuclear proteins. This data suggests that RP2 is a multifunctional protein and may have a role in the nucleus or nuclear envelope perhaps by transporting proteins to the nucleus through interactions mediated by its C-terminus. The missense mutations found in both domains suggest that the potential differential functions mediated by the two

homologous domains in RP2 are both important for RP2's function in retina. It is also interesting to speculate as to how RP2 differentiates between the C-terminal interacting partners, it is possible for example that they compete for binding to RP2. It was not possible to detect TNPO3, SPAG7, RAN or CDKN1B bound to RP2 in alternative binding assays but the optimum conditions for each interaction are unknown and it is possible that there was no binding detected due to competition from the other interactors. Competition assays could be performed to test this hypothesis. Also, it is possible that the interactions occur in different cellular compartments or under different cellular conditions. The use of site directed mutagenesis (SDM) could define the interaction domain for each protein more precisely, for example by mutating residues conserved in the NDK-homology domain between *E.coli* NDK, human NDK 1 and 2 and RP2, and as such assist in understanding the mechanisms by which RP2 is able to differentiate between the interactors.

As described in Chapter 1 RP causative mutations in *RP2* and *RPGR* result in indistinguishable phenotypes. RCC1 is the only currently reported GEF for RAN, but it is possible that there are alternative GEFs for RAN. The RCC1 domain of RPGR suggests that RPGR could have some GEF activity towards RAN. There are no reports of RPGR having any GEF activity for RAN but it may be that this function of RPGR is dependent on an adaptor protein or very particular cellular conditions which are not yet defined. RPGR and Arl3 also have a mutual interacting partner in PDEδ (Linari *et al.* 1999a, Linari *et al.*, 1999b). Thus a putative pathway involving both RPGR and RP2 appears to be emerging.

The investigation of the RP2-RAN interaction led to an interesting observation regarding the effect that RP2-GFP appeared to exert over myc-RAN. Expression of myc-tagged wild type RAN resulted in myc-RAN expression in the cytoplasm and amorphic cells rather than the expected nuclear distribution (Figure 5.7). However in the presence of RP2-GFP there was a reduction in the number of amorphic cells and a significant number of cells were now observed to have myc-RAN localised in the nucleus. It is possible that RP2 is acting as a GEF for RAN or recruiting a GEF, such as RPGR, to facilitate the conversion of RAN-GDP to RAN-GTP which localises to the nucleus. A further possibility is that RP2 has a chaperone function for RAN. As RP2 has homology to TBCC it has been speculated that RP2 may also have some chaperone activity. Whether RP2 functions as a chaperone for RAN or is involved in the recruitment of other proteins involved in the targeting of RAN to the nucleus and

hence to RCC1 remains to be investigated but the data does provide another interesting potential link to RPGR. RPGR has been shown to interact with Nucelophosmin 1, which is a nuclear chaperone (Frehlick *et al.*, 2006), through the retinal-dominant ORF15 isoform (Shu *et al.*, 2005). Since there is potential of RPGR to act as a GEF for RAN it is possible that RP2 and RPGR act in concert to initiate the localisation of RAN to the nucleus possibly through Nucleophosmin 1 (Figures 5.7 and 5.8).

The potential link between RP2 and RPGR could be investigated further through the study of RPGR animal models. There are canine and murine models for *RPGR* mutations which could be utilised to observe expression and localisation changes in key proteins in the predicted pathway such as HRG4, PDEδ, RAN, Nucleophosmin 1, Arl3, and RPGRIP1 (Hong *et al.*, 2000, Beltran *et al.*, 2006).

The importance of ubiquitously expressed splicing factors in normal retinal function is apparent due to identification of pathogenic mutations in four such genes that result in autosomal dominant retinitis pigmentosa (Sullivan *et al.*, 2006, McKie *et al.*, 2001, Chakarova *et al.*, 2002, Maita *et al.*, 2004). The identification of TNPO3 as a putative interacting partner for RP2 further suggests that splicing is an important aspect of normal retinal function. TNPO3 is involved in the transport of SR splicing factors to the nucleus (Lai *et al.*, 2000, Lai *et al.*, 2001) as well as being shown to interact with a non-SR splicing factor (Lai *et al.*, 2003). Interestingly, a study in *Drosophila melanogaster* using co-immunoprecipitations and microarray screening techniques identified groups of mRNAs that were regulated by specific SR proteins (Gabut *et al.*, 2007). One of the SR proteins studied by Gabut *et al* (2007) was dASF/SF2, the *D.melanogaster* homolog of ASF/SF2, which was one of the SR proteins Lai *et al* (2000) showed interacted with TNPO3 (Gabut *et al.*, 2007, Lai *et al.*, 2000). dASF/SF2 was also shown to be important for the regulation of splicing of a number of genes involved in eye development (Gabut *et al.*, 2007). A hypothesis for the reason that mutations in splicing factors may cause RP is that alteration in their activity may result in aberrant splicing, which is supported by the work by Mordes and colleagues (2007) showing reduced expression of the retinal-specific gene *RDS* when the splicing factor *PRPF31* was mutated (Mordes *et al.*, 2007).

The RP2-TNPO3 interaction may be important for the downstream effects of TNPO3, in that if the interaction between RP2 and TNPO3 is disrupted by mutations in RP2, TNPO3 may not be able to bind to the SR splicing factors (e.g. ASF/SF2) and as

such they would not be transported to the nucleus where they are able to regulate the splicing of important retinal genes. Furthermore, it has been shown that murine RPGR, which undergoes alternative splicing, has purine-rich exonic splicing enhancers (ESEs) in the sequence, elements that have been shown to interact with SR splicing factors (Lavigueur *et al.*, 1993, Hong and Li, 2002). The authors suggest that the alternative splicing of RPGR may indeed be regulated by SR proteins binding to these ESEs and affecting the alternative splicing of the ORF15 exon shown to contain RP-causing mutations (Hong and Li, 2002).

CDKN1B has been shown to be important in both the development and function of the retina through studies using retinal progenitor cells (Dyer and Cepko, 2001) and a knock out mouse model (Nakayama *et al.*, 1996). Furthermore there is evidence that CDKN1B acts as a modifier for the Chx10 null mutation, a homeobox gene which acts to regulate the proliferation of retinal progenitor cells (Liang *et al.*, 2007). As such the murine model, a knock out of *Chx10*, has been described as having a reduced number of retinal cells which may be explained by the loss of repression of CDKN1B which is normally mediated by Chx10 (Liang *et al.*, 2007). These data clearly implicate the correct regulation and function of CDKN1B is vital to normal retinal function. If, therefore, the RP2-CDKN1B interaction was important for the regulation of CDKN1B then disruption of the interaction may indeed have implications for the retina.

CDKN1B has three potential phosphorylation sites (Figure 5.10), the phosphorylation at each residue has been shown to have different effects on the CDKN1B's localisation (Lee *et al.* 2007) and that there are different mechanisms involved in the phosphorylation of CDKN1B at the Ser10 and Thr187 residues (Lee *et al.* 2007). Therefore, the possibility that there are at least two different populations of CDKN1B (Lee *et al.*, 2007) leads to the question whether RP2 would preferentially interact with differently phosphorylated forms of CDKN1B.

The physiological significance of the interaction between RP2 and SPAG7 still remains to be elucidated but does provide a link with data published by Yoon *et al* (2006) indicating that RP2 has the ability to translocate to the nucleus under DNA damaging conditions (Yoon *et al.*, 2006). As with all the novel interactors that are nuclear proteins the reported ability of RP2 to translocate to the nucleus offers the possibility that the interactions occur in the nucleus or on the nuclear envelope. For SPAG7, however, this is more likely due to the R3H domain in SPAG7 potentially

mediating the ability of SPAG7 to bind to ssDNA, thus it is possible that the RP2-SPAG7 interaction only occurs when RP2 translocates to the nucleus upon DNA damage in which instance it may facilitate the binding of SPAG7 to the damaged ssDNA. The potential phosphorylation of SPAG7 may also potentially shed further light on the optimal conditions for the RP2-SPAG7 interaction as RP2 may preferentially bind to SPAG7 if it is phosphorylated.

There are links emerging not only between RP2 and other retinal disease proteins but also between the novel interactors themselves. CDKN1B and TNPO3 have both been shown to interact with RAN (Lai *et al.*, 2000, Connor *et al.*, 2003). Although whether the interaction with RAN is simply due to the proteins' nuclear targeting being mediated by RAN, or whether it may be more complex and related to the putative interaction with RP2 remains to be seen.

The use of yeast two-hybrid to discover new interacting partners and delineate pathways is a widely used approach and more recently large scale screening has become possible leading to the generation of large scale interactome maps. Using such screens and other published interactors it has been possible to create a putative RP2 interactome (Figure 6.1) (Stelzl *et al.*, 2005, Colland *et al.*, 2004). This approach highlights the potential links RP2 has to other retinal disease proteins, for example there are several proteins that link RP2 to HRG4 as well as the links between RP2 and RPGR and hence RPGRIP1 and RPGRIP1L. A clearly important emerging theme appears to be the importance of cilia in the pathogenesis of retinal disease, a link already clearly established, and although RP2 has not been detected in a recent cilia proteome screen (Liu *et al.*, 2007) it may be that RP2 plays a role in signalling or at the cilia base rather than within the cilia itself.

The importance of RAN in retinal degeneration also requires further investigation. RAN has been shown to interact with the nucleoporin RanBP2 (Nup358) (Yokoyama *et al.*, 1995) and RanBP2 has been shown to associate with RPGRIP1 in amacrine cells in retina (Castagnet *et al.* 2003) (Figure 6.1). Another of RPGR's interacting partners, Nucleophosmin 1, has also been shown to be regulated by RAN and Exportin 1 (Wang *et al.*, 2005), further strengthening the connection between RAN and RPGR (Figure 6.1). In a similar way it is possible to see connections between HRG4 and PDE δ and Centrin 3, a protein thought to be involved in transducin regulation in the photoreceptor connecting cilium (Friedberg, 2006) (Figure 6.1).

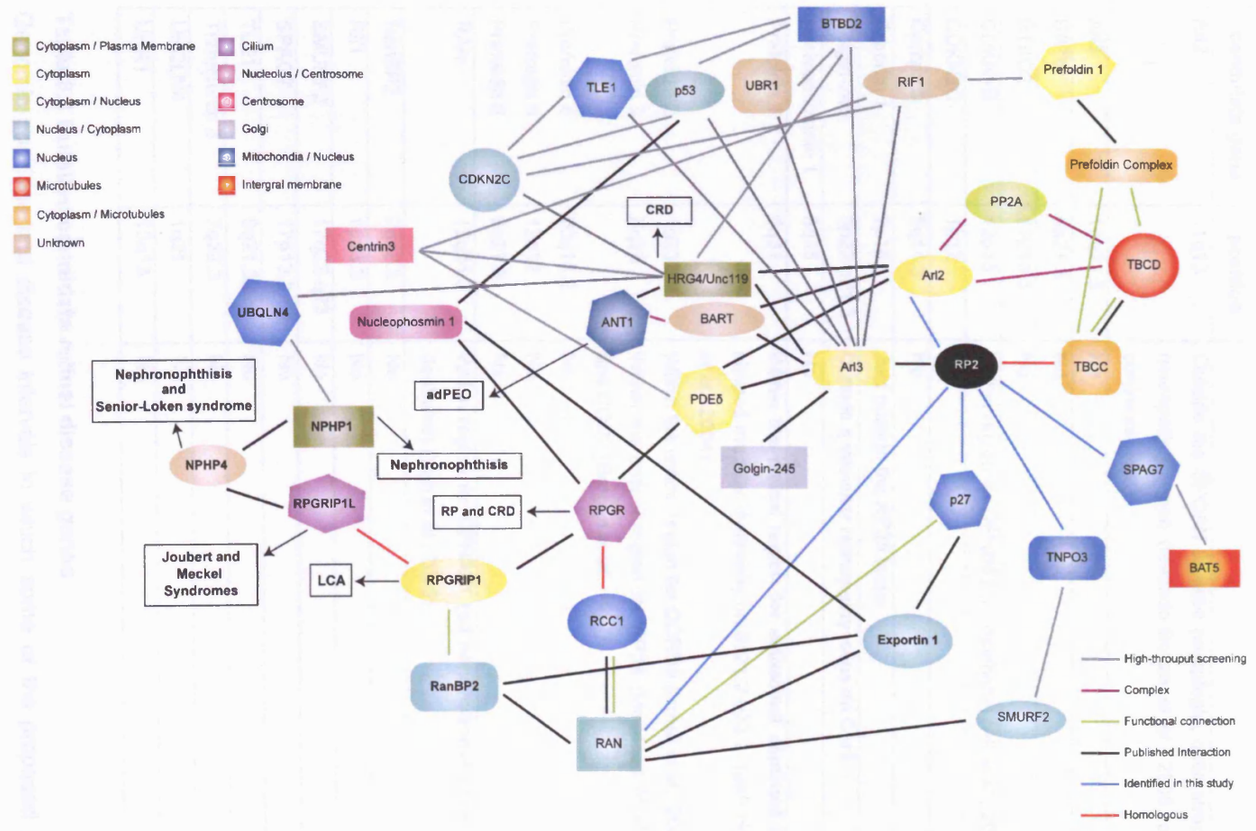

Figure 6.1 The RP2 interactome

Putative candidate gene	Genomic position	Disease loci ?
Arl2	11q13	Outside the SPOAN (spastic paraplegia, optic atrophy and neuropathy) region (Macedo-Souza *et al.*, 2005, personal communication)
Arl3	10q23.3	No
BAT5	6p21.3	No
BTBD2	19p13.3	No
CDKN1B	12p13	Within region for DFNB62 (ar deafness) (Ali *et al.*, 2006)
CDKN2C	1p32	No
Centrin 3	5q14.3	No
Exportin 1	2p16	Just outside the RP28 locus
Golgin-245	3p22-p21.3	Outside a vascular retinopathy locus on Chr3
Nucleophosmin 1	5q35	No
Prefoldin 1	5q31	Within the critical region for autosomal dominant butterfly shaped macular dystrophy on 5q21.2-q33.2. (den Hollander *et al.*, 2004)
Prefoldin 2	1q23.3	Within the critical region for CORD8 (Ismail *et al.*, 2006)
Prefoldin 3	Xq28	Within the critical region for RP34 (Melamud *et al.*, 2006) and COD2 (Bergen *et al., 1997)*
Prefoldin 4	20q13.2	No
Prefoldin 5	12q12	No
Prefoldin 6	6p21.3	No
RAN	12q24.3	Within region for DFNA41 (ad nonsyndromic sensorineural deafness) (Yan *et al.*, 2005)
RanBP2	2q12.3	No
Rif1	1p13.3	No
SMURF2	17q22-q23	No
SPAG7	17p13.2	No
TLE1	9q21.32	No
Transportin 3	7q32.3	No
UBQLN4	1q21	No
UBR1	15q13	No

Table 6.1 Putative candidate retinal disease genes

Genomic positions and disease intervals in which some of the proposed putative ocular candidate disease genes lie (see Figure 6.1).

Therefore it may be interesting to investigate any association Centrin 3 may have with other retinal disease proteins in the connecting cilium such as RPGR.

Figure 6.1 shows the putative links between RP2 and other retinal degeneration proteins, it also provides a means to highlight possible candidate disease genes. Table 6.1 shows the genomic position of several putative candidate retinal disease genes and whether there are any ocular or cilia-related disease loci mapping to their genomic regions (Table 6.1). Several proteins shown in Figure 6.1 are located within the mapped critical regions for ocular diseases, for example members of the Prefoldin complex (Table 6.1).

The ubiquitous expression profile of RP2 and its known and putative interacting partners means that the pathogenesis of RP2 mutations in RP remains unclear. However, there are several emerging pathways which when further investigated, will assist in not only the understanding of RP2's retinal function, but that of many other retinal disease proteins.

REFERENCES

Aijaz, S., Erskine, L., Jeffery, G., Bhattacharya, S. S., and Votruba, M. (2004). Developmental expression profile of the optic atrophy gene product: OPA1 is not localized exclusively in the mammalian retinal ganglion cell layer. *Invest Ophthalmol.Vis.Sci.* **45**, 1667-1673.

Alberts B, Bray D, Lewis J, Raff M, Roberts K, Watson JD. Molecular Biology of the Cell, 3rd Edition (1994). *Garland Publishing.*

Ali, G., Santos, R. L., John, P., Wambangco, M. A., Lee, K., Ahmad, W., and Leal, S. (2006). The mapping of DFNB62, a new locus for autosomal recessive non-syndromic hearing impairment, to chromosome 12p13.2-p11.23. *Clin.Genet.* **69**, 429-433.

Allikmets, R., Singh, N., Sun, H., Shroyer, N. F., Hutchinson, A., Chidambaram, A., Gerrard, B., Baird, L., Stauffer, D., Peiffer, A., Rattner, A., Smallwood, P., Li, Y., Anderson, K. L., Lewis, R. A., Nathans, J., Leppert, M., Dean, M., and Lupski, J. R. (1997). A photoreceptor cell-specific ATP-binding transporter gene (ABCR) is mutated in recessive Stargardt macular dystrophy. *Nat.Genet.* **15**, 236-246.

Allikmets, R. (2004). Leber congenital amaurosis: a genetic paradigm. *Ophthalmic Genet.* **25**, 67-79.

Amor, J. C., Horton, J. R., Zhu, X., Wang, Y., Sullards, C., Ringe, D., Cheng, X., and Kahn, R. A. (2001). Structures of yeast ARF2 and ARL1: distinct roles for the N terminus in the structure and function of ARF family GTPases. *J.Biol.Chem.* **276**, 42477-42484.

Andreasson, S., Breuer, D., Eksandh, L., Ponjavic, V., Frennesson, C., Hiriyanna, S., Filippova, E., Yashar, B., and Swaroop, A. (2003). Clinical studies of X-linked retinitis pigmentosa in three Swedish families with newly identified mutations in the RP2 and RPGR-ORF15 genes. *Ophthalmic Genet.* **24**, 215-223.

Antoshechkin, I. and Han, M. (2002). The C. elegans evl-20 gene is a homolog of the small GTPase ARL2 and regulates cytoskeleton dynamics during cytokinesis and morphogenesis. *Dev.Cell* **2**, 579-591.

Apodaca, G. (2001). Endocytic traffic in polarized epithelial cells: role of the actin and microtubule cytoskeleton. *Traffic.* **2**, 149-159.

Arikawa, K., Molday, L. L., Molday, R. S., and Williams, D. S. (1992). Localization of peripherin/rds in the disk membranes of cone and rod photoreceptors: relationship to disk membrane morphogenesis and retinal degeneration. *J.Cell Biol.* **116**, 659-667.

Aronheim, A., Engelberg, D., Li, N., al Alawi, N., Schlessinger, J., and Karin, M. (1994). Membrane targeting of the nucleotide exchange factor Sos is sufficient for activating the Ras signaling pathway. *Cell* **78**, 949-961.

Arts, H. H., Doherty, D., van Beersum, S. E., Parisi, M. A., Letteboer, S. J., Gorden, N. T., Peters, T. A., Marker, T., Voesenek, K., Kartono, A., Ozyurek, H., Farin, F. M., Kroes, H. Y., Wolfrum, U., Brunner, H. G., Cremers, F. P., Glass, I. A., Knoers, N. V., and Roepman, R. (2007). Mutations in the gene encoding the basal body protein RPGRIP1L, a nephrocystin-4 interactor, cause Joubert syndrome. *Nat.Genet.* **39**, 882-888.

Azarian, S. M. and Travis, G. H. (1997). The photoreceptor rim protein is an ABC transporter encoded by the gene for recessive Stargardt's disease (ABCR). *FEBS Lett.* **409**, 247-252.

Bader, I., Brandau, O., Achatz, H., Apfelstedt-Sylla, E., Hergersberg, M., Lorenz, B., Wissinger, B., Wittwer, B., Rudolph, G., Meindl, A., and Meitinger, T. (2003). X-linked retinitis pigmentosa: RPGR mutations in most families with definite X linkage and clustering of mutations in a short sequence stretch of exon ORF15. *Invest Ophthalmol.Vis.Sci.* **44**, 1458-1463.

Banerjee, P., Kleyn, P. W., Knowles, J. A., Lewis, C. A., Ross, B. M., Parano, E., Kovats, S. G., Lee, J. J., Penchaszadeh, G. K., Ott, J., Jacobson, S. G., and Gilliam, T. C. (1998). TULP1 mutation in two extended Dominican kindreds with autosomal recessive retinitis pigmentosa. *Nat.Genet.* **18**, 177-179.

Bareil, C., Hamel, C. P., Delague, V., Arnaud, B., Demaille, J., and Claustres, M. (2001). Segregation of a mutation in CNGB1 encoding the beta-subunit of

the rod cGMP-gated channel in a family with autosomal recessive retinitis pigmentosa. *Hum.Genet.* **108**, 328-334.

Bartolini, F., Bhamidipati, A., Thomas, S., Schwahn, U., Lewis, S. A., and Cowan, N. J. (2002). Functional overlap between retinitis pigmentosa 2 protein and the tubulin-specific chaperone cofactor C. *J.Biol.Chem.* **277**, 14629-14634.

Bartolini, F., Tian, G., Piehl, M., Cassimeris, L., Lewis, S. A., and Cowan, N. J. (2005). Identification of a novel tubulin-destabilizing protein related to the chaperone cofactor E. *J.Cell Sci.* **118**, 1197-1207.

Bayes, M., Giordano, M., Balcells, S., Grinberg, D., Vilageliu, L., Martinez, I., Ayuso, C., Benitez, J., Ramos-Arroyo, M. A., Chivelet, P., and . (1995). Homozygous tandem duplication within the gene encoding the beta-subunit of rod phosphodiesterase as a cause for autosomal recessive retinitis pigmentosa. *Hum.Mutat.* **5**, 228-234.

Beales, P. L. (2005). Lifting the lid on Pandora's box: the Bardet-Biedl syndrome. *Curr.Opin.Genet.Dev.* **15**, 315-323.

Beaton, S., Cleary, A., ten Have, J., and Bradley, M. P. (1994). Cloning and characterization of a fox sperm protein FSA-1. *Reprod.Fertil.Dev.* **6**, 761-770.

Beltran, W. A., Hammond, P., Acland, G. M., and Aguirre, G. D. (2006). A frameshift mutation in RPGR exon ORF15 causes photoreceptor degeneration and inner retina remodeling in a model of X-linked retinitis pigmentosa. *Invest Ophthalmol.Vis.Sci.* **47**, 1669-1681.

Bennett, S. E., Chen, C. Y., and Mosbaugh, D. W. (2004). Escherichia coli nucleoside diphosphate kinase does not act as a uracil-processing DNA repair nuclease. *Proc.Natl.Acad.Sci.U.S.A* **101**, 6391-6396.

Bergen, A.A and Pinckers, A.J. (1997). Localization of a novel X-linked progressive cone dystrophy gene to Xq27: evidence for genetic heterogeneity. *Am J Hum Genet.* **60**(6): 1468-73

Besharse JC and Horst CJ. The photoreceptor connecting cilium. A model for the transition zone. (1990). *Ciliary and Flagelluar Membranes*. Plenum Press, pp389-443.

Bessant, D. A., Payne, A. M., Mitton, K. P., Wang, Q. L., Swain, P. K., Plant, C., Bird, A. C., Zack, D. J., Swaroop, A., and Bhattacharya, S. S. (1999). A mutation in NRL is associated with autosomal dominant retinitis pigmentosa. *Nat.Genet.* **21**, 355-356.

Bhamidipati, A., Lewis, S. A., and Cowan, N. J. (2000). ADP ribosylation factor-like protein 2 (Arl2) regulates the interaction of tubulin-folding cofactor D with native tubulin. *J.Cell Biol.* **149**, 1087-1096.

Bird, A. C. (1975). X-linked retinitis pigmentosa. *Br.J.Ophthalmol.* **59** , 177-199.

Blacque, O. E., Reardon, M. J., Li, C., McCarthy, J., Mahjoub, M. R., Ansley, S. J., Badano, J. L., Mah, A. K., Beales, P. L., Davidson, W. S., Johnsen, R. C., Audeh, M., Plasterk, R. H., Baillie, D. L., Katsanis, N., Quarmby, L. M., Wicks, S. R., and Leroux, M. R. (2004). Loss of C. elegans BBS-7 and BBS-8 protein function results in cilia defects and compromised intraflagellar transport. *Genes Dev.* **18** , 1630-1642.

Bok, D. (1993). The retinal pigment epithelium: a versatile partner in vision. *J.Cell Sci.Suppl* **17**, 189-195.

Bomont, P., Cavalier, L., Blondeau, F., Ben Hamida, C., Belal, S., Tazir, M., Demir, E., Topaloglu, H., Korinthenberg, R., Tuysuz, B., Landrieu, P., Hentati, F., and Koenig, M. (2000). The gene encoding gigaxonin, a new member of the cytoskeletal BTB/kelch repeat family, is mutated in giant axonal neuropathy. *Nat.Genet.* **26**, 370-374.

Borriello, A., Cucciolla, V., Oliva, A., Zappia, V., and Della, R. F. (2007). p27Kip1 metabolism: a fascinating labyrinth. *Cell Cycle* **6**, 1053-1061.

Bourne, H. R., Sanders, D. A., and McCormick, F. (1990). The GTPase superfamily: a conserved switch for diverse cell functions. *Nature* **348**, 125-132.

Bowne, S. J., Daiger, S. P., Hims, M. M., Sohocki, M. M., Malone, K. A., McKie, A. B., Heckenlively, J. R., Birch, D. G., Ingleheam, C. F., Bhattacharya, S. S., Bird, A., and Sullivan, L. S. (1999). Mutations in the RP1 gene causing autosomal dominant retinitis pigmentosa . *Hum.Mol.Genet.* **8**, 2121-2128.

Boylan, J. P. and Wright, A. F. (2000). Identification of a novel protein interacting with RPGR. *Hum.Mol.Genet.* **9**, 2085-2093.

Brady, S. T. (1991). Molecular motors in the nervous system. *Neuron* **7**, 521-533.

Breuer, D. K., Yashar, B. M., Filippova, E., Hiriyanna, S., Lyons, R. H., Mears, A. J., Asaye, B., Acar, C., Vervoort, R., Wright, A. F., Musarella, M. A., Wheeler, P., MacDonald, I., Iannaccone, A., Birch, D., Hoffman, D. R., Fishman, G. A., Heckenlively, J. R., Jacobson, S. G., Sieving, P. A., and Swaroop, A. (2002). A comprehensive mutation analysis of RP2 and RPGR in a North American cohort of families with X-linked retinitis pigmentosa. *Am.J.Hum.Genet.* **70**, 1545-1554.

Bridges, C. D. (1985). The interphotoreceptor matrix--functions and possible role in hereditary retinal degenerations. *Prog.Clin.Biol.Res.* **190**, 195-212.

Broder, Y. C., Katz, S., and Aronheim, A. (1998). The ras recruitment system, a novel approach to the study of protein-protein interactions. *Curr.Biol.* **8**, 1121-1124.

Bron AJ, Tripathi RC and Tripathi BJ. Wolff's Anatomy of the eye and orbit, 8th edition (1997). *Chapman & Hall.*

Burd, C. G., Strochlic, T. I., and Gangi, S., Sr. (2004). Arf-like GTPases: not so Arf-like after all. *Trends Cell Biol.* **14**, 687-694.

Caldon, C. E., Daly, R. J., Sutherland, R. L., and Musgrove, E. A. (2006). Cell cycle control in breast cancer cells. *J.Cell Biochem.* **97**, 261-274.

Carazo-Salas, R. E., Guarguaglini, G., Gruss, O. J., Segref, A., Karsenti, E., and Mattaj, I. W. (1999). Generation of GTP-bound Ran by RCC1 is required for chromatin-induced mitotic spindle formation. *Nature* **400**, 178-181.

Carelli, V., Ross-Cisneros, F. N., and Sadun, A. A. (2004). Mitochondrial dysfunction as a cause of optic neuropathies. *Prog.Retin.Eye Res.* **23**, 53-89.

Carrano, A. C., Eytan, E., Hershko, A., and Pagano, M. (1999). SKP2 is required for ubiquitin-mediated degradation of the CDK inhibitor p27. *Nat.Cell Biol.* **1**, 193-199.

Castagnet, P., Mavlyutov, T., Cai, Y., Zhong, F., and Ferreira, P. (2003). RPGRIP1s with distinct neuronal localization and biochemical properties

associate selectively with RanBP2 in amacrine neurons. *Hum.Mol.Genet.* **12**, 1847-1863.

Caudron, M., Bunt, G., Bastiaens, P., and Karsenti, E. (2005). Spatial coordination of spindle assembly by chromosome-mediated signaling gradients. *Science* **309**, 1373-1376.

Causier, B. and Davies, B. (2002). Analysing protein-protein interactions with the yeast two-hybrid system. *Plant Mol.Biol.* **50**, 855-870.

Cen, O., Gorska, M. M., Stafford, S. J., Sur, S., and Alam, R. (2003). Identification of UNC119 as a novel activator of SRC-type tyrosine kinases. *J.Biol.Chem.* **278**, 8837-8845.

Chakarova, C. F., Hims, M. M., Bolz, H., Abu-Safieh, L., Patel, R. J., Papaioannou, M. G., Inglehearn, C. F., Keen, T. J., Willis, C., Moore, A. T., Rosenberg, T., Webster, A. R., Bird, A. C., Gal, A., Hunt, D., Vithana, E. N., and Bhattacharya, S. S. (2002). Mutations in HPRP3, a third member of pre-mRNA splicing factor genes, implicated in autosomal dominant retinitis pigmentosa. *Hum.Mol.Genet.* **11**, 87-92.

Chapple, J. P., Hardcastle, A. J., Grayson, C., Spackman, L. A., Willison, K. R., and Cheetham, M. E. (2000). Mutations in the N-terminus of the X-linked retinitis pigmentosa protein RP2 interfere with the normal targeting of the protein to the plasma membrane. *Hum.Mol.Genet.* **9**, 1919-1926.

Chapple, J. P., Hardcastle, A. J., Grayson, C., Willison, K. R., and Cheetham, M. E. (2002). Delineation of the plasma membrane targeting domain of the X-linked retinitis pigmentosa protein RP2. *Invest Ophthalmol.Vis.Sci.* **43**, 2015-2020.

Chen, S., Wang, Q. L., Nie, Z., Sun, H., Lennon, G., Copeland, N. G., Gilbert, D. J., Jenkins, N. A., and Zack, D. J. (1997). Crx, a novel Otx-like paired-homeodomain protein, binds to and transactivates photoreceptor cell-specific genes. *Neuron* **19**, 1017-1030.

Chiang, A. P., Nishimura, D., Searby, C., Elbedour, K., Carmi, R., Ferguson, A. L., Secrist, J., Braun, T., Casavant, T., Stone, E. M., and Sheffield, V. C. (2004). Comparative genomic analysis identifies an ADP-ribosylation factor-like gene as the cause of Bardet-Biedl syndrome (BBS3). *Am.J.Hum.Genet.* **75**, 475-484.

Colland, F., Jacq, X., Trouplin, V., Mougin, C., Groizeleau, C., Hamburger, A., Meil, A. , Wojcik, J., Legrain, P., and Gauthier, J. M. (2004). Functional proteomics mapping of a human signaling pathway. *Genome Res.* **14**, 1324-1332.

Connor, M. K., Kotchetkov, R., Cariou, S., Resch, A., Lupetti, R., Beniston, R. G., Melchior, F., Hengst, L., and Slingerland, J. M. (2003). CRM1/Ran-mediated nuclear export of p27(Kip1) involves a nuclear export signal and links p27 export and proteolysis. *Mol.Biol.Cell* **14**, 201-213.

Coppieters, F., Leroy, B. P., Beysen, D., Hellemans, J., De Bosscher, K., Haegeman, G., Robberecht, K., Wuyts, W., Coucke, P. J., and De Baere, E. (2007). Recurrent Mutation in the First Zinc Finger of the Orphan Nuclear Receptor NR2E3 Causes Autosomal Dominant Retinitis Pigmentosa. *Am.J.Hum.Genet.* **81**, 147-157.

Cremers, F. P., van de Pol, D. J., van Driel, M., den Hollander, A. I., van Haren, F. J., Knoers, N. V., Tijmes, N., Bergen, A. A., Rohrschneider, K., Blankenagel, A., Pinckers, A. J., Deutman, A. F., and Hoyng, C. B. (1998). Autosomal recessive retinitis pigmentosa and cone-rod dystrophy caused by splice site mutations in the Stargardt's disease gene ABCR. *Hum.Mol.Genet.* **7**, 355-362.

Curcio, C. A., Sloan, K. R., Kalina, R. E., and Hendrickson, A. E. (1990). Human photoreceptor topography. *J.Comp Neurol.* **292**, 497-523.

Cuvillier, A., Redon, F., Antoine, J. C., Chardin, P., DeVos, T., and Merlin, G. (2000). LdARL-3A, a Leishmania promastigote-specific ADP-ribosylation factor-like protein, is essential for flagellum integrity. *J.Cell Sci.* **113 (Pt 11)**, 2065-2074.

Daiger, S. P., Bowne, S. J., and Sullivan, L. S. (2007). Perspective on genes and mutations causing retinitis pigmentosa. *Arch.Ophthalmol.* **125**, 151-158.

Dandekar, S. S., Ebenezer, N. D., Grayson, C., Chapple, J. P., Egan, C. A., Holder, G. E., Jenkins, S. A., Fitzke, F. W., Cheetham, M. E., Webster, A. R., and Hardcastle, A. J. (2004). An atypical phenotype of macular and peripapillary retinal atrophy caused by a mutation in the RP2 gene. *Br.J.Ophthalmol.* **88**, 528-532.

Davies, V. J., Hollins, A. J., Piechota, M. J., Yip, W., Davies, J. R., White, K. E., Nicols, P. P., Boulton, M. E., and Votruba, M. (2007). Opa1 deficiency in a mouse model of autosomal dominant optic atrophy impairs mitochondrial morphology, optic nerve structure and visual function. *Hum.Mol.Genet.* **16**, 1307-1318.

De Luca, A., Torrente, I., Mangino, M., Danesi, R., Dallapiccola, B., and Novelli, G. (2001). Three novel mutations causing a truncated protein within the RP2 gene in Italian families with X-linked retinitis pigmentosa. *Mutat.Res.* **432**, 79-82.

Defoe, D. M., Adams, L. B., Sun, J., Wisecarver, S. N., and Levine, E. M. (2007). Defects in retinal pigment epithelium cell proliferation and retinal attachment in mutant mice with p27(Kip1) gene ablation. *Mol.Vis.* **13**, 273-286.

Delous, M., Baala, L., Salomon, R., Laclef, C., Vierkotten, J., Tory, K., Golzio, C., Lacoste, T., Besse, L., Ozilou, C., Moutkine, I., Hellman, N. E., Anselme, I., Silbermann, F., Vesque, C., Gerhardt, C., Rattenberry, E., Wolf, M. T., Gubler, M. C., Martinovic, J., Encha-Razavi, F., Boddaert, N., Gonzales, M., Macher, M. A., Nivet, H., Champion, G., Bertheleme, J. P., Niaudet, P., McDonald, F., Hildebrandt, F., Johnson, C. A., Vekemans, M., Antignac, C., Ruther, U., Schneider-Maunoury, S., Attie-Bitach, T., and Saunier, S. (2007). The ciliary gene RPGRIP1L is mutated in cerebello-oculo-renal syndrome (Joubert syndrome type B) and Meckel syndrome. *Nat.Genet.* **39**, 875-881.

den Hollander, A. I., ten Brink, J. B. , de Kok, Y. J., van Soest, S., van den Born, L. I., van Driel, M. A., van de Pol, D. J., Payne, A. M., Bhattacharya, S. S., Kellner, U., Hoyng, C. B., Westerveld, A., Brunner, H. G., Bleeker-Wagemakers, E. M., Deutman, A. F., Heckenlively, J. R. , Cremers, F. P., and Bergen, A. A. (1999). Mutations in a human homologue of Drosophila crumbs cause retinitis pigmentosa (RP12). *Nat.Genet.* **23**, 217-221.

den Hollander, A. I., Heckenlively, J. R., van den Born, L. I., de Kok, Y. J., Velde-Visser, S. D., Kellner, U., Jurklies, B., van Schooneveld, M. J., Blankenagel, A., Rohrschneider, K., Wissinger, B., Cruysberg, J. R., Deutman, A. F., Brunner, H. G., Apfelstedt-Sylla, E., Hoyng, C. B., and Cremers, F. P. (2001). Leber congenital amaurosis and retinitis pigmentosa with Coats-like

exudative vasculopathy are associated with mutations in the crumbs homologue 1 (CRB1) gene. *Am.J.Hum.Genet.* **69**, 198-203.

den Hollander, A. I., Lith-Verhoeven, J. J., Kersten, F. F., Heister, J. G., de Kovel, C. G., Deutman, A. F., Hoyng, C. B., and Cremers, F. P. (2004). Identification of novel locus for autosomal dominant butterfly shaped macular dystrophy on 5q21.2-q33.2. *J.Med.Genet.* **41**, 699-702.

Dodatko, T., Fedorov, A. A., Grynberg, M., Patskovsky, Y., Rozwarski, D. A., Jaroszewski, L., Aronoff-Spencer, E., Kondraskina, E., Irving, T., Godzik, A., and Almo, S. C. (2004). Crystal structure of the actin binding domain of the cyclase-associated protein. *Biochemistry* **43**, 10628-10641.

Dryja, T. P., McGee, T. L., Hahn, L. B., Cowley, G. S., Olsson, J. E., Reichel, E., Sandberg, M. A., and Berson, E. L. (1990). Mutations within the rhodopsin gene in patients with autosomal dominant retinitis pigmentosa. *N.Engl.J.Med.* **323**, 1302-1307.

Dryja, T. P., Berson, E. L., Rao, V. R., and Oprian, D. D. (1993). Heterozygous missense mutation in the rhodopsin gene as a cause of congenital stationary night blindness. *Nat.Genet.* **4**, 280-283.

Dryja, T. P., Rucinski, D. E., Chen, S. H., and Berson, E. L. (1999). Frequency of mutations in the gene encoding the alpha subunit of rod cGMP-phosphodiesterase in autosomal recessive retinitis pigmentosa. *Invest Ophthalmol.Vis.Sci.* **40**, 1859-1865.

Dryja, T. P., Adams, S. M., Grimsby, J. L., McGee, T. L., Hong, D. H., Li, T., Andreasson, S., and Berson, E. L. (2001). Null RPGRIP1 alleles in patients with Leber congenital amaurosis. *Am.J.Hum.Genet.* **68**, 1295-1298.

Dyer, M. A. and Cepko, C. L. (2001). p27Kip1 and p57Kip2 regulate proliferation in distinct retinal progenitor cell populations. *J.Neurosci.* **21**, 4259-4271.

Edwards, A. O., Ritter, R., III, Abel, K. J., Manning, A., Panhuysen, C., and Farrer, L. A. (2005). Complement factor H polymorphism and age-related macular degeneration. *Science* **308**, 421-424.

Eisenberg, E. and Levanon, E. Y. (2003). Human housekeeping genes are compact. *Trends Genet.* **19**, 362-365.

Eley, L., Yates, L. M., and Goodship, J. A. (2005). Cilia and disease. *Curr.Opin.Genet.Dev.* **15**, 308-314.

Eudy, J. D., Weston, M. D., Yao, S., Hoover, D. M., Rehm, H. L., Ma-Edmonds, M., Yan, D., Ahmad, I., Cheng, J. J., Ayuso, C., Cremers, C., Davenport, S., Moller, C., Talmadge, C. B., Beisel, K. W., Tamayo, M., Morton, C. C., Swaroop, A., Kimberling, W. J., and Sumegi, J. (1998). Mutation of a gene encoding a protein with extracellular matrix motifs in Usher syndrome type IIa. *Science* **280**, 1753-1757.

Fan, Y., Esmail, M. A., Ansley, S. J., Blacque, O. E., Boroevich, K., Ross, A. J., Moore, S. J., Badano, J. L., May-Simera, H., Compton, D. S., Green, J. S., Lewis, R. A., van Haelst, M. M., Parfrey, P. S., Baillie, D. L., Beales, P. L., Katsanis, N., Davidson, W. S., and Leroux, M. R. (2004). Mutations in a member of the Ras superfamily of small GTP-binding proteins causes Bardet-Biedl syndrome. *Nat.Genet.* **36**, 989-993.

Fields, S. and Song, O. (1989). A novel genetic system to detect protein-protein interactions. *Nature* **340**, 245-246.

Frehlick, L. J., Eirin-Lopez, J. M., and Ausio, J. (2007). New insights into the nucleophosmin/nucleoplasmin family of nuclear chaperones. *Bioessays* **29**, 49-59.

Freund, C. L., Gregory-Evans, C. Y., Furukawa, T., Papaioannou, M., Looser, J., Ploder, L., Bellingham, J., Ng, D., Herbrick, J. A., Duncan, A., Scherer, S. W. , Tsui, L. C., Loutradis-Anagnostou, A., Jacobson, S. G., Cepko, C. L. , Bhattacharya, S. S., and McInnes, R. R. (1997). Cone-rod dystrophy due to mutations in a novel photoreceptor-specific homeobox gene (CRX) essential for maintenance of the photoreceptor. *Cell* **91**, 543-553.

Friedberg, F. (2006). Centrin isoforms in mammals. Relation to calmodulin. *Mol.Biol.Rep.* **33**, 243-252.

Gabut, M., Dejardin, J., Tazi, J., and Soret, J. (2007). The SR family proteins B52 and dASF/SF2 modulate development of the Drosophila visual system by regulating specific RNA targets. *Mol.Cell Biol.* **27**, 3087-3097.

Gal, A., Orth, U., Baehr, W., Schwinger, E., and Rosenberg, T. (1994). Heterozygous missense mutation in the rod cGMP phosphodiesterase beta-subunit gene in autosomal dominant stationary night blindness. *Nat.Genet.* **7**, 64-68.

Garcia-Hoyos, M., Garcia-Sandoval, B., Cantalapiedra, D., Riveiro, R., Lorda-Sanchez, I., Trujillo-Tiebas, M. J., Rodriguez, d. A., Millan, J. M., Baiget, M., Ramos, C., and Ayuso, C. (2006). Mutational screening of the RP2 and RPGR genes in Spanish families with X-linked retinitis pigmentosa. *Invest Ophthalmol.Vis.Sci.* **47**, 3777-3782.

Gerber, S., Rozet, J. M., Takezawa, S. I., dos Santos, L. C., Lopes, L., Gribouval, O., Penet, C., Perrault, I., Ducroq, D., Souied, E., Jeanpierre, M., Romana, S., Frezal, J., Ferraz, F., Yu-Umesono, R., Munnich, A., and Kaplan, J. (2000). The photoreceptor cell-specific nuclear receptor gene (PNR) accounts for retinitis pigmentosa in the Crypto-Jews from Portugal (Marranos), survivors from the Spanish Inquisition. *Hum.Genet.* **107**, 276-284.

Gerber, S., Perrault, I., Hanein, S., Barbet, F., Ducroq, D., Ghazi, I., Martin-Coignard, D., Leowski, C., Homfray, T., Dufier, J. L., Munnich, A., Kaplan, J., and Rozet, J. M. (2001). Complete exon-intron structure of the RPGR-interacting protein (RPGRIP1) gene allows the identification of mutations underlying Leber congenital amaurosis. *Eur.J.Hum.Genet.* **9**, 561-571.

Gietz, D., St Jean, A., Woods, R. A., and Schiestl, R. H. (1992). Improved method for high efficiency transformation of intact yeast cells. *Nucleic Acids Res.* **20**, 1425.

Grabowski, P. J. and Black, D. L. (2001). Alternative RNA splicing in the nervous system. *Prog.Neurobiol.* **65**, 289-308.

Graveley, B. R. (2000). Sorting out the complexity of SR protein functions. *RNA.* **6**, 1197-1211.

Grayson, C., Bartolini, F., Chapple, J. P., Willison, K. R., Bhamidipati, A., Lewis, S. A., Luthert, P. J., Hardcastle, A. J., Cowan, N. J., and Cheetham, M. E. (2002). Localization in the human retina of the X-linked retinitis pigmentosa protein RP2, its homologue cofactor C and the RP2 interacting protein Arl3 . *Hum.Mol.Genet.* **11**, 3065-3074.

Grayson, C., Chapple, J. P., Willison, K. R., Webster, A. R., Hardcastle, A. J., and Cheetham, M. E. (2002). In vitro analysis of aminoglycoside therapy for the Arg120stop nonsense mutation in RP2 patients. *J.Med.Genet.* **39**, 62-67.

Gu, S. M., Thompson, D. A., Srikumari, C. R., Lorenz, B., Finckh, U., Nicoletti, A., Murthy, K. R., Rathmann, M., Kumaramanickavel, G., Denton, M. J., and Gal, A. (1997). Mutations in RPE65 cause autosomal recessive childhood-onset severe retinal dystrophy. *Nat.Genet.* **17**, 194-197.

Haines, J. L., Hauser, M. A., Schmidt, S., Scott, W. K., Olson, L. M., Gallins, P., Spencer, K. L., Kwan, S. Y., Noureddine, M., Gilbert, J. R., Schnetz-Boutaud, N., Agarwal, A., Postel, E. A. , and Pericak-Vance, M. A. (2005). Complement factor H variant increases the risk of age-related macular degeneration. *Science* **308**, 419-421.

Hanein, S., Perrault, I., Gerber, S., Tanguy, G., Barbet, F., Ducroq, D., Calvas, P., Dollfus, H., Hamel, C., Lopponen, T., Munier, F., Santos, L., Shalev, S., Zafeiriou, D., Dufier, J. L., Munnich, A., Rozet, J. M., and Kaplan, J. (2004). Leber congenital amaurosis: comprehensive survey of the genetic heterogeneity, refinement of the clinical definition, and genotype-phenotype correlations as a strategy for molecular diagnosis. *Hum.Mutat.* **23**, 306-317.

Hanzal-Bayer, M., Renault, L., Roversi, P., Wittinghofer, A., and Hillig, R. C. (2002). The complex of Arl2-GTP and PDE delta: from structure to function. *EMBO J.* **21**, 2095-2106.

Hardcastle, A. J., Thiselton, D. L., Van Maldergem, L., Saha, B. K., Jay, M., Plant, C., Taylor, R., Bird, A. C., and Bhattacharya, S. (1999). Mutations in the RP2 gene cause disease in 10% of families with familial X-linked retinitis pigmentosa assessed in this study. *Am.J Hum.Genet.* **64**, 1210-1215.

Helou, J., Otto, E. A., Attanasio, M., Allen, S. J., Parisi, M., Glass, I., Utsch, B., Hashmi, S., Fazzi, E., Omran, H., O' Toole, J., Sayer, J., and Hildebrandt, F. (2007). Mutation analysis of NPHP6/CEP290 in patients with Joubert-Syndrome and Senior-Loken-Syndrome. *J.Med.Genet.*

Hendrickson, A. E. and Yuodelis, C. (1984). The morphological development of the human fovea. *Ophthalmology* **91**, 603-612.

Hetzer, M., Bilbao-Cortes, D., Walther, T. C., Gruss, O. J., and Mattaj, I. W. (2000). GTP hydrolysis by Ran is required for nuclear envelope assembly. *Mol.Cell* **5**, 1013-1024.

Hinchcliffe, E. H., Li, C., Thompson, E. A., Maller, J. L., and Sluder, G. (1999). Requirement of Cdk2-cyclin E activity for repeated centrosome reproduction in Xenopus egg extracts. *Science* **283**, 851-854.

Hong, D. H., Pawlyk, B. S., Shang, J., Sandberg, M. A., Berson, E. L., and Li, T. (2000). A retinitis pigmentosa GTPase regulator (RPGR)-deficient mouse model for X-linked retinitis pigmentosa (RP3). *Proc.Natl.Acad.Sci.U.S.A* **97**, 3649-3654.

Hong, D. H., Yue, G., Adamian, M., and Li, T. (2001). Retinitis pigmentosa GTPase regulator (RPGRr)-interacting protein is stably associated with the photoreceptor ciliary axoneme and anchors RPGR to the connecting cilium. *J.Biol.Chem.* **276**, 12091-12099.

Hong, D. H. and Li, T. (2002). Complex expression pattern of RPGR reveals a role for purine-rich exonic splicing enhancers. *Invest Ophthalmol.Vis.Sci.* **43**, 3373-3382.

Hong, D. H., Pawlyk, B., Sokolov, M., Strissel, K. J., Yang, J., Tulloch, B., Wright, A. F., Arshavsky, V. Y., and Li, T. (2003). RPGR isoforms in photoreceptor connecting cilia and the transitional zone of motile cilia. *Invest Ophthalmol.Vis.Sci.* **44**, 2413-2421.

Hong, J. X., Lee, F. J., Patton, W. A., Lin, C. Y., Moss, J., and Vaughan, M. (1998). Phosphol. *J.Biol.Chem.* **273**, 15872-15876.

Hoyt, M. A., Stearns, T., and Botstein, D. (1990). Chromosome instability mutants of Saccharomyces cerevisiae that are defective in microtubule-mediated processes. *Mol.Cell Biol.* **10**, 223-234.

Iannaccone, A., Wang, X., Jablonski, M. M., Kuo, S. F., Baldi, A., Cosgrove, D., Morton, C. C., and Swaroop, A. (2004). Increasing evidence for syndromic phenotypes associated with RPGR mutations. *Am.J.Ophthalmol.* **137**, 785-786.

Ishida, N., Hara, T., Kamura, T., Yoshida, M., Nakayama, K., and Nakayama, K. I. (2002). Phosphorylation of p27Kip1 on serine 10 is required for its binding to CRM1 and nuclear export. *J.Biol.Chem.* **277**, 14355-14358.

Ismail, M., Abid, A., Anwar, K., Mehdi, S. Q., and Khaliq, S. (2006). Refinement of the locus for autosomal recessive cone-rod dystrophy (CORD8) linked to chromosome 1q23-q24 in a Pakistani family and exclusion of candidate genes. *J.Hum.Genet.* **51**, 827-831.

Ito, H., Fukuda, Y., Murata, K., and Kimura, A. (1983). Transformation of intact yeast cells treated with alkali cations. *J.Bacteriol.* **153**, 163-168.

Jaijo, T., Aller, E., Beneyto, M., Najera, C., Graziano, C., Turchetti, D., Seri, M., Ayuso, C., Baiget, M., Moreno, F., Morera, C., Perez-Garrigues, H., and Millan, J. M. (2007). MYO7A mutation screening in Usher syndrome type I patients from diverse origins. *J.Med.Genet.* **44**, e71.

Joseph, J. (2006). Ran at a glance. *J.Cell Sci.* **119**, 3481-3484.

Kalab, P., Weis, K., and Heald, R. (2002). Visualization of a Ran-GTP gradient in interphase and mitotic Xenopus egg extracts. *Science* **295**, 2452-2456.

Kataoka, N., Bachorik, J. L., and Dreyfuss, G. (1999). Transportin-SR, a nuclear import receptor for SR proteins. *J.Cell Biol.* **145**, 1145-1152.

Keeler, L. C., Marsh, S. E., Leeflang, E. P., Woods, C. G., Sztriha, L., Al Gazali, L., Gururaj, A., and Gleeson, J. G. (2003). Linkage analysis in families with Joubert syndrome plus oculo-renal involvement identifies the CORS2 locus on chromosome 11p12-q13.3. *Am.J.Hum.Genet.* **73**, 656-662.

Khaliq, S., Abid, A., Ismail, M., Hameed, A., Mohyuddin, A., Lall, P., Aziz, A., Anwar, K., and Mehdi, S. Q. (2005). Novel association of RP1 gene mutations with autosomal recessive retinitis pigmentosa. *J.Med.Genet.* **42**, 436-438.

Kirschner, M. and Mitchison, T. (1986). Beyond self-assembly: from microtubules to morphogenesis . *Cell* **45**, 329-342.

Klein, M. L., Schultz, D. W., Edwards, A., Matise, T. C., Rust, K., Berselli, C. B., Trzupek, K., Weleber, R. G., Ott, J., Wirtz, M. K., and Acott, T. S. (1998). Age-

related macular degeneration. Clinical features in a large family and linkage to chromosome 1q. *Arch.Ophthalmol.* **116**, 1082-1088.

Kobayashi, A., Higashide, T., Hamasaki, D., Kubota, S., Sakuma, H., An, W., Fujimaki, T., McLaren, M. J., Weleber, R. G., and Inana, G. (2000). HRG4 (UNC119) mutation found in cone-rod dystrophy causes retinal degeneration in a transgenic model. *Invest Ophthalmol.Vis.Sci.* **41**, 3268-3277.

Kogelnik, A. M., Lott, M. T., Brown, M. D., Navathe, S. B., and Wallace, D. C. (1996). MITOMAP: a human mitochondrial genome database. *Nucleic Acids Res.* **24**, 177-179.

Kornbluth, S., Dasso, M., and Newport, J. (1994). Evidence for a dual role for TC4 protein in regulating nuclear structure and cell cycle progression. *J.Cell Biol.* **125**, 705-719.

Kremer, H., van Wijk, E., Marker, T., Wolfrum, U., and Roepman, R. (2006). Usher syndrome: molecular links of pathogenesis, proteins and pathways. *Hum.Mol.Genet.* **15 Spec No 2**, R262-R270.

Kubota, S., Kobayashi, A., Mori, N., Higashide, T., McLaren, M. J., and Inana, G. (2002). Changes in retinal synaptic proteins in the transgenic model expressing a mutant HRG4 (UNC119). *Invest Ophthalmol.Vis.Sci.* **43**, 308-313.

Kuhnel, K., Veltel, S., Schlichting, I., and Wittinghofer, A. (2006). Crystal structure of the human retinitis pigmentosa 2 protein and its interaction with Arl3. *Structure.* **14**, 367-378.

Lai, M. C., Lin, R. I., Huang, S. Y., Tsai, C. W., and Tarn, W. Y. (2000). A human importin-beta family protein, transportin-SR2, interacts with the phosphorylated RS domain of SR proteins. *J.Biol.Chem.* **275**, 7950-7957.

Lai, M. C., Lin, R. I., and Tarn, W. Y. (2001). Transportin-SR2 mediates nuclear import of phosphorylated SR proteins. *Proc.Natl.Acad.Sci.U.S.A* **98**, 10154-10159.

Lai, M. C., Kuo, H. W., Chang, W. C., and Tarn, W. Y. (2003). A novel splicing regulator shares a nuclear import pathway with SR proteins. *EMBO J.* **22**, 1359-1369.

Lamminen, T., Huoponen, K., Sistonen, P., Juvonen, V., Lahermo, P., Aula, P., Nikoskelainen, E., and Savontaus, M. L. (1997). mtDNA haplotype analysis in Finnish families with leber hereditary optic neuroretinopathy. *Eur.J.Hum.Genet.* **5**, 271-279.

Lamond, A. I. and Spector, D. L. (2003). Nuclear speckles: a model for nuclear organelles. *Nat.Rev.Mol.Cell Biol.* **4**, 605-612.

Lavigueur, A., La Branche, H., Kornblihtt, A. R., and Chabot, B. (1993). A splicing enhancer in the human fibronectin alternate ED1 exon interacts with SR proteins and stimulates U2 snRNP binding. *Genes Dev.* **7**, 2405-2417.

Lee, J. G. and Kay, E. P. (2007). Two populations of p27 use differential kinetics to phosphorylate Ser-10 and Thr-187 via phosphatidylinositol 3-Kinase in response to fibroblast growth factor-2 stimulation. *J.Biol.Chem.* **282**, 6444-6454.

Lehner, B., Semple, J. I., Brown, S. E., Counsell, D., Campbell, R. D., and Sanderson, C. M. (2004). Analysis of a high-throughput yeast two-hybrid system and its use to predict the function of intracellular proteins encoded within the human MHC class III region. *Genomics* **83**, 153-167.

Liang, L. and Sandell, J. H. (2007). Focus on molecules: Homeobox protein Chx10. *Exp.Eye Res.*

Linari, M., Ueffing, M., Manson, F., Wright, A., Meitinger, T., and Becker, J. (1999). The retinitis pigmentosa GTPase regulator, RPGR, interacts with the delta subunit of rod cyclic GMP phosphodiesterase. *Proc.Natl.Acad.Sci.U.S.A* **96**, 1315-1320.

Linari, M., Hanzal-Bayer, M., and Becker, J. (1999). The delta subunit of rod specific cyclic GMP phosphodiesterase, PDE delta, interacts with the Arf-like protein Arl3 in a GTP specific manner. *FEBS Lett.* **458**, 55-59.

Liu, L., Wei, Y., and Chen, H. (2001). [Identification of a nonsense mutation causing X-linked RP2 in two Chinese families]. *Zhonghua Yi.Xue.Za Zhi.* **81**, 71-72.

Liu, Q., Zhou, J., Daiger, S. P., Farber, D. B., Heckenlively, J. R., Smith, J. E., Sullivan, L. S., Zuo, J., Milam, A. H., and Pierce, E. A. (2002). Identification and

subcellular localization of the RP1 protein in human and mouse photoreceptors. *Invest Ophthalmol.Vis.Sci.* **43**, 22-32.

Liu, Q., Tan, G., Levenkova, N., Li, T., Pugh, E. N., Jr., Rux, J., Speicher, D. W., and Pierce, E. A. (2007). The proteome of the mouse photoreceptor sensory cilium complex. *Mol.Cell Proteomics.*

Liu, X., Vansant, G., Udovichenko, I. P., Wolfrum, U., and Williams, D. S. (1997). Myosin VIIa, the product of the Usher 1B syndrome gene, is concentrated in the connecting cilia of photoreceptor cells. *Cell Motil.Cytoskeleton* **37**, 240-252.

Lounsbury, K. M., Richards, S. A., Carey, K. L., and Macara, I. G. (1996). Mutations within the Ran/TC4 GTPase. Effects on regulatory factor interactions and subcellular localization. *J.Biol.Chem.* **271**, 32834-32841.

Macara, I. G. (2001). Transport into and out of the nucleus. *Microbiol.Mol.Biol.Rev.* **65**, 570-94, table.

Macedo-Souza, L. I., Kok, F., Santos, S., Amorim, S. C., Starling, A., Nishimura, A., Lezirovitz, K., Lino, A. M., and Zatz, M. (2005). Spastic paraplegia, optic atrophy, and neuropathy is linked to chromosome 11q13. *Ann.Neurol.* **57**, 730-737.

Maita, H., Kitaura, H., Keen, T. J., Inglehearn, C. F., Ariga, H., and Iguchi-Ariga, S. M. (2004). PAP-1, the mutated gene underlying the RP9 form of dominant retinitis pigmentosa, is a splicing factor. *Exp.Cell Res.* **300**, 283-296.

Mansergh, F. C., Millington-Ward, S., Kennan, A., Kiang, A. S., Humphries, M., Farrar, G. J., Humphries, P., and Kenna, P. F. (1999). Retinitis pigmentosa and progressive sensorineural hearing loss caused by a C12258A mutation in the mitochondrial MTTS2 gene. *Am.J.Hum.Genet.* **64**, 971-985.

Maria, B. L., Boltshauser, E., Palmer, S. C., and Tran, T. X. (1999). Clinical features and revised diagnostic criteria in Joubert syndrome. *J.Child Neurol.* **14**, 583-590.

Martin, J. (2000). Group II chaperonins as mediators of cytosolic protein folding. *Curr.Protein Pept.Sci.* **1**, 309-324.

Martinez-Gimeno, M., Gamundi, M. J., Heman, I., Maseras, M., Milla, E., Ayuso, C., Garcia-Sandoval, B., Beneyto, M., Vilela, C., Baiget, M., Antinolo, G., and Carballo, M. (2003). Mutations in the pre-mRNA splicing-factor genes PRPF3, PRPF8, and PRPF31 in Spanish families with autosomal dominant retinitis pigmentosa. *Invest Ophthalmol.Vis.Sci.* **44**, 2171-2177.

Mashima, Y., Saga, M., Akeo, K., and Oguchi, Y. (2001). Phenotype associated with an R120X nonsense mutation in the RP2 gene in a Japanese family with X-linked retinitis pigmentosa. *Ophthalmic Genet.* **22**, 43-47.

Matunis, M. J., Coutavas, E., and Blobel, G. (1996). A novel ubiquitin-like modification modulates the partitioning of the Ran-GTPase-activating protein RanGAP1 between the cytosol and the nuclear pore complex. *J.Cell Biol.* **135**, 1457-1470.

Maw, M. A., Kennedy, B., Knight, A., Bridges, R., Roth, K. E., Mani, E. J., Mukkadan, J. K., Nancarrow, D., Crabb, J. W., and Denton, M. J. (1997). Mutation of the gene encoding cellular retinaldehyde-binding protein in autosomal recessive retinitis pigmentosa. *Nat.Genet.* **17**, 198-200.

McKie, A. B., McHale, J. C., Keen, T. J., Tarttelin, E. E., Goliath, R., Lith-Verhoeven, J. J., Greenberg, J., Ramesar, R. S., Hoyng, C. B., Cremers, F. P., Mackey, D. A., Bhattacharya, S. S., Bird, A. C., Markham, A. F., and Inglehearn, C. F. (2001). Mutations in the pre-mRNA splicing factor gene PRPC8 in autosomal dominant retinitis pigmentosa (RP13). *Hum.Mol.Genet.* **10**, 1555-1562.

McIntyre, D. (2002) Colour blindness: Causes and Effects. Dalton Publishers, UK. ISBN 0-954 1886-0-8.

Mears, A. J., Kondo, M., Swain, P. K., Takada, Y., Bush, R. A., Saunders, T. L., Sieving, P. A., and Swaroop, A. (2001). Nrl is required for rod photoreceptor development. *Nat.Genet.* **29**, 447-452.

Mehalow, A. K., Kameya, S., Smith, R. S., Hawes, N. L., Denegre, J. M., Young, J. A., Bechtold, L., Haider, N. B., Tepass, U., Heckenlively, J. R., Chang, B., Naggert, J. K., and Nishina, P. M. (2003). CRB1 is essential for external limiting membrane integrity and photoreceptor morphogenesis in the mammalian retina. *Hum.Mol.Genet.* **12**, 2179-2189.

Meindl, A., Dry, K., Herrmann, K., Manson, F., Ciccodicola, A., Edgar, A., Carvalho, M. R., Achatz, H., Hellebrand, H., Lennon, A., Migliaccio, C., Porter, K., Zrenner, E., Bird, A., Jay, M., Lorenz, B., Wittwer, B., D'Urso, M., Meitinger, T., and Wright, A. (1996). A gene (RPGR) with homology to the RCC1 guanine nucleotide exchange factor is mutated in X-linked retinitis pigmentosa (RP3). *Nat.Genet.* **13**, 35-42.

Melamud, A., Shen, G. Q., Chung, D., Xi, Q., Simpson, E., Li, L., Peachey, N. S., Zegarra, H., Hagstrom, S. A., Wang, Q. K., and Traboulsi, E. I. (2006). Mapping a new genetic locus for X linked retinitis pigmentosa to Xq28. *J.Med.Genet.* **43**, e27.

Miano, M. G., Testa, F., Filippini, F., Trujillo, M., Conte, I., Lanzara, C., Millan, J. M., De Bernardo, C., Grammatico, B., Mangino, M., Torrente, I., Carrozzo, R., Simonelli, F., Rinaldi, E., Ventruto, V., D'Urso, M., Ayuso, C., and Ciccodicola, A. (2001). Identification of novel RP2 mutations in a subset of X-linked retinitis pigmentosa families and prediction of new domains. *Hum.Mutat.* **18**, 109-119.

Michaelides, M., Hardcastle, A. J., Hunt, D. M., and Moore, A. T. (2006). Progressive cone and cone-rod dystrophies: phenotypes and underlying molecular genetic basis. *Surv.Ophthalmol.* **51**, 232-258.

Miller, J. and Stagljar, I. (2004). Using the yeast two-hybrid system to identify interacting proteins. *Methods Mol.Biol.* **261**, 247-262.

Mitton, K. P., Swain, P. K., Chen, S., Xu, S., Zack, D. J., and Swaroop, A. (2000). The leucine zipper of NRL interacts with the CRX homeodomain. A possible mechanism of transcriptional synergy in rhodopsin regulation. *J.Biol.Chem.* **275**, 29794-29799.

Molday, L. L., Rabin, A. R., and Molday, R. S. (2000). ABCR expression in foveal cone photoreceptors and its role in Stargardt macular dystrophy. *Nat.Genet.* **25**, 257-258.

Mordes, D., Yuan, L., Xu, L., Kawada, M., Molday, R. S., and Wu, J. Y. (2007). Identification of photoreceptor genes affected by PRPF31 mutations associated with autosomal dominant retinitis pigmentosa. *Neurobiol.Dis.* **26**, 291-300.

Morimura, H., Fishman, G. A., Grover, S. A., Fulton, A. B., Berson, E. L., and Dryja, T. P. (1998). Mutations in the RPE65 gene in patients with autosomal

recessive retinitis pigmentosa or leber congenital amaurosis. *Proc.Natl.Acad.Sci.U.S.A* **95**, 3088-3093.

Moritz, M., Braunfeld, M. B., Sedat, J. W., Alberts, B., and Agard, D. A. (1995). Microtubule nucleation by gamma-tubulin-containing rings in the centrosome. *Nature* **378**, 638-640.

Muresan, V., Joshi, H. C., and Besharse, J. C. (1993). Gamma-tubulin in differentiated cell types: localization in the vicinity of basal bodies in retinal photoreceptors and ciliated epithelia. *J.Cell Sci.* **104 (Pt 4)**, 1229-1237.

Nakayama, K., Ishida, N., Shirane, M., Inomata, A., Inoue, T., Shishido, N., Horii, I., Loh, D. Y., and Nakayama, K. (1996). Mice lacking p27(Kip1) display increased body size, multiple organ hyperplasia, retinal dysplasia, and pituitary tumors. *Cell* **85**, 707-720.

Nickerson, J. A. and Wells, W. W. (1984). The microtubule-associated nucleoside diphosphate kinase. *J.Biol.Chem.* **259**, 11297-11304.

Nishimura, D. Y., Searby, C. C., Carmi, R., Elbedour, K., Van Maldergem, L., Fulton, A. B., Lam, B. L., Powell, B. R., Swiderski, R. E., Bugge, K. E., Haider, N. B., Kwitek-Black, A. E., Ying, L., Duhl, D. M., Gorman, S. W., Heon, E., Iannaccone, A., Bonneau, D., Biesecker, L. G., Jacobson, S. G., Stone, E. M., and Sheffield, V. C. (2001). Positional cloning of a novel gene on chromosome 16q causing Bardet-Biedl syndrome (BBS2). *Hum.Mol.Genet.* **10**, 865-874.

Ohno, M., Fornerod, M., and Mattaj, I. W. (1998). Nucleocytoplasmic transport: the last 200 nanometers. *Cell* **92**, 327-336.

Orozco, J. T., Wedaman, K. P., Signor, D., Brown, H., Rose, L., and Scholey, J. M. (1999). Movement of motor and cargo along cilia. *Nature* **398**, 674.

Otto, E., Hoefele, J., Ruf, R., Mueller, A. M., Hiller, K. S., Wolf, M. T., Schuermann, M. J., Becker, A., Birkenhager, R., Sudbrak, R., Hennies, H. C., Nurnberg, P., and Hildebrandt, F. (2002). A gene mutated in nephronophthisis and retinitis pigmentosa encodes a novel protein, nephroretinin, conserved in evolution. *Am.J.Hum.Genet.* **71**, 1161-1167.

Palacios, I., Weis, K., Klebe, C., Mattaj, I. W., and Dingwall, C. (1996). RAN/TC4 mutants identify a common requirement for snRNP and protein import into the nucleus. *J.Cell Biol.* **133**, 485-494.

Pan, J., Wang, Q., and Snell, W. J. (2005). Cilium-generated signaling and cilia-related disorders. *Lab Invest* **85**, 452-463.

Patel-King, R. S., Gorbatyuk, O., Takebe, S., and King, S. M. (2004). Flagellar radial spokes contain a Ca2+-stimulated nucleoside diphosphate kinase. *Mol.Biol.Cell* **15**, 3891-3902.

Pawlyk, B. S., Smith, A. J., Buch, P. K., Adamian, M., Hong, D. H., Sandberg, M. A., Ali, R. R., and Li, T. (2005). Gene replacement therapy rescues photoreceptor degeneration in a murine model of Leber congenital amaurosis lacking RPGRIP. *Invest Ophthalmol.Vis.Sci.* **46**, 3039-3045.

Pazour, G. J., Baker, S. A., Deane, J. A., Cole, D. G., Dickert, B. L., Rosenbaum, J. L., Witman, G. B., and Besharse, J. C. (2002). The intraflagellar transport protein, IFT88, is essential for vertebrate photoreceptor assembly and maintenance. *J.Cell Biol.* **157**, 103-113.

Pelletier, V., Jambou, M., Delphin, N., Zinovieva, E., Stum, M., Gigarel, N., Dollfus, H., Hamel, C., Toutain, A., Dufier, J. L., Roche, O., Munnich, A., Bonnefont, J. P., Kaplan, J., and Rozet, J. M. (2007). Comprehensive survey of mutations in RP2 and RPGR in patients affected with distinct retinal dystrophies: genotype-phenotype correlations and impact on genetic counseling. *Hum.Mutat.* **28**, 81-91.

Peng, G. H., Ahmad, O., Ahmad, F., Liu, J., and Chen, S. (2005). The photoreceptor-specific nuclear receptor Nr2e3 interacts with Crx and exerts opposing effects on the transcription of rod versus cone genes. *Hum.Mol.Genet.* **14**, 747-764.

Pierce, E. A. (2001). Pathways to photoreceptor cell death in inherited retinal degenerations. *Bioessays* **23**, 605-618.

Ponting, C. P., Mott, R., Bork, P., and Copley, R. R. (2001). Novel protein domains and repeats in Drosophila melanogaster: insights into structure, function, and evolution. *Genome Res.* **11**, 1996-2008.

Postel, E. H. and Abramczyk, B. M. (2003). Escherichia coli nucleoside diphosphate kinase is a uracil-processing DNA repair nuclease. *Proc.Natl.Acad.Sci.U.S.A* **100**, 13247-13252.

Provis, J. M., Diaz, C. M., and Dreher, B. (1998). Ontogeny of the primate fovea: a central issue in retinal development. *Prog.Neurobiol.* **54**, 549-580.

Radcliffe, P. A., Garcia, M. A., and Toda, T. (2000). The cofactor-dependent pathways for alpha- and beta-tubulins in microtubule biogenesis are functionally different in fission yeast. *Genetics* **156**, 93-103.

Rattner, A., Sun, H., and Nathans, J. (1999). Molecular genetics of human retinal disease. *Annu.Rev.Genet.* **33**, 89-131.

Rehemtulla, A., Warwar, R., Kumar, R., Ji, X., Zack, D. J., and Swaroop, A. (1996). The basic motif-leucine zipper transcription factor Nrl can positively regulate rhodopsin gene expression. *Proc.Natl.Acad.Sci.U.S.A* **93**, 191-195.

Ribbeck, K., Lipowsky, G., Kent, H. M., Stewart, M., and Gorlich, D. (1998). NTF2 mediates nuclear import of Ran. *EMBO J.* **17**, 6587-6598.

Rittinger, K., Walker, P. A., Eccleston, J. F., Smerdon, S. J., and Gamblin, S. J. (1997). Structure at 1.65 A of RhoA and its GTPase-activating protein in complex with a transition-state analogue. *Nature* **389**, 758-762.

Rivolta, C., Sweklo, E. A., Berson, E. L., and Dryja, T. P. (2000). Missense mutation in the USH2A gene: association with recessive retinitis pigmentosa without hearing loss. *Am.J.Hum.Genet.* **66**, 1975-1978.

Rivolta, C., Berson, E. L., and Dryja, T. P. (2001). Dominant Leber congenital amaurosis, cone-rod degeneration, and retinitis pigmentosa caused by mutant versions of the transcription factor CRX. *Hum.Mutat.* **18**, 488-498.

Rivolta, C., Sharon, D., DeAngelis, M. M., and Dryja, T. P. (2002). Retinitis pigmentosa and allied diseases: numerous diseases, genes, and inheritance patterns. *Hum.Mol.Genet.* **11**, 1219-1227.

Roepman, R., van Duijnhoven, G., Rosenberg, T., Pinckers, A. J., Bleeker-Wagemakers, L. M., Bergen, A. A., Post, J., Beck, A., Reinhardt, R., Ropers, H. H., Cremers, F. P., and Berger, W. (1996). Positional cloning of the gene for X-

linked retinitis pigmentosa 3: homology with the guanine-nucleotide-exchange factor RCC1. *Hum.Mol.Genet.* **5**, 1035-1041.

Roepman, R., Bernoud-Hubac, N., Schick, D. E., Maugeri, A., Berger, W., Ropers, H. H., Cremers, F. P., and Ferreira, P. A. (2000). The retinitis pigmentosa GTPase regulator (RPGR) interacts with novel transport-like proteins in the outer segments of rod photoreceptors. *Hum.Mol.Genet.* **9**, 2095-2105.

Rohlich, P. (1975). The sensory cilium of retinal rods is analogous to the transitional zone of motile cilia. *Cell Tissue Res.* **161**, 421-430.

Rosenberg, T., Schwahn, U., Feil, S., and Berger, W. (1999). Genotype-phenotype correlation in X-linked retinitis pigmentosa 2 (RP2). *Ophthalmic Genet.* **20**, 161-172.

Rosenfeld, P. J., Cowley, G. S., McGee, T. L., Sandberg, M. A., Berson, E. L., and Dryja, T. P. (1992). A null mutation in the rhodopsin gene causes rod photoreceptor dysfunction and autosomal recessive retinitis pigmentosa. *Nat.Genet.* **1**, 209-213.

Rowe MH. Functional organization of the retina. (1991). *Neuroanatomy of the visual pathways and their development.* McMillian, pp1-68.

Scheffzek, K., Ahmadian, M. R., Kabsch, W., Wiesmuller, L., Lautwein, A., Schmitz, F., and Wittinghofer, A. (1997). The Ras-RasGAP complex: structural basis for GTPase activation and its loss in oncogenic Ras mutants. *Science* **277**, 333-338.

Scheffzek, K., Ahmadian, M. R., and Wittinghofer, A. (1998). GTPase-activating proteins: helping hands to complement an active site. *Trends Biochem.Sci.* **23**, 257-262.

Schmitt, A. and Wolfrum, U. (2001). Identification of novel molecular components of the photoreceptor connecting cilium by immunoscreens. *Exp.Eye Res.* **73**, 837-849.

Schrick, J. J., Vogel, P., Abuin, A., Hampton, B., and Rice, D. S. (2006). ADP-ribosylation factor-like 3 is involved in kidney and photoreceptor development. *Am.J.Pathol.* **168**, 1288-1298.

Schultz, D. W., Klein, M. L., Humpert, A. J., Luzier, C. W., Persun, V., Schain, M., Mahan, A., Runckel, C., Cassera, M., Vittal, V., Doyle, T. M., Martin, T. M., Weleber, R. G., Francis, P. J., and Acott, T. S. (2003). Analysis of the ARMD1 locus: evidence that a mutation in HEMICENTIN-1 is associated with age-related macular degeneration in a large family. *Hum.Mol.Genet.* **12**, 3315-3323.

Schwahn, U., Lenzner, S., Dong, J., Feil, S., Hinzmann, B., van Duijnhoven, G., Kirschner, R., Hemberger, M., Bergen, A. A., Rosenberg, T., Pinckers, A. J., Fundele, R., Rosenthal, A., Cremers, F. P., Ropers, H. H., and Berger, W. (1998). Positional cloning of the gene for X-linked retinitis pigmentosa 2. *Nat.Genet.* **19**, 327-332.

Schwahn, U., Paland, N., Techritz, S., Lenzner, S., and Berger, W. (2001). Mutations in the X-linked RP2 gene cause intracellular misrouting and loss of the protein. *Hum.Mol.Genet.* **10**, 1177-1183.

Seddon, J. M., Ajani, U. A., and Mitchell, B. D. (1997). Familial aggregation of age-related maculopathy. *Am.J.Ophthalmol.* **123**, 199-206.

Seewald, M. J., Korner, C., Wittinghofer, A., and Vetter, I. R. (2002). RanGAP mediates GTP hydrolysis without an arginine finger. *Nature* **415**, 662-666.

Seyedahmadi, B. J., Rivolta, C., Keene, J. A., Berson, E. L., and Dryja, T. P. (2004). Comprehensive screening of the USH2A gene in Usher syndrome type II and non-syndromic recessive retinitis pigmentosa. *Exp.Eye Res.* **79** , 167-173.

Sharer, J. D. and Kahn, R. A. (1999). The ARF-like 2 (ARL2)-binding protein, BART. Purification, cloning, and initial characterization. *J.Biol.Chem.* **274**, 27553-27561.

Sharon, D., Sandberg, M. A., Rabe, V. W., Stillberger, M., Dryja, T. P., and Berson, E. L. (2003). RP2 and RPGR Mutations and Clinical Correlations in Patients with X-Linked Retinitis Pigmentosa. *Am.J Hum.Genet.* **73**, 1131-1146.

Shu, X., Fry, A. M., Tulloch, B., Manson, F. D., Crabb, J. W., Khanna, H., Faragher, A. J., Lennon, A., He, S., Trojan, P., Giessl, A., Wolfrum, U., Vervoort, R., Swaroop, A., and Wright, A. F. (2005). RPGR ORF15 isoform co-localizes with RPGRIP1 at centrioles and basal bodies and interacts with nucleophosmin. *Hum.Mol.Genet.* **14**, 1183-1197.

Shu, X., Black, G. C., Rice, J. M., Hart-Holden, N., Jones, A., O'Grady, A., Ramsden, S. , and Wright, A. F. (2007). RPGR mutation analysis and disease: an update. *Hum.Mutat.* **28**, 322-328.

Signor, D., Wedaman, K. P., Orozco, J. T., Dwyer, N. D., Bargmann, C. I., Rose, L. S., and Scholey, J. M. (1999). Role of a class DHC1b dynein in retrograde transport of IFT motors and IFT raft particles along cilia, but not dendrites, in chemosensory neurons of living Caenorhabditis elegans. *J.Cell Biol.* **147**, 519-530.

Song, X. Q., Meng, F., Ramsey, D. J., Ripps, H., and Qian, H. (2005). The GABA rho1 subunit interacts with a cellular retinoic acid binding protein in mammalian retina. *Neuroscience* **136**, 467-475.

Stelzl, U., Worm, U., Lalowski, M., Haenig, C., Brembeck, F. H., Goehler, H., Stroedicke, M., Zenkner, M., Schoenherr, A., Koeppen, S., Timm, J., Mintzlaff, S., Abraham, C., Bock, N., Kietzmann, S., Goedde, A. , Toksoz, E., Droege, A., Krobitsch, S., Korn, B., Birchmeier, W., Lehrach, H., and Wanker, E. E. (2005). A human protein-protein interaction network: a resource for annotating the proteome. *Cell* **122**, 957-968.

Stevenson, V. A. and Theurkauf, W. E. (2000). Actin cytoskeleton: putting a CAP on actin polymerization. *Curr.Biol.* **10**, R695-R697.

Sullivan, L. S., Bowne, S. J., Seaman, C. R., Blanton, S. H., Lewis, R. A., Heckenlively, J. R., Birch, D. G., Hughbanks-Wheaton, D., and Daiger, S. P. (2006). Genomic rearrangements of the PRPF31 gene account for 2.5% of autosomal dominant retinitis pigmentosa. *Invest Ophthalmol.Vis.Sci.* **47**, 4579-4588.

Sun, H. and Nathans, J. (1997). Stargardt's ABCR is localized to the disc membrane of retinal rod outer segments. *Nat.Genet.* **17**, 15-16.

Tamkun, J. W., Kahn, R. A., Kissinger, M., Brizuela, B. J., Rulka, C., Scott, M. P., and Kennison, J. A. (1991). The arflike gene encodes an essential GTP-binding protein in Drosophila. *Proc.Natl.Acad.Sci.U.S.A* **88**, 3120-3124.

Thiselton, D. L., Zito, I., Plant, C., Jay, M., Hodgson, S. V., Bird, A. C., Bhattacharya, S. S., and Hardcastle, A. J. (2000). Novel frameshift mutations in the RP2 gene and polymorphic variants. *Hum.Mutat.* **15**, 580.

Thompson, D. A., Li, Y., McHenry, C. L., Carlson, T. J., Ding, X., Sieving, P. A., Apfelstedt-Sylla, E., and Gal, A. (2001). Mutations in the gene encoding lecithin retinol acyltransferase are associated with early-onset severe retinal dystrophy. *Nat.Genet.* **28**, 123-124.

Tian, G., Huang, Y., Rommelaere, H., Vandekerckhove, J., Ampe, C., and Cowan, N. J. (1996). Pathway leading to correctly folded beta-tubulin. *Cell* **86**, 287-296.

Tian, G., Bhamidipati, A., Cowan, N. J., and Lewis, S. A. (1999). Tubulin folding cofactors as GTPase-activating proteins. GTP hydrolysis and the assembly of the alpha/beta-tubulin heterodimer. *J.Biol.Chem.* **274**, 24054-24058.

Vainberg, I. E., Lewis, S. A., Rommelaere, H., Ampe, C., Vandekerckhove, J., Klein, H. L., and Cowan, N. J. (1998). Prefoldin, a chaperone that delivers unfolded proteins to cytosolic chaperonin. *Cell* **93**, 863-873.

Valverde, D., Riveiro-Alvarez, R., Aguirre-Lamban, J., Baiget, M., Carballo, M., Antinolo, G., Millan, J. M., Garcia, S. B., and Ayuso, C. (2007). Spectrum of the ABCA4 gene mutations implicated in severe retinopathies in Spanish patients. *Invest Ophthalmol.Vis.Sci.* **48**, 985-990.

Van Valkenburgh, H., Shern, J. F., Sharer, J. D., Zhu, X., and Kahn, R. A. (2001). ADP-ribosylation factors (ARFs) and ARF-like 1 (ARL1) have both specific and shared effectors: characterizing ARL1-binding proteins. *J.Biol.Chem.* **276**, 22826-22837.

Vervoort, R., Lennon, A., Bird, A. C., Tulloch, B., Axton, R., Miano, M. G., Meindl, A., Meitinger, T., Ciccodicola, A., and Wright, A. F. (2000). Mutational hot spot within a new RPGR exon in X-linked retinitis pigmentosa. *Nat.Genet.* **25**, 462-466.

Vervoort, R. and Wright, A. F. (2002). Mutations of RPGR in X-linked retinitis pigmentosa (RP3). *Hum.Mutat.* **19**, 486-500.

Vithana, E. N., Abu-Safieh, L., Allen, M. J., Carey, A., Papaioannou, M., Chakarova, C., Al Maghtheh, M., Ebenezer, N. D., Willis, C., Moore, A. T., Bird, A. C. , Hunt, D. M., and Bhattacharya, S. S. (2001). A human homolog of yeast

pre-mRNA splicing gene, PRP31, underlies autosomal dominant retinitis pigmentosa on chromosome 19q13.4 (RP11). *Mol.Cell* **8**, 375-381.

Vorster, A. A., Rebello, M. T., Coutts, N., Ehrenreich, L., Gama, A. D., Roberts, L. J., Goliath, R., Ramesar, R., and Greenberg, L. J. (2004). Arg120stop nonsense mutation in the RP2 gene: mutational hotspot and germ line mosaicism? *Clin.Genet.* **65**, 7-10.

Wada, Y., Kubota, H., Maeda, M., Taniwaki, M., Hattori, M., Imamura, S., Iwai, K., and Minato, N. (1997). Mitogen-inducible SIPA1 is mapped to the conserved syntenic groups of chromosome 19 in mouse and chromosome 11q13.3 centromeric to BCL1 in human. *Genomics* **39**, 66-73.

Wada, Y., Nakazawa, M., Abe, T., and Tamai, M. (2000). A new Leu253Arg mutation in the RP2 gene in a Japanese family with X-linked retinitis pigmentosa. *Invest Ophthalmol.Vis.Sci.* **41**, 290-293.

Wang, G., Miskimins, R., and Miskimins, W. K. (1999). The cyclin-dependent kinase inhibitor p27Kip1 is localized to the cytosol in Swiss/3T3 cells. *Oncogene* **18**, 5204-5210.

Wang, W., Ding, J., Allen, E., Zhu, P., Zhang, L., Vogel, H., and Yang, Y. (2005). Gigaxonin interacts with tubulin folding cofactor B and controls its degradation through the ubiquitin-proteasome pathway. *Curr.Biol.* **15**, 2050-2055.

Wang, W., Budhu, A., Forgues, M., and Wang, X. W. (2005). Temporal and spatial control of nucleophosmin by the Ran-Crm1 complex in centrosome duplication. *Nat.Cell Biol.* **7**, 823-830.

Weil, D., Blanchard, S., Kaplan, J., Guilford, P., Gibson, F., Walsh, J., Mburu, P., Varela, A., Levilliers, J., Weston, M. D., and . (1995). Defective myosin VIIA gene responsible for Usher syndrome type 1B. *Nature* **374**, 60-61.

Weis, K., Dingwall, C., and Lamond, A. I. (1996). Characterization of the nuclear protein import mechanism using Ran mutants with altered nucleotide binding specificities. *EMBO J.* **15** , 7120-7128.

Wright, A. F. and Shu, X. (2007). Focus on Molecules: RPGR. *Exp.Eye Res.* **85**, 1-2.

Wu, M., Lu, L., Hong, W., and Song, H. (2004). Structural basis for recruitment of GRIP domain golgin-245 by small GTPase Arl1. *Nat.Struct.Mol.Biol.* **11**, 86-94.

Yan, D., Ouyang, X. M., Zhu, X., Du, L. L., Chen, Z. Y., and Liu, X. Z. (2005). Refinement of the DFNA41 locus and candidate genes analysis. *J.Hum.Genet.* **50**, 516-522.

Yang, Y., Allen, E., Ding, J., and Wang, W. (2007). Giant axonal neuropathy. *Cell Mol.Life Sci.* **64**, 601-609.

Yaroslavskiy, B., Watkins, S., Donnenberg, A. D., Patton, T. J., and Steinman, R. A. (1999). Subcellular and cell-cycle expression profiles of CDK-inhibitors in normal differentiating myeloid cells. *Blood* **93**, 2907-2917.

Yates, J. R., Sepp, T., Matharu, B. K., Khan, J. C., Thurlby, D. A., Shahid, H., Clayton, D. G., Hayward, C., Morgan, J., Wright, A. F., Armbrecht, A. M., Dhillon, B., Deary, I. J., Redmond, E., Bird, A. C., and Moore, A. T. (2007). Complement C3 Variant and the Risk of Age-Related Macular Degeneration. *N.Engl.J.Med.*

Yau, K. W. (1994). Phototransduction mechanism in retinal rods and cones. The Friedenwald Lecture. *Invest Ophthalmol.Vis.Sci.* **35**, 9-32.

Yokoyama, N., Hayashi, N., Seki, T., Pante, N., Ohba, T., Nishii, K., Kuma, K., Hayashida, T., Miyata, T., Aebi, U., and . (1995). A giant nucleopore protein that binds Ran/TC4. *Nature* **376**, 184-188.

Yoon, J. H., Qiu, J., Cai, S., Chen, Y., Cheetham, M. E., Shen, B., and Pfeifer, G. P. (2006). The retinitis pigmentosa-mutated RP2 protein exhibits exonuclease activity and translocates to the nucleus in response to DNA damage. *Exp.Cell Res.* **312**, 1323-1334.

Young, R. W. and Bok, D. (1969). Participation of the retinal pigment epithelium in the rod outer segment renewal process. *J.Cell Biol.* **42**, 392-403.

Zhang, C. and Clarke, P. R. (2001). Roles of Ran-GTP and Ran-GDP in precursor vesicle recruitment and fusion during nuclear envelope assembly in a human cell-free system. *Curr.Biol.* **11**, 208-212.

Zhang, H., Liu, X. H., Zhang, K., Chen, C. K., Frederick, J. M., Prestwich, G. D., and Baehr, W. (2004). Photoreceptor cGMP phosphodiesterase delta subunit (PDEdelta) functions as a prenyl-binding protein. *J.Biol.Chem.* **279**, 407-413.

Zhou, C., Cunningham, L., Marcus, A. I., Li, Y., and Kahn, R. A. (2006). Arl2 and Arl3 regulate different microtubule-dependent processes. *Mol.Biol.Cell* **17**, 2476-2487.

Zito, I., Downes, S. M., Patel, R. J., Cheetham, M. E., Ebenezer, N. D., Jenkins, S. A., Bhattacharya, S. S., Webster, A. R., Holder, G. E., Bird, A. C., Bamiou, D. E., and Hardcastle, A. J. (2003). RPGR mutation associated with retinitis pigmentosa, impaired hearing, and sinorespiratory infections. *J.Med.Genet.* **40**, 609-615.

Website Addresses:

OMIM:
http://www.ncbi.nlm.nih.gov/sites/entrez?db=OMIM

RetNet:
http://www.sph.uth.tmc.edu/Retnet/

NCBI:
http://www.ncbi.nlm.nih.gov/

ExPASy:
http://www.expasy.ch/tools/

APPENDIX 1

REAGENTS, SOLUTIONS AND MEDIA

General Reagents

6x loading dye:

0.4% Orange G, 0.03% Bromophenol Blue, 0.03% Xylene cyanol, 15% Ficoll 400, 10 mM 1 M Tris-HCl (pH 7.5), 50mM EDTA (pH 8.0)

TAE buffer:

40 mM Tris-HCl, 40 mM Acetic Acid, 1 mM EDTA

SOC media:

2% (w/v) tryptone, 0.5% (w/v) yeast extract, 0.2% (v/v) 5 M NaCl, 0.25% (v/v) 1 M KCl, 1% (v/v) 1 M $MgCl_2$, 1% (v/v) 1 M $MgSO_4$, 2% (v/v) 1 M glucose

Phosphate buffered saline (PBS):

145 mM NaCl, 3.6 mM NaH_2PO_4, 10.5 mM Na_2HPO_4

L-agar antibiotic plates:

1% (w/v) Bacto®-tryptone, 0.5% (w/v) Bacto®-yeast extract, 1% (w/v) NaCl, 1.5% (w/v) Bacto®-agar

L-broth (LB):

1% (w/v) Bacto®-tryptone, 0.5% (w/v) Bacto®-yeast extract, 1% (w/v) NaCl

Tris-EDTA (TE) buffer:

10 mM Tris-HCl (pH 7.5), 1 mM EDTA

SDS-PAGE resolving gel:

375 mM Tris-HCl pH 8.8, 8-15% (v/v) acrylamide, 0.2-0.4% (v/v) bisacrylamide, 0.15% (w/v) ammonium persulphate (APS), 0.1% (w/v) SDS, 0.05% (v/v) TEMED

SDS-PAGE stacking gel:

125 mM Tris-HCl pH6.8, 3% (v/v) acrylamide, 0.1% (v/v) bisacrylamide, 0.05% (w/v) ammonium persulphate (APS), 0.1% (w/v) SDS, 0.08% (v/v) TEMED

SDS-PAGE running buffer:
25 mM Tris-HCl, 190 mM Glycine, 3.5 mM SDS

2 x SDS-PAGE sample buffer:
125 mM Tris-HCl (pH6.8), 20% (v/v) Glycerol, 4% (v/v) SDS, 10% (v/v) 2-β Mercaptoethanol, 0.2% (w/v) Bromophenol Blue

Coomassie stain:
25% (v/v) Methanol, 25% (v/v) Acetic acid, 0.25% (w/v) Coomassie brilliant blue (R-250)

Coomassie de-stain solution:
25% (v/v) Methanol, 25% (v/v) Acetic acid

PBS-Tween20:
0.05% (v/v) Tween-20® in PBS

1 x Western blotting transfer buffer:
25 mM Tris-HCl, 190 mM Glycine, 20% (v/v) Methanol

Western blotting blocking buffer:
5% (w/v) "Marvel®" milk powder, 0.05% (v/v) Tween-20® in PBS

Southern blotting denaturation buffer:
1.5M NaCl, 0.5M NaOH

Southern blotting hybridisation solution:
0.05M PO_4 (pH 6.8), 2 x SSC, 5 ml 100x Denhardts solution (2% Ficoll, 2% BSA, 2% PVP), 10 µg/ml salmon sperm DNA, 10% dextran sulphate, 0.3% SDS, 0.15% NaPPi ($Na_4P4O_7.10H_2O$)

Yeast-specific Reagents

YPAD media:
1% (w/v) Yeast extract, 2% (w/v) Bacto®-peptone, 2% (w/v) Dextrose, 0.004% (w/v) Adenine Sulfate

YPAD agar plates:
1% (w/v) Yeast extract, 2% (w/v) Bacto®-peptone, 2% (w/v) Dextrose, 0.004% (w/v) Adenine Sulfate, 15% (w/v) Agar

LiOAc/TE:
10 mM LiOAC in TE

SD/glucose plates:
0.17% (w/v) Yeast nitrogen base without amino acids, 0.5% (w/v) Ammonium sulphate, 2% (w/v) Dextrose, 15% (w/v) Agar, 10% (v/v) appropriate x10 dropout solution

SD/galactose plates:
0.17% (w/v) Yeast nitrogen base without amino acids, 0.5% (w/v) Ammonium sulphate, 2% (w/v) Galactose, 1% (w/v) Raffinose, 15% (w/v) Agar, 10% (v/v) appropriate x10 dropout solution

NaOH/β-ME buffer:
1.85 M NaOH, 7.5% β-Mercaptoethanol

SU buffer:
5% (w/v) SDS, 125 mM Tris-HCl (pH 6.8), 0.1 mM EDTA, 0.005% (w/v) Bromophenol blue, 8 M Urea, 15 mg DTT/ml

10x Dropout Solution:

Amino Acid	Weight (mg/litre)
L-Isoleucine	300
L-Valine	1500
L-Adenine hemisulphate salt	200
L-Arginine HCl	500
L-Histidine HCl monohydrate	200
L-Leucine	1000
L-Lysine HCl	500
L-Methionine	200
L-Phenylalanine	500

L-Threonine*	2000
L-Tryptophan	500
L-Tyrosine	500
L-Uracil	200
L-Glutamic Acid	1000
L-Aspartic Acid*	1000
L-Serine	400

All amino acids can be autocalved with the exception of those marked *. These should be filter sterilised and added after the auoclaved solution has cooled to 55°C.

PRIMER SEQUENCES

Oligo Name	Sequence 5'-3'	Cloning Restriction Site	Purpose And Host Vector
RP2 Start (F)	CGCCATGGGCTGCTTCTTCTCCAAGAG	*Nco*I	PCR pSos
RP2 41 (F)	CGCCATGGGAATGTTCAGTGGACTGAAGGATG	*Nco*I	PCR pSos
RP2 190 (F)	CGCCATGGGACCAGAAGATGCTGTGGTTCAG	*Nco*I	PCR pSos
RP2 238 (F)	CGCCATGGGAGTGGTATTATTTGCTGGTGATTAC	*Nco*I	PCR pSos
RP2 200 (R)	CGGTCGACTTAAGGAACATAGTCCTGAACCACAGC	*Sal*I	PCR pSos
RP2 End (R)	CGGTCGACTCATATTCCCATCTGTATATCAGC	SalI	PCR pSos
pMyr Forward	ACTACTAGCAGCTGTAATAC	-	Sequencing pMyr
pMyr Reverse	CGTGAATGTAAGCGTGACAT	-	Sequencing pMyr
pSos Forward	CCAAGACCAGGTACCATG	-	Sequencing pSos
pSos Reverse	GCCAGGGTTTTCCCAGT	-	Sequencing pSos
Arl3 Forward	CGGAATTCATGGGCTTGCTCTCAATTTTG	*Eco*RI	PCR pMyr
Arl3 Reverse	CGGTCGACTCCCGCAGCTCCTGCATC	*Sal*I	PCR pMyr
Arl6 Forward	CGCTCGAGTATGGGATTGCTAGACAGACTTTC	*Xho*I	PCR pMyr
Arl6 Reverse	CGGTCGACGCTGAGGTTTTCCAACTATTATC	*Sal*I	PCR pMyr
M13 Forward	GTAAAACGACGGCCAGT	-	Sequencing pGem TEasy
M13 Reverse	GGAAACAGCTATGACCATG	-	Sequencing pGem TEasy
Arl3 C-term F	CGGAATTCATGGGCTTGCTCTCAATTTTG	*Eco*RI	PCR pcDNA4/TO/

			VSV
Arl3 C-term R	CCGCGGTATAATTTCTTCTTTGCATTGAC	*Sac*II	PCR pcDNA4/TO/ VSV
RP2 pMyr F	CGGAATTCATGGGCTGCTTCTTCTCCAAGAG	*Eco*RI	PCR pMyr
RP2 pMyr R	CGCTCGAGTCATATTCCCATCTGTATATCAG	*Xho*I	PCR pMyr
Arl3 pSos F	CGCCATGGTCATGGGCTTGCTCTCAATTTTG	*Nco*I	PCR pSos
Arl3 pSos R	CGGCGGCCGCTCCCGCAGCTCCTGCATC	*Not*I	PCR pSos
Arl6 pSos F	CGCCATGGTTATGGGATTGCTAGACAGACTTTC	*Nco*I	PCR pSos
Arl6 pSos R	CGGCGGCCGCGCTGAGGTTTTCCAACTATTATC	*Not*I	PCR pSos
Arl6 pCMV3 F	GCGGATCCCATGGGATTGCTAGACAGAC	*Bam*HI	PCR pCMVTag3b
Arl6 pCMV3 R	GCCTCGAGTCATGTCTTCACAGTCTGG	*Xho*I	PCR pCMVTag3b
SPAG7 pCMV3b F	GCGAATTCATGGCGGACCTACTGGGCTCC	*Eco*RI	PCR pCMVTag3b
SPAG7 pCMV3b R	GCCTCGAGCGCCTAGGAGGTTGGCGGCAAC	*Xho*I	PCR pCMVTag3b
540-562 F	GTACGGTGGGAGGTCTATATAAG	-	Sequencing pEGFP-N1
745-724 R	GTCGCCGTCCAGCTCGACCAGG	-	Sequencing pEGFP-N1
Bovine Arl2 F	CCATCCTCAAGAAGTTCAACGG	-	PCR
Bovine Arl2 R	GATGAGGAGGGTCGCTCCG	-	PCR
Bovine Arl3 F	GAAGACATCAGCCACATCACAC	-	PCR
Bovine Arl3 R	GTTCCTGACCTGTCTCTTCAAATC	-	PCR

Table 7.1 Oligonucleotide primers used for PCR and sequencing

Oligo Name	Sequence 5'-3'	Resultant Change
RP2 Cys67Tyr F	CTCATTCAAGAC**TAT**GAGAACTGTAACATC	TGT to TAT
RP2 Cys67Tyr R	GATGTTACAGTTCTC**ATA**GTCTTGAATGAG	TGT to TAT
RP2 Cys86Tyr F	GTTACCATTGATGAC**TAT**ACTAACTGC	TGT to TAT
RP2 Cys86Tyr R	GCAGTTAGT**ATA**GTCATCAATGGTAAC	TGT to TAT
RP2 Arg118His F	CCTGCCAACAATTT**CAT**GTGCGAGATTG	CGT to CAT
RP2 Arg118His R	CAATCTCGCAC**ATG**AAATTGTTGGCAGG	CGT to CAT
RP2 Leu253Arg F	GCCAGAAAA**CGA**ATTGATGAGATGGTTG	CTA to CGA
RP2 Leu253Arg R	CAACCATCTCATCAAT**TCG**TTTTCTGGC	CTA to CGA
Arl3 T31N F	GCTGGCAAG**AAC**ACTCTTCTGAAGCAG	ACC to AAC
Arl3 T31N R	CTGCTTCAGAAGAGT**GTT**CTTGCCAGC	ACC to AAC
Arl3 Q71L F	GACATTGGTGGA**CTG**AGGAAAATCAG	CAG to CTG
Arl3 Q71L R	CTGATTTTCCT**GAG**TCCACCAATGTC	CAG to CTG
Arl2 T30N F	GCT GGA AAG **AAC** ACC ATC CTG	ACA to AAC
Arl2 T30N R	CAG GAT GGT **GTT** CTT TCC AGC	ACA to AAC
Arl2 Q70L F	GTG GGT GGC **CTG** AAG TCC CTG	CAG to CTG
Arl2 Q70L R	CAG GGA CTT **CAG** GCC ACC CAC	CAG to CTG
RAN T24N F	CT GGA AAA **AAT** ACA TTC GTT AAG	ACT to AAT
RAN T24N R	CTT AAC GAA TGT **ATT** TTT TCC AG	ACT to AAT
RAN 43E F	GTA GCT ACC **GAG** GGT GAG	TTG to GAG
RAN 43E R	CTC AAC ACC **CTC** GGT AGC TAC	TTG to GAG
RAN Q69L F	CA GCT GGT **CTG** GAG AAA TTT G	CAG to CTG
RAN Q69L R	C AAA TTT CTC **CAG** ACC AGC TG	CAG to CTG

Table 7.2 Mutant oligonucleotide primers used for SDM

APPENDIX 2

PUBLICATIONS ARISING FROM THIS STUDY

Evans, R. J., Chapple, J. P., Grayson, C., Hardcastle, A. J., and Cheetham, M. E. (2005). Assay and functional analysis of the ARL3 effector RP2 involved in X-linked retinitis pigmentosa. *Methods Enzymol.* **404**, 468-480.

Evans, R. J., Hardcastle, A. J., and Cheetham, M. E. (2006). Focus on molecules: X-linked Retinitis Pigmentosa 2 protein, RP2. *Exp.Eye Res.* **82**, 543-544.